

Wind Resource Assessment: Statistical and Computational Fluid-Dynamic Analysis

Wahid Irshad

MSc. Applied Physics (Specialisation in Electronics)

MSc. IT (Mechatronics)

A thesis submitted in partial fulfilment of the requirements of
Edinburgh Napier University, for the award of Doctor of
Philosophy

February 2012

ABSTRACT

Wind is an important source of renewable energy and is widely available, despite the changing condition. In recent years a growing number of manufacturers have produced small wind turbines suitable for utilisation by individual householders or small businesses. These systems are designed to install in towns or cities. This raises the question about the potential of wind energy resource in build-up areas. This thesis sets to investigate the wind energy resource implication in the build-up areas by understanding the wind climatology of urban areas. As well as the overall mean wind speed, knowledge of the wind speed distribution (due to the non-linear relationship between wind speed and wind power) and the wind-direction distribution for optimum turbine siting is required. Other areas that have been considered are short-duration fluctuations in both speed and direction as these can affect the efficiency of the turbine.

The aims of this research are to study the local wind conditions and estimate the available wind resource for the wind-energy driven generation of electricity in Edinburgh by taking into account of its climate, wind data and topographical effects. To achieve these aims eleven years of Met office data was investigated in addition to analysis of the data collected from locally installed weather station. Diurnal effect on wind condition was studied and found to be more pronounced in Edinburgh's rural area than its urban conurbation. It was also found that the available wind energy in the urban area is 30% less than that of the rural area. Turbulence in wind speed and direction of flow was also investigated. Careful consideration of all the parameters defining and affecting the prevailing wind revealed the wind resource in Edinburgh's urban area to be insufficient for viable generation of wind energy through the available technology of micro WEC (wind energy converter) systems.

A CFD analysis was also performed to determine wind resource differences because of different mounting locations of wind equipment over the building under consideration. As a part of the project, a commercially available wind turbine was installed and monitored to investigate its performance in urban area. The research study finally suggests that the available grid connected micro WEC system cannot provide a cost effective contribution to urban Edinburgh's renewable energy generation.

ACKNOWLEDGEMENTS

I would like to thank my Director of studies, Dr. Keng Goh. Thank you for your constant support, guidance and motivation, giving me the drive to succeed. In addition I would like to thank to an important member of my supervisory team, Professor Jorge Kubie for the support and advice that you have given me.

I would also like to thank the technical and administrative staff at the Faculty and the school of engineering and built environment: Ian Campbell, Derek Cogle, and all the other technicians who were always so helpful in providing technical insight and support.

Finally I would like to thank my family, friends and peers for their unconditional support over the years; I am very grateful.

DECLARATION

I hereby declare that the work presented in this thesis was solely carried out by myself at Edinburgh Napier University, Edinburgh, except where due acknowledgement is made, and that it has not been submitted for any other degree.

.....
Wahid Irshad (Candidate)

.....
Date

TABLE OF CONTENTS

ABSTRACT	ii
ACKNOWLEDGEMENTS	iii
DECLARATION	iv
TABLE OF CONTENTS	v
LIST OF TABLES.....	xxi
NOMENCLATURE.....	xxiii

1 INTRODUCTION **1**

1.1 CLIMATE CHANGE.....	1
1.2 INCREASING ENERGY COST.....	1
1.3 GROWTH OF WIND ENERGY	3
1.4 AIMS AND OBJECTIVES	4
1.5 OUTLINE OF THE THESIS	5

2 REVIEW OF RELEVANT LITERATURE..... **7**

2.1 INTRODUCTION.....	7
2.2 METEOROLOGICAL ASPECT OF WIND	8
2.2.1 ATMOSPHERIC LAYERS	9
2.2.2 ATMOSPHERIC CIRCULATIONS	10
2.2.3 TEMPERATURE AND PRESSURE IN ATMOSPHERE	12
2.2.4 LOCAL WINDS SYSTEM.....	12
2.2.4.1 Katabatic and Anabatic winds	13
2.2.4.2 Wind due to topographic barriers	14
2.2.4.3 Land and sea breezes.....	15
2.2.5 BOUNDARY LAYER	16
2.3 URBAN WIND	18
2.4 CHARACTERISTICS OF WIND	20
2.4.1 SCALE OF MOTION.....	20
2.4.1.1 Inter-annual variation.....	20
2.4.1.2 Annual variation	22
2.4.1.3 Diurnal variation.....	22
2.4.1.4 Short-term variation	22

2.4.2	WIND TURBULENCE AND GUST	23
2.5	COMPUTATIONAL FLUID DYNAMICS (CFD)	24
2.5.1	INTRODUCTION	24
2.5.2	CFD SIMULATION MODELS.....	26
2.5.2.1	Direct Numerical Simulations (DNS).....	26
2.5.2.2	Large Eddy Simulation (LES).....	26
2.5.2.3	Reynolds Averaged Navier-Stokes (RANS).....	27
2.5.2.4	Detached Eddy Simulations (DES)	27
2.5.3	WORKING METHODOLOGY OF CFD.....	27
2.5.3.1	Pre-processing stage.....	28
2.5.3.2	Processing stage	28
2.5.3.3	Post processing stage	29
2.5.4	LIMITATIONS AND ERRORS OF CFD	29
2.6	WIND AS A SOURCE OF ENERGY	30
2.6.1	POWER AVAILABLE IN WIND	30
2.6.2	ASSESSMENT OF WIND ENERGY POTENTIAL	31
2.6.2.1	Approaches and objectives	32
2.6.2.2	Software packages.....	33
2.7	WIND MEASUREMENTS AND INSTRUMENTATION.....	34
2.7.1	WIND SPEED MEASUREMENTS.....	34
2.7.2	WIND DIRECTION MEASUREMENTS.....	35
2.7.3	TEMPERATURE MEASUREMENTS.....	35
2.7.4	BAROMETRIC PRESSURE MEASUREMENTS.....	35
2.8	WIND ENERGY CONVERTOR (WEC).....	35
2.8.1	DRAG TYPE WEC.....	36
2.8.2	LIFT TYPE WEC	36
2.8.3	HORIZONTAL AXIS WIND TURBINE (HAWT).....	37
2.8.4	VERTICAL-AXIS WIND TURBINE (VAWT)	39
2.8.5	WIND TURBINE SIZES	40
2.8.6	WIND TURBINE END-USE CATEGORIES	41
2.8.6.1	Off grid applications	41
2.8.6.2	On grid applications.....	41
2.9	WIND ENERGY IN UK.....	42
2.10	WARWICK WIND TRIAL REPORT.....	43

<u>3</u>	<u>DESCRIPTION OF EDINBURGH'S TOPOGRAPHY</u>	<u>45</u>
3.1	EDINBURGH'S GEOGRAPHY	45
3.2	SEVEN HILLS OF EDINBURGH	47
3.3	WOODLAND IN EDINBURGH	47
3.4	URBAN HABITATS IN EDINBURGH	49
3.5	RIVERS OF EDINBURGH	49
3.6	FARMLANDS IN EDINBURGH	50
3.7	EDINBURGH GREEN BELT	51
3.8	CLIMATE IN EDINBURGH	52
3.9	POPULATION DENSITY	54
3.10	TOWN AND VILLAGE DISTRIBUTION	54
<u>4</u>	<u>EQUIPMENT INSTALLATION AND CALIBRATION</u>	<u>55</u>
4.1	INTRODUCTION	55
4.2	WINDSAVE TURBINE WS1200PS	55
4.2.1	SENSING EQUIPMENT	59
4.2.1.1	DC voltage sensing	59
4.2.1.2	DC Current sensing	62
4.2.1.3	AC voltage sensing	62
4.2.1.4	AC current sensing	63
4.3	PRESSURE SENSOR	63
4.4	METPAK WEATHER STATION	64
4.4.1	INTRODUCTION	64
4.4.2	WORKING PRINCIPLE	64
4.4.3	INSTALLATION	65
4.4.4	SCALING ERROR	66
4.4.5	WINDCOM SOFTWARE PLATFORM	69
4.5	DATA LOGGING EQUIPMENT	69
4.5.1	SETUP SETTINGS FOR LOGGING	72
4.5.2	DATA DOWNLOADING	72
4.6	PROCESSING OF RAW DATA	73
<u>5</u>	<u>ANALYSIS OF MET OFFICE WIND DATA</u>	<u>76</u>

5.1	INTRODUCTION.....	76
5.2	MET OFFICE DATA	76
5.3	LOCATION OF DATA COLLECTION POINT.....	78
5.4	ELEVATION OF MET OFFICE WEATHER STATION AND SURROUNDING AREA	80
5.5	PREVAILING WIND DIRECTION	86
5.6	AVERAGE WIND SPEED	86
5.7	STANDARD DEVIATION OF WIND SPEED.....	88
5.8	STANDARD DEVIATION VS. MEAN WIND SPEED	90
5.9	FREQUENCY DISTRIBUTION	91
5.10	PROBABILITY DISTRIBUTION FUNCTION (PDF).....	93
5.11	CUMULATIVE DISTRIBUTION FUNCTION (CDF).....	96
5.12	VELOCITY DURATION CURVE	99
5.13	VERTICAL WIND PROFILE	100
5.13.1	LOG LAW	101
5.13.2	POWER LAW	102
5.14	DIURNAL VARIATION IN WIND.....	104
5.15	RELATION BETWEEN WIND SPEED AND METEOROLOGICAL PARAMETERS	109
5.15.1	TEMPERATURE	109
5.15.2	ATMOSPHERIC PRESSURE.....	116
5.15.3	RELATIVE HUMIDITY.....	121
5.16	AIR DENSITY IN EDINBURGH	123
5.17	WIND POWER DENSITY AND ENERGY ESTIMATION.....	125
5.18	SAVINGS ON GHG EMISSIONS.....	129
5.19	CONCLUSION.....	129

6 ANALYSIS OF LOCALLY COLLECTED WIND DATA 130

6.1	INTRODUCTION.....	130
6.2	LOCATION OF MERCHISTON CAMPUS.....	130
6.3	TERRAIN AT THE MERCHISTON CAMPUS	130
6.4	WIND DATA SOURCE	139
6.5	PREVAILING WIND DIRECTION	139
6.6	MEAN WIND SPEED AND STANDARD DEVIATION	143
6.7	PROBABILITY DISTRIBUTION FUNCTION (PDF).....	145
6.8	CUMULATIVE DISTRIBUTION FUNCTION (CDF)	148

6.9	EFFECT OF SAMPLING TIME ON FREQUENCY DISTRIBUTION OF DATA.....	151
6.10	VELOCITY DURATION CURVE	153
6.11	DIURNAL VARIATION IN DATA AT MERCHISTON	154
6.12	COMPARISON OF MET OFFICE AND MERCHISTON WIND DATA.....	157
6.13	WIND POWER DENSITY AND ENERGY ESTIMATION.....	158
6.14	TURBULENCE ANALYSIS.....	161
6.14.1	INTRODUCTION	161
6.14.2	SAMPLING TIME FOR TURBULENCE INTENSITY	162
6.14.3	STANDARD DEVIATION AND MEAN WIND SPEED	165
6.14.4	VARIATION IN WIND PROFILE WITH HEIGHT NEAR TO BUILDINGS	168
6.15	VARIATION IN WIND DIRECTION	171
6.16	CONCLUSION.....	174
7	<u>CFD ANALYSIS</u>	<u>175</u>
7.1	INTRODUCTION.....	175
7.2	PHOENICS CFD SOFTWARE	175
7.2.1	INTRODUCTION	175
7.2.2	THE COMPONENTS OF PHOENICS	175
7.2.3	GEOMETRY CONSTRUCTION	177
7.2.4	DOMAIN CREATION	180
7.2.5	MESH SIZING	180
7.2.6	BOUNDARY CONDITIONS.....	183
7.2.6.1	Wind object.....	183
7.2.7	SELECTION OF TURBULENCE MODEL	185
7.2.7.1	KECHEN Turbulence model.....	187
7.2.8	CONVERGENCE CRITERIA.....	187
7.2.9	LIMITATIONS AND POTENTIAL ERRORS IN CFD ANALYSIS	188
7.3	SIMULATION RESULTS	189
7.3.1	CFD INVESTIGATION OF WIND FLOW OVER A CUBIC OBSTACLE	189
7.3.1.1	Wind speed results and analysis	190
7.3.1.2	Turbulence intensity analysis.....	194
7.3.2	CFD SIMULATION OVER MERCHISTON CAMPUS.....	195
7.3.2.1	Effect of roughness height on wind flow	196
7.3.2.2	Vertical wind flow pattern at Merchiston campus.....	197

7.3.2.3	Effect of wind direction on wind flow	199
7.3.2.4	Turbulence intensity analysis at Merchiston	202
7.4	LIMITATIONS OF THIS CFD STUDY AND FUTURE DIRECTIONS.....	203
7.5	CONCLUSION.....	204
8	<u>PERFORMANCE ANALYSIS OF WEC SYSTEM.....</u>	205
8.1	INTRODUCTION.....	205
8.2	WIND RESOURCE AT METPAK-L AND WEC LOCATION.....	205
8.3	PERFORMANCE OF WEC SYSTEM.....	209
8.3.1	AVAILABLE WIND RESOURCE FOR WEC.....	209
8.3.2	PERFORMANCE OF WIND TURBINE	211
8.3.3	PERFORMANCE OF INVERTER SYSTEM	214
8.4	CONCLUSION.....	217
9	<u>CONCLUSIONS AND FUTURE WORK.....</u>	218
9.1	ANALYSIS OF WIND DATA AT MET OFFICE SITE AND MERCHISTON CAMPUS.....	218
9.2	RESULTS OF CFD INVESTIGATION.....	219
9.3	PERFORMANCE OF THE WEC SYSTEM.....	220
9.4	FUTURE WORK.....	220
	REFERENCES.....	222
	APPENDICES.....	234
	Appendix A: Wind turbine efficiency	235
	Appendix B: Data sheets	237
	Appendix C: List of Publications.....	241

LIST OF FIGURES

Figure 1-1: Average annual UK domestic electricity bills trend based on DECC data.....	2
Figure 1-2: Average price of fuels paid by UK power producers (DECC, 2011a).	3
Figure 2-1: Wind Spectrum Farm Brookhaven based on work by Van der Hoven (1957) (Burton <i>et al.</i> 2001).....	9
Figure 2-2: Layers of the atmosphere and temperature gradient line (Pidwirny, 2010).....	10
Figure 2-3: Schematic picture of the general circulation (WMO, 1981).....	11
Figure 2-4: Atmospheric pressure gradient graph (Ahrens, 2009).	13
Figure 2-5: Formation and flow of Katabatic wind (BBC Weather, 2006).....	13
Figure 2-6: Formation and flow of Anabatic wind (BBC Weather, 2006).....	14
Figure 2-7: The flow of air over the mountain range based on WMO, 1981.....	15
Figure 2-8: Diurnal land and sea breeze. A and B: sea breeze circulation and pressure distribution. C and D: land breeze circulation and pressure distribution (Barry & Chorley, 2010).	16
Figure 2-9: Typical daily pattern of BLH for hot and cold season during 2005 (Contini, <i>et al.</i> 2008).....	17
Figure 2-10: Relative distribution of BLH for hot and cold season during 2005 (Contini, <i>et al.</i> 2008).....	18
Figure 2-11: Various scales related to urban wind climate based on Murakami, 1999.....	19
Figure 2-12: The scales of atmospheric motion with the phenomenon's average size and life span based on Ahrens, 2009.	20

Figure 2-13: Example of vertical wind shear and change in wind speed with height (calculations are for given wind speed of 10 m/s at 10 m height, wind shear exponent is around 1/7 (Nelson, 2009).	23
Figure 2-14: An air parcel moving towards a wind turbine.	30
Figure 2-15: Drag and lift forces on airfoil (Mathew, 2006).	37
Figure 2-16: Upwind and downwind turbines based on Mathew, 2006.	38
Figure 2-17: Classification of wind turbines based on Mathew, 2006.	39
Figure 2-18: Theoretical power production for different wind turbines when the wind speed is 10 m/s, based on Clarke, 2003.....	40
Figure 2-19: Graph of UK wind farm growth based on BWEA data.	42
Figure 3-1: Edina generated Edinburgh map in terms of elevation (Courtesy of Edina Digimap).	46
Figure 3-2: Seven Hills of Edinburgh (Courtesy Of Google Earth).	47
Figure 3-3: Woodland in Edinburgh (Scottish Gov, 2006).....	48
Figure 3-4: Urban Habitats in Edinburgh (Scottish Gov, 2006).	49
Figure 3-5: Rivers in Edinburgh (Scottish Gov, 2006).....	50
Figure 3-6: Farmland in Edinburgh (Scottish Gov, 2006).....	51
Figure 3-7: Edinburgh Green Belt (Scottish Gov, 2004).....	52
Figure 3-8: Edinburgh Climate over view (Wikimedia, 2007)	53
Figure 3-9: south-westerly Wind flow in Edinburgh (courtesy of Edina).	53
Figure 3-10: Urban and rural distribution of Edinburgh (Edinburgh city local plan, 2007).....	54
Figure 4-1: Windsave WS1000 wind turbine installed on Merchiston roof top (continue).....	56

Figure 4-2: Windsave WS1000 wind turbine installed on Merchiston roof top. .	57
Figure 4-3: Power connection and proposed data logging with WindSave turbine.....	59
Figure 4-4: Circuit diagram of VDC.	60
Figure 4-5: VDC components and connections.....	61
Figure 4-6: DC current sensor.....	62
Figure 4-7: AC current sensor.....	63
Figure 4-8: Pressure sensor HCA0811ARG inside of the sensor box.....	64
Figure 4-9: Time of flight details (Gill Instruments, 2006a).....	65
Figure 4-10: MetPak weather station on the right side and MetPak installed on the Merchiston roof on the left side.	66
Figure 4-11: Comparison between MetPak and Airflow meter data.	67
Figure 4-12: Comparison between Corrected MetPak data and Airflow meter data.....	68
Figure 4-13: RS-232 Connection available in MetPak	68
Figure 4-14: WindCom scale setting screen.	69
Figure 4-15: System setup at the Merchiston roof for logging and downloading data.....	70
Figure 4-16: SquirrelView main screen with all possible options.....	71
Figure 4-17: Squirrel 2020 data logger setup settings	72
Figure 5-1: European Wind Atlas.....	77
Figure 5-2: NOABL wind speed atlas for the UK (source: BWEA).	78
Figure 5-3: Met office weather station at Gogarbank Edinburgh (obtained from Google map).	79

Figure 5-4: Met office weather station location's satellite picture and surrounding terrain's photograph at Gogarbank Edinburgh (obtained from Google map).....	80
Figure 5-5: Sectors around Met office weather station drawn on Google Earth.	81
Figure 5-6: 24 Elevation graphs of the surrounding area covering a 10 km distance around the Met office weather station (continue).....	82
Figure 5-7: 24 Elevation graphs of the surrounding area covering a 10 km distance around the Met office weather station (continue).....	83
Figure 5-8: 24 Elevation graphs of the surrounding area covering a 10 km distance around the Met office weather station (continue).....	84
Figure 5-9: 24 Elevation graphs of the surrounding area covering a 10 km distance around the Met office weather station.....	85
Figure 5-10: Wind directions frequency in rose diagram for year 2000-2009.....	87
Figure 5-11: Graph of monthly mean wind speeds.	88
Figure 5-12: Graph of monthly wind speed standard deviation.	89
Figure 5-13: Monthly mean wind speed versus monthly standard deviation of eleven years of data.....	91
Figure 5-14: Sample plot of 1999 wind speed data.....	92
Figure 5-15: Comparison between probability distribution of real data, Weibull distribution and Rayleigh distribution for 1999 to 2009 (continue).....	95
Figure 5-16: Comparison between probability distribution of real data, Weibull distribution and Rayleigh distribution for 1999 to 2009.	96
Figure 5-17: Comparison between cumulative distribution curves of real data, Weibull distribution and Rayleigh distribution for 1999-2009 (continue).....	97
Figure 5-18: Comparison between cumulative distribution curves of real data, Weibull distribution and Rayleigh distribution for 1999-2009.....	98

Figure 5-19: Velocity duration curve A : Velocity duration curve from 1999 to 2009. B : Velocity duration curve of 1999, 2002 and 2003.....	100
Figure 5-20: Lograthimic profile of 1999 to 2009 with surface roughness (Z_0) 0.03 m.....	103
Figure 5-21: Lograthimic profile of eleven years mean wind speed for diferent surface roughnesses.....	104
Figure 5-22: Graph between hour of the day and hourly mean wind speed for March 2009.....	105
Figure 5-23: Graph between hour of the day and hourly mean wind speed for 3 days of March 2009.	105
Figure 5-24: Graph of monthly diurnal wind speed for 1999 to 2009 (continue).	107
Figure 5-25: Graph of monthly diurnal wind speed for 1999 to 2009.	108
Figure 5-26: Graph of hourly wind direction data against hours of the day for March 2009.....	109
Figure 5-27: Monthly minimum, maximum and mean temperature for year 2009.	110
Figure 5-28: Graph of daily mean wind speed and temperature against days.	110
Figure 5-29: Graph of hourly mean temperature against hours of the day for March 2009.....	111
Figure 5-30: Monthly diurnal temperature variation for 2009.....	112
Figure 5-31: Graph of one day (i.e. 24 hours) hourly wind speed and temperature for March 2009.....	113
Figure 5-32: Graph of average hourly wind speed and temperature for March 2009.....	113

Figure 5-33: Graph of average hourly wind speed and temperature for December 2009.	114
Figure 5-34: Graph of coefficient of correlation between diurnal mean wind speed and temperature against months for 1999 to 2009.....	115
Figure 5-35: Graph of hourly wind speed and atmospheric pressure for one day.	117
Figure 5-36: Graph of diurnal hourly average wind speed and atmospheric pressure for March 2009.....	117
Figure 5-37: Graph A : diurnal atmospheric pressure variation for year 2009. B : diurnal wind speed variation for year 2009.....	118
Figure 5-38: Graph A :Hourly atmospheric pressure variation fo Jan 2009. B : hourly wind speed variation for Jan 2009.....	120
Figure 5-39: Graph of diurnal hourly average relative humidity for May 2007.	122
Figure 5-40: Graph of diurnal hourly average wind speed and relative humidity for May 2007.....	122
Figure 5-41: Graph of coefficient of correlation between diurnal mean wind speed and relative humidity against months for 1999 to 2009.	123
Figure 5-42: Wind power density against wind speed frequency for year 2008.	128
Figure 6-1: Relative location and elevation of Met office weather station and Merchiston campus (Courtesy of Google Earth).	131
Figure 6-2: 24 Sectors around Merchiston campus drawn on Google Earth... ..	132
Figure 6-3: 24 Elevation graphs around Merchiston campus up to 15 km in distance (continue).....	133
Figure 6-4: 24 Elevation graphs around Merchiston campus up to 15 km in distance (continue).....	134

Figure 6-5: 24 Elevation graphs around Merchiston campus up to 15 km in distance (continue).....	135
Figure 6-6: 24 Elevation graphs around Merchiston campus up to 15 km in distance.....	136
Figure 6-7: Photographs of surrounding area from roof top of Merchiston campus (continue).	137
Figure 6-8: Photographs of surrounding area from roof top of Merchiston campus.	138
Figure 6-9: Wind rose diagrams of wind flow direction at Met Pack1 & 2 from July 2009 to June 2010 (continue).....	140
Figure 6-10: Wind rose diagrams of wind flow direction at Met Pack1 & 2 from July 2009 to June 2010 (continue).....	141
Figure 6-11: Wind rose diagrams of wind flow direction at Met Pack1 & 2 from July 2009 to June 2010.....	142
Figure 6-12: Comparison of monthly mean wind speed from MetPak 1 and MetPak 2.....	144
Figure 6-13: Comparison between Probability distribution of MetPak-H (MetPak1) data, Weibull distribution and Rayleigh distribution for year 2010 (continue).....	145
Figure 6-14: Comparison between Probability distribution of MetPak-H (MetPak1) data, Weibull distribution and Rayleigh distribution for year 2010 (continue).....	146
Figure 6-15: Comparison between Probability distribution of MetPak-H (MetPak1) data, Weibull distribution and Rayleigh distribution for year 2010.	147
Figure 6-16: Comparison between monthly cumulative distribution of real data, Weibull distribution and Rayleigh distribution year 2010 (continue).	149

Figure 6-17: Comparison between monthly cumulative distribution of real data, Weibull distribution and Rayleigh distribution year 2010.	150
Figure 6-18: Comparison between Probability distribution of real data, Weibull distribution and Rayleigh distribution based on different sampling time.	152
Figure 6-19: Velocity duration curve of MetPak-H and MetPak-L for year 2010.	154
Figure 6-20: Graph of monthly diurnal wind speed at MetPak-L and MetPak-H for 2010.	155
Figure 6-21: Monthly diurnal temperature variation at Merchiston campus for 2010.	156
Figure 6-22: Graph of coefficient of correlation for MetPak-H and MetPak-L between diurnal mean wind speed and temperature against months for 2010.	156
Figure 6-23: Daily wind direction in rose diagram for 2 days of July 2010.	157
Figure 6-24: Wind power density bar graph in relation with Wind Speed Frequency distribution for year 2010 at MetPak-H.	160
Figure 6-25: Wind speed data for a 5-minutes sampling period at 0.5 Hz.	161
Figure 6-26: Mean wind speed and standard deviation versus sampling period.	163
Figure 6-27: Turbulence intensity (TINT) versus sampling period with power trend.	163
Figure 6-28: Turbulence intensity versus sampling period of 1 to 60 minutes.	164
Figure 6-29: Rate of change (slope) between consecutive turbulence intensity values.	165
Figure 6-30: Turbulence intensity versus sampling period 10 to 60 minutes.	165
Figure 6-31: Standard deviation versus mean wind speed.	166

Figure 6-32: Turbulence intensity (TINT) versus mean wind speed.	167
Figure 6-33: Turbulence intensity versus standard deviation in wind speed. ...	167
Figure 6-34: Wind speed at lower Matpak versus wind speed at higher Matpak.	169
Figure 6-35: TINT at lower Metpak versus TINT at higher Metpak.	169
Figure 6-36: Lower MetPak turbulence (TINT-L) and higher MetPak turbulence (TINT-H) on hourly time scale and ratio between them.	170
Figure 6-37: Probability density of wind turbulence intensity at higher MetPak (TINT-H) and lower MetPak (TINT-L).....	170
Figure 6-38: Wind approaching angle with the increment of time.	172
Figure 6-39: Cumulative probability distribution of wind direction variations for different months and logarithmic trend line.	173
Figure 6-40: Turbulence intensity (std dev / mean) of wind directional variation versus mean wind speed.	174
Figure 7-1: interrelationships of different modules of PHOENICS.....	176
Figure 7-2: Isometric and Plan view of Merchiston campus CFD geometric model.	179
Figure 7-3: Domain dimensions of CFD model.	180
Figure 7-4: Grid on Merchiston model.....	182
Figure 7-5: CFD software error because of resources deficiency.	182
Figure 7-6: Screen short of Wind attributes dialog box.	183
Figure 7-7: Convergence monitor plot generated by the EARTH solver.	188
Figure 7-8: Wind flow pattern over cubic blocks, view; X-Z plan Y=0.....	191
Figure 7-9: vertical wind speed profile at roof top of cubic building.	192

Figure 7-10: Wind speed at the leading edge of the building, wind blowing from front, view; Y-Z plan X=0.....	193
Figure 7-11: Wind speed variation over cubic building with respect to height plan view (X-Y plan Z=0).....	194
Figure 7-12: Turbulence layer over the top of the cubic building A : view; Y-Z plan X=0, where wind coming from front. B : View; X-Z plan Y=0, where wind coming from left.	195
Figure 7-13: Simulation of wind flow at Merchiston, view; X-Z plan Y=0.....	196
Figure 7-14: Vertical wind profile at Merchiston (view; X-Z plan Y=0) when A : wind blow from 240 degrees. B : when wind blow from 60 degrees.	197
Figure 7-15: Vertical wind profile graph for Merchiston at MetPak location, when A : wind blow from 240 degrees. B : when wind blow from 60 degrees.....	198
Figure 7-16: Wind speed at turbine and MetPak-L positions from different angles. A : Rose diagram. B : X-Y plot.	201
Figure 7-17: Turbulence intensity at Merchiston (view; X-Z plan Y=0). A : When wind flow from 240 degrees. B : When wind flow from 60 degrees.....	202
Figure 7-18: Change in TINT with height at MetPak location for different wind directions.....	203
Figure 8-1: Relative location of MetPak and wind turbine at the top of Merchiston Campus roof.....	205
Figure 8-2: Rose diagram for MetPak-L wind directional data	207
Figure 8-3: Hourly wind frequency and power available in wind per m ² . A : at MetPak-L location. B : at Turbine location.....	208
Figure 8-4: Available wind speed at turbine location in terms of turbine operation.....	210
Figure 8-5: Monthly voltage output of wind turbine generator.	213

Figure 8-6: Graph of DC voltage and DC current of 30000 data points.215

Figure 8-7: Graph of DC voltage and AC current of 30000 data points.....215

LIST OF TABLES

Table 1-1: The top 10 countries with highest installed wind power capacity in the first half of 2011 (WWEA, 2011).....4

Table 4-1: Accumulator reading and monthly energy generation of WindSave’s grid connected inverter.....58

Table 4-2: Lab test of VDC.....61

Table 5-1: Monthly mean wind speed (m/s) and yearly average wind speed (m/s) from Met office data (1999-2009) at Edinburgh GogarBank station.88

Table 5-2: Monthly standard deviation (m/s) and yearly average standard deviation (m/s) from Met office data (1999-2009) at Edinburgh Gogarbank station.90

Table 5-3: Wind speed frequency for different ranges of speed, %.92

Table 5-4: Yearly PDF parameters of Weibull and Rayleigh distribution with goodness of fit value (R^2) to real data.....94

Table 5-5: Typical roughness lengths for different terrain surface characteristics according to the European Wind Atlas based on ISES, 2007. 102

Table 5-6: Correlation coefficient between monthly mean diurnal temperature and wind speed..... 115

Table 5-7: Correlation coefficient between monthly mean diurnal relative humidity and wind speed..... 123

Table 5-8: Monthly available wind energy in kWh/m²..... 128

Table 6-1: Mean wind speed and standard deviation based on MetPak H (MetPak1) and MetPak L (MetPak2) data. 144

Table 6-2: Weibull and Rayleigh parameters for MetPak-H wind speed data for year 2010.....	148
Table 6-3: Mean, standard deviation and PDF parameters based on different sampling time.....	153
Table 6-4: Monthly mean wind speed and standard deviation at Met office weather station and Merchiston campus.....	158
Table 6-5: Monthly mean wind speed, power density derived from mean wind speed and from hourly data.	159
Table 6-6: Comparison of results for wind energy estimation based on different methods for year 2010 MetPak-H.	161
Table 7-1: Effect of roughness height on wind flow.....	197
Table 7-2: Wind speed at turbine and MetPak positions when wind blow from different angles and their ratio.....	199
Table 8-1: Comparison of wind speed and wind energy available at MetPak-L and turbine location.....	209
Table 8-2: Monthly input, output energy and energy consumed by inverter with inverter efficiency and net energy export.	216

NOMENCLATURE

ABL	Atmospheric Boundary Layer
BLH	Boundary Layer Height
CFD	Computational fluid dynamics
CWE	Computational Wind Engineering
GW	Giga watt (10^9)
hpa	hectopascal
kW	Kilo watt (10^3)
Lidar	Light Detection and Ranging
TWh	Terawatt hour (10^{12})
SODAR	SONic Detection Aand Ranging
WECs	Wind Energy Converters
WAsP	Wind Atlas Analysis and Application Program
A_T	Area covered by turbine blades, m^2
C	Scale factor
C_p	power coefficient of turbine
k	Shape factor
V	Wind speed, m/s
V_m	Mean wind speed, m/s
v	Volume, m^3
P	Atmospheric pressure, mbar
P_v	Vapor pressure, mbar, hpa
P_{sat}	Saturation vapor pressure, hpa
ρ_a	Air density, kg/m^3
σ	Standard deviation
ϕ	Relative humidity

1 INTRODUCTION

This thesis investigates the available wind resource in the local area; one of the major sources of renewable energy that has recently witnessed a keen interest from energy suppliers and/or investors in the United Kingdom (UK). This paradigm shift in the energy market is mainly driven by increasing energy prices and a desire by many to combat the causes of climate change.

1.1 Climate change

The Sun is the main source of energy in our world. On earth, energy from the sun is absorbed by oceans, land and air and the rest is reflected back to space. The energy absorbed by the land and oceans is released to the atmosphere as heat. This heat is then absorbed by Green House Gases (GHGs) and later re-emitted back to the earth's surface. This heat, in normal circumstances, will keep the earth comfortably warm but due to increased GHGs concentrations this effect is intensified leading to temperature rises globally (Kiehl & Trenberth, 1997).

GHGs consist of water vapour, CO₂, methane, ozone, oxygen, etc. and clouds. Of all these GHGs, water vapour and CO₂ have the greatest effect in absorbing and emitting the heat from both the sun and earth. A higher concentration of CO₂ traps more heat or radiation emitted from the earth's surface hence increasing the earth's temperature. One of the main GHG contributors is the burning of fossil fuels to obtain energy, which releases a large amount of CO₂ in the atmosphere responsible for global warming.

The UK government is committed to reducing GHG emissions by at least 80% by 2050, relative to 1990 levels (DECC, 2011b). The issue of climate change and reducing CO₂ emissions is of greater importance as the global energy demand is expected to increase by more than 50% by 2020 (U.S. EIA, 1999).

1.2 Increasing energy cost

Figures from the Department of Energy and Climate Change show that the average 2010 electricity bill (i.e. £446) across all payment types fell by £11,

compared to 2009 (i.e. £456), but increased by 46.7% (£142) of the price in 2005 (i.e. £304) (see Figure 1-1). The outlook for 2011 also indicates a rise in energy bills (DECC, 2011a).

The main cause for these electricity price rises reflects tightness in the market due to the lack of generation. Other contributing factors include the impacts of higher fossil fuel prices (see Figure 1-2). Such price hikes will encourage energy users to adopt energy efficiency measures and look at alternative energy sources, renewable micro-generation being one of them.

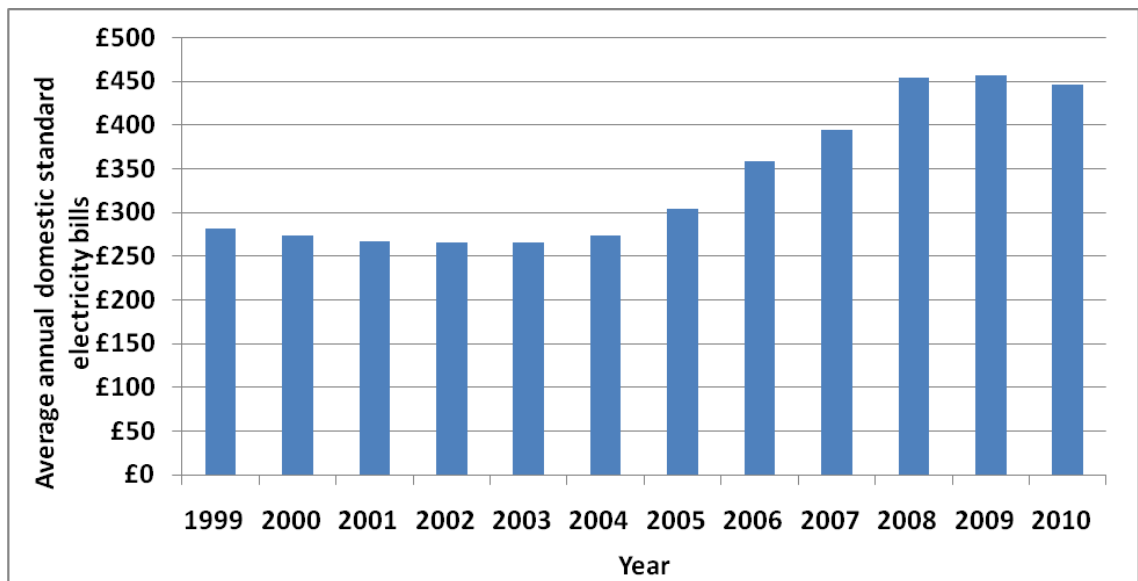


Figure 1-1: Average annual UK domestic electricity bills trend based on DECC data.

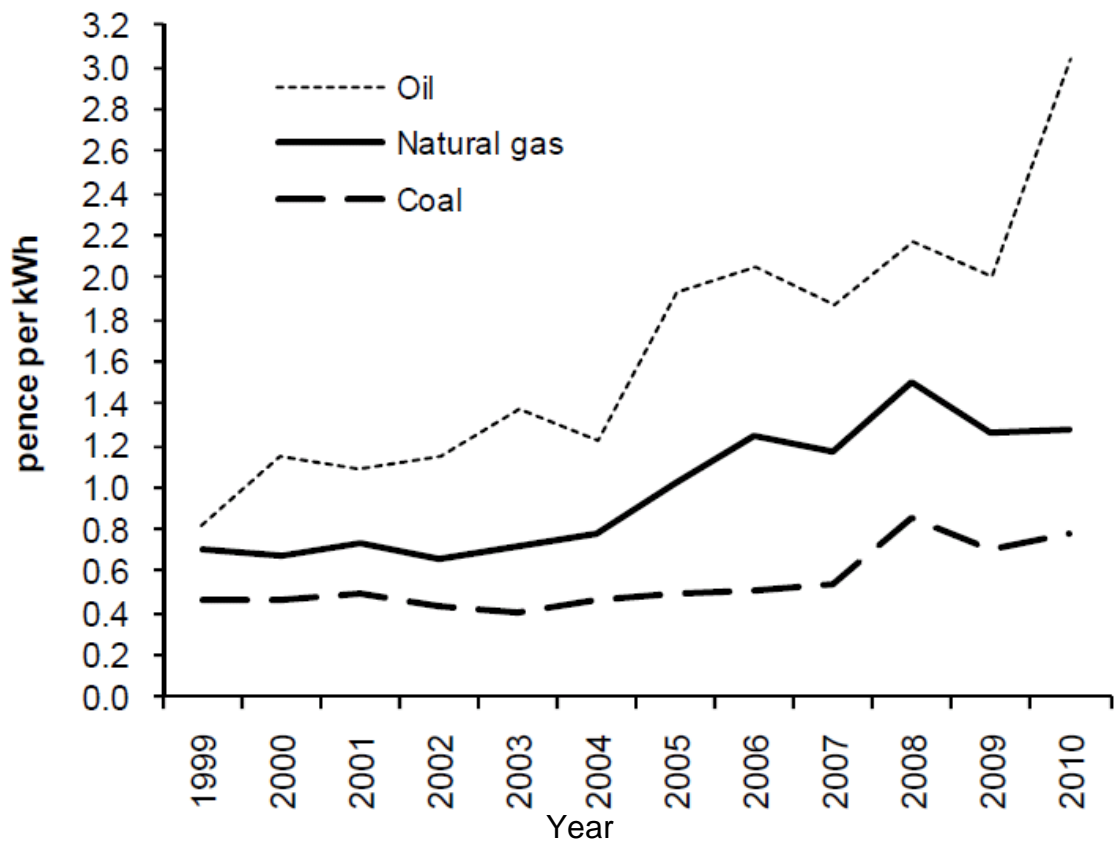


Figure 1-2: Average price of fuels paid by UK power producers (DECC, 2011a).

1.3 Growth of wind energy

Wind energy has seen rapid growth in recent years. The worldwide wind capacity, extended to 215 MW by the end of June 2011, out of which 18.405 MW were added in the first six months of 2011. This increase represents 15 % more than in the first half of 2010, when only 16 MW were added. Worldwide wind capacity grew by 9.3 % within six months and by 22.9 % on an annual basis (mid-2011 compared with mid-2010). In comparison, the annual growth rate in 2010 was 23.6 %. In this growth five leading countries have the lion's share of the world capacity of wind turbines i.e. China, USA, Germany, Spain and India, together they represent a total share of 74 % of the global wind capacity as shown in Table 1-1. In the second half of 2011, an additional capacity of 25.500 MW is expected to be erected worldwide, which would bring new annual installations to 43.900 MW, compared with 37.642 MW in the year 2010. The total installed wind capacity is projected to reach 240.500 MW by the

end of this year. This capacity can cover almost 3 % of the electricity demand all over the world (WWEA, 2011).

Table 1-1: The top 10 countries with highest installed wind power capacity in the first half of 2011 (WWEA, 2011).

Position	Country	Total Capacity by June 2011 [MW]	Added Capacity first half 2011 [MW]	Total Capacity end 2010 [MW]	Added Capacity first half 2010 [MW]	Total Capacity end 2009 [MW]
1	China	52.800	8.000	44.733	7.800	25.810
2	USA	42.432	2.252	40.180	1.200	35.159
3	Germany	27.981	766	27.215	660	25.777
4	Spain	21.150	480	20.676	400	19.149
5	India	14.550	1.480	13.065	1.200	11.807
6	Italy	6.200	460	5.797	450	4.850
7	France	6.060	400	5.660	500	4.574
8	United Kingdom	5.707	504	5.203	500	4.092
9	Canada	4.611	603	4.008	310	3.319
10	Portugal	3.960	260	3.702	230	3.357
	Rest of the World	29.500	3.200	26.441	2.750	21.872
	Total	215.000	18.405	196.682	16.000	159.766

Increased relevance of renewable energy, owing to rising concerns about climate change and energy security, has led to a growing demand of wind energy generation including micro wind projects. These micro wind systems can be installed either in an urban area or in a remote rural area which does not have a grid connection with the mains.

The most striking characteristic of the wind resource is its variability; it is highly variable, both geographically and temporally. Therefore, for any wind energy project the first step is to determine the characteristics of the prevailing wind. Such wind analysis becomes more complicated when it deals with an urban area or a complex terrain.

1.4 Aims and objectives

The aim of this research is to investigate the local wind condition for the purpose of harnessing its energy and attempts to answer the following questions: How is the wind energy is distributed in urban and rural areas? What are the wind variation patterns and the terrain which affect the wind flow in the region? This aim is followed through by a number of objectives, namely,

- ✓ Installation of wind equipment.
- ✓ Data collection and analysis
- ✓ Computational fluid dynamic (CFD) simulations
- ✓ Performance analysis of a commercially available micro WEC system in an urban environment.

To achieve these objectives Edinburgh topography was studied in detail and eleven years of Met office wind data was statistically analysed. To assess the effect of mounting location on the wind resource, CFD simulations were carried out. Performance of locally installed micro WEC system was evaluated. Turbulence at the top of the local building was also analysed.

1.5 Outline of the thesis

Chapter 1 gives the introduction to the thesis, which broadly covers the progress in the field of wind energy. The chapter throws light on the global wind energy scenario with particular reference to the UK market. The chapter also outlines the aims and objectives which this thesis will investigate.

Chapter 2, the literature review, covers the following areas of interest: meteorological aspect of wind; urban wind; characteristics of wind; CFD simulations of wind flow; wind as a source of energy; wind measurement and instrumentation; WEC systems; wind energy in UK and the Warwick wind trial report.

Chapter 3 examines different aspects of the topography in the Edinburgh region.

Chapter 4 covers the equipment installation and calibration; it includes the installation of a WindSave WEC system and a MetPak weather station with calibration of sensing equipments. It also details the data processing done in this research.

Chapter 5 investigates the eleven years of hourly wind data bought from the Met office. It includes terrain investigation around the weather station, average wind speed and standard deviation analysis, probability and cumulative distribution analysis, velocity duration curve, vertical wind profile, diurnal effects and its relation with other atmospheric parameters. In this chapter air density in Edinburgh was calculated and the available wind energy resource, based on the data, was estimated.

Chapter 6 analyses wind energy within urban environment based on wind data collected from the roof of Edinburgh Napier University, Merchiston campus. It also includes turbulence analysis in wind speed and wind direction.

Chapter 7 presents CFD investigation; it includes the working methodology of PHOENICS CFD software, analysis of wind flow over a cuboids object and model of Merchiston campus to find out the wind differences on two mounting locations.

Chapter 8 investigates the performance of the installed WEC system.

Chapter 9 draws important conclusions from each aspect of the presented work. The potential for future work is also discussed.

2 REVIEW OF RELEVANT LITERATURE

2.1 Introduction

This chapter presents a review of relevant literature about wind analysis as it is a subject of common interest within various disciplines, like meteorology, environment, construction, aero dynamics, engineering etc. Different disciplines have different research aims and therefore, their research approach also differs from each other. Nevertheless, inter-disciplinary exchange of research outcomes not only instils research motivation but also helps in improvisation of approach.

Under the flag of meteorology, very detailed and versatile research approaches to assess the wind condition have been adopted. The Salford experiment (Barlow *et al.*, 2008) is one of the very good examples of meteorological approach towards wind condition. In this experiment the researchers selected three urban sites to explore their wind condition through three different approaches. On one site they used sonic anemometer, in the second SODAR (Sonic Detection and Ranging) system and in the third Doppler LIDAR (Light Detection and Ranging) system. In conclusion the research emphasised that every layer of wind behaves differently, therefore the wind condition should be studied on layer basis and modelling should also be done on the basis of wind layers (Barlow *et al.*, 2008). In building construction field researches have been done to shape the buildings in such a way so as to concentrate and harness the wind energy (Blanch, 2002). Environmental research on wind condition emphasises temperature and pressure differences. Some researchers also study the urban wind condition by considering canyons and do modelling on that basis (Georgakis & Santamouris. 2008).

Wind engineering research deals with data collection and computer simulation. The research in Portugal (Palma *et al.*, 2008) in this field is a brilliant combination of both data collection and CFD (Computational Fluid Dynamics) simulation. In this particular research, the researchers collected wind data (wind direction and speed) from five different locations in a complex terrain, analyzed it to make models for wind flow and then simulated it in CFD software. The

results they presented, although not excellent in their entirety, provided sufficient evidence for the effectiveness of CFD simulation to predict wind conditions in a complex terrain. Another research based on CFD simulation (Zhou & Stathopoulos, 1997) shows that modification in the wind layer models can decrease the difference between the experimental data and simulation outcomes.

2.2 Meteorological aspect of wind

Air is a mixture of gases. The Earth's atmosphere contains approximately 5.243×10^{18} kg of air which covers it to the height of 15 km. Kinetic energy in the air, which causes wind, is the result of conversion of the potential energy (WMO, 1981). This potential energy originates by the phenomena that the Earth's equatorial regions receive more solar energy than the polar Regions and this causes large-scale convection currents in the atmosphere. Thus, in a simple pattern, air rises at the equator and sinks at the poles. This develops a macro scale wind circulation around the globe which is greatly influenced by the effects of the rotation of the earth (at a speed of about 600 kilometers per hour at the equator, decreasing to zero at the poles) called Coriolis Effect. In addition, seasonal variations in the distribution of solar energy give rise to variations in the circulation (Manwell, McGowan & Rogers, 2009). The spatial variations in heat transfer create variations in the pressure field and in response to forces directed from high-to-low pressure, air in the atmosphere moves. In the vertical direction, the pressure gradient force is usually cancelled by the downward gravitational force; therefore, the winds blow predominantly in the horizontal plane in response to the horizontal pressure gradients (Hiester & Pennell, 1981). Meteorologists estimate that about 1% of the incoming solar radiation is converted into wind energy which is extremely large because the solar energy received by earth in ten days has an energy content equal to the world's entire fossil fuel reserves (Freris, 1990).

There are four main atmospheric forces which lead the macro-level wind pattern. These include pressure forces due to pressure gradient, the Coriolis force caused by the rotation of the earth, inertial forces due to large-scale

circular motion, and frictional forces at the earth's surface. In contrast there are many small-scale wind and weather systems which might or might not play a role in the general circulation, like land and sea temperature contrast or concentration of strong vertical currents.

Wind is generated in different time and space scales. The large amount of energy found for larger periods of variation, called 'synoptic' variations, roughly 4-5 days is caused by the large-scale motion systems as shown in Figure 2-1. The relatively small amount of energy found for periods of 10-15 hours corresponds to diurnal variations of wind speed while 2-3 minutes variation reflects the fact that motion closes to the surface is almost always turbulent or gusty (WMO, 1981).

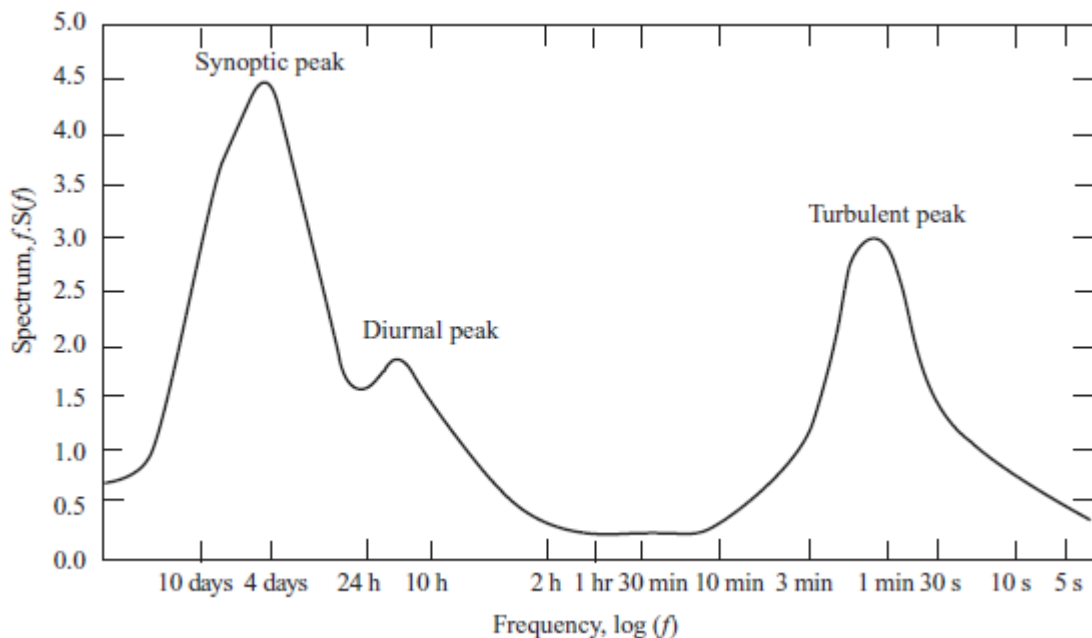


Figure 2-1: Wind Spectrum Farm Brookhaven based on work by Van der Hoven (1957) (Burton *et al.* 2001).

2.2.1 Atmospheric layers

The atmosphere is divided into several layers as shown in Figure 2-2. It is denser near the surface and lighter with increasing height until it ultimately merges with space. The first layer above the earth's surface is called the troposphere. About 80 % of the total mass of the atmosphere is contained in the

troposphere. Weather occurs in this layer. The height of the troposphere is about 11 km and it varies with the seasons. Generally, the troposphere is higher in summer and lower in winter at all latitudes. It is normally found at higher elevations over equatorial regions and decreases towards pole regions. The second layer is known as the stratosphere. Aircrafts fly in this layer because it is very stable. Ozone is also formed in this layer which absorbs harmful rays from the sun. On top of the stratosphere, the mesosphere layer exists in which Meteors or rock fragments burn up when entering in the earth's atmosphere. The hot layer above the mesosphere is the thermosphere. The atmosphere merges into space in the extremely thin exosphere which is the upper limit of the atmosphere (Ahrens, 2009).

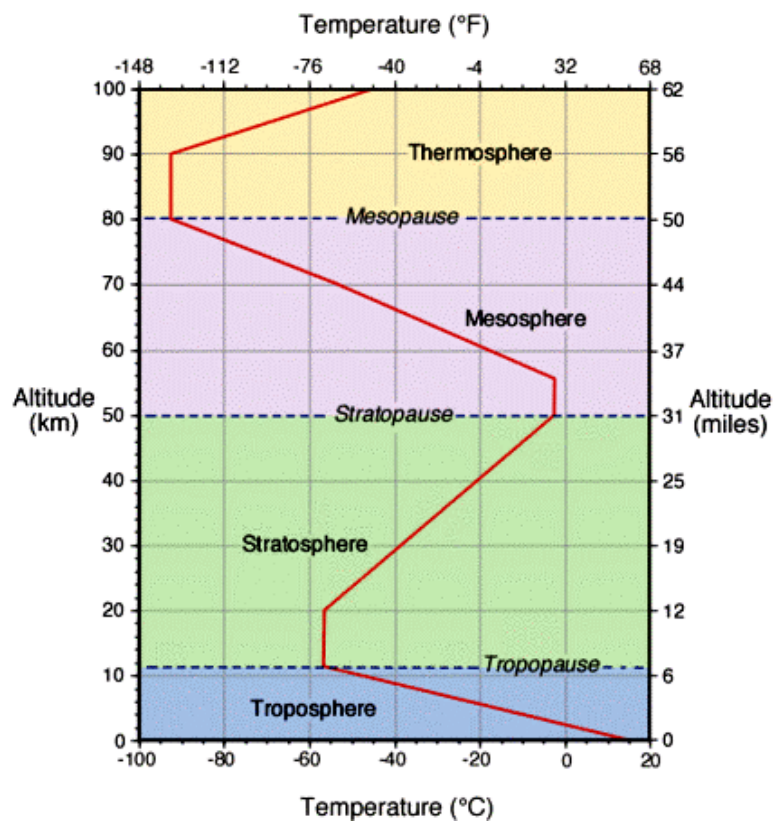


Figure 2-2: Layers of the atmosphere and temperature gradient line (Pidwirny, 2010).

2.2.2 Atmospheric circulations

There are different kinds of atmospheric circulations based on the scale and time. One is called Hadley circulation named after the British scientist George

Hadley (1935) who first suggested it. In this circulation, heated air over the Equator becomes lighter and starts to rise; the cold air in the northern hemisphere starts sinking, which causes the rising warm air in the south to move northward to replace it. At the same time the sinking cold air flows towards the south to replace the rising air over the equator. In this close circulation warm air flows towards the north in the upper atmosphere, cooling at the same time, while cold air moves towards the south, being heated as it does so, as shown in Figure 2-3. Conditions are similar at the southern hemisphere. In this way the atmosphere eliminates the temperature differences between the Poles and the Equator (Schneider, 2006).

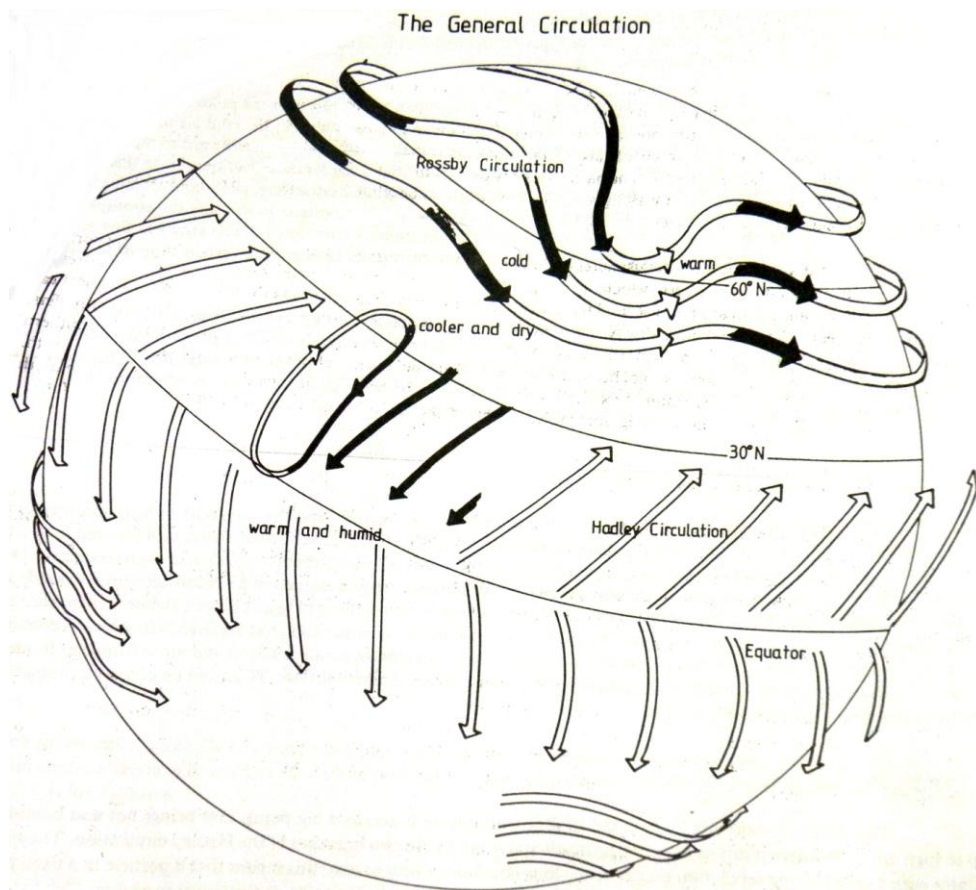


Figure 2-3: Schematic picture of the general circulation (WMO, 1981).

One type of circulation called monsoon circulation is caused by the weather variations between different regions of the world in summer and winter. Another type of circulation is known as Rossby circulation, which is a wavy jet stream at very high altitude as shown in Figure 2-3, is caused by the large temperature

contrast across the west wind belt. The net result of this long wavy pattern will be that the warm air is transported towards the north in the north-moving branches and cold air towards the south in the south-moving branches. This circulation is a source of enormous stirring of the atmosphere, heating the northerly altitudes and cooling the southerly ones (WMO, 1981).

2.2.3 Temperature and pressure in atmosphere

Atmosphere is full of temperature and pressure gradients which drives the contents of atmosphere. Temperature near the earth's surface is relatively high and decreases with height up to the end of troposphere as shown in Figure 2-2.

Cold air has greater density than warm air; the atmospheric pressure in cold air decreases more rapidly with height than in warm air, change in atmospheric pressure with respect to height is shown in Figure 2-4. When there is temperature difference in different regions there is also a pressure difference; pressure being lowest where temperature is the lowest. Because of the different rates of pressure drop with height in cold and warm air, the pressure difference increases more rapidly with height in cold regions thus increasing the pressure force and consequently resulting in an increase in geotropic wind with height. This geotropic wind, also called thermal wind, moves according to the temperature and pressure gradient and if temperature and pressure gradient are not in the same direction geotropic wind also turns with height. Thermal wind has important effects on the boundary layer especially at night (WMO, 1981).

2.2.4 Local winds system

Besides global atmospheric variations which drive the wind, there will always be some local atmospheric variations which control the local wind like valley and mountain winds, land and sea breezes, Foehn winds (dry high-temperature winds on the downwind side of mountain ranges) etc.

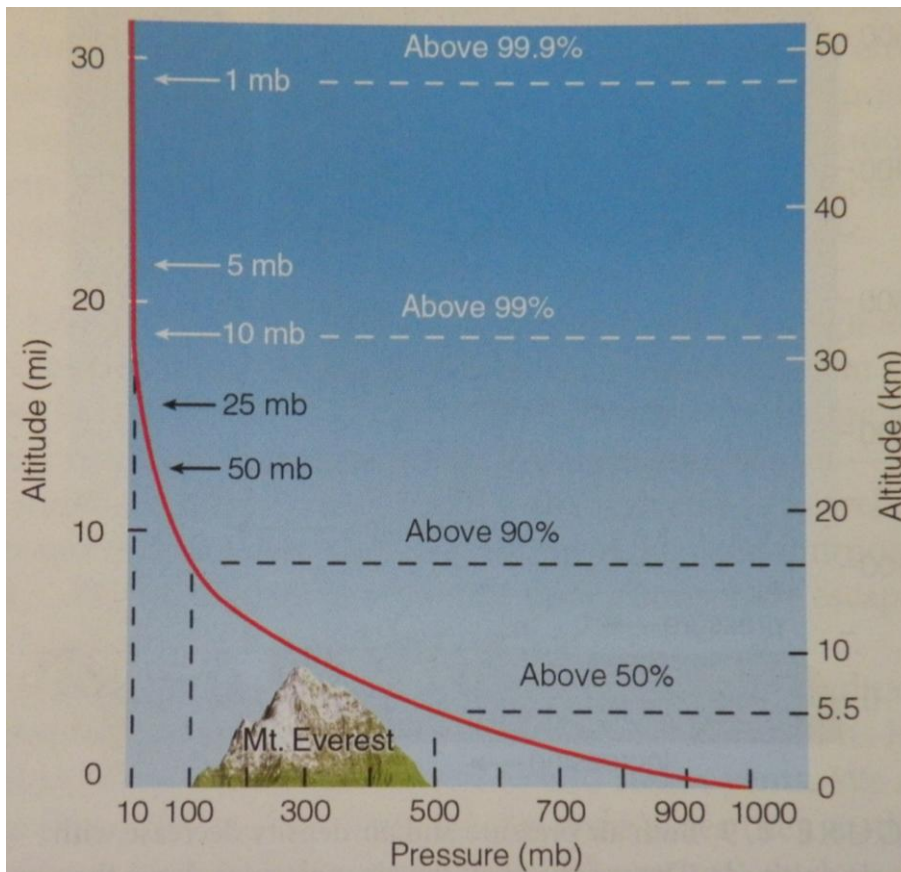


Figure 2-4: Atmospheric pressure gradient graph (Ahrens, 2009).

2.2.4.1 Katabatic and Anabatic winds

These are important type of local winds which occur in many places around the world but more often become extraordinarily strong in high latitudes in mountain areas. Katabatic winds are formed as a result of gravitational force which pulls high density air from a higher elevation down to the slope as shown in Figure 2-5. This occurs at night when cool air sinks down from mountain slopes. Such winds are sometimes also called drainage or fall winds (WMO, 1981).

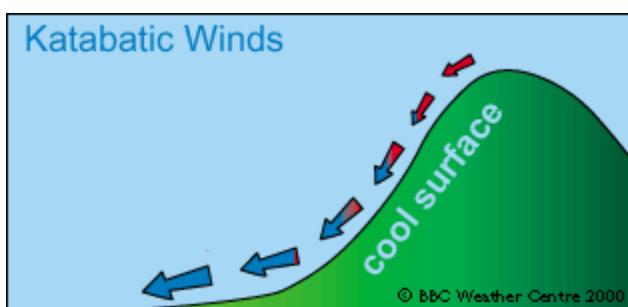


Figure 2-5: Formation and flow of Katabatic wind (BBC Weather, 2006).

Anabatic winds are formed when warmed air rises and gently flows up mountain slopes and valleys as shown in Figure 2-6. These winds usually occur during the daytime in calm sunny weather when warm wind on the mountain slope moves upward (Barry & Chorley, 2010).

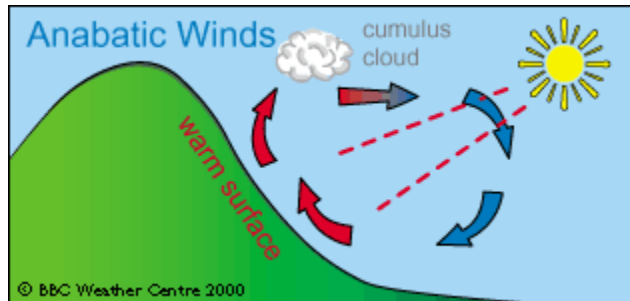


Figure 2-6: Formation and flow of Anabatic wind (BBC Weather, 2006).

2.2.4.2 Wind due to topographic barriers

Mountain ranges have important effects on the air flow across them. Wind is either forced to flow around a mountain or to move over it, and normally both routes are taken as shown in Figure 2-7. On the wind ward side of a mountain cloudiness and precipitation are amplified because of the strained ascent and the condensation of the water vapour in the air. On the lee ward side of the mountain range it is a strong, gusty, dry and warm wind, when stable air is forced to flow across the barrier by a regional pressure gradient, called foehn or Chinook (Barry & Chorley, 2010). Mountains also have another important effect on the local wind, namely, the air shrinks in the vertical when forced upwards, so that the air parcel becomes compressed as shown in Figure 2-7. The air tends to move as around an anticyclone and over the mountain a high-pressure ridge is formed. On the downstream the air starts sinking again; it is stretched in the vertical and the air parcel becomes slimmer. Instead of inward, air moves outward in a more cyclonic fashion and an extension of a low-pressure system is formed in the lee of the mountain range (WMO, 1981).

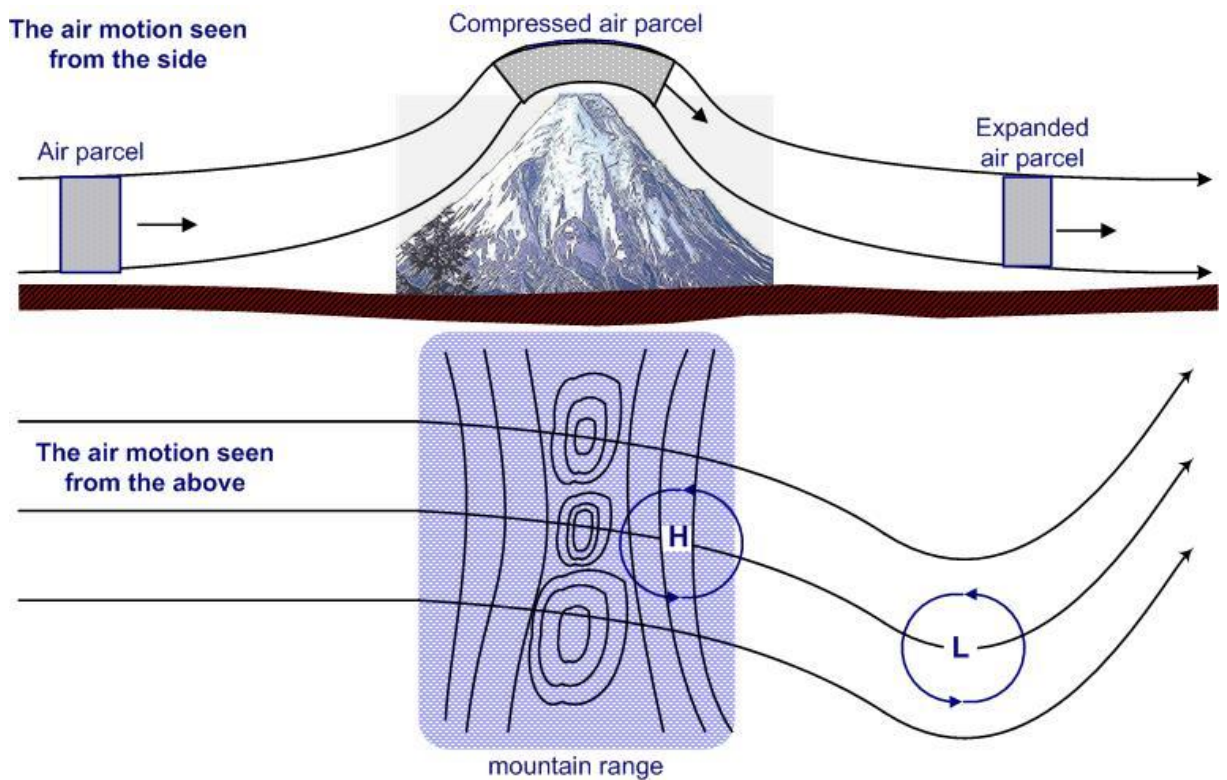


Figure 2-7: The flow of air over the mountain range based on WMO, 1981.

2.2.4.3 Land and sea breezes

Coastal areas are frequently affected by regular wind variations known as sea breeze during the day and land breeze during the night. Sea and land breezes are caused by the temperature contrast between the sea and the land and it forms a close circulation. In day time solar heating over the land gives high surface temperature while the sea-surface temperature is fairly low. This lifts up the land air and sea breeze blows towards the land to cover the gap as shown in Figure 2-8. At night the process is reversed (WMO, 1981). The vertical expansion of the air column creates pressure differences typically in the order of 2 mb which leads the breeze (Barry & Chorley, 2010).

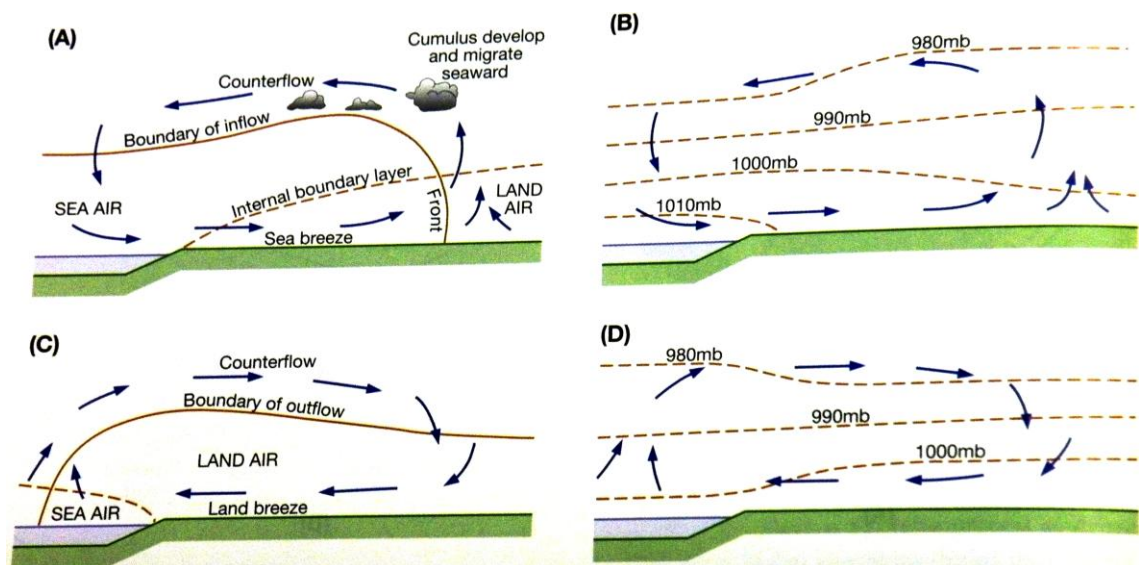


Figure 2-8: Diurnal land and sea breeze. A and B: sea breeze circulation and pressure distribution. C and D: land breeze circulation and pressure distribution (Barry & Chorley, 2010).

2.2.5 Boundary layer

The atmospheric boundary layer (ABL) is the transition region between the surface and the free atmosphere, where the motion is unaffected by surface friction or turbulence induced at lower levels. The height of the boundary layer is usually 1000m, but it varies significantly between day and night and between seasons (i.e. winter, summer) (Ahrens, 1994). ABL also varies with wind speed. All ground based WECs (wind energy converters) are installed in this region. Therefore, properties of the boundary layer are very important to assess wind energy (WMO, 1981).

Main effects governing the properties of the boundary layer are the strength of the geotropic wind, the surface roughness, Coriolis effects due to the earth's rotation, and thermal effects (Burton *et al.*, 2001).

To study the urban or a complex terrain wind condition, study of boundary layer is very important. In research (Contini, *et al.* 2008), meteorologists measure the height of the boundary layer by using SODAR and ultrasonic anemometers. Figure 2-9 shows that the boundary layer height (BLH) varies with hours of a

day. And boundary layer height is higher in hot than in the cold weather. Figure 2-10 shows that the probability of BLH in between 200m to 400m is higher in cold weather than in the hot weather. From these results one can assume that regions having cold weather have lower boundary layer than hot regions. But roughness of the area also effects significantly on the height of the boundary.

In the atmospheric boundary layer, horizontal wind speed increases with height; it can be zero at ground level. This variation in wind speed with elevation is known as vertical wind shear (Manwell, McGowan & Rogers, 2009).

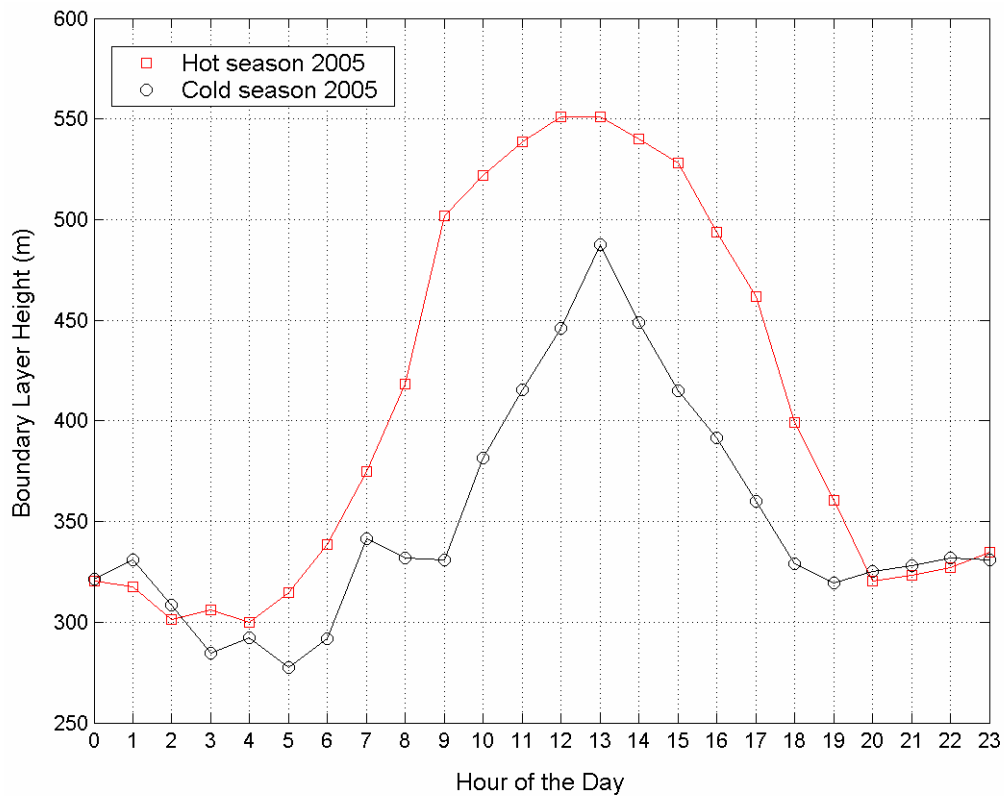


Figure 2-9: Typical daily pattern of BLH for hot and cold season during 2005 (Contini, *et al.* 2008).

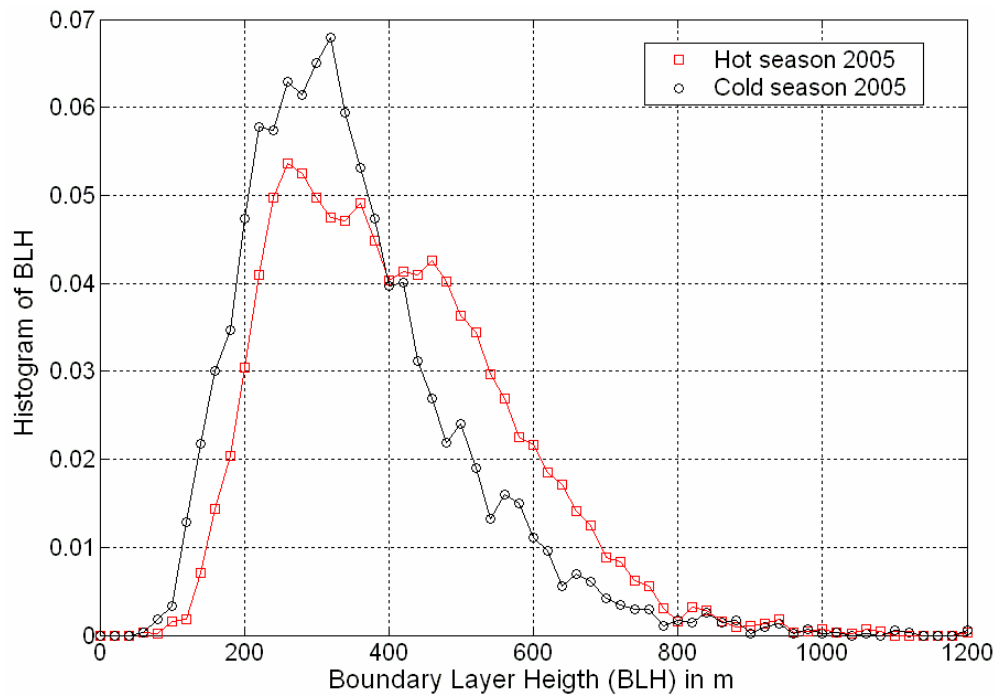


Figure 2-10: Relative distribution of BLH for hot and cold season during 2005 (Contini, et al. 2008).

Due to the boundary layer effect, wind speed increases with height in a logarithmic pattern. If wind data is available at a height Z and the roughness height is Z_0 , then the velocity at a height Z_R is given by the following equation:

$$V(Z_R) = V(Z) \frac{\ln\left(\frac{Z_R}{Z_0}\right)}{\ln\left(\frac{Z}{Z_0}\right)} \quad \text{Equation 2-1}$$

Where, $V(Z_R)$ and $V(Z)$ are the velocities at heights Z_R and Z , respectively (Mathew, 2006).

2.3 Urban wind

Urban wind is a part of local wind but it also has additional parameters which significantly affects the wind speed and direction as shown in Figure 2-11. Due to the resistance offered to wind by buildings, flow through the city exits downstream is lower than the flow entering the city upstream. It is known that, in some cases, street networks have a specific flow capacity i.e. the flow rate

along a street canyon will attain a constant value or flow capacity (Buccolieri, Sandberg & Sabatino, 2010).

Due to the nature of urban structure, studying prevailing wind condition by statistical analysis is difficult. Therefore, it also requires CFD analysis of the area for better results.

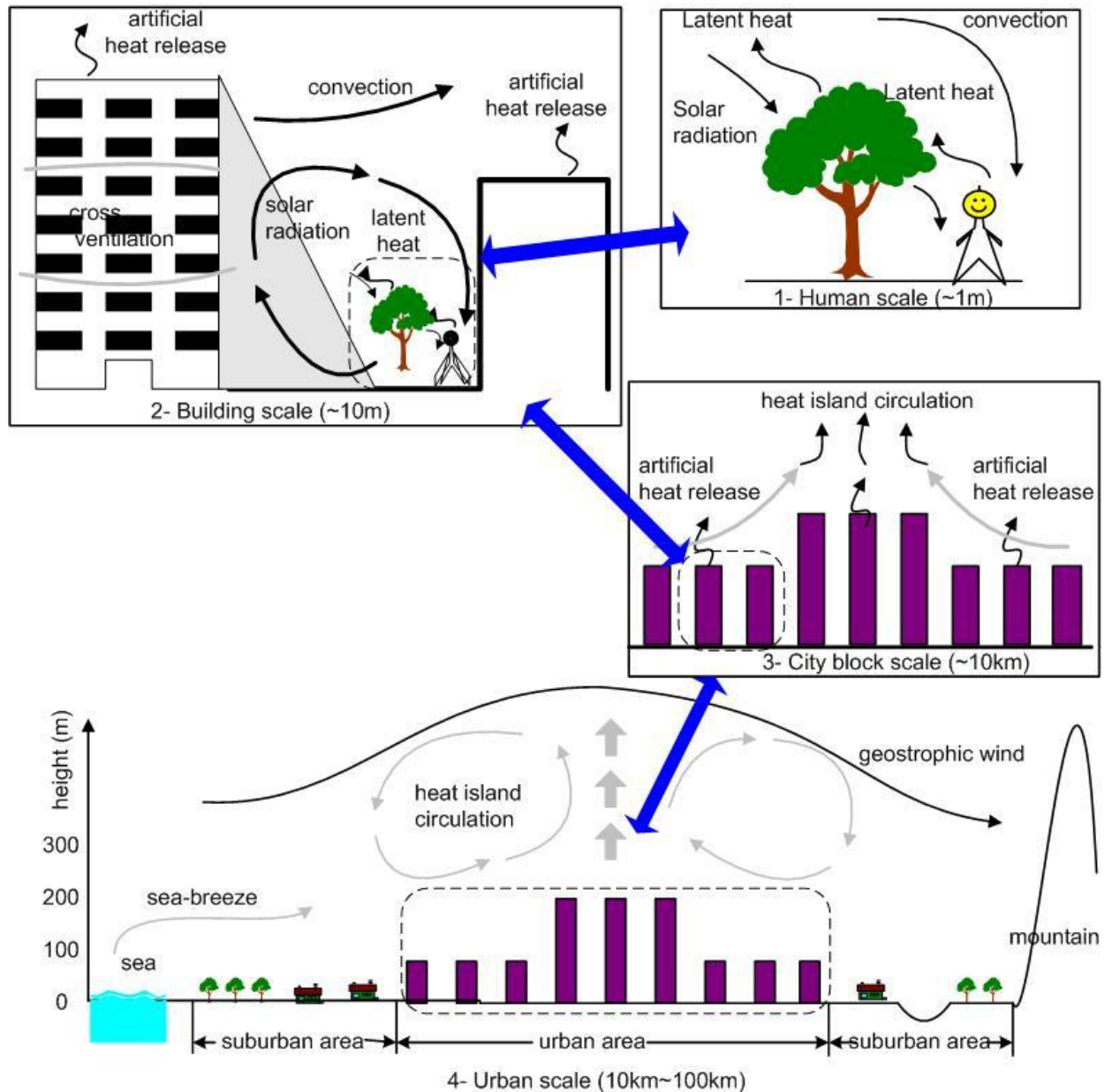


Figure 2-11: Various scales related to urban wind climate based on Murakami, 1999.

2.4 Characteristics of Wind

2.4.1 Scale of motion

Wind in the atmosphere varies in both time (seconds to months) and space (centimetres to thousands of kilometres). Figure 2-12 summarizes the time and space variations of atmospheric motion as applied to wind energy. Space variations are generally dependent on height above the ground and local geographical conditions. Variations of wind speed in time can be divided into the following groups:

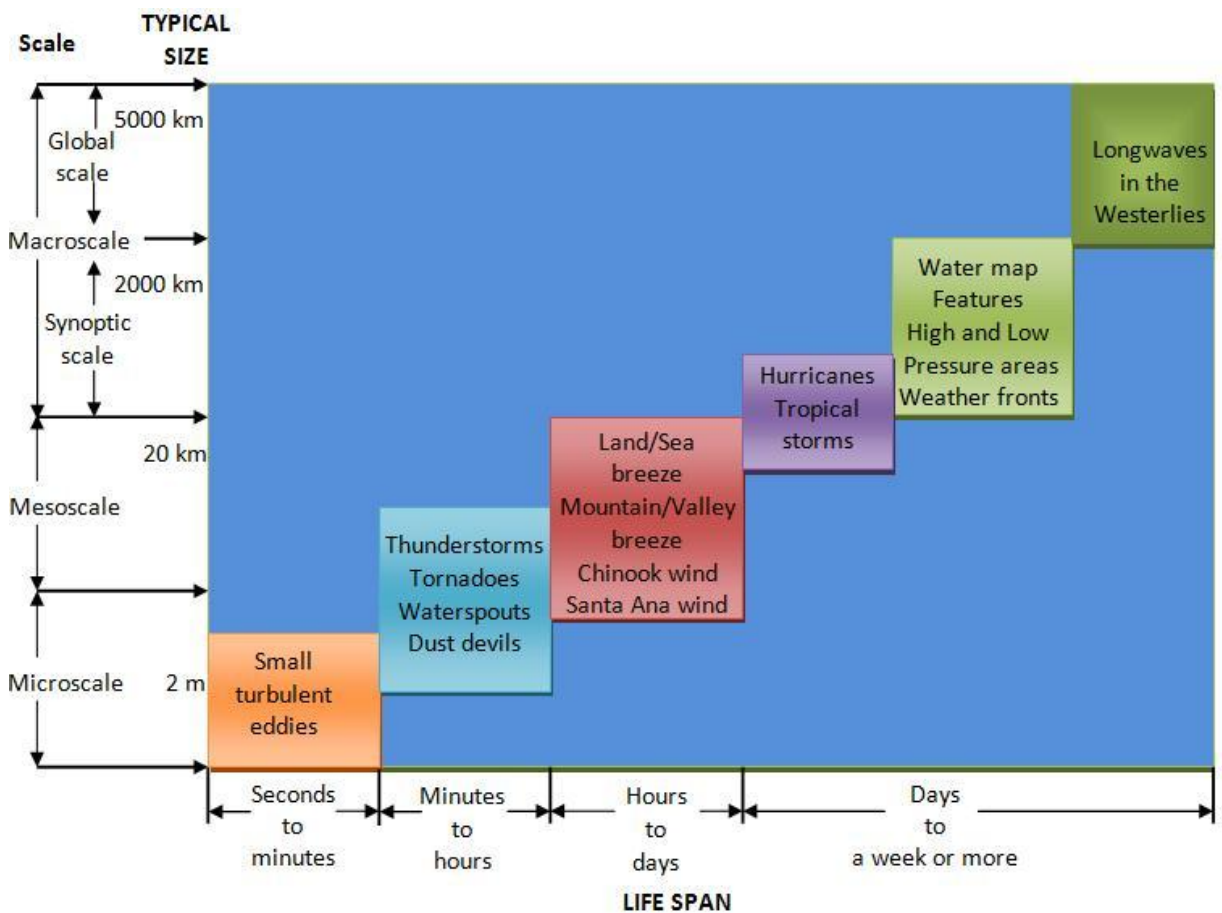


Figure 2-12: The scales of atmospheric motion with the phenomenon's average size and life span based on Ahrens, 2009.

2.4.1.1 Inter-annual variation

Inter-annual variations in wind speed take place over greater time scale i.e. more than one year. They can have a large effect on long-term wind energy

estimation. Estimating inter-annual variability is important as it helps in estimating long-term mean wind at a site. Meteorologists generally conclude that it takes at least five years to arrive at a reliable average annual wind speed at a given location. On the other hand shorter data records can be useful (Manwell, McGowan & Rogers, 2009).

2.4.1.2 Annual variation

Variations in seasonal or monthly averaged wind speeds are significant and common over most of the world. A seasonal change of monthly wind speed variation is not defined by a single year of data but wind speed variations during the year can be well characterized in terms of a probability distribution. One year of record data is generally sufficient to predict long-term seasonal mean wind speeds within an accuracy of 10% with a confidence level of 90% (Manwell, McGowan & Rogers, 2009).

2.4.1.3 Diurnal variation

Large wind variations also occur on a diurnal or daily time scale. This type of wind speed variation is due to differential heating of the earth's surface during the daily radiation cycle. A typical diurnal variation is an increase in wind speed during the day with the wind speeds lowest during the hours from midnight to sunrise. Daily variations in solar radiation are responsible for diurnal wind variations in temperate latitudes over relatively flat land areas. The largest diurnal changes generally occur in spring and summer, and the smallest in winter. The diurnal variations in wind speed vary with location and altitude above sea level. For example, at higher altitudes surrounding terrain, e.g., mountains or ridges, the diurnal pattern is very different from the lower altitude or relatively flat areas. There may be significant year-to-year differences in diurnal behaviour, even at fairly windy locations. Although coarse features of the diurnal cycle can be established with a single year of data but more detailed features such as the amplitude of the diurnal oscillation and the time of day that the maximum winds occur cannot be determined precisely (Manwell, McGowan & Rogers, 2009).

2.4.1.4 Short-term variation

Short-term wind speed variations normally include turbulence and gusts. These types of variations usually mean variations over time intervals of 10 minutes or less. Ten-minute averages are typically determined using a sampling rate of about 1 second. In general, variations in wind speed with periods from less than

a second to 10 minutes and having arbitrary character are considered to represent turbulence (Manwell, McGowan & Rogers, 2009).

2.4.2 Wind Turbulence and gust

Wind flowing smoothly on horizontal plane is called laminar flow. But as a result of the ground forces the wind could be zero directly at the surface and it creates a zone of strong vertical variation of wind speed close to the ground. This variation of wind speed or shear is a source of turbulence. Wind shear is the change in wind speed or direction over some distance. There can even be a vertical wind shear as shown in Figure 2-13, caused by the interaction between upward moving warm air and downward moving cold air (Nelson, 2009).

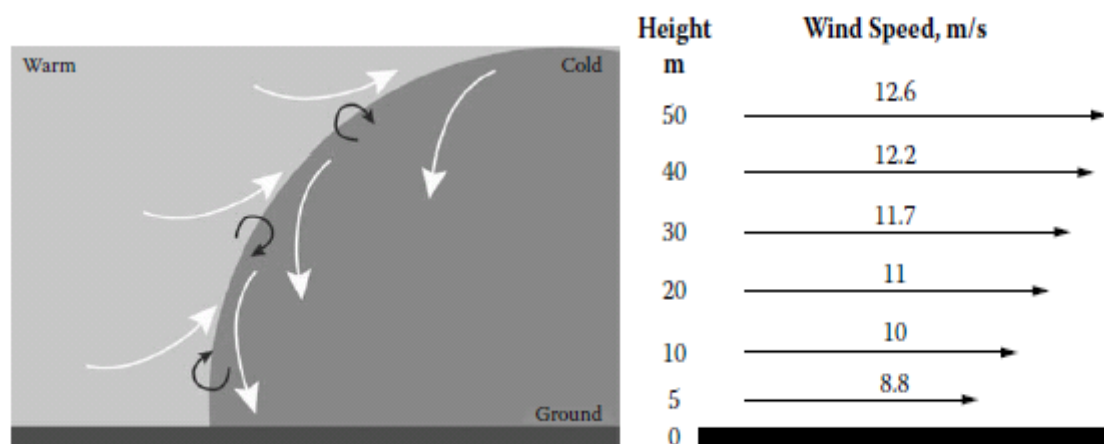


Figure 2-13: Example of vertical wind shear and change in wind speed with height (calculations are for given wind speed of 10 m/s at 10 m height, wind shear exponent is around 1/7 (Nelson, 2009).

Friction of wind flow, called wind viscosity, is also a cause of turbulence. The speed and direction of wind change rapidly as it passes through rough surfaces and obstacles like buildings, trees and rocks (Mathew, 2006). Turbulence can be considered as random wind speed fluctuations imposed on the mean wind speed. These fluctuations occur in all three directions: longitudinal (in the direction of the wind), lateral (perpendicular to the average wind), and vertical (Manwell, McGowan & Rogers, 2009). Surface heating and instability are also a source of turbulence which extends to greater altitudes. As the earth's surface heats up, thermals rise and convection cells form. The resulting vertical motion

creates thermal turbulence, which increase with the instability of surface heating and the degree of atmospheric instability (Ahrens, 2009).

A gust is a discrete event within a turbulent wind field. Wind flowing through an obstacle in a stable and light air produces small eddies and little vertical mixing. In contrast, greater winds in unstable air create deep vertical mixing and eddies that produce strong, gusty surface wind (Ahrens, 2009).

Forecasting the turbulence intensity and spectrum at a given point within an area of a complex terrain is not straightforward. Hilly terrain upwind of the site in question will lead to generally higher turbulence levels, and some researchers have suggested that this can be calculated from a regional roughness length which takes the topography into account as well as the surface roughness (Tieleman, 1992). On the other hand, distortion of the flow by the local terrain may reduce the turbulence intensity. At heights above ground which are of importance for wind turbines, rapid distortion theory applies which means that the variance of the turbulent fluctuations will not change much as the flow passes over terrain features such as hills. Therefore, if there is acceleration of the flow in the wind when it passes over a hill, the turbulence intensity will decrease, while the length scale will increase, resulting in a shift of turbulence spectrum towards lower frequencies, without any change of shape (Schlez, 2000). This effect is therefore easily estimated once a model such as WASP has been used to calculate the speed-up factor at a particular point. However, the effect is also accompanied by a shift of turbulent energy from the longitudinal to the lateral and vertical components of turbulence, causing the turbulence on hilltops to be more isotropic (Petersen *et al.*, 1998) (Burton *et al.* 2001).

2.5 Computational Fluid Dynamics (CFD)

2.5.1 Introduction

Computational Fluid Dynamics (CFD) is a numerical technique in which equations describing the fluid flow are solved by computer software. It can be used to solve numerous problems involving fluid flow and heat transfer whether it is on an atomic particle scale or a planetary scale. CFD technique has

become a powerful tool in various branches of industry and the sciences: from the aerodynamics of aircraft and vehicles and combustion in gas turbines, to cooling of electronic micro-circuits and blood flows through arteries and veins. It can be used to analyse a variety of thermal, chemical and physical phenomena (Versteeg & Malalasekera, 1995). In wind engineering CFD is increasingly being used to assess the wind flow over buildings, mountains, urban areas and street canopy etc. It is also used to assess the atmospheric boundary layer (ABL) flow and turbulence effect. CFD application in wind engineering, also known as Computational Wind Engineering (CWE), has significantly increased in the last two decades from micro level to macro level (Franke *et al.*, 2004).

To the best of available knowledge, Raithby *et al.*, (1987) were present at one of the early studies using CFD to simulate the flow over hills. In their work they concluded that their model predicts the mean flow variables with good accuracy but there are disagreements in the quantities related to the turbulence.

CFD analysis in wind engineering plays an important role to predict wind climate from human scale to urban scale but because of the complexity of the urban environment where many physical processes affect the wind climate, the results are not perfect and need some more work in the field to improve it (Murakami, *et al.* 1999).

Endalew, *et al.* (2009) presents CFD modelling of airflow within plant canopies using 3D canopy architecture to understand the effect of the canopy and compare it with wind tunnel experimental results. They found the average longitudinal velocity measurements in good agreement with the simulation results with minimum accuracies of 92%. Its main disadvantage however, when compared with full-scale and wind tunnel modelling of rooftop wind flows, is that any flow problems that are solved are based on theoretical models rather than actual flow data. Nevertheless, as this branch of fluid dynamics develops and computer processing power increases, CFD is becoming more accurate and its capabilities and limits getting better understood.

2.5.2 CFD Simulation Models

CFD models are based on the fluid dynamic equations for mass, momentum and energy conservation (Versteeg & Malalasekera, 1995). Different CFD models are used depending on the physics included in the flow problem. There are established practices for a specific class of problem, the level of accuracy required, the available computational resource, the amount of time available for the simulation and especially the turbulence involved in the simulation. The different models currently available are as follows:

2.5.2.1 Direct Numerical Simulations (DNS)

These models integrate the equations numerically without any tuning or modelling assumption (Martilli, Santiago & Martin, (2007). In order to solve turbulent flow finitely with high Reynolds numbers, the size (mesh size) must be no larger than the smallest scales in turbulent flow; this scale is called the Kolmogorov length. However, even with modern computing power the cost and time required to do this is prohibitively expensive. Therefore, DNS is currently restricted to flows with low Reynolds numbers and relatively simple aerodynamic geometry i.e. it cannot be used in multiple bluff bodies where flow separation is likely.

2.5.2.2 Large Eddy Simulation (LES)

This is based on the spatial filtering of the fluid dynamic equations i.e. averaged in space. The large eddies are determined, while the small eddies are filtered out and their effects parameterized. In LES models, the spatially filtered, time-dependent equations are solved for a period of time large enough to allow the computation of a statistic. LES models are computationally less expensive than DNS models and they are increasingly used to simulate flows over complex geometries (Xie & Castro, 2006). However, this method is too computationally expensive to be used extensively in micrometeorological studies over urban areas (Martilli, Santiago & Martin, 2007).

2.5.2.3 Reynolds Averaged Navier-Stokes (RANS)

Simulating the flow fluctuations directly is computationally expensive. The instantaneous governing equations can, therefore, be time-averaged to remove the small scales, resulting in a set of modified equations that are computationally less expensive to solve. But these modified equations contain other unknown variables and turbulence models are needed to determine these variables in terms of known quantities. RANS models are currently widely used for micrometeorological flows. Although LES and DNS results would predict the wind flow with higher accuracy since fewer features are parameterized, they need a much higher computational capability (Murakami, 1998).

2.5.2.4 Detached Eddy Simulations (DES)

Detached Eddy Simulation (DES) is a modification of RANS model in which the model shifts into a sub grid scale i.e. it formulates in regions fine enough for LES calculations. Regions near solid boundaries and where the turbulent length scale is less than the maximum, grid dimensions are assigned the RANS mode of solution. As the turbulent length scale exceeds the grid dimension, the regions are solved using the LES mode. Thus, the grid resolution for DES is not as demanding as pure LES thereby reducing the computational cost considerably. Although DES was initially formulated for the Spalart-Allmaras model in 1997, it can be implemented with other RANS models by appropriately modifying the length scale which is explicitly or implicitly involved in the RANS model. DES is a non-zonal approach and provides a single smooth velocity field across the RANS and the LES regions of the solutions (Bunge, Mockett & Thiele, 2007).

2.5.3 Working methodology of CFD

The process of a CFD simulation consists of a number of steps that can be split into three stages outlined below.

2.5.3.1 Pre-processing stage

This stage involves the setting up of the flow problem into a model that can be processed by a CFD solver package. The user's activities at this stage are:

- Definition of the physical bounds of the problem by creating the 2-D or 3-D geometry and the construction of a computational domain / control volume.
- Generation of a suitable grid, if necessary, by sub-division of computational domain into smaller, non-overlapping sub-domains.
- Definition of appropriate boundary conditions for the computational domain.

Most of this pre-processing can be achieved using a software package known as a pre-processor and some CFD software, like PHOENICS, provide this within the CFD package. Other examples include Gambit, Poly flow and CFX-Pre. These packages are used to generate a 2-D or 3-D model of the computational domain (either directly or by importing a model from an alternative CAD package). Once the domain has been defined, it is divided into discrete cells. The solution to the flow problem is defined at the nodes of each cell. Consequently the accuracy of the CFD solution is governed by the size of the cells in the mesh. It is generally observed that the smaller the size of the cells, the more accurate the solution is. Unfortunately, the more cells there are, the more processing time and power is needed to find a solution. Consequently, grid construction is crucial when performing CFD analysis. A good grid will drastically increase the speed at which a solution is processed, saving precious processing time and effort. Most pre-processing software packages include a function for analysing and assessing the quality of the mesh. Once these user activities are complete, a mesh file can be exported for use in the next stage (Versteeg & Malalasekera, 1995).

2.5.3.2 Processing stage

The completed mesh is imported into a solver software package and once various parameters and options have been set, the solver will apply the fluid

flow equations to the domain. There are several numerical methods that can be applied; these include the finite difference method, the finite element method, the finite volume method and spectral methods. The finite volume technique is currently the method of choice in the CFD industry. Examples of solver software packages include FLUENT, CFX, PHOENICS, RAMPANT, NEKTON, POLYFLOW and FIDAP (Versteeg & Malalasekera, 1995).

2.5.3.3 Post processing stage

This stage involves the analysis and visualisation of the result. Recent advances in the CFD software and its subsequent take-up by industry and research institutions has meant a lot of development work has been conducted at the post processing stage in order to equip the engineer with a range of analysis and visualisation tools. These include:

- Domain geometry and grid display
- Vector plots
- Line and filled contour plots
- 2D and 3D surface plots
- Particle tracking
- View manipulation (translation, rotation, scaling, etc.)
- Animation for dynamic result display
- Data export facilities for further manipulation

2.5.4 Limitations and errors of CFD

Although the potential for CFD is certainly enormous, it is acknowledged that it also has limitations. CFD solutions are based on the physical model of real world processes, e.g., turbulence, compressibility, chemistry, multiphase flow, etc. Therefore, CFD solutions can only be as accurate as the physical models on which they are based. The second main thing which limits the effectiveness of CFD is numerical errors. Solving equations on a computer always introduces numerical errors. Because of the finite word size available in the computers there is a round-off error and round-off errors will always exist (though they can

be small in most cases). Approximations in the numerical models also a source of error called truncation error. Mesh refinement is one way to deal with truncation error as truncation errors will go to zero as the grid is refined but it also has its limitation because a fine grid is very expensive in terms of computation. As with physical models, the accuracy of the CFD solution is only as good as the initial or boundary conditions provided to the numerical model (Franke *et al.* 2007).

2.6 Wind as a source of Energy

Energy available in wind is essentially the kinetic energy of moving air over the earth's surface. Wind energy converters (WEC) or wind turbines' blades receive this kinetic energy, which is then transformed to mechanical or electrical forms, depending on end use. The efficiency of converting wind into other useful energy forms greatly depends on the efficiency with which the WEC interacts with the wind stream (Mathew, 2006).

2.6.1 Power available in wind

If m is the mass of the air and V is the velocity of wind then the kinetic energy available in wind stream can be express as below (Mathew 2006):

$$K.E = \frac{1}{2}mV^2 \quad \text{Equation 2-2}$$

If a wind turbine rotor having cross sectional area A is exposed to this wind stream as shown in Figure 2-14.

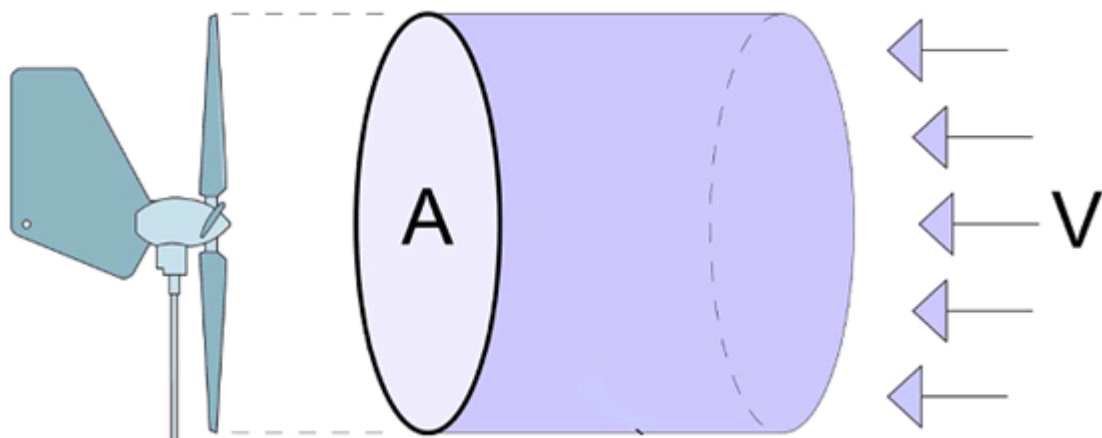


Figure 2-14: An air parcel moving towards a wind turbine.

If ℓ_a is the density of air and v is the volume of air then mass of air can be:

$$m = \ell_a v \quad \text{Equation 2-3}$$

The kinetic energy of the air stream available for the turbine can be expressed as in equation 2-4.

$$K.E = \frac{1}{2} \ell_a v V^2 \quad \text{Equation 2-4}$$

Here v is the volume of air parcel available to the rotor. The air parcel interacting with the rotor per unit time has a cross-sectional area, equal to the swept area of the rotor (A_T) and thickness equal to the wind velocity (V) (Mathew, 2006).

$$v = A_T V \quad \text{Equation 2-5}$$

Hence, the power available in the wind stream can be expressed as:

$$P = \frac{1}{2} \ell_a A_T V^3 \quad \text{Equation 2-6}$$

Equation 2-6 shows that the factors influencing the power available in the wind stream are the air density, area of the wind turbine rotor and the wind velocity. Effect of the wind velocity is more prominent due to its cubic relationship with power.

2.6.2 Assessment of wind energy potential

Assessment of wind energy potential is the first step for all types of wind energy projects, either big or small. Precise information of the wind characteristics at the potential sites is essential for the successful planning and implementation of wind energy projects. The vital information required for such an analysis is the speed and direction of the wind. Ecological factors may also be considered in identifying process of a candidate site for a wind power project. Wind data from the nearby meteorological stations can give a better understanding on the wind spectra available at the site. However, for an accurate analysis, the wind

velocity and direction at the particular site has to be measured with the help of precise and reliable instruments (Mathew, 2006).

Available energy in the wind is directly proportional to the cube of the wind speed as shown in equation 2-6. Therefore, wind resource assessment is primarily based on the wind speed in the region. Wind resources of a region also significantly depend on the local topographical and terrain variations (Manwell, McGowan & Rogers, 2009).

A wind resource assessment program requires planning and coordination. It demands a clear set of objectives so that the best assessment approach is selected. Wind resource assessment's success crucially depends on the quality of the assessment's assembled assets; sound siting and measurement techniques, quality equipment, and methodical data analysis techniques. However, it is sometimes constrained by budget and schedule limitations.

2.6.2.1 Approaches and objectives

Several approaches are available when investigating the wind resource within a given land area. These approaches can be categorized as three basic scales or stages of wind resource assessment: preliminary area identification, area wind resource evaluation and micro siting.

a) Preliminary Area Identification

In the first stage of wind resource assessment, a relatively large region (e.g., state or utility service territory) is screened up for suitable wind resource areas based on information such as airport wind data, topography, flagged trees, and other indicators. At this stage new wind measurement sites can be selected.

b) Area Wind Resource Evaluation

The second stage applies to wind measurement programs to characterise the wind resource in a defined area or set of areas where

wind power development is being considered. The most common objectives of this scale of wind measurement are to:

- Determine or verify whether sufficient wind resources exist within the area to justify further site-specific investigations.
- Compare areas to distinguish relative development potential.
- Obtain representative data for estimating the performance and the economic viability of selected wind turbines.
- Screen for potential wind turbine installation sites.

c) Micro-siting

And finally the smallest scale of wind resource assessment is micro-siting. Its main objective is to quantify the small-scale variability of the wind resource over the terrain of interest. Ultimately, micro-siting is used to position one or more wind turbines on a parcel of land to maximize the overall energy output of the wind plant (AWS Scientific, 1997).

2.6.2.2 Software packages

There are several software packages available to model or estimate the wind regime e.g. windFarm, WAsP, WERA, ALWIN, CALLaLOG 98 etc. Wind flow modelling software predicts wind characteristics at locations where measurements are not available. Some other CFD models are Meteodyn WT, WindSim and WindieTM. However, this comes at the price of being more computationally expensive (Onat & Ersoz, 2010).

WAsP is the most popular software package; it was created at Denmark's Risø National Laboratory and is available commercially. This can model wind regimes to aid the design of a wind farm. WAsP uses a potential flow model to predict how wind flows over the terrain at a site. This software program works on the statistics of wind climate by vertical and horizontal extrapolation. And it takes account of terrain roughness and the sheltering effects from obstacles. This software helps to calculate wind resources for a potential wind farm and

develop a detailed wind atlas for wind farm planning (Wind Atlas Analysis and Application Program, 2009).

2.7 Wind measurements and instrumentation

Precise information about wind characteristics at the potential area is critical for the successful planning and implementation of a wind energy project. It requires instruments to measure different meteorological parameters in the area. The vital information needed for such an analysis is the speed and direction of the prevailing wind at different time scales. For each wind energy application, the type and amount of instrumentation required varies widely. Wind energy applications typically use the following types of meteorological instruments (Manwell, McGowan & Rogers, 2009):

- I. Anemometers to measure wind velocity.
- II. Wind vanes to measure wind direction.
- III. Thermometers to measure the ambient air temperature
- IV. Barometers to measure the air pressure

2.7.1 Wind Speed measurements

Wind speed data are the most important indicator of a wind energy resource. Measurement of wind speed at multiple heights are encouraged for determining wind shear characteristics, conducting turbine performance simulations at several turbine hub heights, and for data backup (AWS Scientific, 1997). Wind measuring instrumentation sensors can be classified according to their principle of operation via the following (Manwell, McGowan & Rogers, 2009):

- Momentum transfer - cups, propellers, and pressure plates.
- Pressure on stationary sensors - Pitot tubes and drag spheres.
- Heat transfer - hot wires and hot films.
- Doppler effects - sonic and laser.
- Special methods - ion displacement, vortex shedding, etc.

2.7.2 Wind Direction measurements

Wind direction frequency information is important for identifying preferred terrain shapes and orientations and for optimizing the layout of wind turbines within a wind region. Wind direction is normally measured via the use of a wind vane but in newer instruments ultra-sonic sensors are also used to measure the wind direction (AWS Scientific, 1997).

2.7.3 Temperature measurements

Air temperature is an important descriptor of a wind farm's operating environment and is normally measured either near ground level (2 to 3 m), or near hub height. In most locations the average near ground level air temperature will be within 1°C of the average at hub height. It is used to calculate air density, a variable required to estimate the wind power density and wind turbines power output (AWS Scientific, 1997).

2.7.4 Barometric Pressure measurements

Barometric pressure is used with air temperature to determine air density. It is difficult to be measured accurately in windy environments because of the dynamic pressures induced when wind flows across an instrument enclosure. An indoor or office environment is a preferred setting for a pressure sensor (AWS Scientific, 1997).

2.8 Wind Energy Convertor (WEC)

Wind energy convertors are classified according to the interaction of the blades with the wind (aerodynamics), orientation of the rotor axis with respect to the ground, size of the power output and end user applications.

The aerodynamic interaction of the blades with the wind is by drag or lift, or a combination of the two.

2.8.1 Drag type WEC

In a drag type WEC, the wind pushes against the blade or sail as shown in Figure 2-15 and drag devices are inherently limited in efficiency since the speed of the device or blades cannot be greater than the wind speed. For a drag type wind turbine, the wind pushes on the blades and forces the rotor to turn on its axis. Examples of drag devices are cup anemometers, vanes, and paddles, which are shielded from the wind or change parallel to the wind on half the rotor cycle (Nelson, 2009).

Clam shells are another example of a drag type device which open on the downwind side and close on the upwind side. There are no commercial drag wind turbines for producing electricity, since they are inefficient and require a lot of material for blades.

2.8.2 Lift type WEC

Lift type WEC devices mostly use airfoils for blades as shown in Figure 2-15 similar to propellers or airplane wings; however, other concepts have also been used. Using lift, the blades can move faster than the wind and are more efficient in terms of aerodynamics and the amount of material needed for the blades. The tip speed ratio is the speed of the tip of the blade divided by the wind speed. At the point of maximum efficiency for a rotor, the tip speed ratio is around 7 for a lift turbine and 0.3 for a drag turbine. For a lift WEC the ratio of amount of power per material area is around 75, which explains why wind turbines using lift are used to produce electricity. The most favourable tip speed ratio also depends on the solidity of the rotor; solidity is the ratio of the blade area to the rotor swept area. Therefore, one blade rotating very fast can in fact extract as much energy from the wind as many blades rotating slowly. A wind turbine with one blade would save on material; however, a counter weight is needed for balance. Most modern wind turbines have two or three blades because of other considerations, and almost all large wind turbines in the commercial market have three blades. The MBB Monopteros and the FLAIR designs were single-bladed wind turbines built in Germany, and a one-bladed (5 kW) unit was built by Riva Calzoni, Italy. MBB and Riva Calzoni collaborated on

a 20 kW one-bladed unit, and then Riva Calzoni built a 330 kW unit. There are some modern wind turbines with four to six blades also (Nelson, 2009).

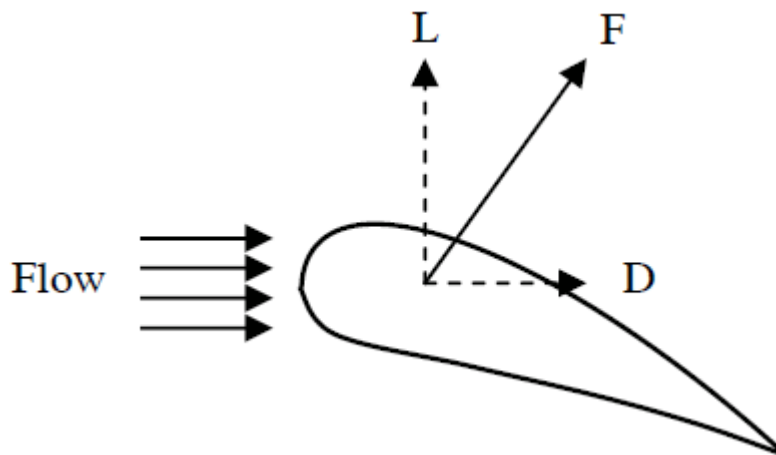


Figure 2-15: Drag and lift forces on airfoil (Mathew, 2006).

Wind turbines are further classified by orientation of the rotor axis with respect to the ground: horizontal-axis wind turbine (HAWT) and vertical-axis wind turbine (VAWT).

2.8.3 Horizontal Axis Wind Turbine (HAWT)

HAWTs always use lift-type blades and can either be upwind or downwind in design. Most of the commercial wind turbines fall under this category. Horizontal axis wind turbines have some distinct advantages such as low cut-in wind speed and easy furling. In general, they show a relatively high power coefficient. However, the generator and gearbox of these turbines are to be placed over the tower which makes its design more complex and expensive (Mathew, 2006). Another disadvantage is the need for the tail or yaw drive, to capture the maximum energy. The rotor on HAWTs needs to be kept perpendicular to the flow of the wind. This rotation of the unit or rotor about the tower axis is called yawing. This is accomplished by a tail on upwind units (as shown in Figure 2-16) of small wind turbines up to 10 kW, although there have been tails on some 50 kW units as well.

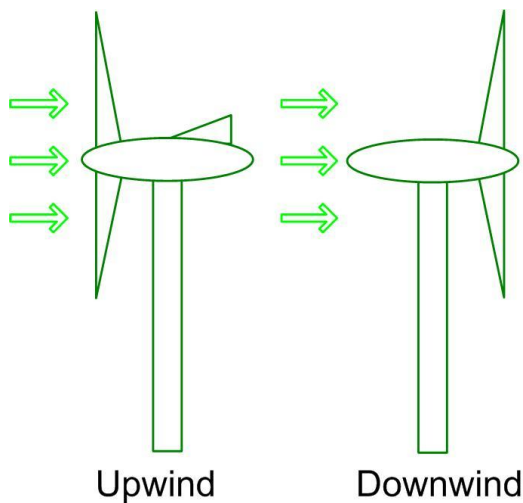


Figure 2-16: Upwind and downwind turbines based on Mathew, 2006.

The downwind version has the advantage that it doesn't require a yawing mechanism or vane (as shown in Figure 2-16); it uses a passive yawing technique called coning (coning is where the blades are at an angle from the plane of rotation). In big turbines a motor (electric or wind {fan tail rotor}) drives the unit around the yaw axis. However, the sound emissions in downwind turbines are often higher due to the approaching airflow being disturbed by the turbine's mast and consequently inducing low-frequency noise as the blades pass through the shadow of the mast. That's why downwind turbines are generally inappropriate for installation in residential areas and have been mainly employed in rural or industrial sites (Nelson, 2009).

The upwind version is the design preferred by UK manufacturers so far, with companies opting for a 3, 5 or 6 blade setup as shown in Figure 2-17. A turbine with a higher number of blades (solidity) will generally have a lower start-up wind speed and a lower tip-speed ratio. A lower tip-speed ratio means a quieter operation.

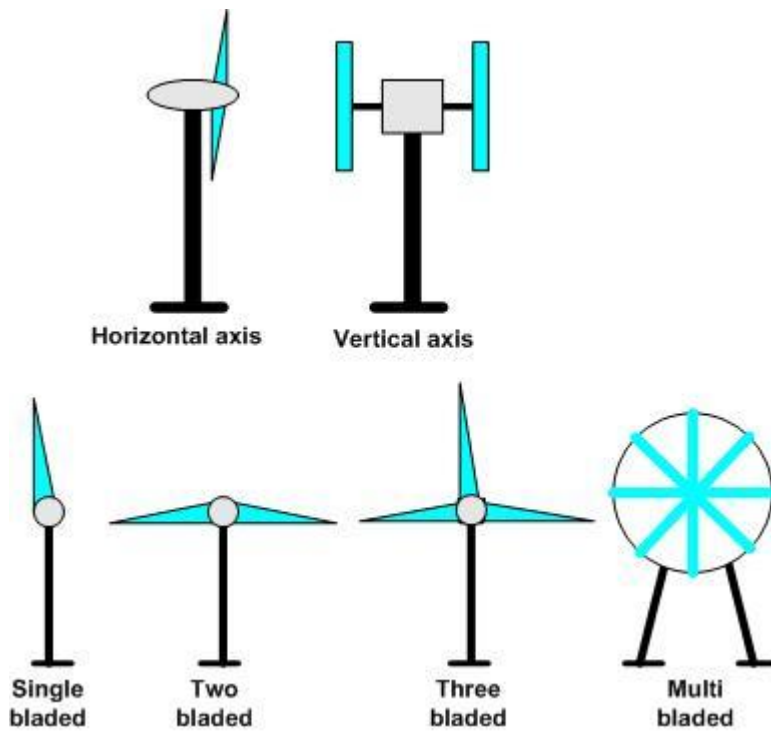


Figure 2-17: Classification of wind turbines based on Mathew, 2006.

2.8.4 Vertical-axis wind turbine (VAWT)

VAWTs use either lift-type or drag-type blades and has the advantage of accepting the wind from all directions as shown in Figure 2-17. The most common drag based design is the Savonius rotor which has an S-shaped cross-section. Drag-type VAWTs have had some limited success in the micro-wind turbine market owing to their quiet operation, low start-up wind speed, and the fact that they are self-starting. Their weak point however is low power output (typically around a tenth that of HAWTs) leading to long payback times.

The lift-based vertical axis design makes use of aerofoil blades that transfer the force of the wind to the rotation of the turbine axis. The 'eggbeater' is the most easily recognised lift-based VAWT, invented by the Frenchman, George Darrieus in the 1930s (Ponta, Seminara & Otero, 2007). However, the Darrieus wind turbine is not reliably self-starting, as the blades have to move faster than the wind to generate power. Therefore the induction motor/generator or another motor is used for start-up to get the blades moving fast enough that they generate positive power. Some designs overcome this problem by incorporating articulated blades, which changes the angle of attack of the aerofoil blades to

continually be optimised for wind direction, so it can be self-starting. Another advantage of VAWTs is that the speed increaser and generator can be at ground level. There are two major disadvantages: the rotor is closer to the ground, and there is cyclic variation of power on every revolution of the rotor (Nelson, 2009).

2.8.5 Wind turbine sizes

The micro, midi and macro wind turbines have been categorized with respect to their nominal output within 0-2 kW, 2-20 kW and greater than 20 kW power bands, as shown in Figure 2-18.

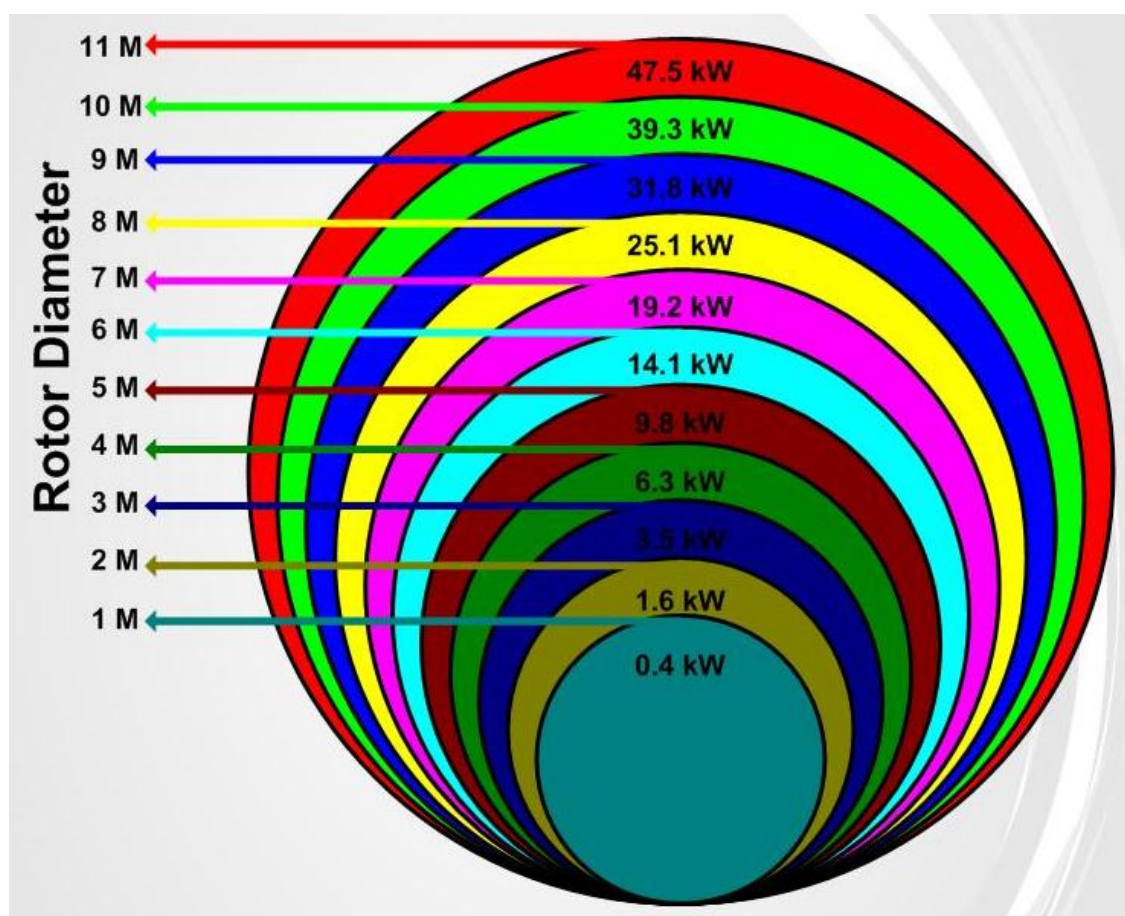


Figure 2-18: Theoretical power production for different wind turbines when the wind speed is 10 m/s, based on Clarke, 2003.

Many different types of wind turbines are available on the market today. Each of them has different performance curves depending on the blades' shape, the axis direction and the wind speed.

2.8.6 Wind turbine end-use Categories

Wind energy markets can be classified on the basis of end-use application of the technology. Wind energy projects are common for off-grid applications. However, the largest market potential for wind energy projects is with on-grid (or grid-connected) applications.

2.8.6.1 Off grid applications

Wind energy is most competitive in remote sites, far from the electric grid and requiring relatively small amounts of power, typically less than 10 kW. In these off-grid applications, wind energy is typically used in the charging of batteries that stores the energy captured by the wind turbines and provides the user with electrical energy on demand. The key competitive area for wind energy in remote off-grid power applications is against electric grid extension and primary (disposable) batteries.

2.8.6.2 On grid applications

In on-grid applications the wind energy system feeds electrical energy directly into the electric utility grid. Two on-grid application types can be distinguished. Isolated-grid electricity generation which is common in remote areas, with wind turbine generation capacity is typically ranging from approximately 10 kW to 200 kW. Central-grid electricity generation have wind turbine generation capacity ranging from approximately 200 kW to 2 MW. Central-grid applications for wind energy projects are becoming more common. In relatively windy areas, larger scale wind turbines are clustered together to create a wind farm with capacities in the multi-megawatt range. The land within the wind farm is usually used for other purposes, such as agriculture or forestry. Central grid application will be the most common scenario for building integrated or standalone applications in the UK.

2.9 Wind energy in UK

UK has been slow on the uptake of wind energy in comparison with the rest of Europe. This is not because UK has a poor wind resource. In reality UK has the best wind resource in Europe both for on and offshore wind energy. In terms of offshore wind, UK has a third of Europe's offshore wind potential which, if utilized, could supply the UK's electricity demand three times over. Up to the end of 2010, there were 283 operational wind farms in the UK, with 3,153 turbines and 5,204 MW of installed capacity as shown in Figure 2-19. A further 2,506 MW worth of schemes are currently under construction, while another 6,208 MW have planning consent and some 9,102 MW are in planning awaiting approval (BWEA, 2011).

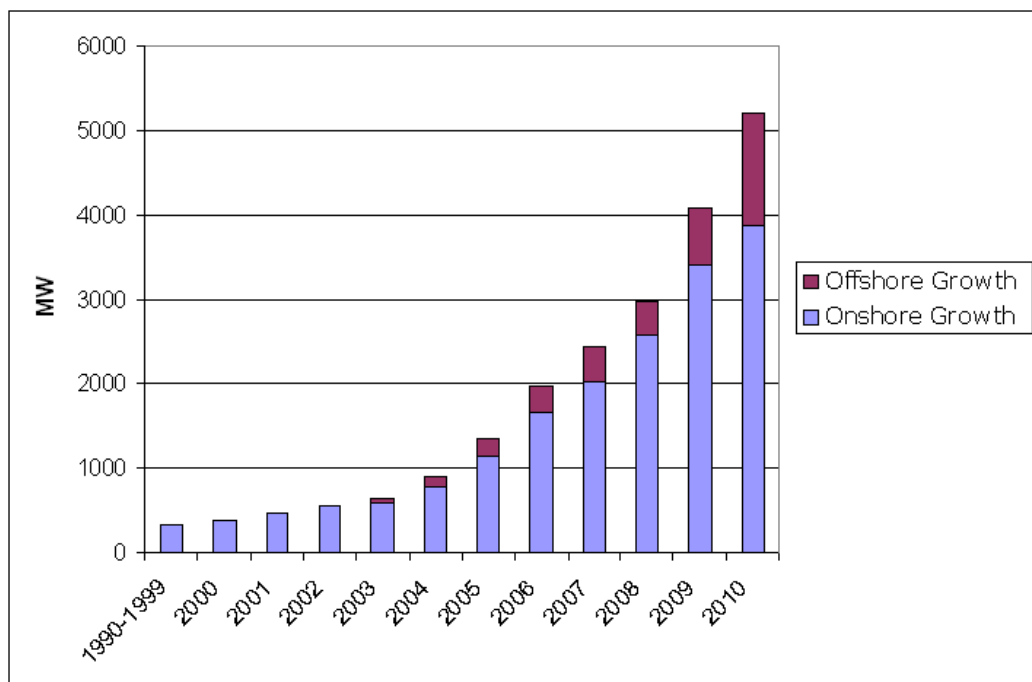


Figure 2-19: Graph of UK wind farm growth based on BWEA data.

There are few key factors which have been slowing the UK's policy down. One is the UK's cumbersome planning legislation and another is painfully slow access to the National Grid. The shortage of turbine supply is another issue which is slowing down the whole process. Typically the given period of time from planning to installation for a wind farm is three years. The UK's planning system is complex, due to the four devolved UK jurisdictions, which has

resulted in the use of four different legislations, making the whole process slow and often inconsistent (BWEA, 2009).

2.10 Warwick wind trial report

The Warwick Wind Trial was an open-access project to provide independent and objective data on the performance of rooftop wind turbines on real sites in the UK, inclusive of Edinburgh Napier University installation. This project was established in 2006 with the partnership of Action21, Warwick District Council and Warwickshire County Council and it is managed by Encraft (Warwick Wind Trials, 2009). The results have provided more evidence that the current method of predicting wind speeds in the UK is inaccurate for micro-wind. In this project micro-wind turbines are cited by using the NOABL wind speed database. However, NOABL is solely a synthetic database which doesn't take account of land topography and the effects of obstructions such as buildings and trees on the mean wind velocities. The project covering 168950 hours of operation of 26 turbines was involved in the trials from Aberdeen to Cornwall. The average capacity factor (the percentage of time that a turbine achieves its rated power) is found to be 0.85% for the building mounted turbines. If only counting the number of times when turbines were switched on and ignoring imported energy; perfect in use capacity factors range from 0.29% to 16.54% and the overall average is 4.15%. At 16 sites out of 26 in the trial, the measured wind speeds were more than 40% lower than the NOABL database. The observed wind speed distributions at most sites fit best to a Weibull distribution with a shape factor (k) that is less than 2. The Derived values for k at 18 sites were less than 1.6 (Warwick Wind Trials, 2009).

This was the first large scale multi turbine / multi-site trial in the world of wind turbines in the 0.5-1.5 kW range. It was investigated in open fields, urban and suburban housing, and high-rise building installations. There is a wide range of mounting systems. All turbines are installed on real client's sites. So far the general marketing excitement is wildly ahead of actual technical deliverability. Some companies are grossly over-representing the potential for energy delivered from urban wind. Most low-rise sheltered urban and suburban sites

make no economic sense at current grid energy costs, as there are many concerns regarding mounting turbines on buildings such as structural integrity which can be overcome, but, at a cost.

The annual outputs range between 18 and 657 kWh, in contrast the average electricity demand for a typical dwelling house in the UK is 3,000 kWh per annum. Thus, there needs to be a reasonably simple and accurate method of determining the mean wind velocity for a site, without carrying out a costly wind survey which may take a year of recording data before the wind velocity characteristics can be assessed.

In conclusion the report suggested scaling factors for NOABL database to improve wind speed predictions and suggested that more work is required to increase the accuracy of wind speed for a particular area. The Warwick wind project also found that urban site conditions that reduce wind speed are not the only reason for low energy production. The accuracy of manufacturers' power curves, losses from balance-of-system components, and losses from additional site conditions (such as very close obstacles causing turbulence and wind shear), have also been acknowledged as major causes. The balance-of-systems and effect of turbulence/wind shear are estimated to reduce energy production by 10–15% and 15–30%, respectively.

3 DESCRIPTION OF EDINBURGH'S TOPOGRAPHY

3.1 Edinburgh's geography

The city of Edinburgh is the capital of Scotland. It is located in the south-east of Scotland, at longitude 55° 57' N and latitude 3°11' W. Edinburgh lies on the east coast of Scotland's most populated region, and along with the Firth of Forth, is also known as "Scottish Midlands" . Edinburgh is surrounded by the Firth of Forth in the north leading to the North Sea, Galashiels in the south, Livingston in the west and Haddington in the east. In the south-west of Edinburgh there is a small town Peebles with a series of mountains having an elevation of up to 600m to 400m. On one side of Edinburgh there is the Forth Road Bridge which connects Edinburgh to Dunfermline and Kirkcaldy.

The city of Edinburgh offers a high value of surface roughness coefficient for wind. Edina (EDiNA Digimap is an online mapping service delivering maps and data) map was downloaded and printed on an A2 sized sheet (attached at the end of thesis) to read out the elevation variations. In this map dark colour shows build up area, green colour shows big grass land and blue colour shows water. Red lines in the map distinguish elevation of different areas and blue line shows river in Edinburgh.

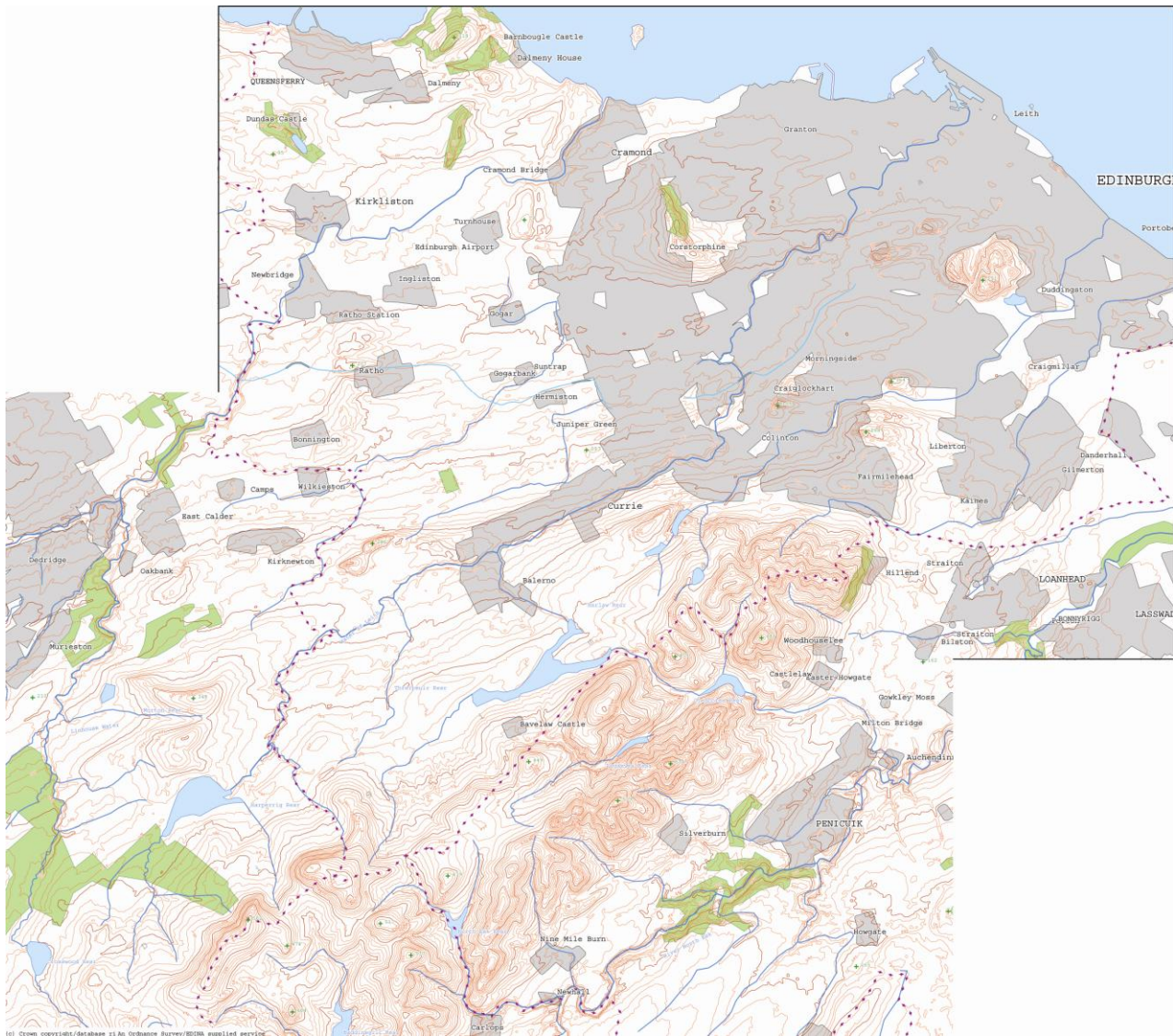


Figure 3-1: Edina generated Edinburgh map in terms of elevation (Courtesy of Edina Digimap).

3.2 Seven hills of Edinburgh

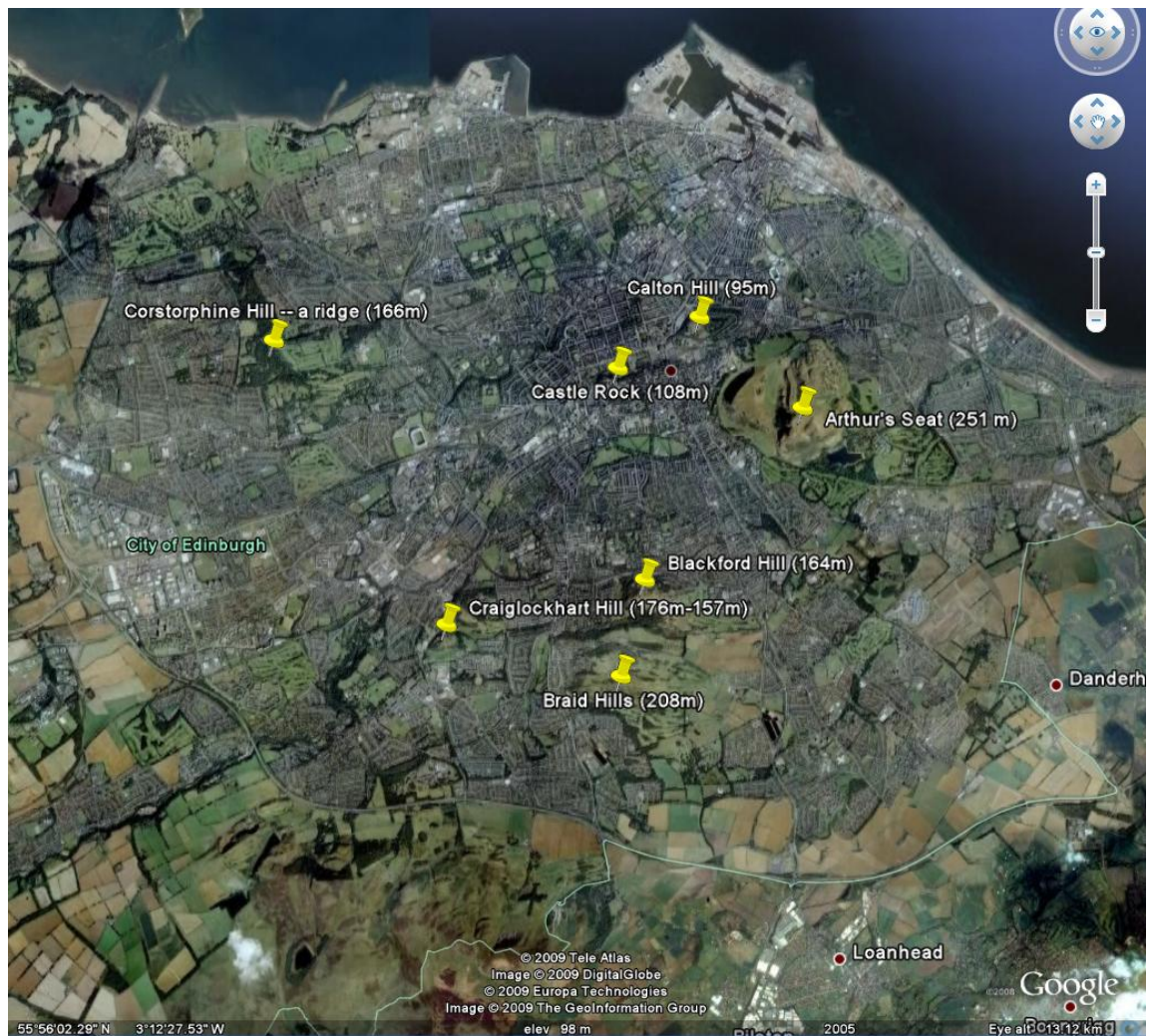


Figure 3-2: Seven Hills of Edinburgh (Courtesy Of Google Earth).

Edinburgh has a land area of 262.28 km² nestled amongst its 'Seven Hills' as shown in Figure 3-2. All seven hills are dead volcanoes located in the heart of the city, which erupted around 400 million years ago. The most important volcanoes, however, were active about 350 million years ago.

3.3 Woodland in Edinburgh

Woodland, the land where the ecological condition is, or will be, strongly influenced by tree canopy, extends over 1,500 hectares (6%) of Edinburgh. This woodland cover is lower than the corresponding Scottish average of about 15% making Edinburgh one of the most sparsely wooded districts in UK. However,

there are several different types of woodland habitat in Edinburgh. Although small and fragmented, many of Edinburgh's woodlands are linked by wildlife corridors, again many of which are tree lined (Scottish Gov, 2006).

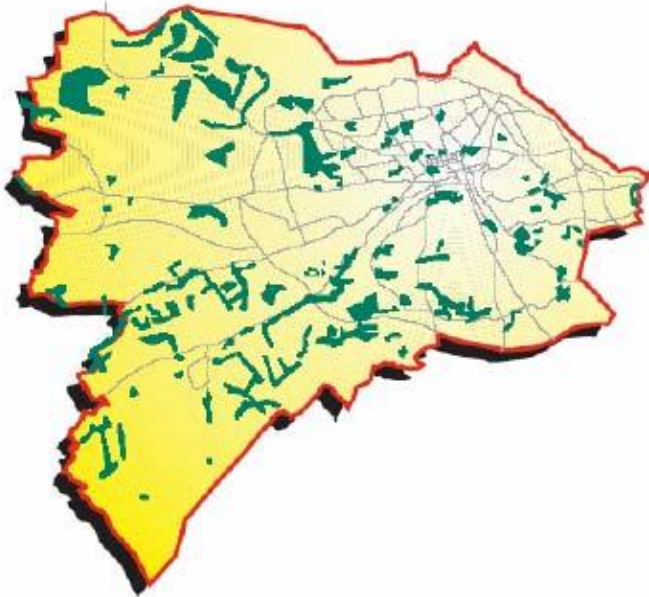


Figure 3-3: Woodland in Edinburgh (Scottish Gov, 2006).

There is diminutive documentation specifically dedicated to the analysis of the effects of trees on wind flow in micrometeorological applications. However, various studies have examined the effects of trees on buildings located within a built up environment (Chiovitti & Dodaro, 1994). Heisler's field study (Heisler, 1989) compared a treeless neighbourhood to a similar neighbourhood with 77% tree density. The neighbourhood with trees acquired a wind speed reduction of 48% and 43% in summer and winter, respectively. This variation, although relatively insignificant, could be attributed to seasonal high winds coupled with deciduous trees shedding their leaves and thus having a lesser effect on wind speed reduction. If one overlooks the wind speed reduction owing to the presence of trees in generation of electricity via wind turbines, then it's important to cite that trees do have positive benefits on the energy demands of buildings. A building surrounded by trees has a lower heating demand in the winter because of reduced wind chill and in the summer months tree shading reduces the building's cooling demand.

3.4 Urban habitats in Edinburgh

Edinburgh is rich with urban habitats which are a valuable haven for wildlife and an important area for the interaction of people with nature. In 1996 sample survey of the 50,000+ gardens in the city (some 3,000 ha in total) identified significant species diversity, including a number of species previously unrecorded for Scotland and the Lothian's. Collectively considered the 130 public parks, 196 churchyards and cemeteries, 25 golf courses, 22 allotments, and 220 vacant and derelict sites in the city, urban habitats probably make up Edinburgh's largest and most diverse wildlife reserve (Scottish Gov, 2006). Some of these locations are ideal for the purpose of harnessing wind energy because of their open plan locations.

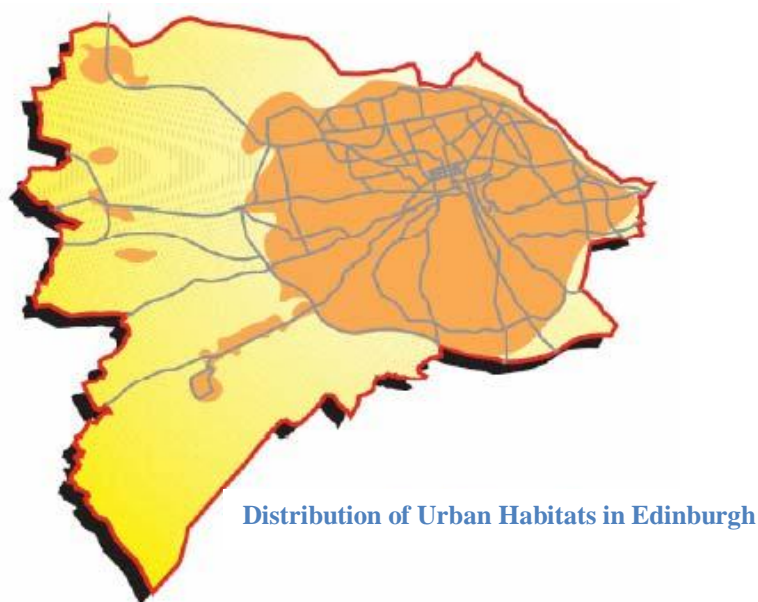


Figure 3-4: Urban Habitats in Edinburgh (Scottish Gov, 2006).

3.5 Rivers of Edinburgh

Almost all rivers of Edinburgh are aligned in south west direction, which is the prevailing wind direction in Edinburgh. Although Edinburgh's rivers are mostly surrounded by trees and houses but at some places they pass through open areas, these water ways can help to exploit wind power. Wind changes its speed as well as direction when crossing a body of water. As air moves from a

relatively rough land to a smooth area (water area) there is less friction with the surface and therefore, its speed increases (Ahrens, 1994).

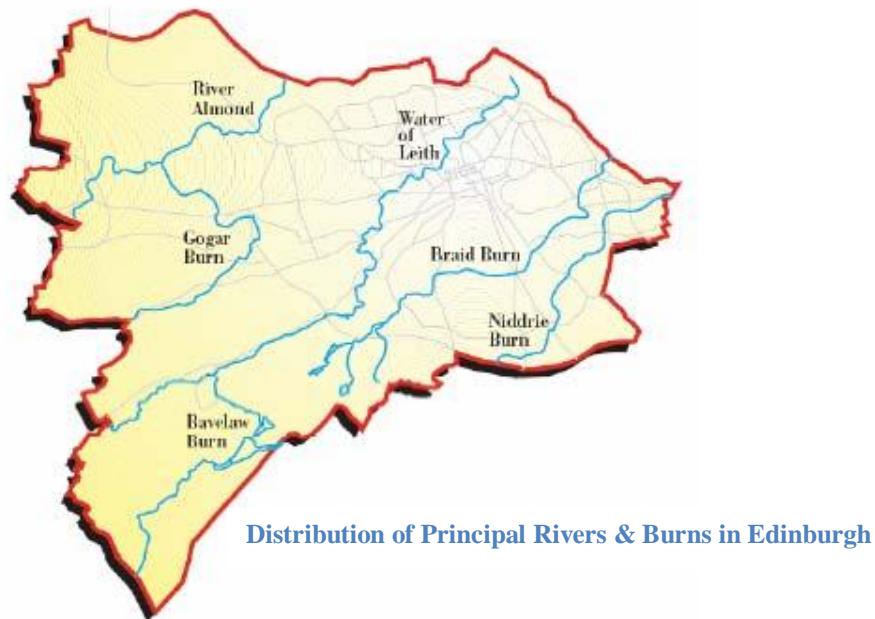


Figure 3-5: Rivers in Edinburgh (Scottish Gov, 2006).

3.6 Farmlands in Edinburgh

Edinburgh has farmland in its rural parts from which three quarters is managed for arable and vegetable crops, the remainder being predominantly improved and semi-improved grassland supporting dairy, beef and sheep production. Grasslands are ideal locations for harnessing wind energy because they have lower surface roughness ($z_0 = 8.00\text{mm}$) than vegetation area (Manwell, McGowan & Rogers, 2009).

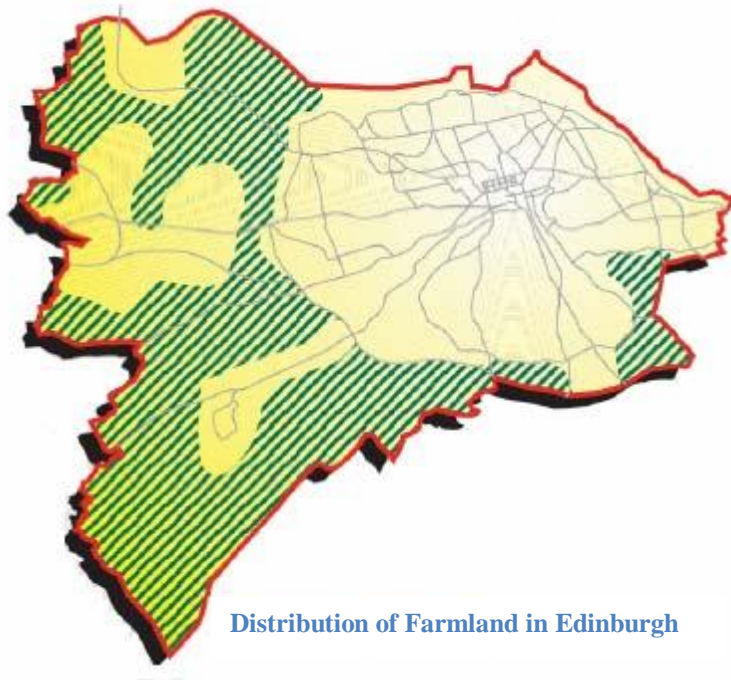


Figure 3-6: Farmland in Edinburgh (Scottish Gov, 2006).

3.7 Edinburgh green belt

The idea of green belt around Edinburgh was first proposed in 1948 and officially designated in 1957. There were two basic objectives of green belt at the time of first design; one to preserve and enhance the landscape setting of the Scotland's Capital and second to prevent the agricultural land from developers and city expansion. However, in 2004 Edinburgh council is facing pressure for economic development pushing it to reassess the aims and objective of the green belt and how much outcomes environment gets from this green belt (Scottish Gov, 2004). Green belt effects on the roughness index of area.

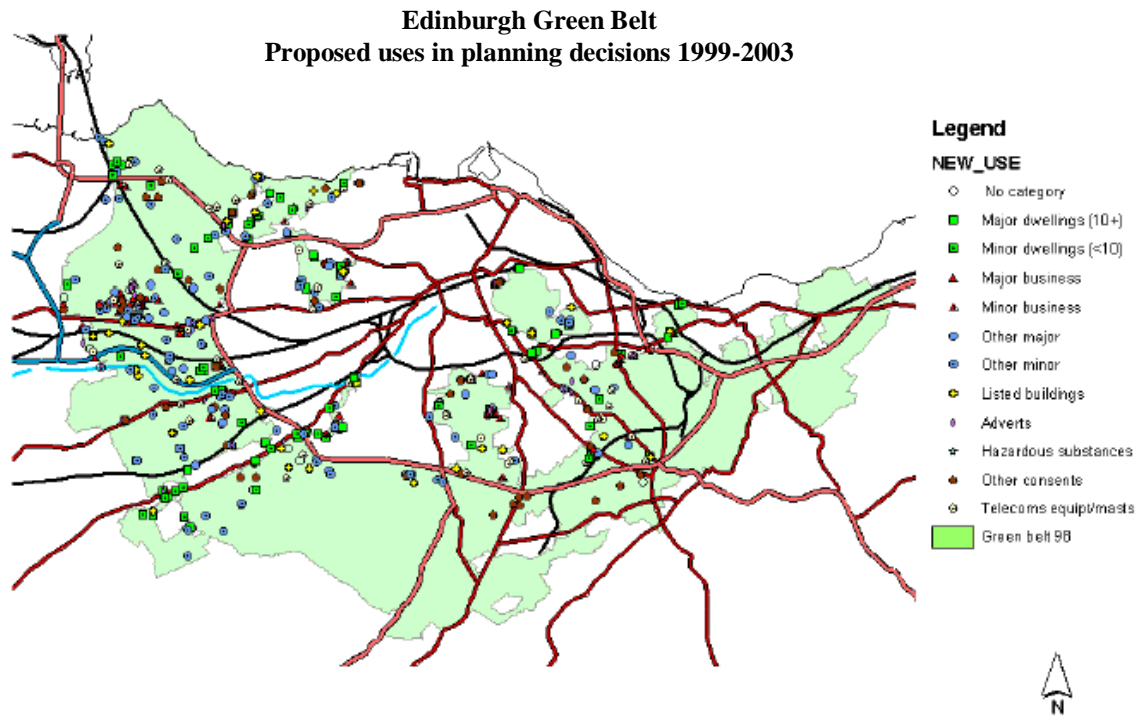


Figure 3-7: Edinburgh Green Belt (Scottish Gov, 2004).

3.8 Climate in Edinburgh

Edinburgh experiences an island's changeability of weather, but it rarely has extreme weather. This is because the city has sea on its one side, thus any large variations in temperature or extremes of climate are minimized. Summer days with sunshine sometimes rapidly change into wet, showery conditions or vice versa. Summers in general are normally fine, with mild temperatures (i.e. maxima rarely exceeds 22 °C) and bright sunshine, although days might start out misty. In winter, day time temperature rarely falls below 0°C. Winters are long and damp with many frosty days. High rainfall occurs normally in December, January and February (graph below shows different months), but snow in winter is infrequent (The City of Edinburgh Council, 2008 & Wordtravels, 2009).

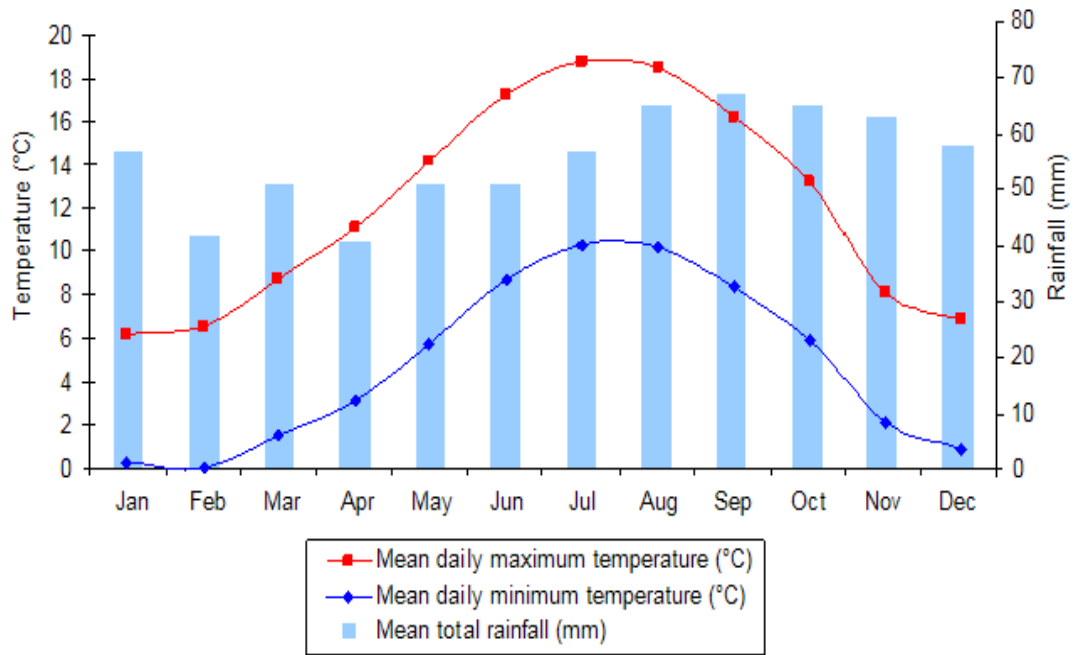


Figure 3-8: Edinburgh Climate over view (Wikimedia, 2007)

Edinburgh is a windy city due to its position between the sea and mountains, with a prevailing south-westerly wind as shown in Figure 3-9.

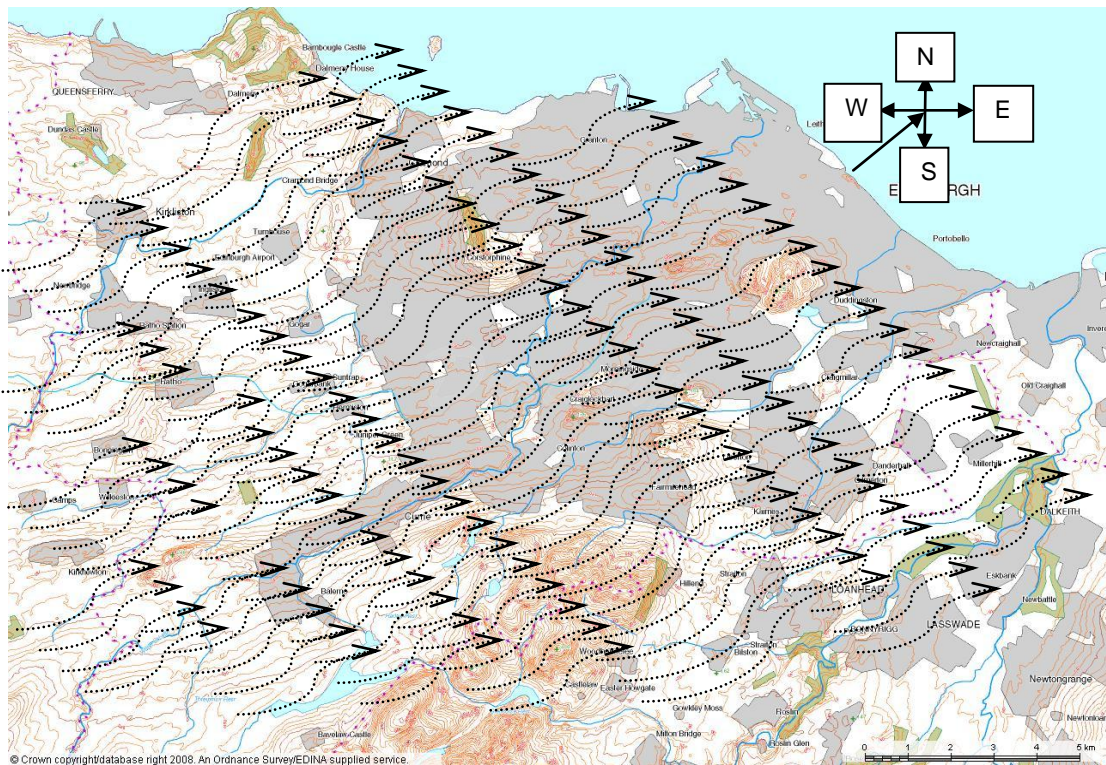


Figure 3-9: south-westerly Wind flow in Edinburgh (courtesy of Edina).

3.9 Population density

According to the City of Edinburgh Council, by 2006 Edinburgh had a population of 463,510 and its population density (persons/km²) was 1,767 (The City of Edinburgh Council's Economic Development service, 2008).

3.10 Town and village distribution

Edinburgh City Council divides Edinburgh into urban and west rural areas. Urban area is denser than rural in terms of development and population. In Edinburgh, over half of the rural area is in the Green Belt zone. Edinburgh's west rural area is characterised as open countryside, much of which is of high landscape quality. Agriculture is likely to remain the dominant land use in rural west Edinburgh. The various towns and villages are distinct urban elements in a predominantly rural landscape, as are the three large areas of non-conforming use at Edinburgh Airport, the Royal Highland Showground and Heriot-Watt University's Edinburgh Campus at Riccarton (The city of Edinburgh Council, 2006).

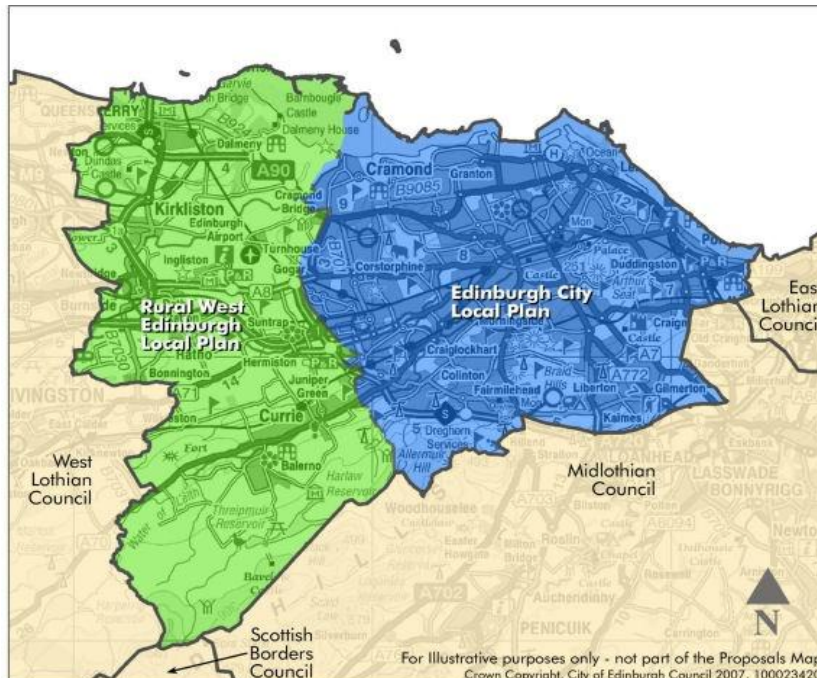


Figure 3-10: Urban and rural distribution of Edinburgh (Edinburgh city local plan, 2007).

4 EQUIPMENT INSTALLATION AND CALIBRATION

4.1 Introduction

This chapter presents the installation and calibration of equipment used in this research. It includes the installation and monitoring of wind equipment to obtain the real time data and analyse it to create the picture of local wind condition. There are basically two categories of wind equipment; one is used to monitor or log the wind data and second is used to convert wind power into electrical power. At the start of this research, all proposed wind equipment installations, however big or small, had to go through the local planning office approval. Due to the lack of experience with micro-generation, local planning departments originally used the governments Planning Policy Statement 22 as a guideline, which is the very basic document with respect to the micro wind power (Office of the Deputy Prime Minister, 2006).

According to “Draft Micro generation Guideline” issued by the City of Edinburgh Council, micro-wind turbines are likely to require planning permission depending on their size, location and surroundings. When applying for planning permission the wind turbine’s noise, visual impact, natural heritage designations and road safety issues have to be taken into account (The City of Edinburgh Council, 2007). Applications would normally be accepted if the proposed turbine were planned to be mounted below the apex of a pitched roof property. This was a result of existing rule that protected the roofline of urban areas by excluding development above the highest part of the existing roof. According to one of the government document called Permitted Development Rights for Domestic Micro-generation Equipment (Scottish Government, 2008), wind turbine on a building is permitted if it planned more than 100m from neighbouring house or flat of roof and that it should not be more than 3m above the top of the roof (including the blade, having length not more than 1.1m).

4.2 Windsave turbine WS1200PS

Windsave 1 kW wind turbine WS1200PS, as shown in Figure 4-2, was installed on 17th July 2008, it cost about £1400. According to the operating manual from Windsave, the turbine has a rated power of 1 kW at the wind speed of 12 m/s;

its power curve is provided in Appendix A. Turbine blade diameter is 1.74m hence its swept area is 2.378m^2 . The turbine is connected to the grid through an inverter which converts turbine's DC (direct current) into AC (alternating current). Inverter has supply from the grid and when turbine voltages reach up to 210V, it starts exporting power until turbine voltages decrease down to 198V. The inverter comes with an LCD display which has accumulator reading for exported power and the level of power generated by turbine. There is no reading available which can show how much power is consumed by the inverter from the grid. Furthermore, one cannot find out the amount of exported power in a particular span of time.



Figure 4-1: Windsave WS1000 wind turbine installed on Merchiston roof top (continue).



Windsave Plug and Save Inverter
DO NOT COVER VENTILATION SLOTS
INDOOR USE ONLY
Model: WS1000PBT
Input: 270-280VAC 50Hz
Output: 270-280VAC 50Hz
Made in China
Serial No: E006420375

Site Record

Site Owner	NAFEE UNIVERSITY	Address	10 GARDEN ROAD
Site Maintainer	AS ABOVE	Postcode	RG10 5DT
Incoming Mains	Make: MELLIN	Model: GREEN MELLIN	
Mains Isolation Switch	Rating: 200 Amps		
MCD of Mined	Type: N/A	Rating: Milliohms	
MCB (Type-B recommended)	Type: B	Rating: 16 Amps	

Notes:
1. All cable 1.5mm minimum, 3 core metal cable BS6347, Conductor wires otherwise stated.
2. Cable from support pole to building entry to be either concealed or protected in HDPE conduit.
3. Connection to Consumer Unit may be either direct or via UK Ring Main, in accordance with BS7671 Wiring Regulations.

Figure 4-2: Windsave WS1000 wind turbine installed on Merchiston roof top.

Table 4-1: Accumulator reading and monthly energy generation of WindSave's grid connected inverter.

Date	Time	Accumulator Reading (Kwh)	Monthly Generation (Kwh)
23/06/2008	1300	7	
17/07/2008	1424	51.1	24.3
18/08/2008	1300	75.4	34.2
18/09/2008	1440	109.6	49.5
16/10/2008	1229	159.1	119.5
18/11/2008	1200	278.6	82.3
18/12/2008	1118	360.9	74.6
19/01/2009	1520	435.5	60.9
18/02/2009	1500	496.4	107.8
18/03/2009	1300	604.2	88.9
17/04/2009	1200	693.1	74.7
18/05/2009	1400	767.8	30.1
17/06/2009	1215	797.9	

As shown in Table 4-1, Windsave wind turbine generates 798 kWh of electric energy in one year and if divided into 12 months equally it yields a monthly average of 66.458 kWh. However, in reality the output is high for a few months and low for the others. In order to calculate the input/output power inverter voltage and current on both its DC and AC side need to be logged, as shown in Figure 4-3. Current can be measured by current sensors and logged to the data logger. For the voltages a small voltage divider circuit has been designed and tested in the lab, which can decrease the voltage level as appropriate for the data logger. This voltage and current measurement installation plan had to be approved from Windsave and permission was subsequently granted in March 2009.

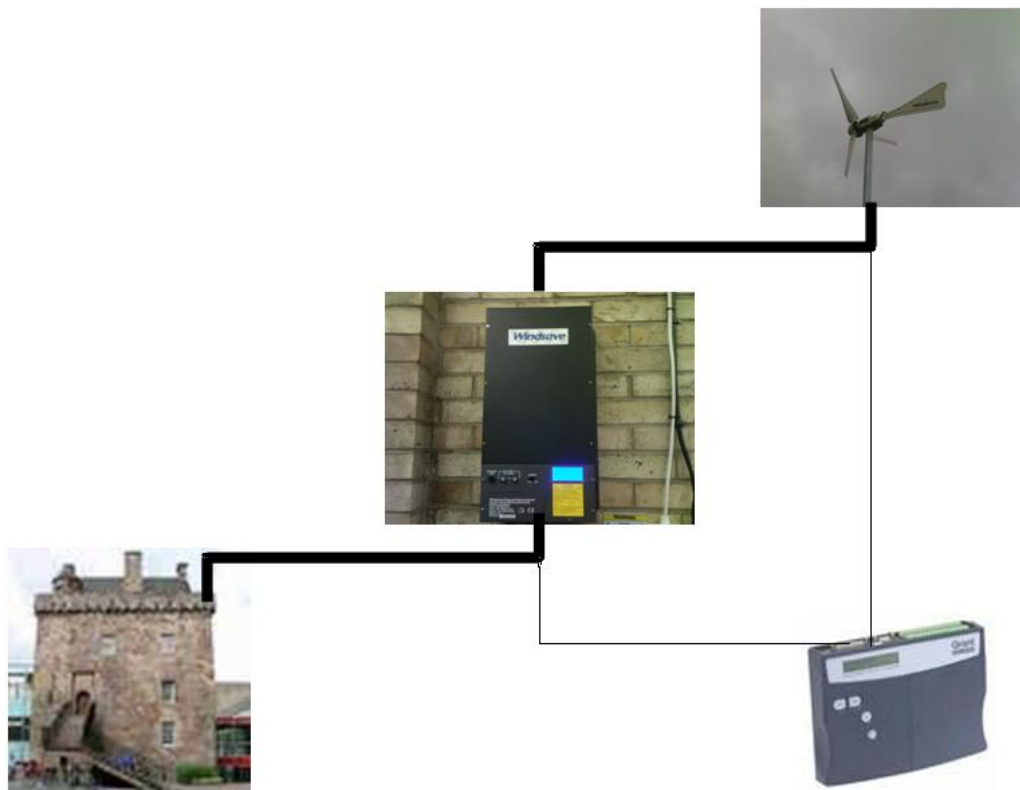


Figure 4-3: Power connection and proposed data logging with WindSave turbine.

4.2.1 Sensing equipment

For monitoring the efficiency of the wind energy converter system (WECS), the following data logging was required: available wind power, output electrical power produced by the turbine, the inverter's intake from and output power (exported power) to the grid. To monitor the available wind resource MetPak (weather stations) were installed. To monitor the turbine's output power, output current and voltages were to be logged. Because the turbine output was in DC, it required sensors which can sense the DC current and DC voltages. The supply from and to the grid was AC, hence AC sensors were installed.

4.2.1.1 DC voltage sensing

Turbine produces electric output in DC voltages which varies with the rotor speed of the turbine. Turbine generates DC output from 0V to 382V at rated speed of 800rpm (@ no load condition) and at 1000rpm 363V (@full load

condition) (Clark, 2006). On the other hand data logger can log maximum 25V in voltage channel. To resolve this issue a Voltage Divider Circuit (VDC) has been designed as shown in Figure 4-4.

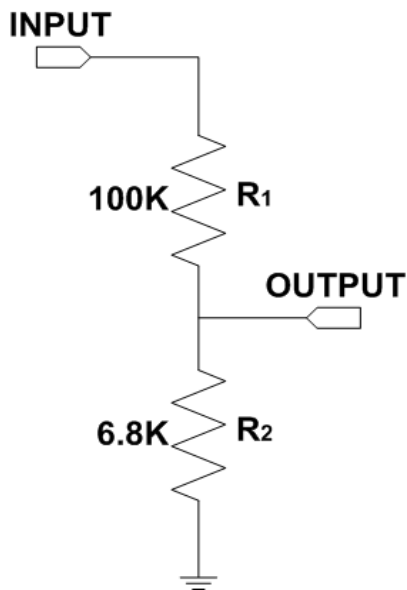


Figure 4-4: Circuit diagram of VDC.

This circuit was designed on the bases of VDC equation as shown in equation below;

$$V_{out} = \frac{R_2}{R_1 + R_2} \times V_{in} \quad \text{Equation 4-1}$$

According to the above equation the VDC shown in Figure 4-4 provides a maximum of 25 volt at the output when input reaches 392 volt. 392 volt is not reachable for turbine generator in normal situation.

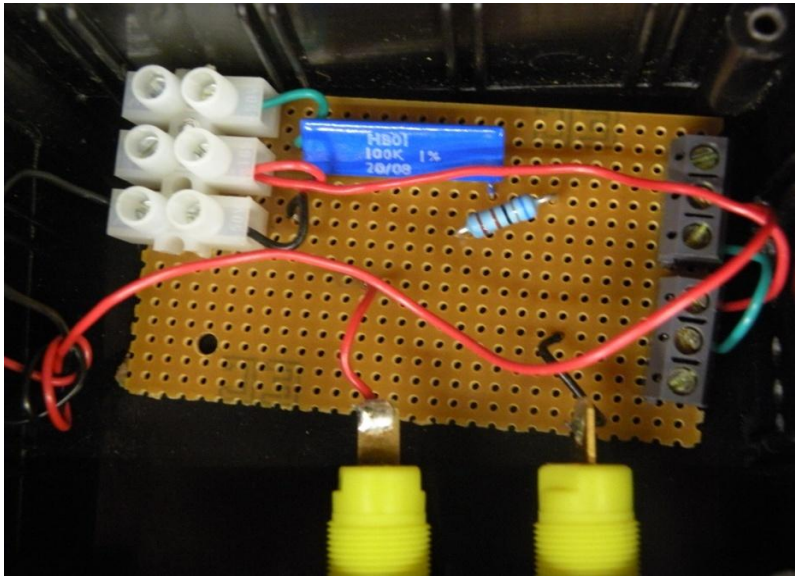


Figure 4-5: VDC components and connections.

Designed VDC has been tested in lab by applying different voltages and measured circuit output as shown in Table 4-2.

Table 4-2: Lab test of VDC.

Input Voltage (V)	Theoretical output (V)	Practical output		Data logger reads out (V)	Error in reading (%)	Error in results (%)
		At volt meter (V)	At data logger (V)			
100.00	6.38	6.38	6.34	99.49	0.50	0.51
150.03	9.57	9.55	9.50	148.97	0.71	0.71
200.04	12.75	12.71	12.65	198.00	0.84	1.03
300.20	19.14	19.01	18.91	296.58	1.22	1.22
355.20	22.65	22.43	22.32	350.07	1.47	1.47

From the lab test results it was found that there is a slight difference in the theoretical (calculated) and practical output of the VDC producing an error of 0.5% to 1.47% in the readings. Error is calculated as per the formula in Equation 4-2.

$$\frac{V_{theoretical} - V_{actual}}{V_{actual}} \times 100 = Error\% \quad \text{Equation 4-2}$$

This error in voltage sensing is corrected when power output of turbine generator and inverter exported power is calculated.

4.2.1.2 DC Current sensing

To log the turbine DC current a current transducer HY 10 has been used as shown in Figure 4-6. This type of sensor can measure DC, AC, pulsed or mixed current with galvanic isolation (of about 2500 volt) between the primary (high power) and secondary circuit, (for data sheet refer to Appendix B). It works on Hall Effect measuring principle, has low power consumption and is considerably immune to external interference. It requires ± 15 volt to power up which is provided by a PCB mount DC power adapter as shown in Figure 4-6.

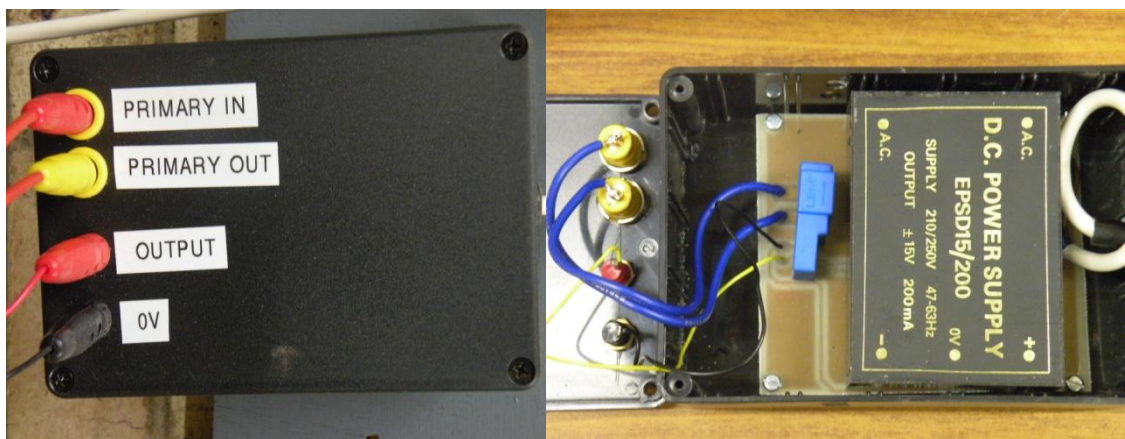


Figure 4-6: DC current sensor.

4.2.1.3 AC voltage sensing

WEC under consideration has a single phase AC grid connection, which is used for inverter supply as well as exporting terminal for the WEC. AC electricity supply in UK is 230 volts (+10% -6%) being used according to Standards & Technical Regulations Directorate (Standards & Technical Regulations Directorate, 2005). AC supply was tested by author also at Merchiston campus and found to be 230 volts in average. Therefore, in all AC calculations 230 volts have been used.

4.2.1.4 AC current sensing

To sense output current of the inverter an AC current transducer “AK 50 C 10” was used as shown in Figure 4-7. It is a split core transducer for the electronic measurement of AC sinusoidal waveforms current, with galvanic isolation between primary (high power) and secondary circuits (electronic circuit). It has jumper selectable ranges and self-powered transducers (for data sheet refer to Appendix B).



Figure 4-7: AC current sensor.

4.3 Pressure sensor

To log the barometric pressure a pressure sensor HCA0811ARG was used and mounted inside the equipment room at Merchiston roof as shown in Figure 4-8. HCA0811ARG is a small PCB mount HCA-BARO Series, miniature amplified barometric pressure sensor. Its input supply is fed from the data logger sensor supply channel and its output directly logged into the data logger.

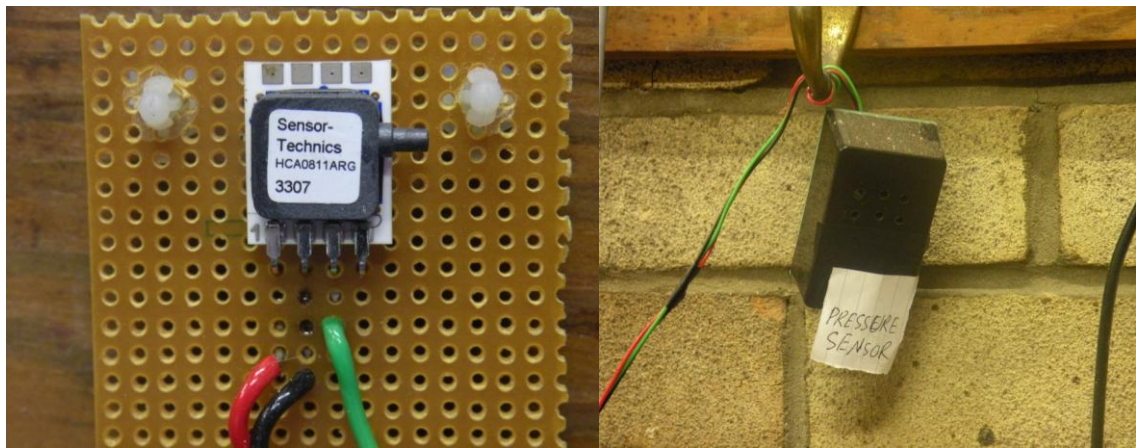


Figure 4-8: Pressure sensor HCA0811ARG inside of the sensor box.

4.4 MetPak weather station

4.4.1 Introduction

MetPak is a compact and lightweight multi-sensor weather station, manufactured by Gill Instruments Ltd Company. MetPak measures wind speed and direction by using ultrasonic technology. It also measures temperature and humidity by using industrial standard probes housed in a naturally aspirated radiation shield. The instrument uses a strong U-bolt mounting clamp that enables it to attach with any vertical pipe up to 50mm in diameter. It can be supplied with either a four channel analogue output option or a digital SDI-12 output. This makes the device suitable for interfacing with industrial standard data loggers. Under current research, four channel analogue output option, which is compatible with Squirrel 2020 data logger, was used. MetPak consumes low power which enables the instrument to be used in remote locations. An electrical junction box fitted to the mounting bracket provides convenient termination of all electrical cables (Gill Instruments, 2006a).

4.4.2 Working Principle

The MetPak uses the WindSonic wind speed and direction sensor, which works on the time of flight theory. Time of flight theory says that the ultrasonic pulse travel time varies with the wind speed. To use this theory WindSonic installed four ultrasonic transducers. The transducers fire ultrasonic pulses to opposing

transducers. In still air all pulses time of flight are equal. When the wind blows, it increases the time of flight for pulses travelling against it. From the changes in the time of flight, the system calculates the wind speed and direction as shown in Figure 4-9 (Gill Instruments, 2006b).

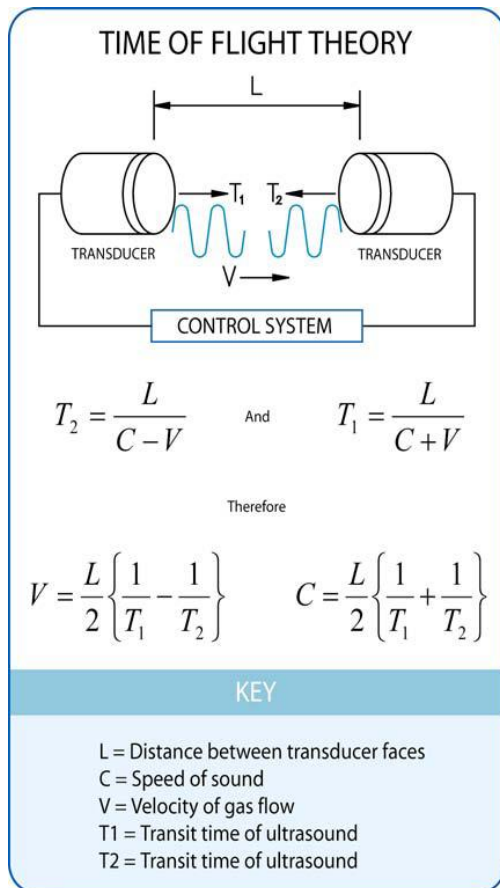


Figure 4-9: Time of flight details (Gill Instruments, 2006a).

4.4.3 Installation

Two MetPak weather stations have been installed on Merchiston roof for the collection of wind data. In MetPak stations wind speed and direction can be sensed by ultrasonic sensors which can give more reliable data than a weather station which has moving parts. The construction height at which MetPak is installed is 20.5m net (height of the main building being 16.3m from ground and another construction having a height of 4.2m). The bottom or lower MetPak is installed at 1.6m from the roof (20.5m+1.6m=22.1m from ground) called MetPak2 or MetPak-L and top MetPak is 3.1 m from the roof (20.5 m + 3.1 m =

23.6 m from ground) called MetPak1 or MetPak-H. The vertical distance between both MetPak stations is 1.5m. There is a yellow mark on the MetPak called North marker arrow pointing in the north direction.



Figure 4-10: MetPak weather station on the right side and MetPak installed on the Merchiston roof on the left side.

4.4.4 Scaling error

The logged data was checked for any errors or outstanding values. It was found that wind speed measurement shows extraordinary high wind when compared to Met office data. The discrepancy is, however, due to different location, altitude and height above ground level. With further investigation, it is found that MetPak measured wind speed was even higher than the data logged by other researchers in the campus. Nevertheless based on this comparison, the MetPak readings cannot be considered unreliable, because other wind speed sensors have a more indirect measuring approach based on:

- Use of moving parts to measure wind speed
- Complex calculation to deduce the wind speed from raw data

- Lack of satisfactory time scale in their data.

MetPak's manufacturers were contacted but a satisfactory response was not received. As a result, the author had decided to take some wind speed measurement. For this purpose, a hand held wind speed meter (Airflow Meter) was used at the same position as MetPak and 1006 data points were logged by one second sampling and logging time (up to 16.76 minutes). Then it was averaged per two seconds and compared to MetPak data. It was found that the data from Airflow meter co-relate to the MetPak data but with almost consistent difference in wind speed as shown in Figure 4-11.

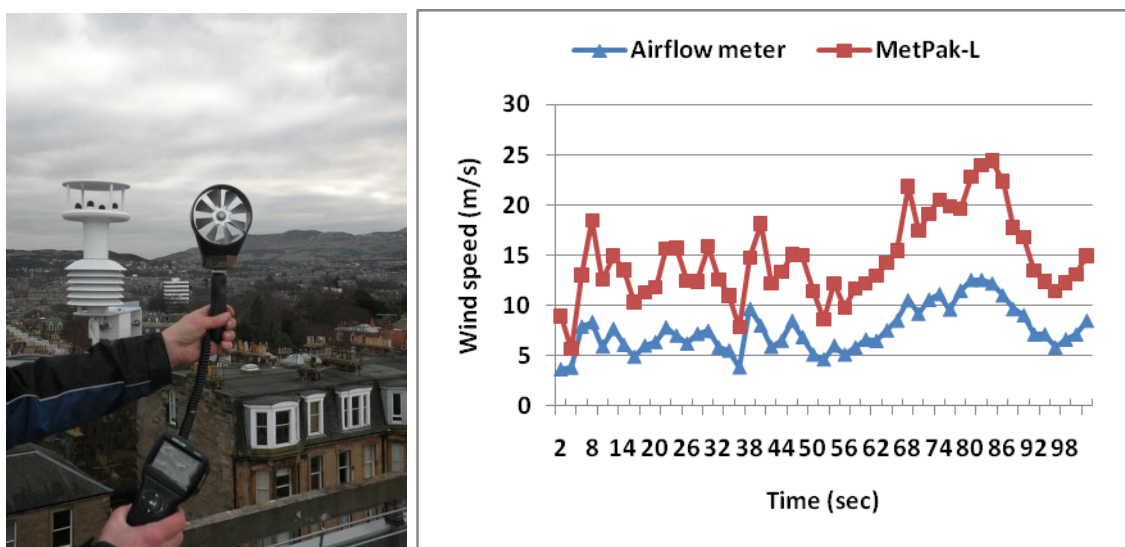


Figure 4-11: Comparison between MetPak and Airflow meter data.

Average ratio between MetPak and Airflow meter was found to be 0.5. This means that MetPak shows a wind speed double than that of Airflow meter and if is divided the MetPak data values by two, it becomes very close to Airflow meter reading as shown in Figure 4-12. This implicates a possible anomaly with the wind speed scale. MetPak has two scales for wind speed: one is from 0 to 60 m/s and another from 0 to 30 m/s. MetPak manual and corresponds to the manufacturer's insistence that the default scale setting is 0 to 30 m/s. Therefore a 0 to 30 m/s scale was set in the data logger setup. However, Airflow meter test confirms that the scale in the MetPak is not set as mentioned in the manual. So MetPak's default scale setting needs be checked and corrected. This

required a connection between MetPak and computer by using available serial port RS-232 on MetPak as shown in

Figure 4-13.

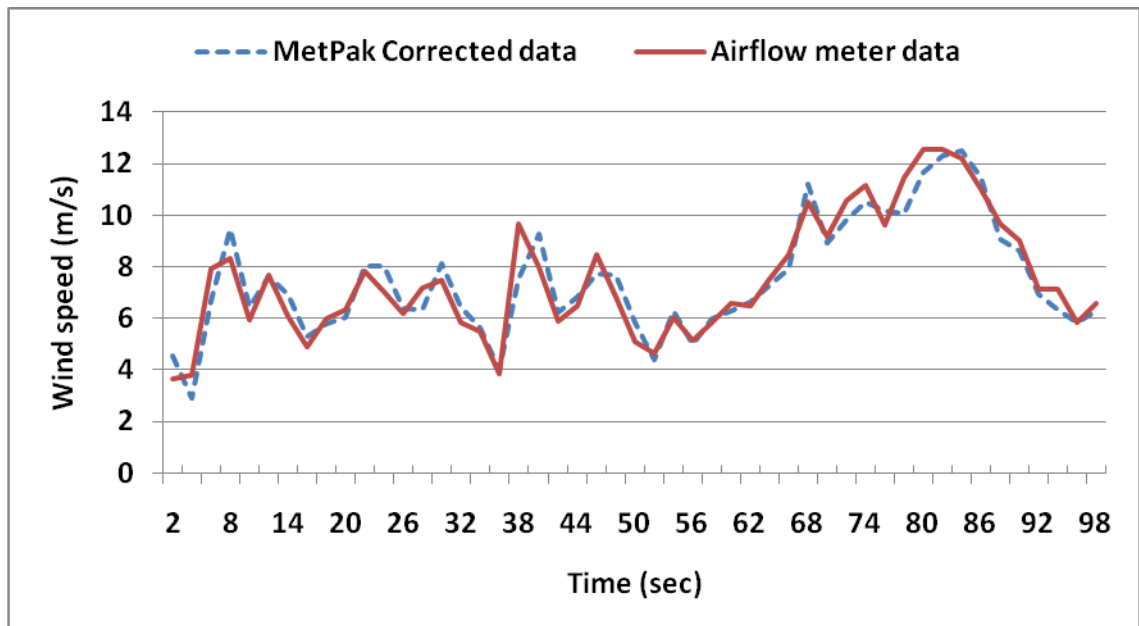


Figure 4-12: Comparison between Corrected MetPak data and Airflow meter data.

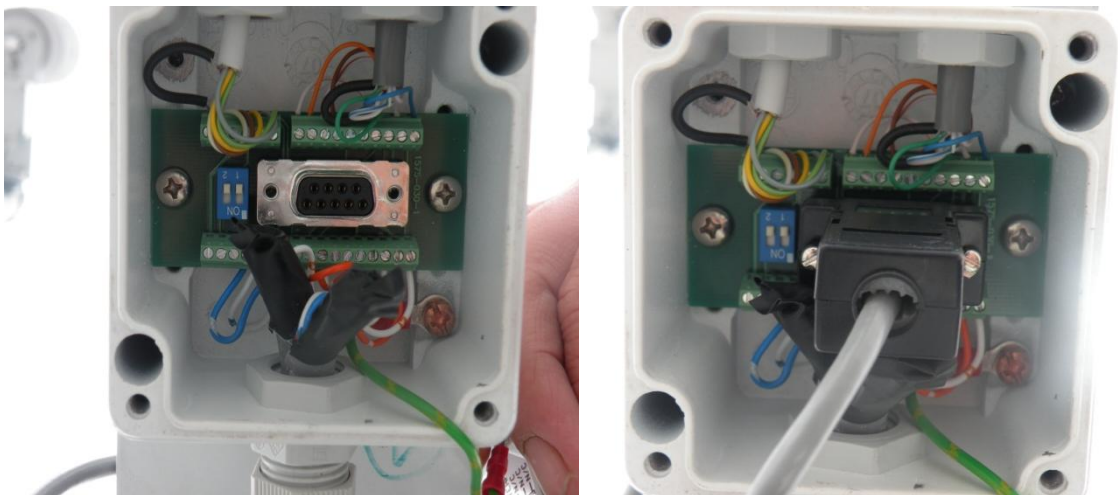


Figure 4-13: RS-232 Connection available in MetPak

4.4.5 Windcom Software platform

Windcom Software is used to establish an interface between user and MetPak setting. On the analogue output module configuration window the default setting for wind speed scale was found to be 0 to 60 m/s. This mismatch between data logger setup setting and MetPak setting led to erroneous wind speed measurements. The MetPak readings were then corrected to 0 to 30 m/s, as shown in Figure 4-14, which removed the error. Windcom also provides scale setting for direction and switching output mode from voltage to current. It also provides instantaneous analysis and data logging of wind speed and direction into PC (personal computer).

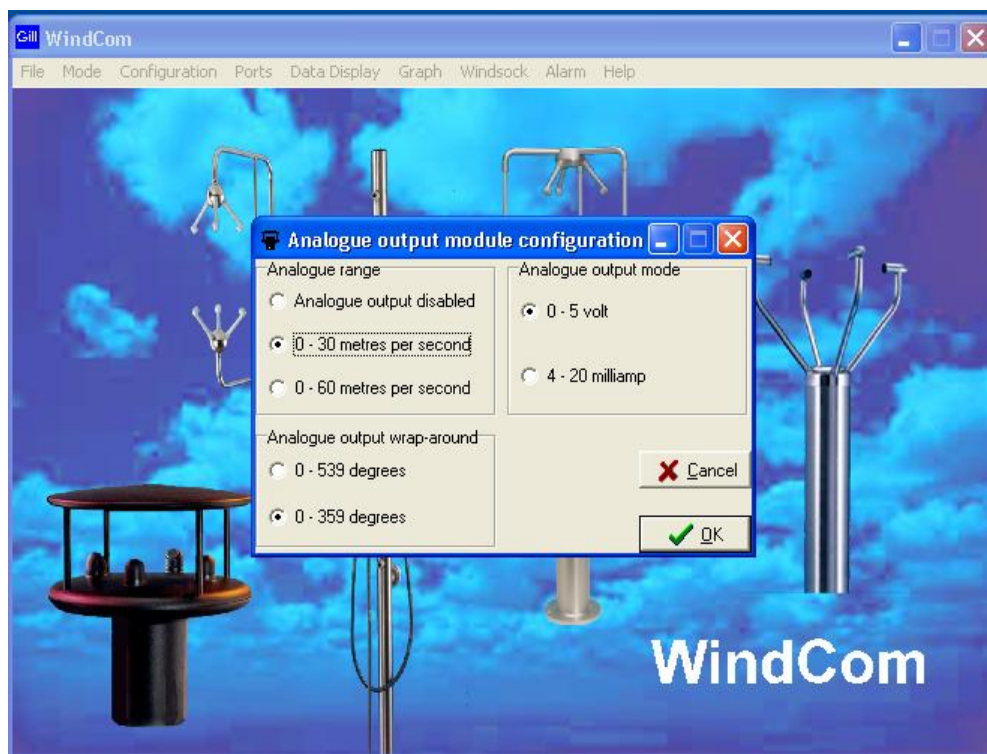


Figure 4-14: WindCom scale setting screen.

4.5 Data logging equipment

In this research, Grant's 2020 series Squirrel Data Logger was used to log the relevant data of the research works. The 2020 Squirrel Data Logger uses six AA size alkaline batteries and can be powered from an external source (10-18V DC). When using external power (as used during this research) it is highly

The first and the main SquirrelView window screen, called SquirrelView Assistant, it has all the available options in the software as shown in Figure 4-16;

- Communication Wizard provides selection option for communication medium: Serial (RS232), USB or Ethernet.
- Logger Control facilitates control i.e. start, stop, pause or continue logging, also provides logger time settings and alarm status.
- Meter Mode provides real time monitoring of the data in numeric format.
- Analysis provides real time data monitoring in graphic format.
- Downloading Data provides downloading and deleting options for stored data.
- Logger Setup provides all setting up options for a particular job of logging i.e. channel settings, scale settings, sampling and logging time settings, sensor power settings, name and save a particular setup in terms of file in PC, uploading and downloading setup into data logger, alarm settings, time settings etc.

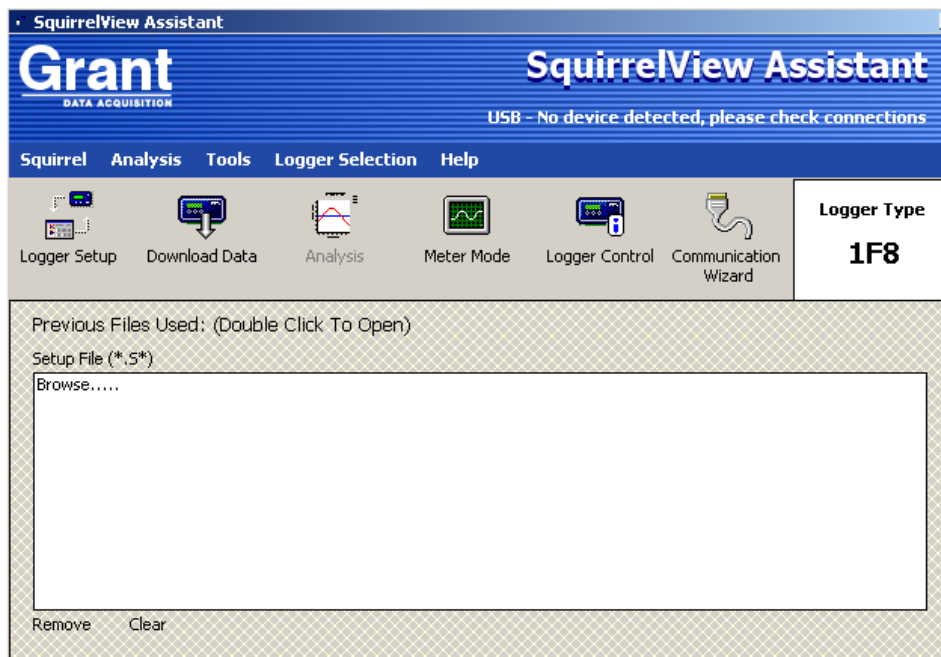


Figure 4-16: SquirrelView main screen with all possible options.

Squirrel 2020 data logger also has easy to read LCD and simple 4 button user interface which can provide manual control and navigation into the data logger. It has 16Mb (up to 1,800,000 readings) internal memory and external memory up to 256Mb removable MMC/SD card. Unfortunately the external memory can only be used for transferring internal memory data or storing setups, it cannot be used for data logging (Grant Data Acquisition, 2008).

4.5.1 Setup settings for logging

In the logger setup one can set the channels for the particular sensor and also scale it according to given specifications as shown in Figure 4-17.

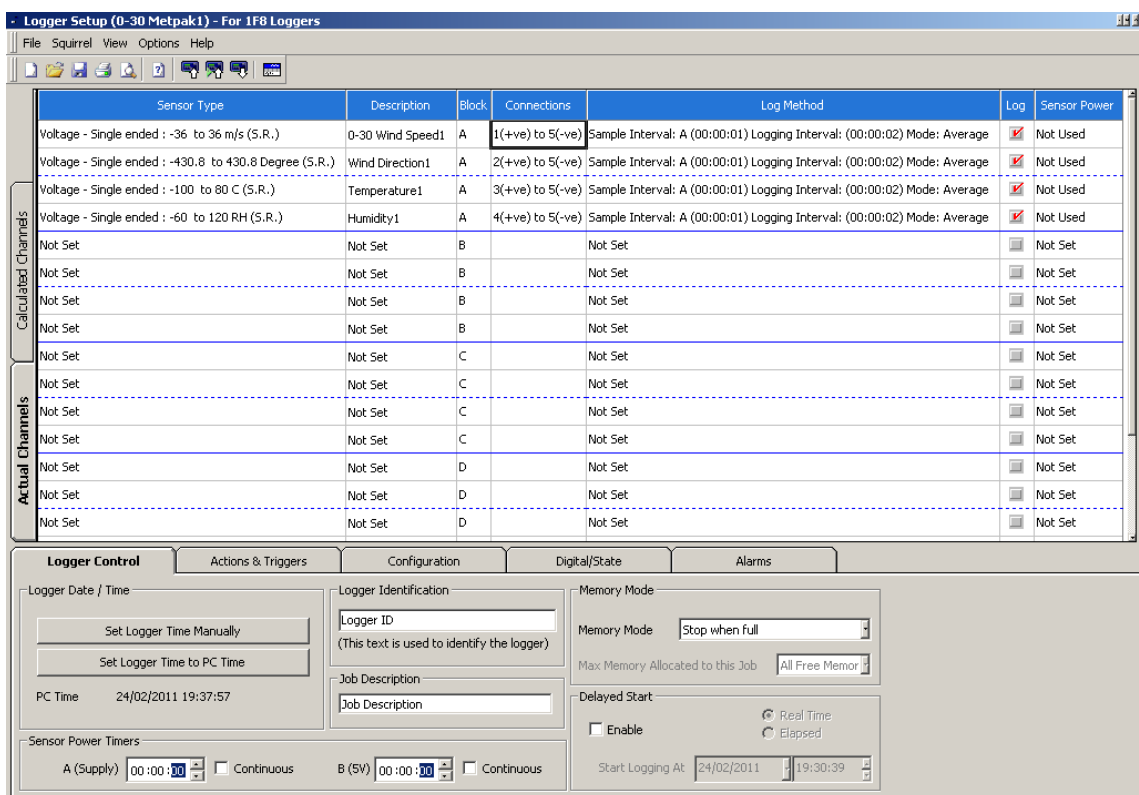


Figure 4-17: Squirrel 2020 data logger setup settings

4.5.2 Data downloading

Downloading the data sometimes interrupts the logging process but by learning the behaviour and functions of the data logger one can adapt a smart way to download the data so its effect on the logging process is as minimum as possible. In this particular research, because of the storage limits (memory

limitations) of the data logger data was downloaded every week. Downloading a week's data from one data logger takes about 13mins. In Squirrel 2020 data logger, data file cannot be downloaded if the process of logging continues in the same file. To avoid the loss of this 13mins data logging during downloading process author disarmed and armed the data logger instantaneously. This action closes the file in which data before the disarm action was being saved and opens a new file to save the data after arm action. Then the old file can be downloaded at the same time as data logging continues in the new file. But in order to clear off the data logger's memory, the downloaded file cannot be deleted in the arm condition. That's why after downloading from the data logger, author disarmed the logger and deleted the downloaded files before arming it again. In this whole process author lost some few seconds of data.

4.6 Processing of raw data

Data processing is a very crucial technical step particularly for large datasets as utilization and effectiveness of data depends on it. The following steps were taken to convert raw data into useable format.

- Squirrel 2020 data logger generated data file in "*.D20" format which is only readable through the logger's supplied software.
- Using export function of Squirrel software, "*.D20" files were exported into comma delimiter text files. Header files were generated separately from data files.
- Downloaded data from three data loggers were divided into three categories:
- Metpak1 (MetPak-H) data files that contain wind speed (m/s), wind direction (Degree), temperature ($^{\circ}\text{C}$), relative humidity (%) at higher height.
- Metpak2 (MetPak-L) data files that contain wind speed (m/s), wind direction (Degree), temperature ($^{\circ}\text{C}$), relative humidity (%) at lower or hub height.
- Vmbar data files contain atmospheric Pressure (mbar) and DC side current (A), DC side Voltages (V), AC side current (A) of turbine system.

- For data processing title row (the first row), which contains the titles of all columns, was removed from each data file.
- All files of one category were copied into one file by using DOS (disk operating system) prompt command “copy”.
- Using VBA code first two columns (which contain date and time) of data files were split into six columns (which contain date, month, year, hour, minute and second).
- Separate files were generated for each month from big data file again through VBA programming.
- “N/A”, which appeared occasionally due to disarm action stopping the logging process, was removed from each month’s data file as it caused problem during data processing.
- Data was then sorted by date and time because during the copying process different weekly and smaller files mangled in the copied file (i.e. rows are not in ascending order of date and time). To perform this task of data organisation following steps were taken:
- Each row of data file was tagged with a unique code (by using VBA) which was generated on the basis of date and time of that particular data line.
- This monthly tagged data was then loaded into MatLab and sorted out. The output was written into two “*.csv” files as there is file opening problem if all data were written in one file.
- Sorted data files were opened in excel and saved as comma delimiter text file because “*.csv” file generated by MatLab couldn’t be successfully processed using VBA code.
- Then both files were recombined using VBA and tags were removed from data.
- Data was again retagged through VBA programming to check three things;
- Was data in correct date and time sequence?
- Was there any missing data or gap in the data, if yes, then for how long?
- Was there any overlap in data? Data overlap could occur because of time conflict between data after re-adjustment of data logger time.

- In some data files, overlapping of data was found (i.e. same time for more than one row or because of time adjustment logging was found every second instead of every two seconds) and removed by MatLab code.
- These fixed files were retagged and rechecked.
- Separate files were generated from “Vmbar category” files for atmospheric pressure data and turbine system data.
- Eventually, monthly text files with up to 1337288 rows of data (depending on the availability of data in a month) were made available for data analysis.

5 ANALYSIS OF MET OFFICE WIND DATA

5.1 Introduction

This chapter describes the topography of the Met office weather station location and its surrounding areas. It also analyses the Met office wind data calculations of wind energy in Edinburgh's rural area.

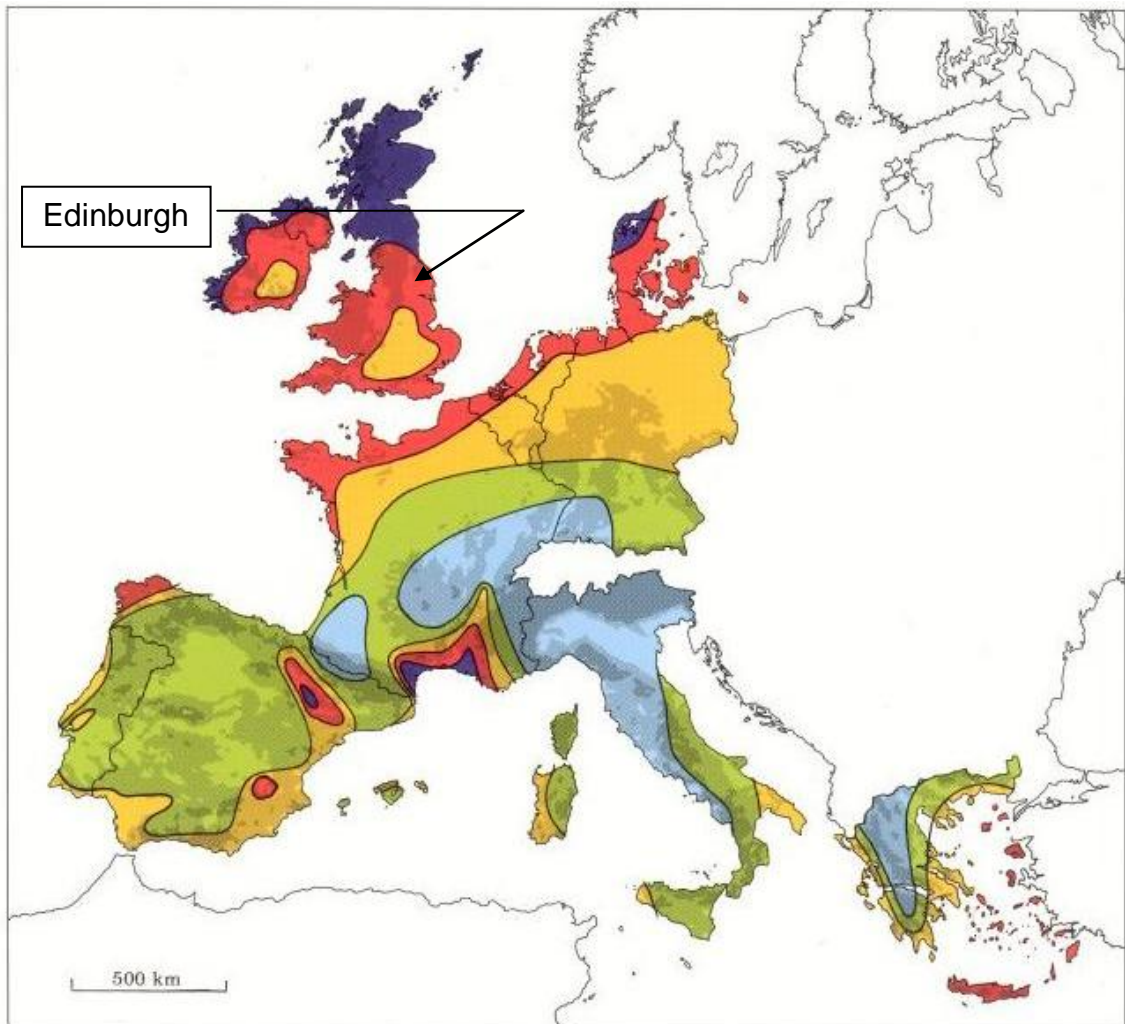
According to European Wind Atlas (which is generated by RisØ National Laboratory, Roskilde, Denmark), Scotland is one of the highest wind resource regions in entire Europe as shown in Figure 5-1. According to the atlas, it has wind speeds of more than: 6 m/s in sheltered terrain regions, 7.5 m/s in open plan areas, 8.5 m/s in coastal areas and 11.5 m/s in hills and ridges.

As discussed in previous chapter, Edinburgh bordered by the coast of Firth of Forth is in the south-east of Scotland. Hence, wind speeds can be expected in the range of 6.0-8.5 m/s as per the European Atlas. In NOABL (wind speed data base) wind speed atlas for UK, wind speed at Edinburgh can be expected in the range of 6-7 m/s as shown in Figure 5-2 (BWEA, 1999).

5.2 Met office data

One set of data (1999-2009) was purchased from UK Meteorological office (called Met office data) and used to analyze the wind conditions. The data sets contain record of hourly wind-mean speed, wind direction, maximum gust speed, mean sea level pressure, relative humidity and temperature. Wind speed and wind direction are sampled every 250 milliseconds, from which a 10 minutes mean is calculated and 3 seconds mean is applied to determine wind gust. Temperature is sampled at every 15 seconds for which one minute mean is calculated. Relative humidity is measured at every 15 seconds and is then combined into a one minute average. All the calculated data above is then converted and averaged to hourly value.

European wind resource at 50 meters above ground level



Wind resources ¹ at 50 metres above ground level for five different topographic conditions										
	Sheltered terrain ²		Open plain ³		At a sea coast ⁴		Open sea ⁵		Hills and ridges ⁶	
	$m s^{-1}$	Wm^{-2}	$m s^{-1}$	Wm^{-2}	$m s^{-1}$	Wm^{-2}	$m s^{-1}$	Wm^{-2}	$m s^{-1}$	Wm^{-2}
	> 6.0	> 250	> 7.5	> 500	> 8.5	> 700	> 9.0	> 800	> 11.5	> 1800
	5.0-6.0	150-250	6.5-7.5	300-500	7.0-8.5	400-700	8.0-9.0	600-800	10.0-11.5	1200-1800
	4.5-5.0	100-150	5.5-6.5	200-300	6.0-7.0	250-400	7.0-8.0	400-600	8.5-10.0	700-1200
	3.5-4.5	50-100	4.5-5.5	100-200	5.0-6.0	150-250	5.5-7.0	200-400	7.0- 8.5	400- 700
	< 3.5	< 50	< 4.5	< 100	< 5.0	< 150	< 5.5	< 200	< 7.0	< 400

From the *European Wind Atlas*. Copyright © 1989 by Risø National Laboratory, Roskilde, Denmark.

Figure 5-1: European Wind Atlas.

Annual mean wind speed
at 25m above ground level [m/s]

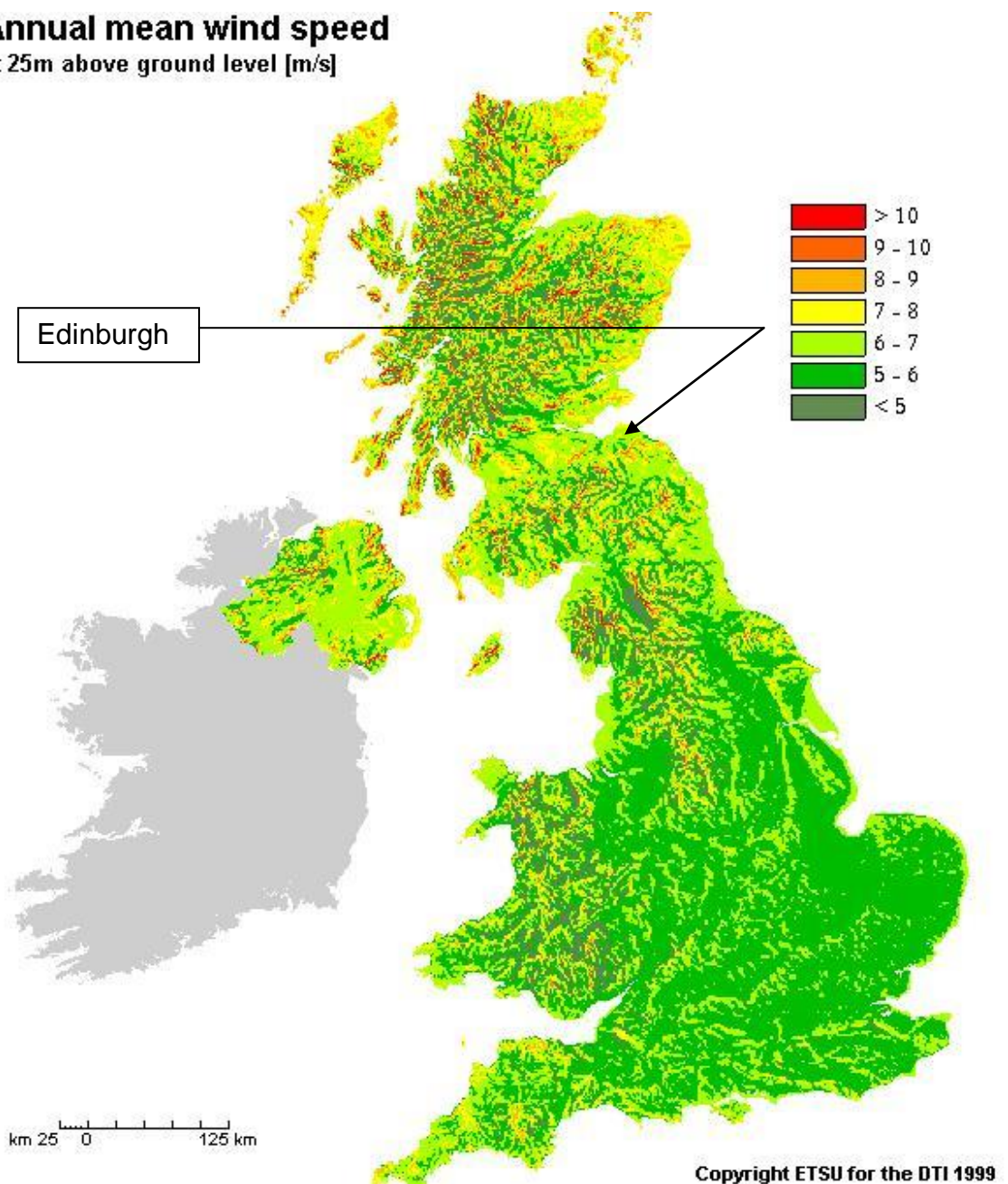


Figure 5-2: NOABL wind speed atlas for the UK (source: BWEA).

5.3 Location of data collection point

The data was recorded from a 10 meters high weather station at Gogarbank Edinburgh (as shown in Figure 5-3) with an altitude of 57 meters (from mean sea level) and coordinate of 55°55'41.87"N (55.93°N), 3°20'38.91"W (03.34°)W. Gogarbank is situated in the rural classified area in west of Edinburgh as shown in Figure 5-4. In Gogarbank, Met office weather station is

located in a relatively open area in all directions apart from the obstruction of few trees and Edinburgh's urban area starting from about 2 km in the east.



Figure 5-3: Met office weather station at Gogarbank Edinburgh (obtained from Google map).



Figure 5-4: Met office weather station location's satellite picture and surrounding terrain's photograph at Gogarbank Edinburgh (obtained from Google map).

5.4 Elevation of Met office weather station and surrounding area

Met office weather station elevation was found, using Google Earth as a tool, to be 57m. To determine the elevation around Met office weather station, surrounding area was divided into 24 sectors with a spacing of 15 degrees.

Twenty four lines were drawn commencing from Met office weather station and terminating up to the length of 10 km in distance as shown in Figure 5-5. Figure 5-9 shows 24 resultant elevations around Met office weather station. It shows that in the North of the weather station, before the sea, some sharp rise in the elevation is in the way and that the nearest sea side is 6.6 km away at 30 degrees from North. At 60 degrees from North there is a 162 m high cliff, 5.15 km away from the weather station. Elevation on and around the south east side of the weather station is much higher (i.e. up to 462 m). Even in the south and the southwest direction weather station seems to be in the bottom of the high rise elevation area having elevation of 256 m. There are higher elevations also in the west direction as shown in Figure 5-9.

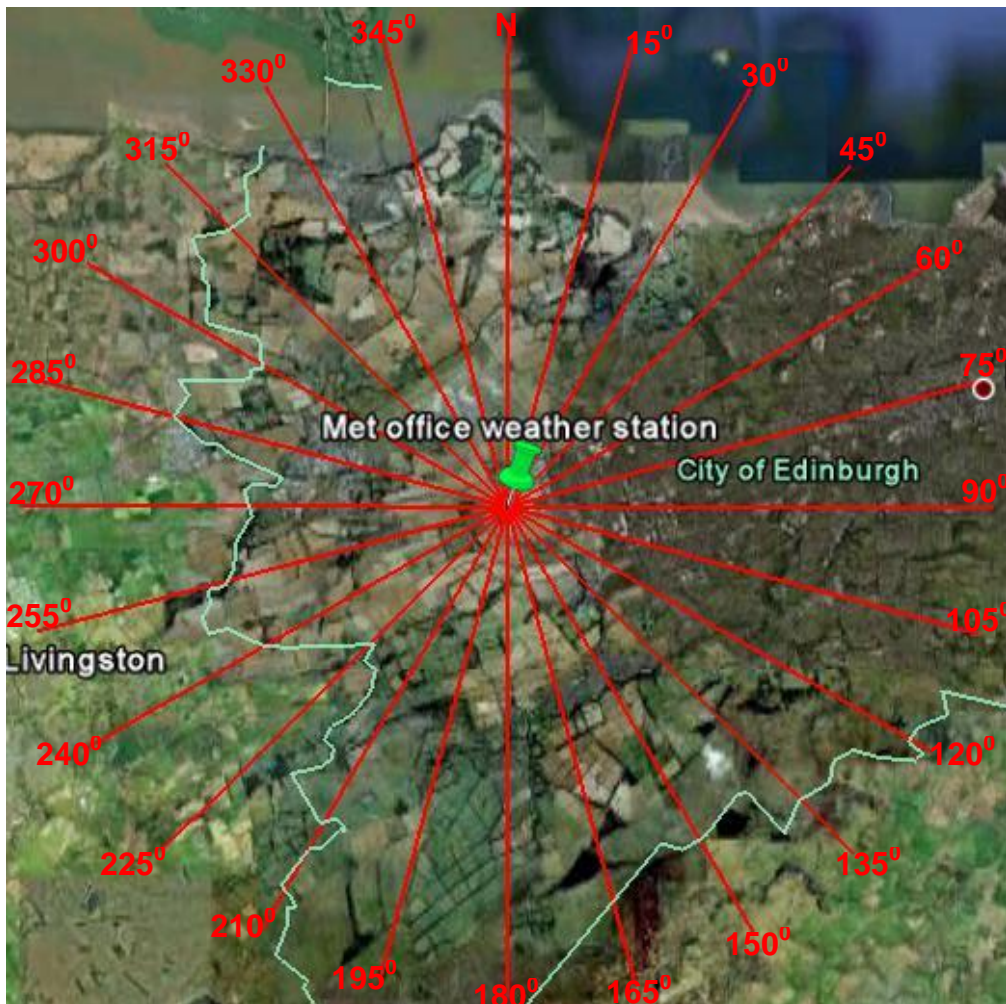


Figure 5-5: Sectors around Met office weather station drawn on Google Earth.

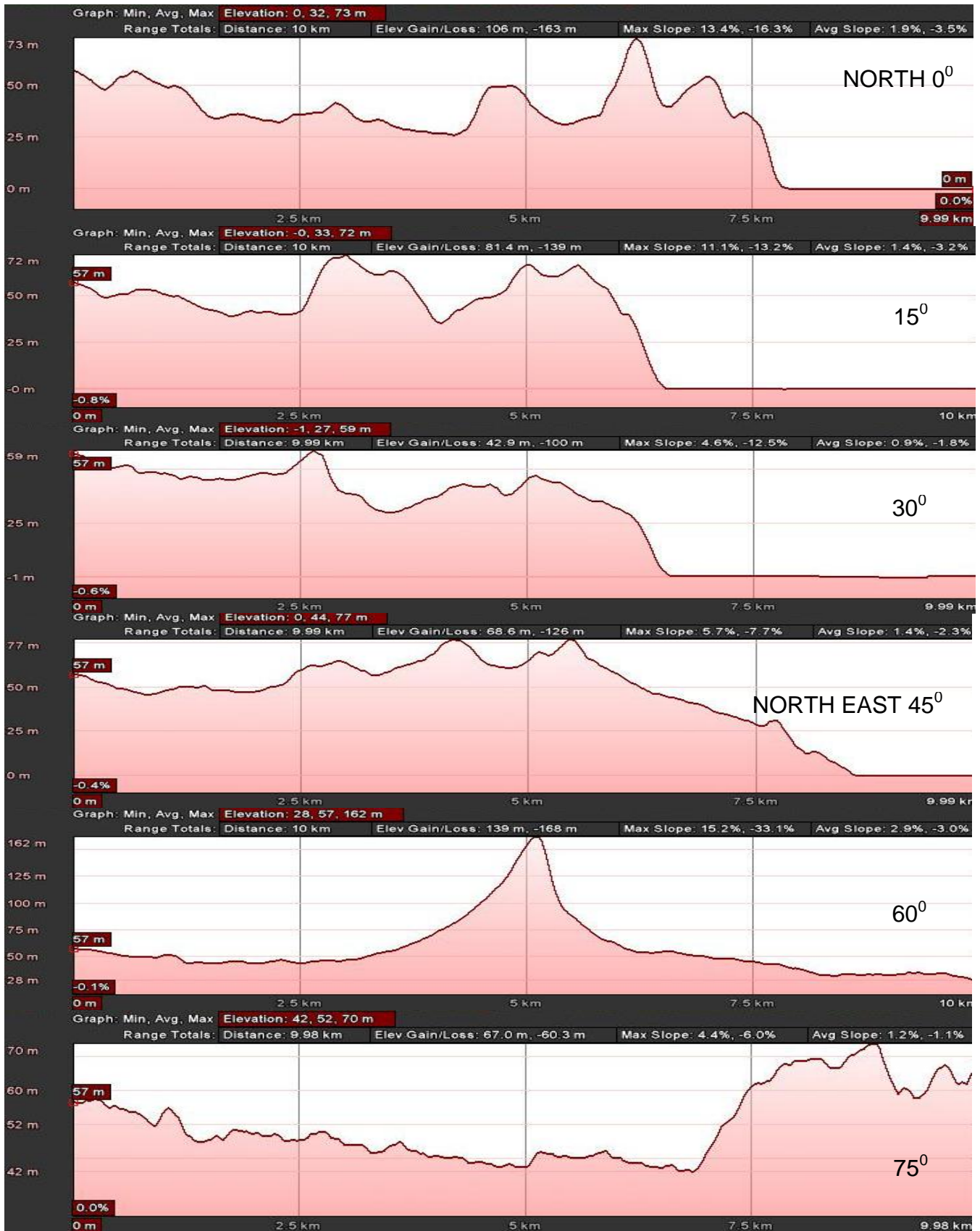


Figure 5-6: 24 Elevation graphs of the surrounding area covering a 10 km distance around the Met office weather station (continue).

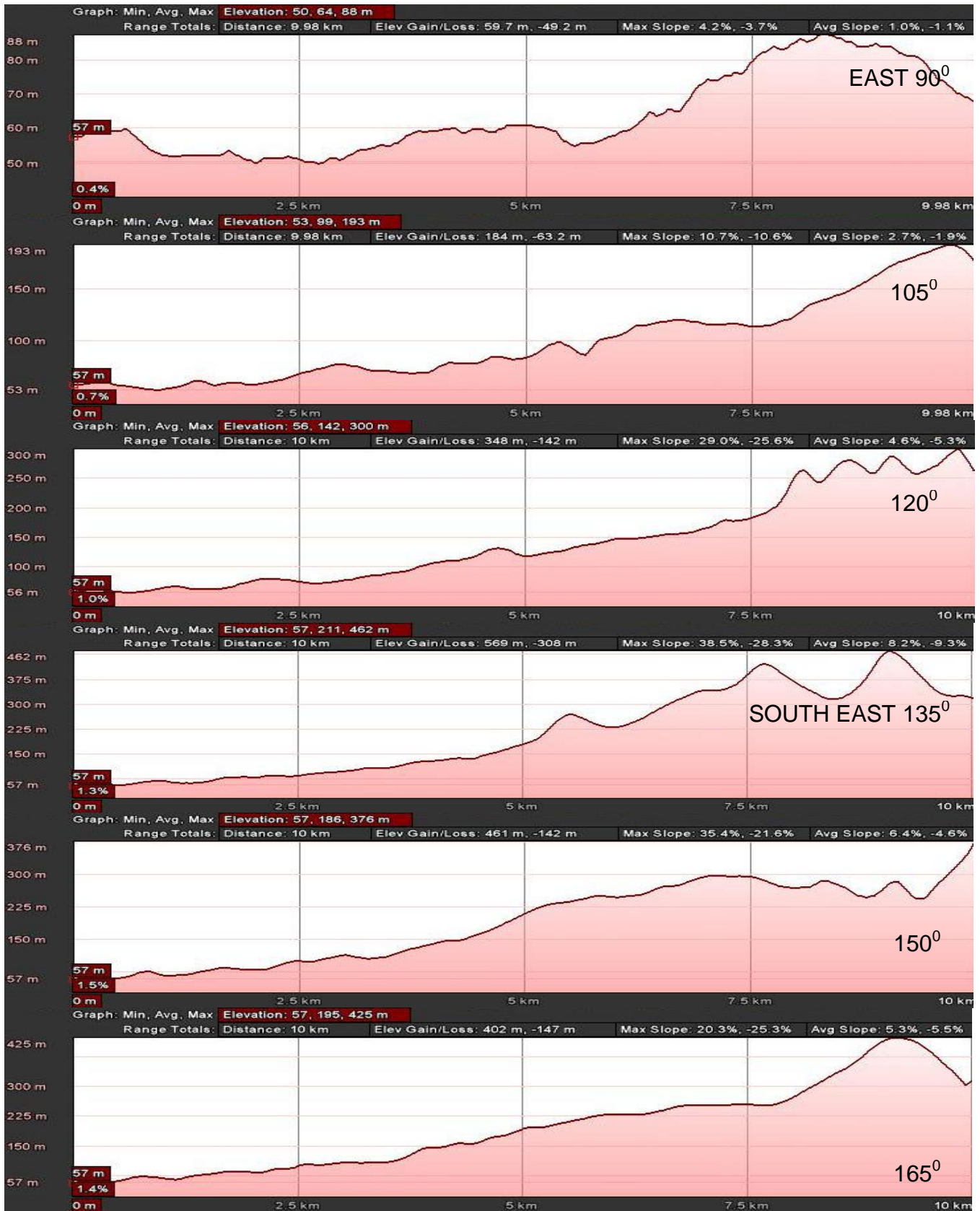


Figure 5-7: 24 Elevation graphs of the surrounding area covering a 10 km distance around the Met office weather station (continue).

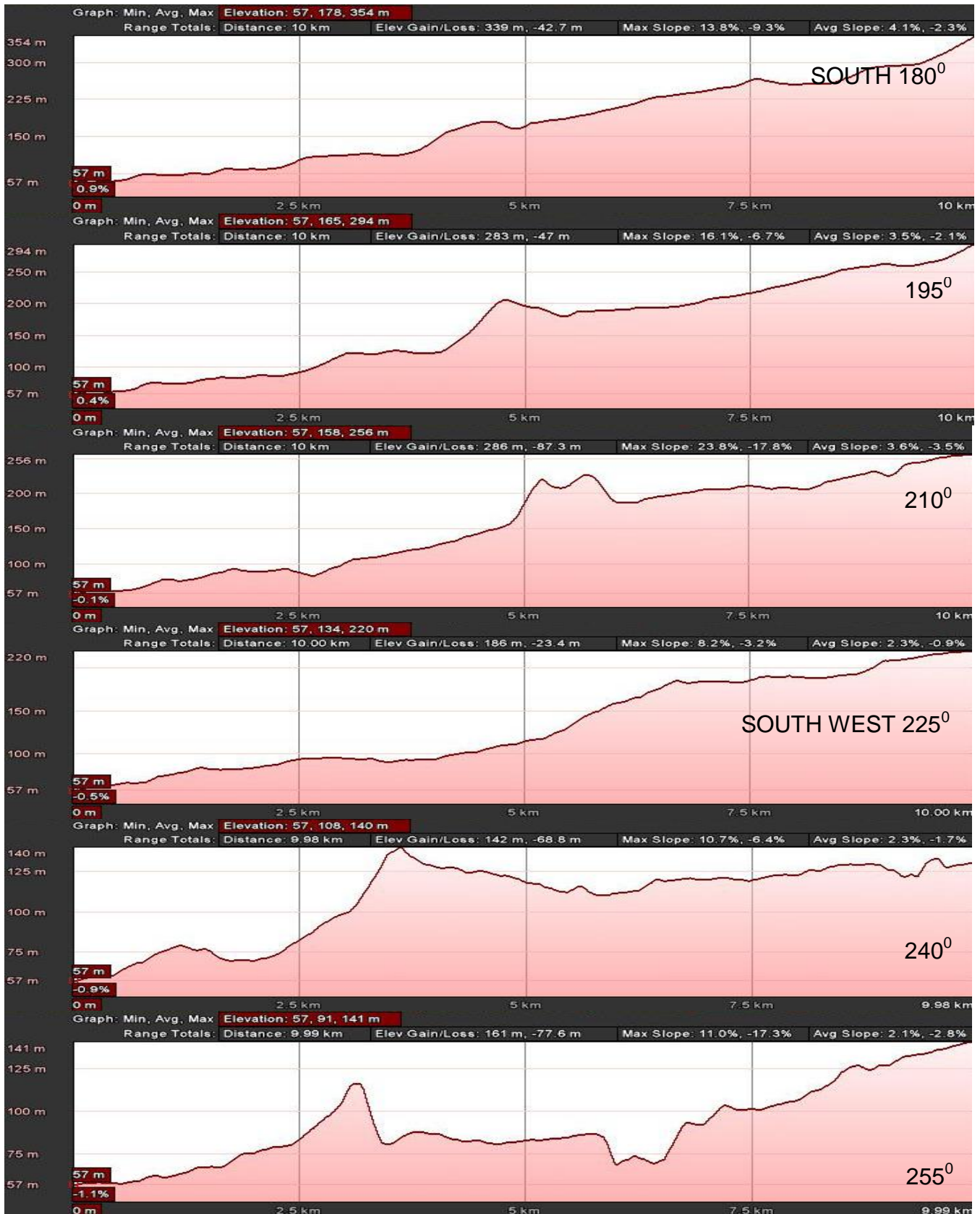


Figure 5-8: 24 Elevation graphs of the surrounding area covering a 10 km distance around the Met office weather station (continue).

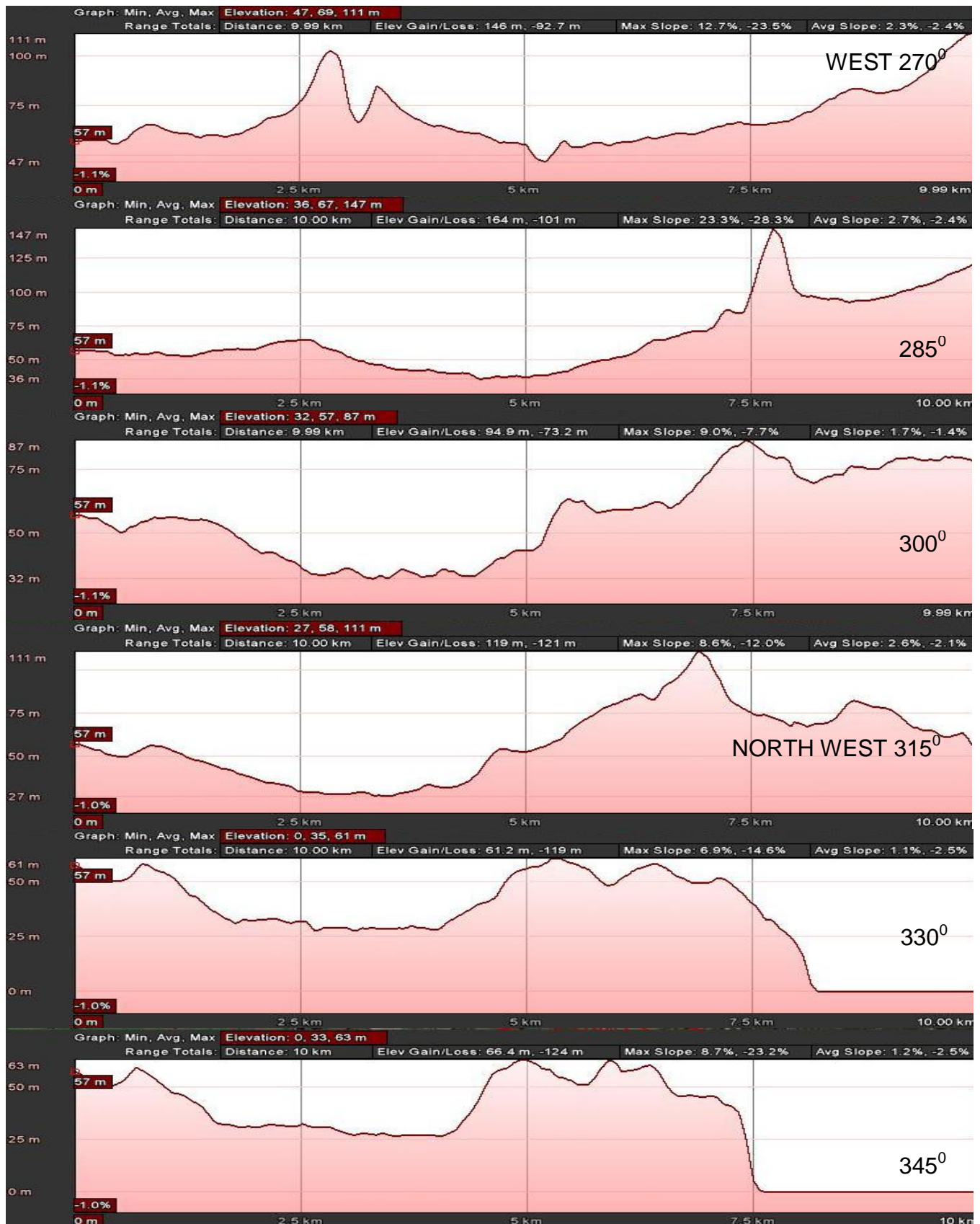


Figure 5-9: 24 Elevation graphs of the surrounding area covering a 10 km distance around the Met office weather station.

5.5 Prevailing wind direction

As a first step, wind speed is converted from knots to meter per second and wind direction from degrees to radians. To investigate wind direction wind rose has been drawn, it is a graphic tool used to give a concise view of how wind direction is typically distributed at a particular location. On analysing met office data, more than 60% of the wind was found to blow from south west direction as shown in Figure 5-10. Some other directions are also shown on the wind rose which can be considered as turbulence.

5.6 Average wind speed

The most widely used and most generally understandable statistical tool is arithmetic mean or simple mean, also known as average. It is a simple tool which describes the central tendency of the data (Hamburg, 1985). It can be calculated by the dividing the sum of the data ($\sum X$) by the total number of data points (n).

$$\bar{X} = \frac{\sum X}{n} \quad \text{Equation 5-1}$$

Figure 5-11 shows the monthly average wind speed of hourly wind data. It presents a general trend of seasonal wind i.e. Edinburgh has high winds from October to March. It has a maximum average wind speed of 6.98 m/s in the month of January 2007 while in January 2001 this value is only 3.3 m/s. It shows that in winter season monthly mean wind speed is high but unsettled and has a large variation. On the other hand in summer season monthly mean wind speed is low but consistent. It has minimum average wind speed of 3.04 m/s, in the month of July 2000, while in July 2007 this value is 3.69 m/s.

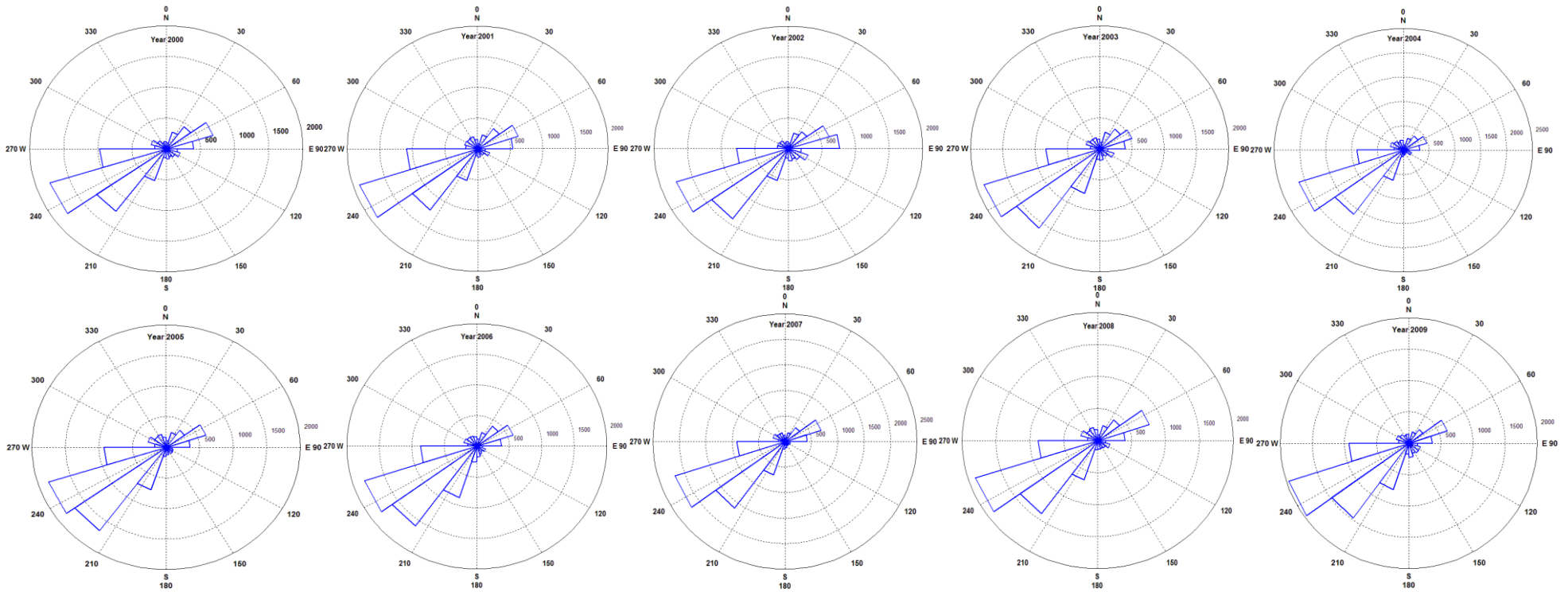


Figure 5-10: Wind directions frequency in rose diagram for year 2000-2009.

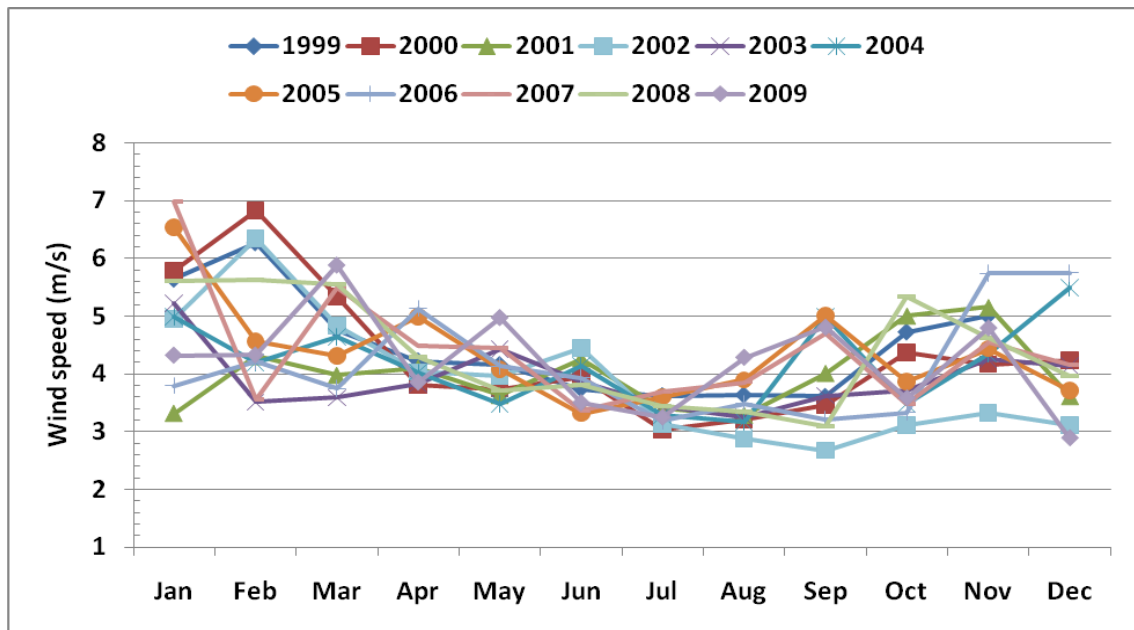


Figure 5-11: Graph of monthly mean wind speeds.

Table 5-1: Monthly mean wind speed (m/s) and yearly average wind speed (m/s) from Met office data (1999-2009) at Edinburgh GogarBank station.

Year	1999	2000	2001	2002	2003	2004	2005	2006	2007	2008	2009
Jan	5.64	5.79	3.31	4.95	5.22	4.99	6.53	3.80	6.98	5.61	4.32
Feb	6.27	6.83	4.30	6.35	3.51	4.20	4.56	4.22	3.56	5.63	4.32
Mar	4.76	5.33	3.97	4.84	3.59	4.64	4.31	3.75	5.50	5.55	5.88
Apr	4.22	3.80	4.10	4.03	3.82	4.03	4.99	5.13	4.49	4.30	3.85
May	4.16	3.74	3.63	3.96	4.42	3.48	4.07	4.13	4.46	3.70	4.97
Jun	3.74	3.95	4.26	4.45	3.88	4.14	3.31	3.93	3.37	3.80	3.50
Jul	3.62	3.04	3.40	3.12	3.44	3.28	3.60	3.19	3.69	3.44	3.24
Aug	3.63	3.21	3.28	2.87	3.25	3.17	3.90	3.48	3.86	3.35	4.28
Sep	3.61	3.46	4.01	2.67	3.62	4.99	5.01	3.21	4.71	3.10	4.81
Oct	4.72	4.37	5.00	3.11	3.71	3.48	3.86	3.33	3.48	5.34	3.58
Nov	5.00	4.16	5.15	3.32	4.25	4.34	4.43	5.74	4.55	4.61	4.79
Dec	5.59	4.23	3.61	3.11	4.14	5.50	3.71	5.75	4.16	3.96	2.89
Average	4.58	4.32	4.00	3.90	3.90	4.19	4.36	4.14	4.40	4.37	4.20

5.7 Standard deviation of wind speed

Standard deviation is another statistical tool which measures the dispersion or variability of the data set. This analysis provides information that how much data points are distant from mean value or each other. Thus, standard deviation is useful in describing the general characteristics of the data (Hamburg, 1985).

$$S = \sqrt{\frac{\sum (X - \bar{X})^2}{n-1}}$$

Equation 5-2

Standard deviation may serve as a measure of uncertainty. It has the same unit as the data points. If the standard deviation is high it shows that variation in the data is high or, in other words, uncertainty is high. Figure 5-12 shows monthly standard deviation of wind data. It shows that during summer time value of standard deviation is low while in winter the value is high. Table 5-2 shows the values of standard deviation in detail. It shows that the minimum value of standard deviation occurs in month of July 2000 i.e. 1.52 m/s and maximum value occurs in month of Feb 2008 i.e. 3.88 m/s.

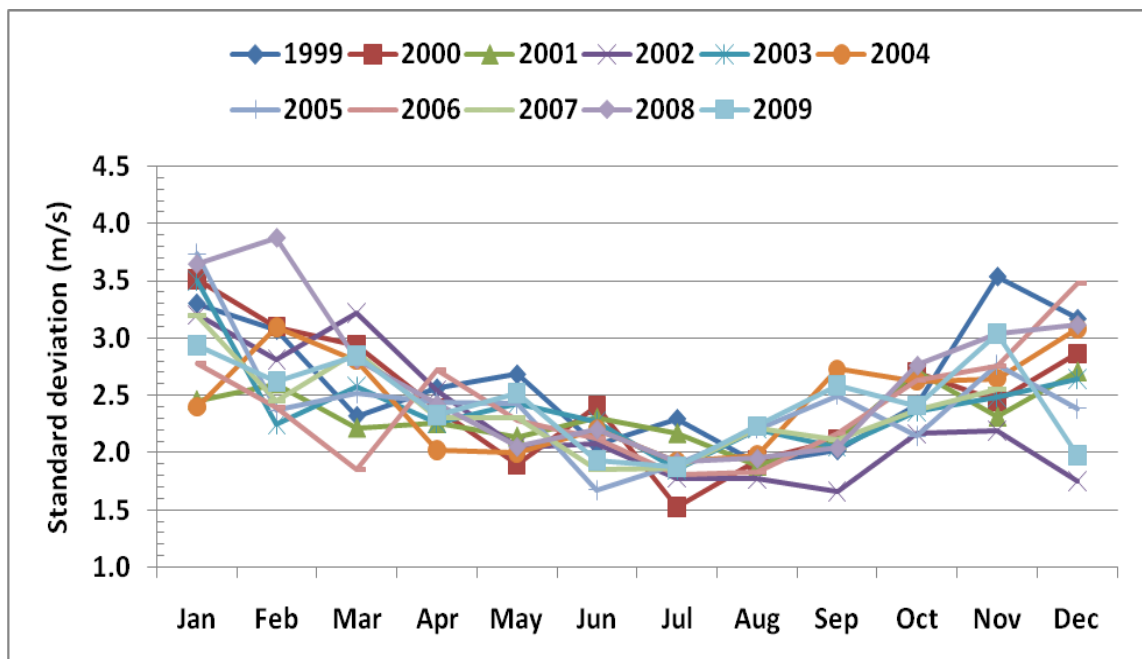


Figure 5-12: Graph of monthly wind speed standard deviation.

Table 5-2: Monthly standard deviation (m/s) and yearly average standard deviation (m/s) from Met office data (1999-2009) at Edinburgh Gogarbank station.

Year	1999	2000	2001	2002	2003	2004	2005	2006	2007	2008	2009
Jan	3.30	3.51	2.46	3.20	3.50	2.40	3.74	2.78	3.20	3.65	2.94
Feb	3.07	3.10	2.60	2.81	2.25	3.09	2.37	2.39	2.45	3.88	2.62
Mar	2.32	2.94	2.22	3.22	2.58	2.81	2.52	1.85	2.89	2.82	2.85
Apr	2.56	2.38	2.26	2.54	2.26	2.02	2.44	2.72	2.31	2.42	2.33
May	2.68	1.90	2.14	2.05	2.43	2.00	2.43	2.28	2.30	2.05	2.52
Jun	2.06	2.41	2.30	2.08	2.27	2.20	1.67	2.12	1.85	2.20	1.93
Jul	2.29	1.52	2.17	1.78	1.85	1.92	1.90	1.81	1.86	1.92	1.88
Aug	1.90	1.93	1.88	1.77	2.21	1.98	2.21	1.83	2.22	1.95	2.23
Sep	2.02	2.12	2.11	1.66	2.05	2.73	2.50	2.17	2.11	2.04	2.58
Oct	2.42	2.70	2.71	2.16	2.36	2.63	2.14	2.63	2.37	2.76	2.41
Nov	3.54	2.45	2.31	2.19	2.48	2.65	2.77	2.75	2.55	3.04	3.04
Dec	3.17	2.86	2.71	1.75	2.64	3.08	2.38	3.48	2.97	3.12	1.97
Average	2.61	2.49	2.32	2.27	2.41	2.46	2.42	2.40	2.42	2.65	2.44

5.8 Standard deviation vs. mean wind speed

In Figure 5-12 it is revealed that standard deviation is relatively high from October to March than in other months. By taking account of Figure 5-11 one can see that October to March normally have high mean wind speeds. It can, thus, be concluded at this initial stage that the months with high mean wind speed have high diversity in the data i.e. wind speed can be very high at one instance and very low in the other. On the other hand the months with low standard deviation have low variation in the data so one can rely on the mean value. It is interesting to note that although in Figure 5-11 mean wind speed of January 2006 and March 2006 are roughly the same, in Figure 5-12 their respective standard deviation values largely differ. It means that some months are more erratic in wind variation than others, irrespective of high or low mean speed.

To determine the correlation between mean wind speed and standard deviation a scatter chart was drawn as shown in Figure 5-13. This graph depicts nearly linear relation between mean wind speed and standard deviation.

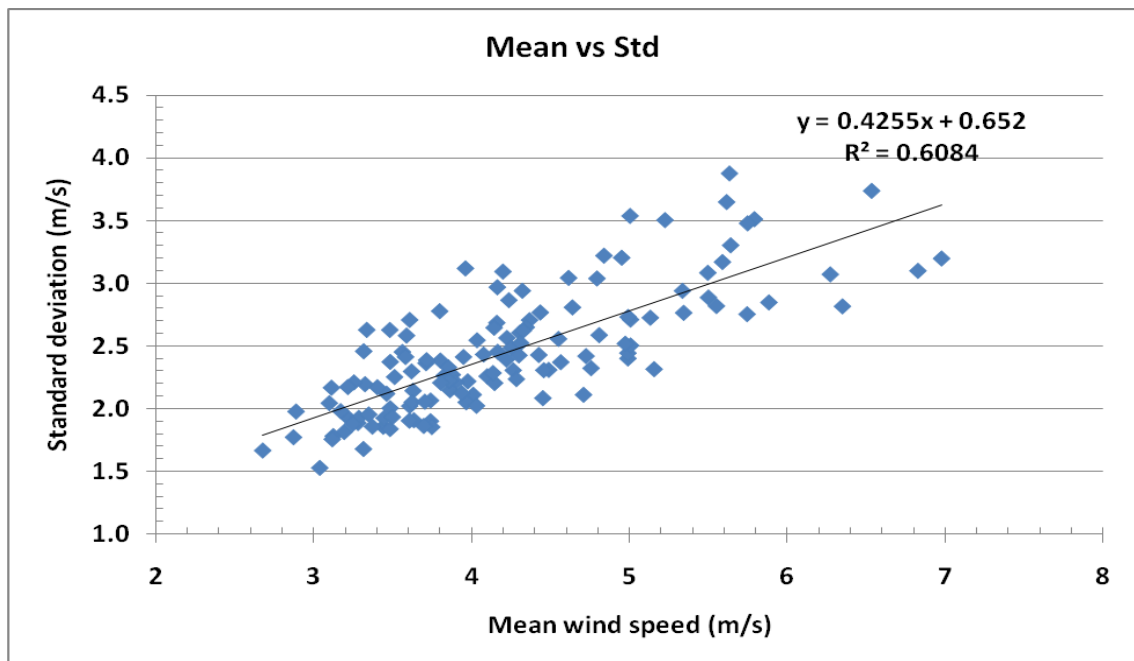


Figure 5-13: Monthly mean wind speed versus monthly standard deviation of eleven years of data.

5.9 Frequency distribution

Frequency distribution is a statistical technique that is used to summarize and describe the characteristics of a large amount of data. Frequency distribution analysis deals with cross-sectional data, which refers to data observed at a point in time (Hamburg, 1985). It is very difficult to generalize the prominent information contained by huge data (e.g. sample graph of 1999 wind speed is presented in Figure 5-14). It shows that fluctuation in wind speed is so high that it is very difficult to analyse the data.

A frequency distribution gives a clearer picture of data. It displays a frequency count and characteristic trend for the distinct values in a column. Table 5-3 provides the frequencies of different wind speeds which are divided into class tags, followed by class ranges. This frequency distribution table gives a very distinct idea about the wind speed pattern. It shows that the concentration of wind speed data resting between 1 and 10 m/s and rarely goes above 13 m/s. Last row in the Table 5-3 shows the available data, the value are not 100 % because of some unavailable data.

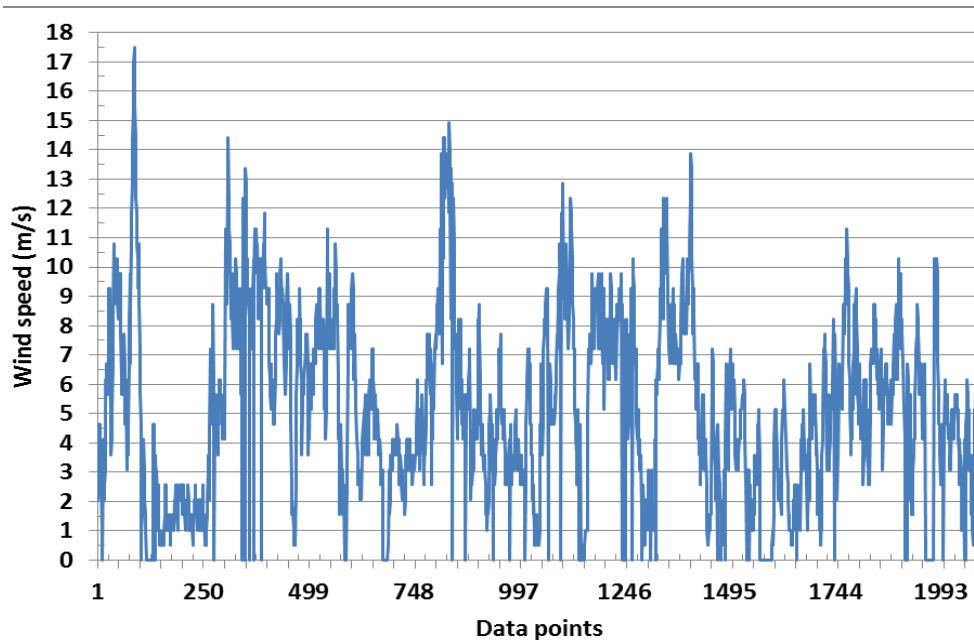


Figure 5-14: Sample plot of 1999 wind speed data.

Table 5-3: Wind speed frequency for different ranges of speed, %.

Wind speed (m/s)		Yearly data frequency										
Class Tag	Class Range	1999	2000	2001	2002	2003	2004	2005	2006	2007	2008	2009
0	0-0.49	0	0	0	0	0	0	0	0	0	0	0
1	0.50-1.49	882	980	1191	1314	1312	1079	894	1178	1005	1186	1114
2	1.50-2.49	1043	1203	1221	1416	1370	1193	1225	1210	1127	1235	1259
3	2.50-3.49	1172	1308	1227	1350	1354	1372	1310	1377	1190	1143	1283
4	3.50-4.49	1282	1281	1273	1176	1334	1339	1333	1313	1288	1216	1257
5	4.50-5.49	1059	1117	1185	1130	1063	1060	1123	1130	1249	1098	1085
6	5.50-6.49	790	812	964	862	770	845	927	888	946	876	869
7	6.50-7.49	677	551	634	551	603	597	745	622	712	640	648
8	7.50-8.49	497	350	381	306	397	439	457	378	497	429	495
9	8.50-9.49	318	255	193	181	230	283	273	282	290	289	271
10	9.50-10.49	188	175	102	103	131	193	170	145	158	192	133
11	10.50-11.49	117	137	49	74	61	89	73	77	96	131	87
12	11.50-12.49	66	44	19	46	25	48	48	50	67	94	47
13	12.50-13.49	48	32	6	25	10	13	24	16	25	49	24
14	13.50-14.49	34	25	2	6	5	4	22	9	12	28	4
15	14.50-15.49	5	17	2	5	3	1	5	6	4	13	2
16	15.50-16.49	1	10	0	2	2	0	4	2	0	5	0
17	16.50-17.49	3	1	0	1	0	0	2	2	0	0	0
18	17.50-18.49	0	0	0	1	0	0	0	2	0	0	0
19	18.50-19.49	0	0	0	0	0	0	0	0	0	0	0
20	19.50-20.49	0	0	0	1	0	0	0	0	0	0	0
21	20.50-21.49	0	0	0	1	0	0	0	0	0	0	0
Hours of data		8182	8298	8449	8551	8670	8555	8635	8687	8666	8624	8578
		93%	94%	96%	98%	99%	97%	99%	99%	99%	98%	98%

5.10 Probability distribution function (PDF)

Probability distribution is a technique which notifies the probability of each data point in the data set. Probability density function of wind speed is important in many wind energy applications (Carta, Ramirez & Velazquez, 2009).

Weibull is a special type of probability distribution which is widely used in wind resource assessments (Mathew, 2006) & (Manwell, McGowan & Rogers, 2009). Weibull distribution can describe the long-term records of wind speeds. It is given as (Jowder, 2009):

$$f(V) = \frac{k}{c} \left(\frac{V}{c} \right)^{k-1} e^{-\left(\frac{V}{c}\right)^k} \quad \text{Equation 5-3}$$

where k is the shape factor, c is the scale factor and V is the wind speed.

There are many methods to calculate Weibull parameters k and c (Mathew, 2006). Some test shows that approximated approach to find out the Weibull parameters predicts the wind speed and wind power more accurately than other approaches (Jowder, 2009).

In approximated method Weibull parameters can be calculated from the mean and standard deviation of the given wind speed data by the following equations:

$$k = \left(\frac{\sigma}{V_m} \right)^{-1.086} \quad (1 \leq k \leq 10) \quad \text{Equation 5-4}$$

$$c = \frac{V_m}{\Gamma\left(1 + \frac{1}{k}\right)} \quad \text{Equation 5-5}$$

Another distribution used in wind resource assessment is called Rayleigh distribution. It is a simplified form of Weibull distribution which has $k = 2$ and the value of c is calculated as follows:

$$c = \frac{2V_m}{\sqrt{\pi}} \quad \text{Equation 5-6}$$

Rayleigh distribution is used when there is no complete wind data available and only mean wind speed over a given time period is known (Mathew, 2006).

If wind speed distribution is unimodal (i.e. probability distribution which has a single mode) as in the case of Met office data, then superiority of the four mixture PDFs (i.e. mixture Gamma and Weibull distribution, mixture normal distribution, Mixture normal and Weibull distribution and Mixture Weibull distribution) and the maximum entropy principle (MEP) PDF (i.e. a probability distribution whose entropy is at least as great as that of all other members of a specified class of distributions) relative to the conventional Weibull PDF is not significant. While if the distribution is bimodal (i.e. probability distribution which has two modes) then all the mixture PDFs and the MEP PDF describes better wind characterizations than the Weibull PDF (Chang, 2010). Table 5-4 shows that Weibull shape factor varies between the values of 1.58 and 1.75, while scale factor varies between the values of 4.33 and 5.13. This implies that scale factor of Weibull varies more than shape factor throughout the data.

Table 5-4: Yearly PDF parameters of Weibull and Rayleigh distribution with goodness of fit value (R^2) to real data.

Year	Weibull		Rayleigh	Goodnees of fit with real data (R^2)	
	K shape factor	C scale factor	C scale factor	Weibull	Rayleigh
1999	1.71	5.13	5.16	0.99	0.96
2000	1.63	4.80	4.85	0.99	0.97
2001	1.74	4.49	4.52	0.96	0.93
2002	1.58	4.33	4.38	0.99	0.93
2003	1.63	4.37	4.41	0.99	0.93
2004	1.69	4.70	4.73	0.99	0.96
2005	1.75	4.89	4.92	0.99	0.98
2006	1.66	4.62	4.66	0.99	0.95
2007	1.74	4.94	4.96	0.98	0.96
2008	1.58	4.87	4.93	0.98	0.91
2009	1.69	4.70	4.74	0.99	0.95

Figure 5-16 shows that each year's wind histogram has one hump i.e. data is unimodal and that hump lies between 2 to 4 m/s wind speed range. The plots in Figure 5-16 compare the probability distribution drawn from real data with Weibull and Rayleigh distribution. Results indicate that Weibull distribution is closer to the real data distribution than Rayleigh distribution. It is obvious as

Weibull uses more information from data than Rayleigh distribution (i.e. standard deviation).

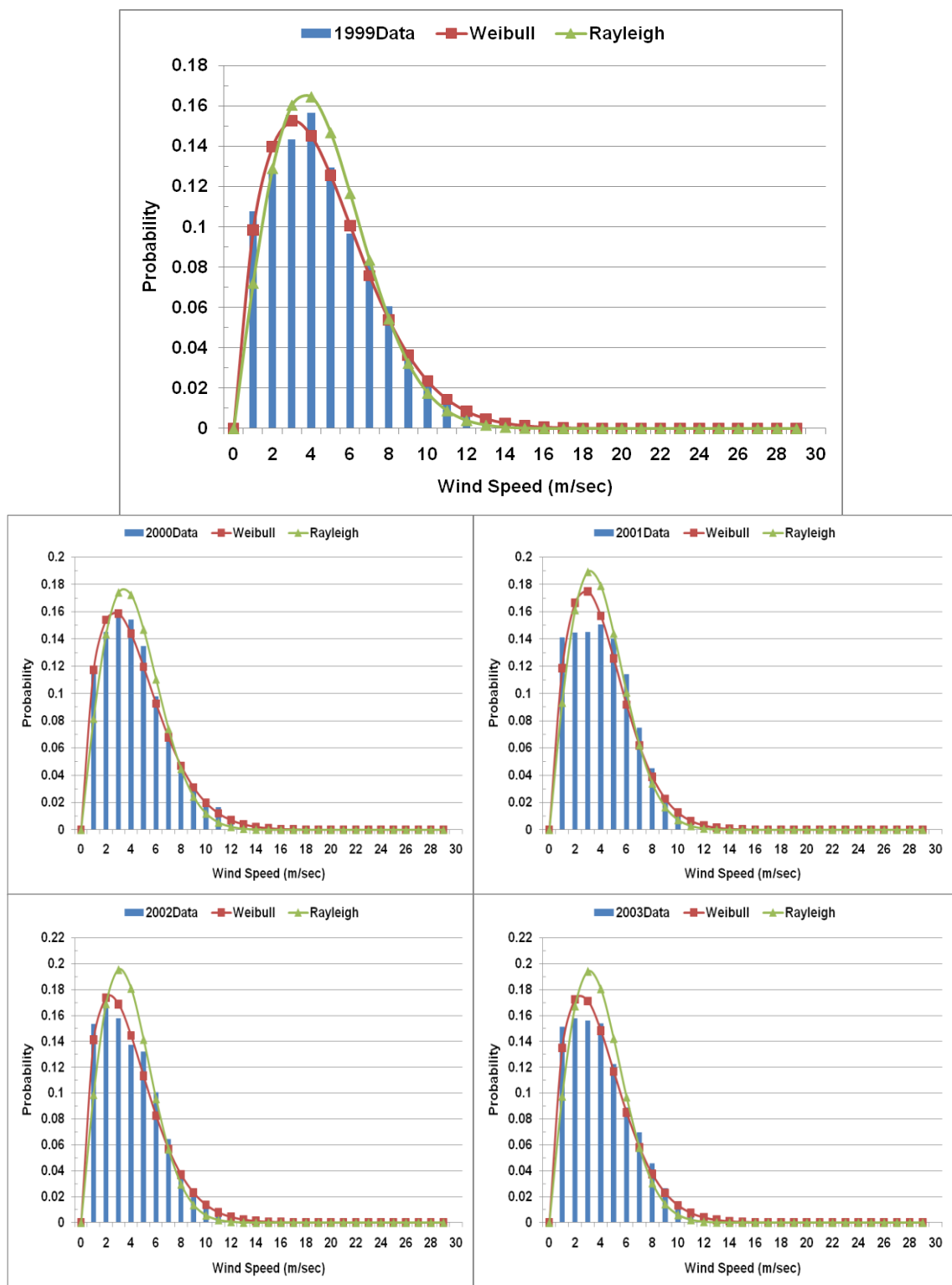


Figure 5-15: Comparison between probability distribution of real data, Weibull distribution and Rayleigh distribution for 1999 to 2009 (continue).

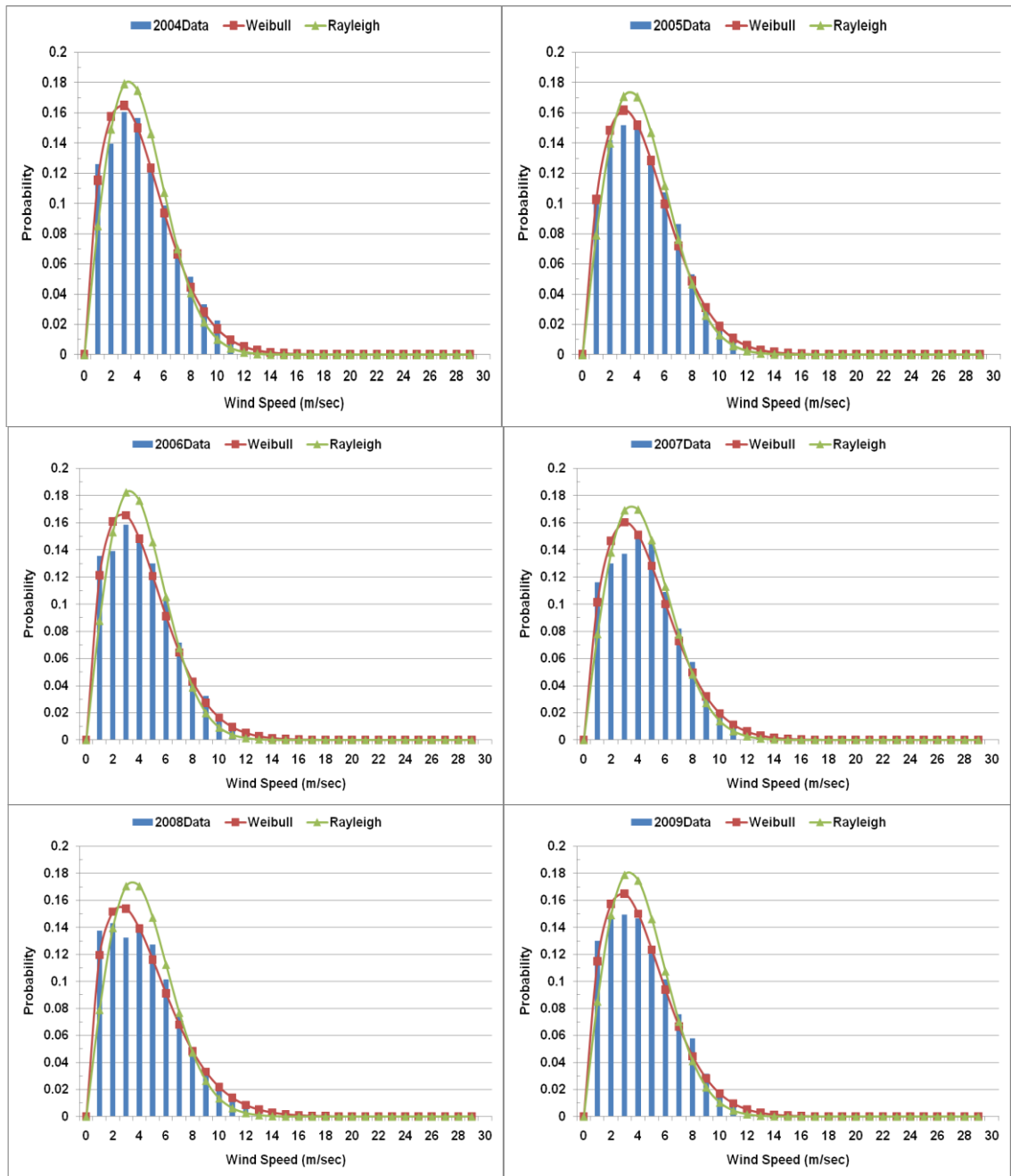


Figure 5-16: Comparison between probability distribution of real data, Weibull distribution and Rayleigh distribution for 1999 to 2009.

5.11 Cumulative distribution function (CDF)

Cumulative distribution function indicates the fraction of time for which the wind is at a given velocity. It can be drawn by accumulating the probability of wind speed in ascending order. CDF is the integral of the probability density function;

if $F(V)$ is the CDF of a given data then for Weibull distribution CDF is evaluated as in the equation below (Mathew, 2006).

$$F(V) = \int_0^{\infty} f(V) dV = 1 - e^{-\left(\frac{V}{c}\right)^k} \quad \text{Equation 5-7}$$

In this calculation Weibull CDF shows that 40% wind speed is lower than 3 m/s and only a friction of wind speed data occurs above 10 m/s. Figure 5-18 compares the cumulative distribution function drawn from real data with Weibull and Rayleigh distribution. It shows that Weibull CDF is closer to the real data distribution than Rayleigh CDF.

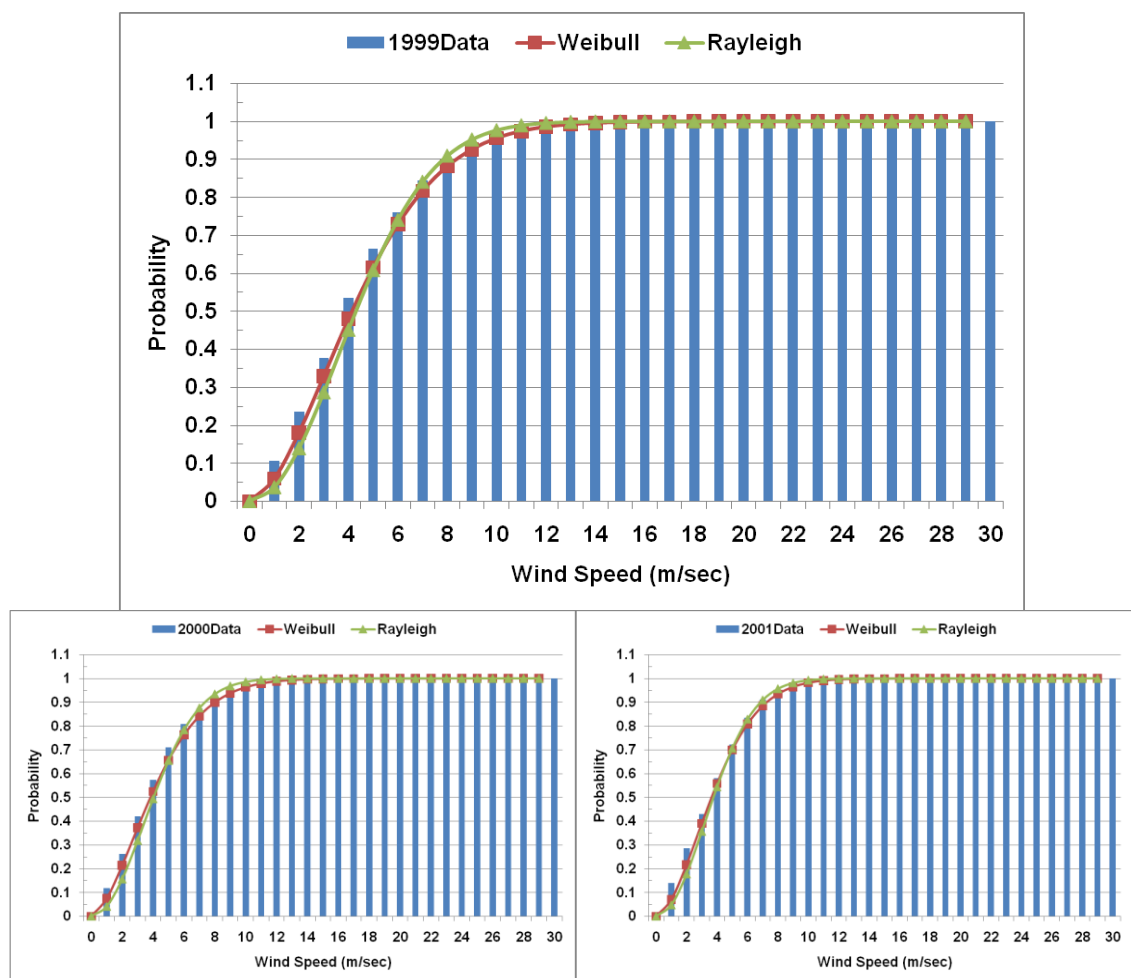


Figure 5-17: Comparison between cumulative distribution curves of real data, Weibull distribution and Rayleigh distribution for 1999-2009 (continue).

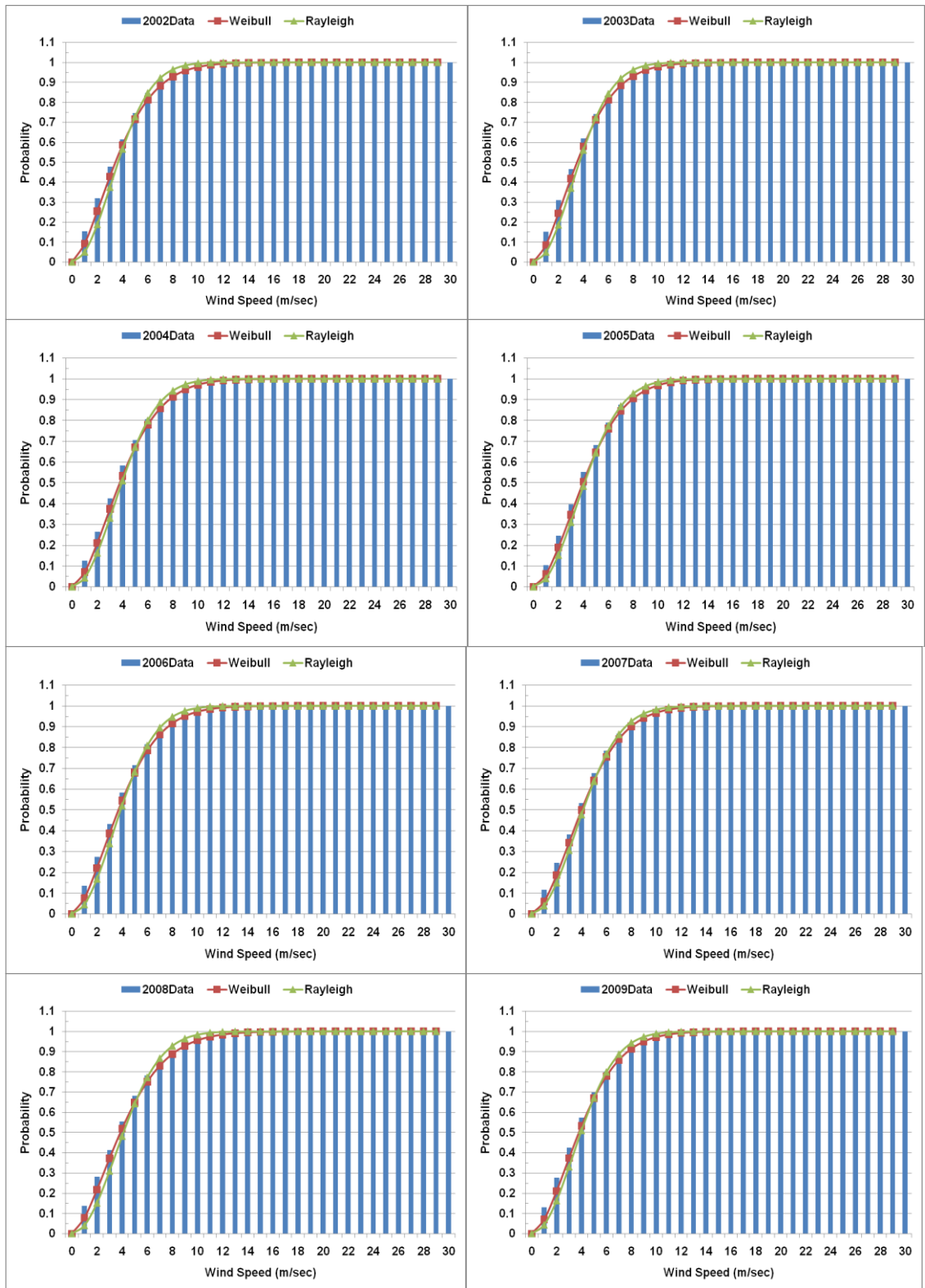


Figure 5-18: Comparison between cumulative distribution curves of real data, Weibull distribution and Rayleigh distribution for 1999-2009.

5.12 Velocity duration curve

Velocity duration curve is normally used to compare the wind potential of different sites (Manwell, McGowan & Rogers, 2009). But it is also useful in getting an approximate idea about the nature of wind regime with the change of time. The velocity duration curve graph has wind speed on the y-axis and the number of hours in the year for which the speed equals or exceeds each particular value on the x-axis as shown in Figure 5-19. Figure 5-19A shows yearly wind duration curve for 1999 to 2009 and it demonstrates that in all eleven years hourly wind duration is correlated to each other, except curvature difference 0 to 2000 hours (on x-axis), which shows that in some years, number of hours are more than others for higher wind speed. In the graph flatter curve indicates more constant wind speeds while steeper curve suggests more irregular wind regime. The termination of curves on x-axis at different points reveals that each annual data set contained different number of available hours (also shown in Table 5-3). Figure 5-19B shows three years velocity duration curve, one is of year 1999 which has higher annual mean wind speed (i.e. 4.58 m/s) and the other two are of 2002 and 2003 having lower annual mean speed (i.e. 3.90 m/s). Figure 5-19B shows that the data with higher annual mean wind speed has steeper curve than the data with lower mean wind speed. Velocity duration curve in Figure 5-19 reveals that about 5000 annual data hour's i.e. 57% of the total number of hours (i.e. 8760) available in a year have mean wind speed equal or greater than 4 m/s. This is a positive indicator of conformance from a wind energy resource perspective but cannot be deemed as excellent.

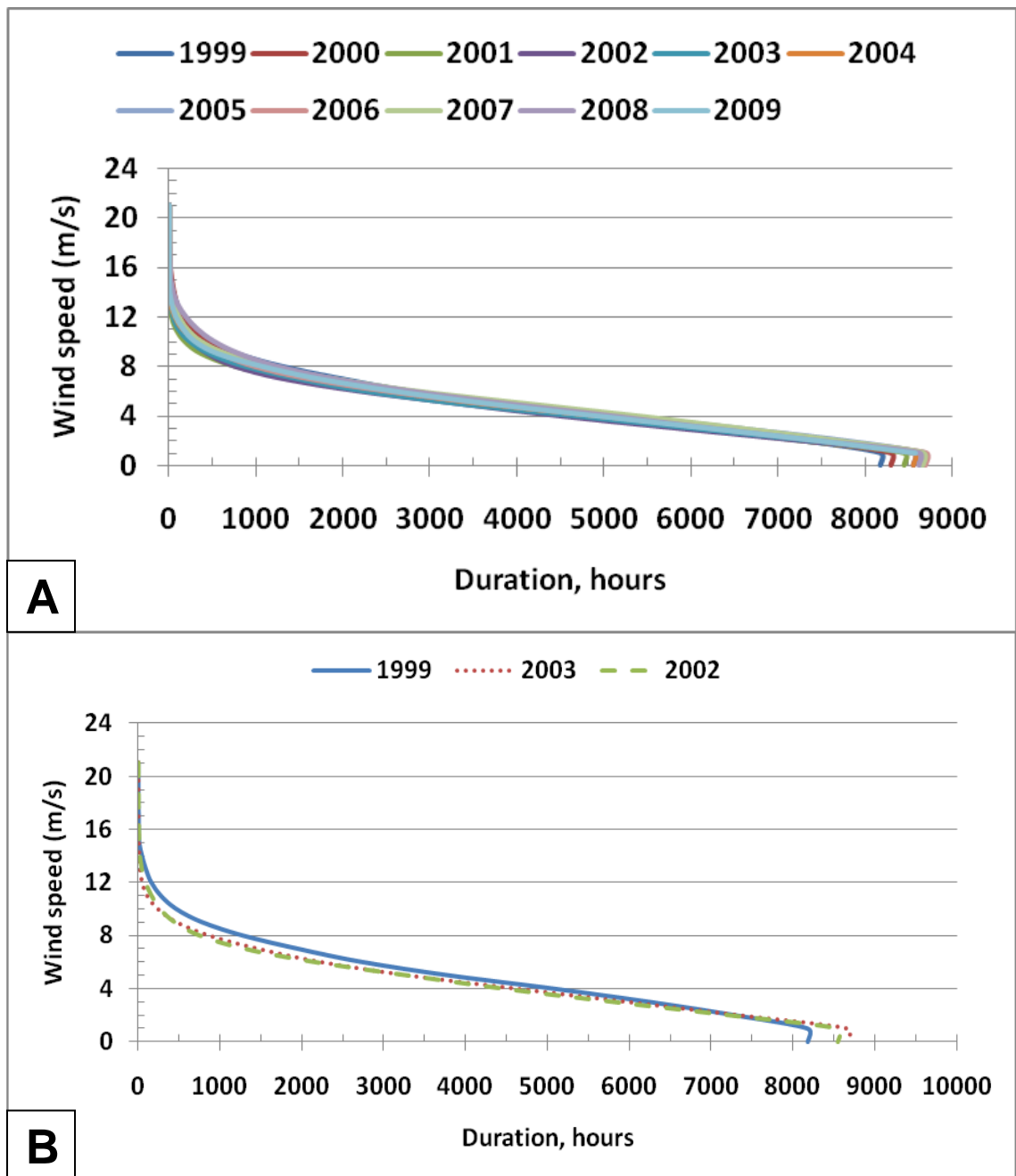


Figure 5-19: Velocity duration curve **A**: Velocity duration curve from 1999 to 2009. **B**: Velocity duration curve of 1999, 2002 and 2003.

5.13 Vertical wind profile

The flow of the wind above the ground is slowed down by frictional resistance presented by the earth's surface (boundary layer effect) (Shaw, Doran & Coulter, 2005). This resistance is caused either by the topography of the area itself or due to vegetations, buildings and other structures present over the

ground. Theoretically, the velocity of wind at ground level should be zero. Velocity increases with height up to a certain elevation and the rate at which the velocity increases with height depends on the roughness of the terrain (Moraes *et al.* 2005). Dense vegetations like plantations, forests, and bushes are significantly effective in slowing down the wind speed. Level and smooth terrains do not have much effect on the wind speed (Mathew, 2006). The variation in wind speed with height is important for both the assessment of wind resources and the design of wind turbines (Manwell, McGowan & Rogers, 2009). Generally wind data collection is done at a height of 10m as in the case of Met office data. But the height of the WEC can be selected as appropriate to achieve better performance.

There are two mathematical models or laws generally used to calculate the vertical wind profile.

5.13.1 Log law

The first one is called the wind profile log law; it is driven from boundary layer flow in fluid mechanics and in atmospheric research. It is based on a combination of theoretical and empirical research (Panofsky & Press, 1962). Log law states that wind speed increases with height in a logarithmic pattern. If the wind data is available at a reference height Z_{ref} and the roughness height is Z_0 , then the velocity at a height Z is given by Equation 5-8.

$$V(Z) = V(Z_{ref}) \frac{\ln\left(\frac{Z}{Z_0}\right)}{\ln\left(\frac{Z_{ref}}{Z_0}\right)} \quad \text{Equation 5-8}$$

The roughness of a particular surface area is determined by the size and distribution of the roughness elements it contains. Roughness is the height where the mean wind speed becomes zero (Tieleman, 2003). In the European Wind Atlas the different terrains have been divided into four types, each characterized by its roughness elements. Table 5-5 indicates the relation between roughness length, terrain surface characteristics and roughness class

given in the European Wind Atlas. Table 5-5 is used as a guideline for assigning roughness length values.

Table 5-5: Typical roughness lengths for different terrain surface characteristics according to the European Wind Atlas based on ISES, 2007.

Z_0 [m]	Terrain surface characteristics	Roughness class
1.00	city	
0.80	forest	
0.50	suburbs	
0.40		3 (0.40 m)
0.30	shelter belts	
0.20	many trees and/or bushes	
0.10	farmland with closed appearance	2 (0.10 m)
0.05	farmland with open appearance	
0.03	farmland with very few buildings/trees	1 (0.03 m)
0.02	airport areas with buildings and trees	
0.01	airport runway areas	
0.008	mown grass	
0.005	bare soil (smooth)	
0.001	snow surfaces (smooth)	
0.0003	sand surfaces (smooth)	
0.0002		0 (0.0002 m)
0.0001	water areas (lakes, fjords, calm sea)	

5.13.2 Power law

The second approach is wind profile power law relationship; it is often used as a substitute for the log wind profile when surface roughness or stability information is not available. Unlike the log law, the power law has no physical basis. The wind profile power law relationship is:

$$V(Z) = V(Z_{ref}) \left(\frac{Z}{Z_{ref}} \right)^\alpha \quad \text{Equation 5-9}$$

where, $V(Z)$ is the wind speed at required height Z , $V(Z_{ref})$ is the reference wind speed at reference height Z_{ref} and α is the power law exponent. The power law exponent (α) varies with such parameters as elevation, time of day, season, nature of the terrain, wind speed, temperature, and various thermal and mechanical mixing parameters.

Both approaches are subjected to uncertainty caused by the variables and complex nature of turbulent flows (Hiester & Pennell, 1981). To overcome the problem, the simplest solution is to classify the land-type around the measuring station following a wind-sector division and assign the roughness length value as parameterised in literature (Pielke, 2002).

Met office weather station location area can be classified as land with few trees as shown in Figure 5-4 and the roughness height is estimated to be 0.03 m. By using yearly mean wind speed as a reference wind speed $V(Z_{ref})$, reference height (Z_{ref}) 10 m and the surface roughness (Z_0) 0.03 m in the log law Equation 5-8, vertical wind profile for eleven years was calculated as shown in Figure 5-20. It shows that at 100 m height, yearly mean wind speed can be found between 5.5 m/s to 6.5 m/s (approx).

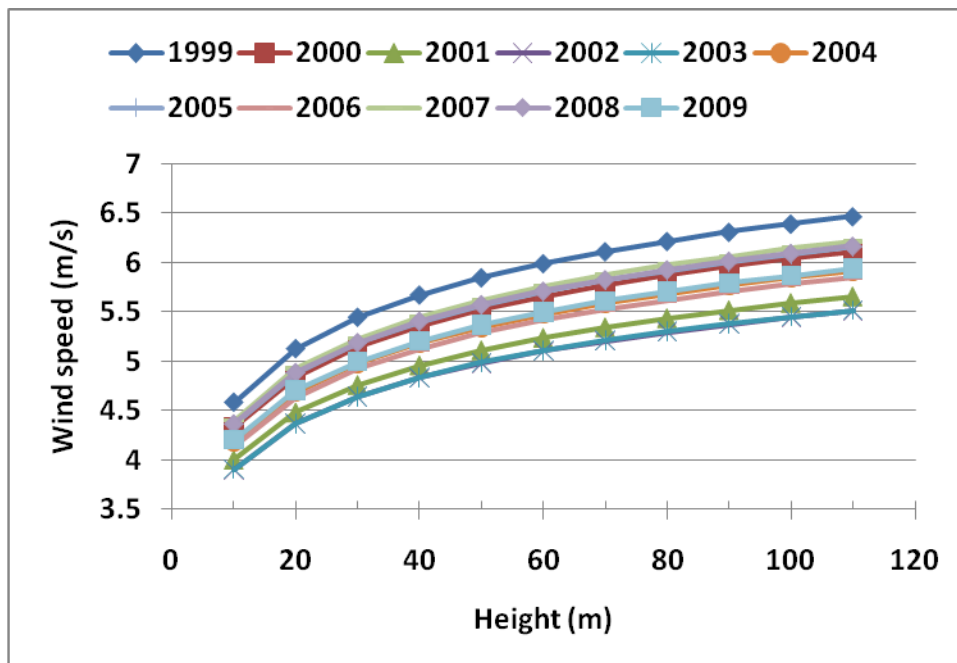


Figure 5-20: Logarithmic profile of 1999 to 2009 with surface roughness (Z_0) 0.03 m.

Eleven years average yearly mean wind speed is 4.21 m/s; it was used to investigate the effect of different surface roughness values from 0.02 m to 1 m as shown in Figure 5-21. It was found that as the surface roughness increases the change in the vertical wind profile increases as well.

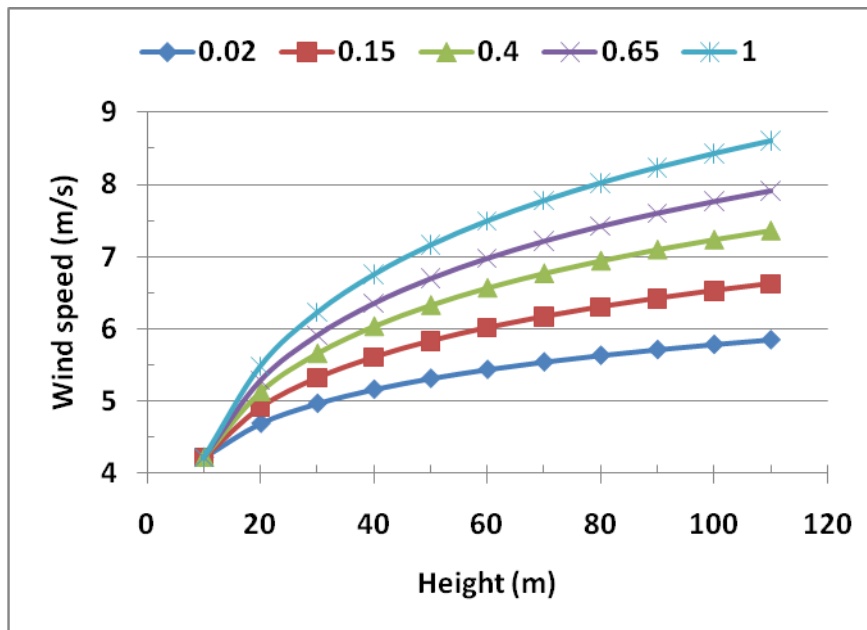


Figure 5-21: Logarithmic profile of eleven years mean wind speed for different surface roughnesses.

5.14 Diurnal variation in wind

Diurnal type of wind speed variation is due to differential heating of the earth's surface during the everyday radiation cycle. A usual diurnal variation is an increase in wind speed during the day with the wind speed lowest during the hours from midnight to sunrise. To check diurnal wind variation a graph between the hour of the day and hourly mean wind speed was drawn for March 2009 as shown in Figure 5-22. It shows that there is a change from 10th hour of a day to 20th hour of a day (on x-axis), but scattering of wind speed data from 0-12 m/s in whole month makes it difficult to judge the significance of the diurnal variation. Even it is not very clear by plotting hourly mean wind speed of individual days, against the hour of the day as shown in Figure 5-23.

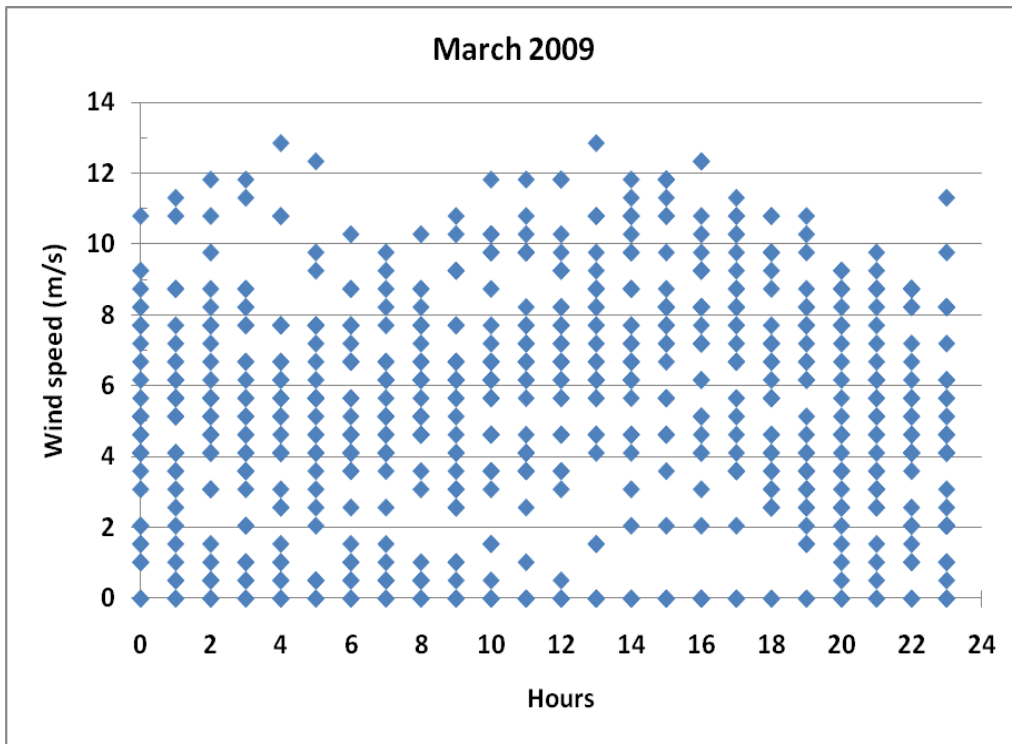


Figure 5-22: Graph between hour of the day and hourly mean wind speed for March 2009.

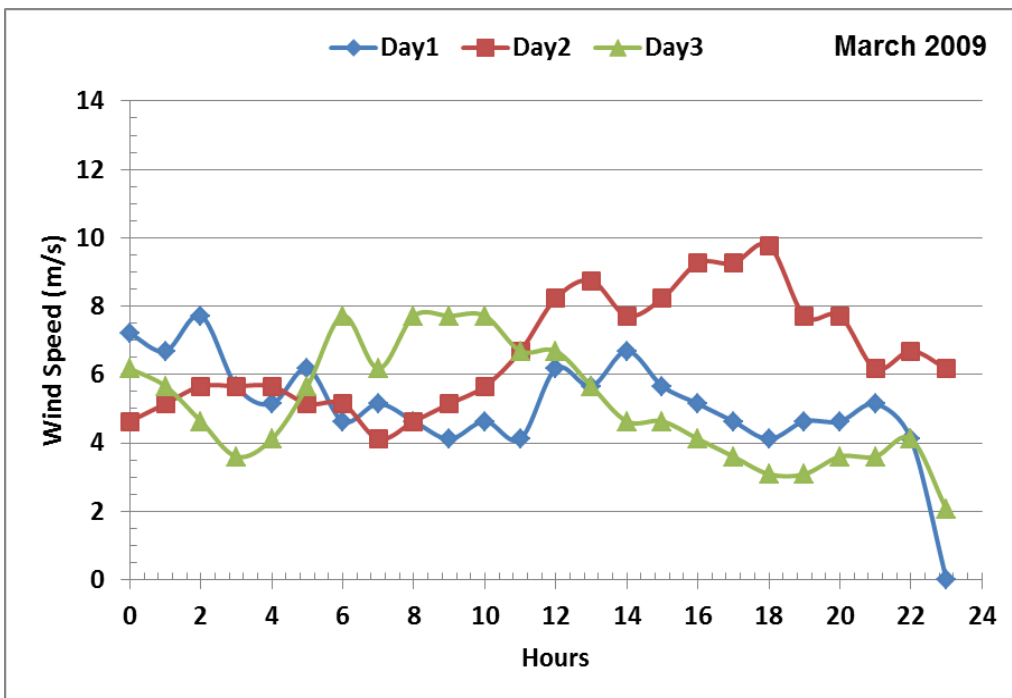


Figure 5-23: Graph between hour of the day and hourly mean wind speed for 3 days of March 2009.

To elaborate the diurnal wind speed variation hourly wind speed data has been used to take average for each hour of a day (i.e. the average of every hour of the day up to a month) as shown in Figure 5-25. In Figure 5-25 graph titled 2009 shows that there is a noticeable trend of increment in wind speed from 7th hour to 20th hour. And it is very significant in March 2009 in which average wind speed increases from 5 m/s to about 8 m/s. The wind speed increases from 7th hour to 15th hour and then starts decreasing settling down on 20th hour. In year 2009 the second significant diurnal variation appears in the month of May, in which wind speed starts increasing from 3.5 m/s on 6th hour up to 6.7 m/s in 14th hour and then starts decreasing until 2nd hour. In 2009 remaining month's diurnal variation amplitude is very low and the month of November and December has minimum change in diurnal wind speed. It shows that the largest diurnal changes generally occur in spring and summer, and the smallest in winter.

In Figure 5-25 by looking at the other years diurnal wind variation, it was found that there is a noteworthy uncertainty in diurnal wind variation. For example in the month of February there was a significant diurnal effect in 2008 but in 2001 it was very low or almost nil. Moreover, the month of January normally does not have diurnal effect; either it has high wind (i.e. 2003, 2005, 2007 and 2008) or low wind. However, in 2002 and 2004 it has significant diurnal effect. It may be because of the atmospheric temperature differences from one year to another, which will further be discussed in next section.

To check diurnal effect on wind direction, hourly wind direction data was plotted against hours of the day for March 2009 (which has a significant diurnal effect on wind speed) as shown in Figure 5-26.

It is found that there is no strong evidence of diurnal effect on wind direction because wind consistently blows from wind ward direction (i.e. south west), such findings also reflect on the wind rose graphs in Figure 5-10. It could be due to the elevation of the location of Met office weather station as shown in Figure 5-9. Figure 5-9 shows that weather station is in the bottom of the higher elevation area on the wind ward direction and has shadow of the abrupt higher

elevation on the lee ward direction. This consistently pointing to the prevailing wind direction i.e. south-west

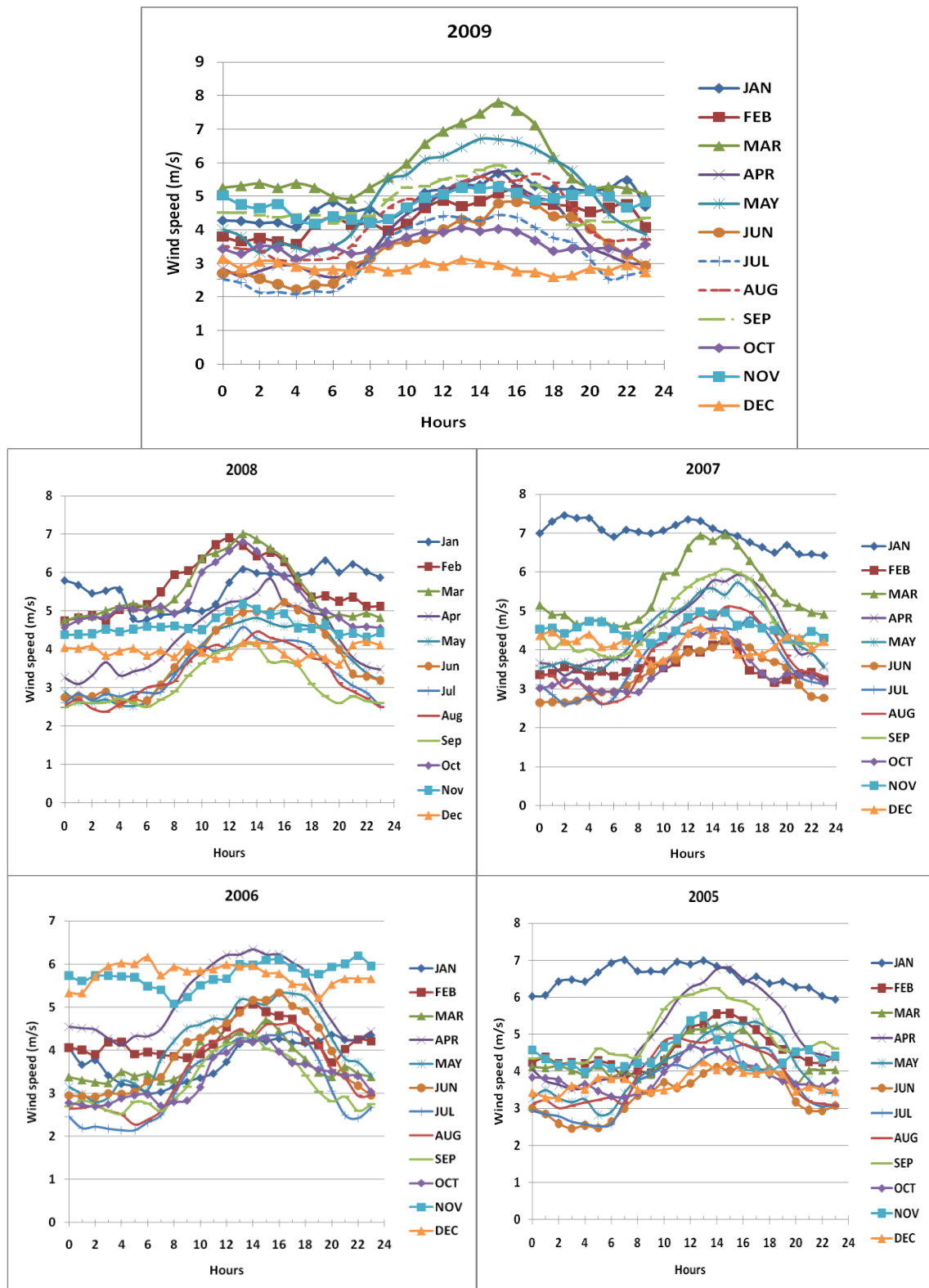


Figure 5-24: Graph of monthly diurnal wind speed for 1999 to 2009 (continue).

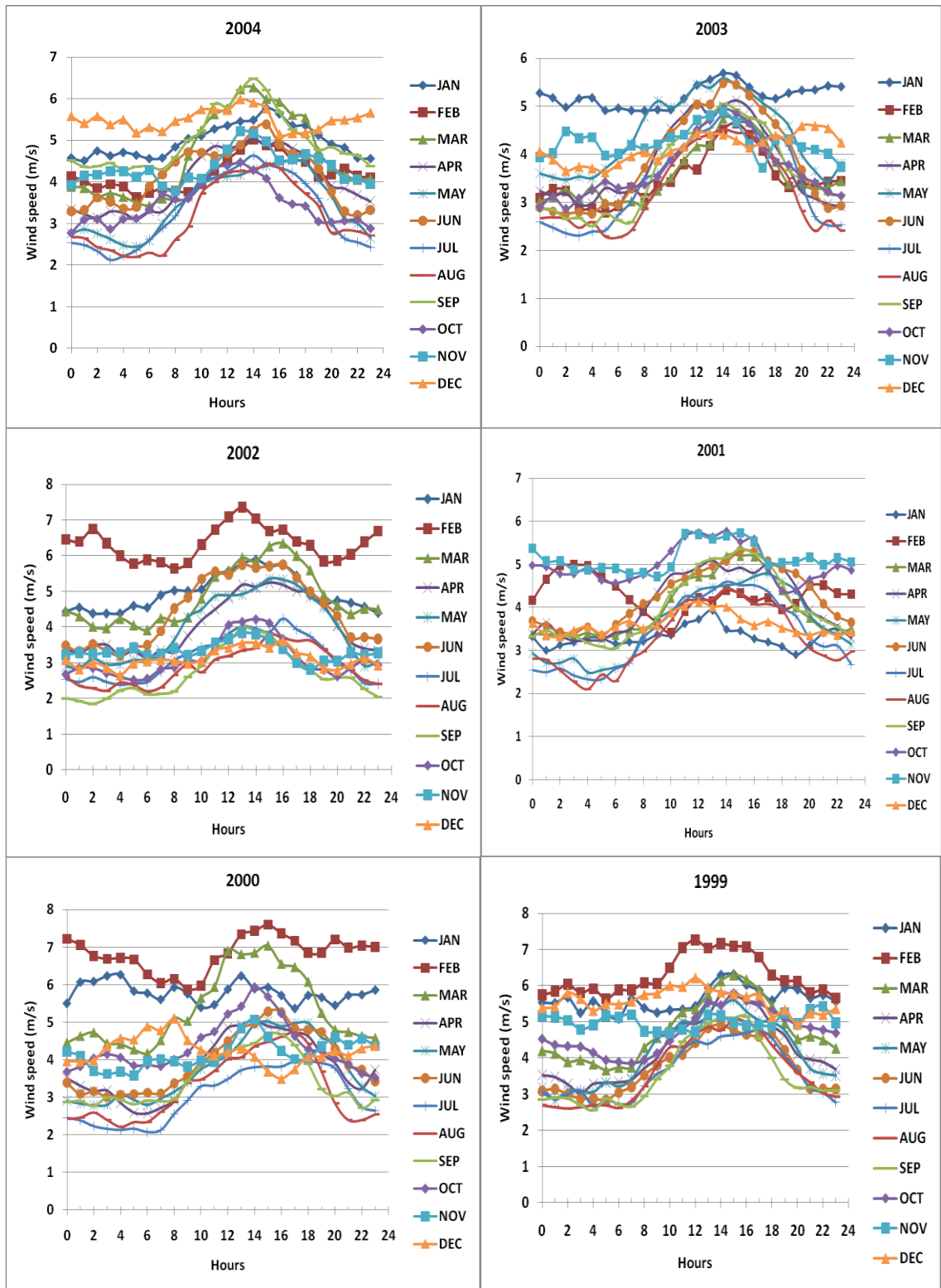


Figure 5-25: Graph of monthly diurnal wind speed for 1999 to 2009.

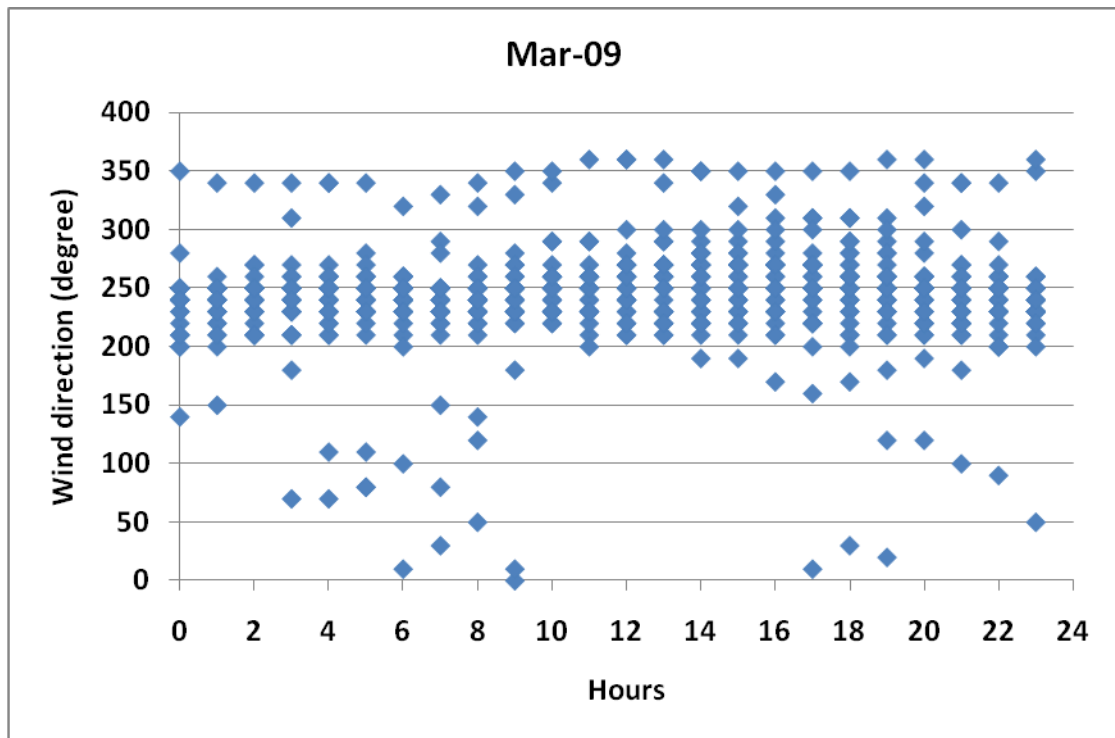


Figure 5-26: Graph of hourly wind direction data against hours of the day for March 2009.

5.15 Relation between wind speed and meteorological parameters

Since wind is a part of meteorological environment, other elements within this environment also affect it. In fact other meteorological parameters drive the wind, depending on the location of the site. The influence of each of these forces on atmospheric wind systems varies in view of the scale of motion considered.

5.15.1 Temperature

Edinburgh experiences an island's irregularity of weather, but it rarely has extreme weather this is because the city has sea on its one edge and elevated mountains on the other, this combination minimizes any large variations in temperature or extremes of climate. By drawing monthly minimum, maximum and mean temperature for year 2009 (as shown in

Figure 5-27) it is found that in summer maximum temperature was raised up to 28.7 °C with the minimum of 6.3 °C and mean 15 °C. In winters maximum

temperature went up to 10.8 °C with minimum of -10.6 °C and mean 1.8 °C. Temperature went below zero in six months of 2009.

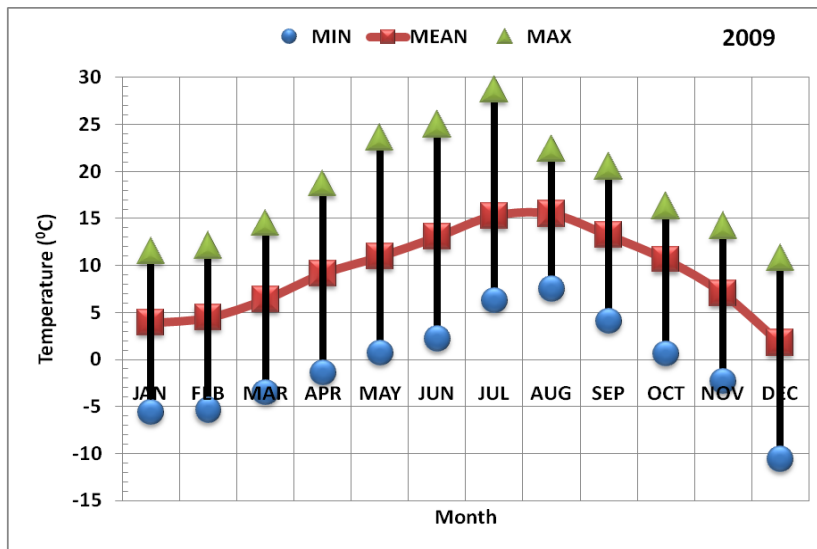


Figure 5-27: Monthly minimum, maximum and mean temperature for year 2009.

To determine the relation between temperature and wind speed graphs were plotted between daily mean wind speed and temperature for Jan 2009 and Mar 2009 as shown in Figure 5-28. But there is no strong relation or agreement found between daily mean wind speed and temperature.

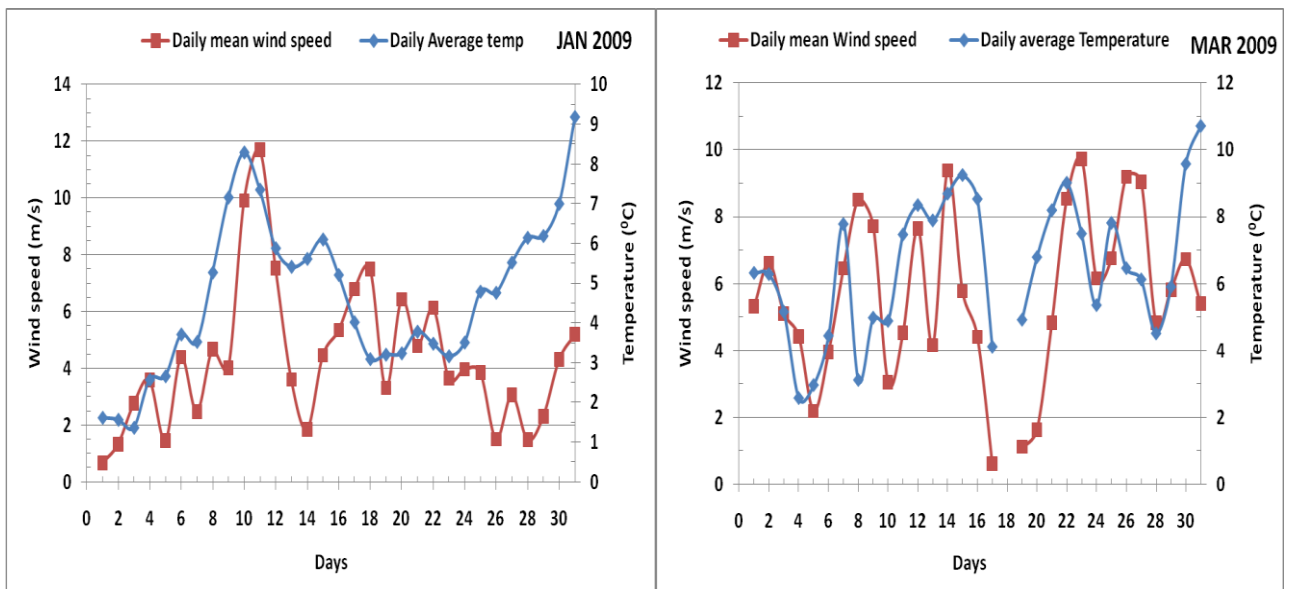


Figure 5-28: Graph of daily mean wind speed and temperature against days.

The solar radiation absorbed by the atmosphere and the heat emitted by the earth increase the air temperature during the day hours. To find out diurnal temperature variation, hourly mean temperature data was drawn against hours of the day for March 2009 as shown in Figure 5-29. Figure 5-29 shows that the atmospheric temperature increases during the day hours and reaches a maximum at 14th hour of the day then decreases until 21st hour of the day. This pattern appears similar as diurnal wind speed pattern as shown in Figure 5-25.

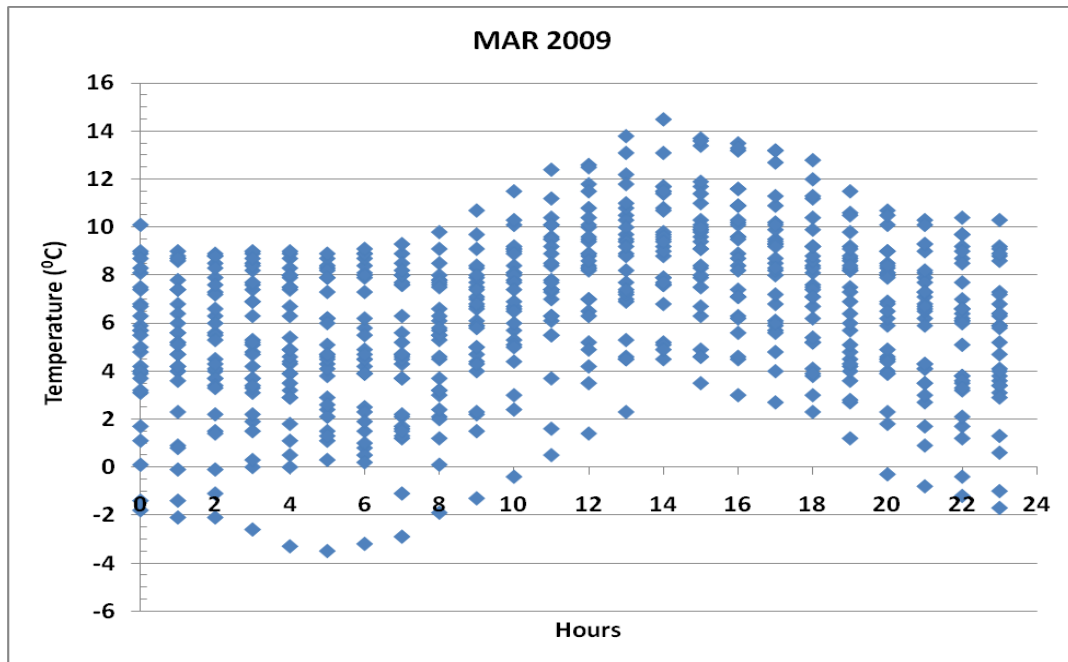


Figure 5-29: Graph of hourly mean temperature against hours of the day for March 2009.

To elaborate the diurnal temperature variation, hourly temperature data was used to take average for each hour of a day (i.e. the average of every hour of the day up to a month) as shown in Figure 5-30. It shows that there is a significant diurnal variation in temperature. Temperature rose during the day time when sun is high in the sky and went down in the night. The height and width of amplified temperature wave is longer in summer time when days are longer than winter. The minimum diurnal variation occurs in the month of December and January when days are shorter and temperature is lower than other months.

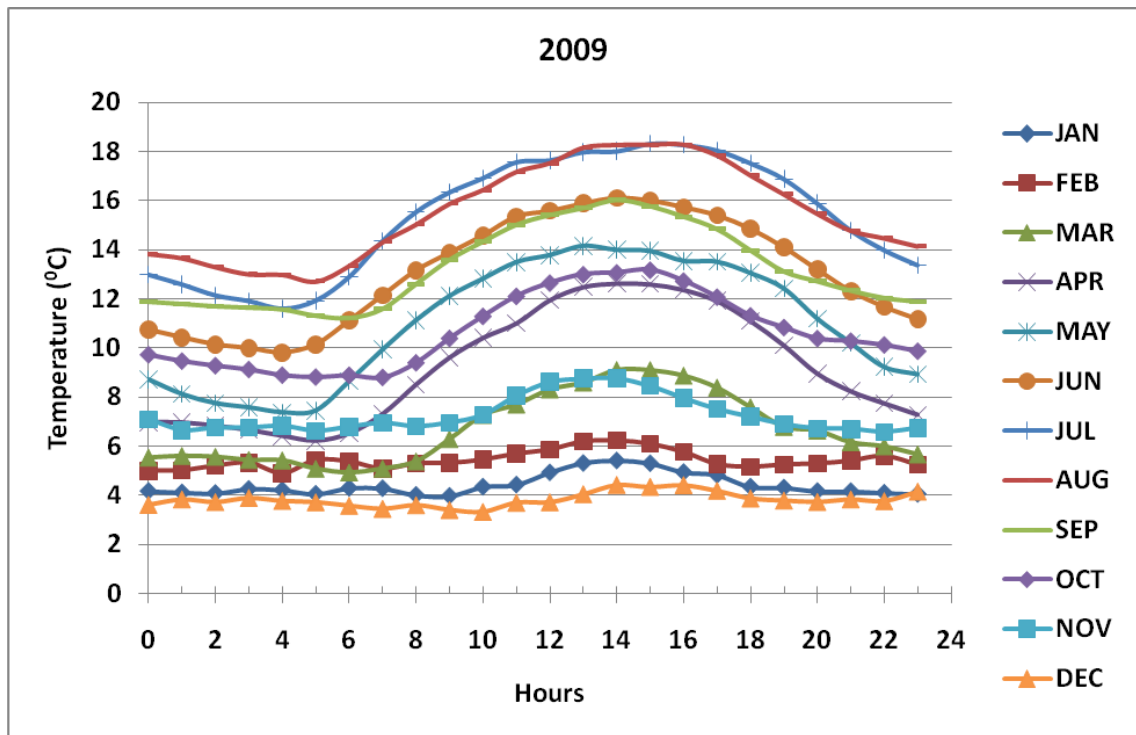


Figure 5-30: Monthly diurnal temperature variation for 2009.

To evaluate the relation between diurnal wind speed variation and diurnal temperature variation, the month of March was selected, as it witnessed highest diurnal wind speed variation in 2009 (as shown in Figure 5-25). One day hourly data of wind speed and temperature is plotted against hours of the day as shown in Figure 5-31. There are some evidences in Figure 5-31 that show the diurnal wind speed varies with diurnal temperature variation. To ascertain the overall relation between diurnal wind speed and temperature, average wind speed and temperature for each hour for the month of March 2009 was taken and plotted against hours as shown in Figure 5-32. Figure 5-32 shows that there is a very strong relation between hourly mean diurnal wind speed and hourly mean diurnal temperature. To further reaffirm the relation between diurnal wind speed and temperature, month of December was selected as it witnessed lowest diurnal wind speed variation in year 2009 (as shown in Figure 5-25). Figure 5-33 shows that in December 2009, the relation between the two parameters is less appearance compared to March 2009 data. This could be explained by the unsettled weather during the winter months.

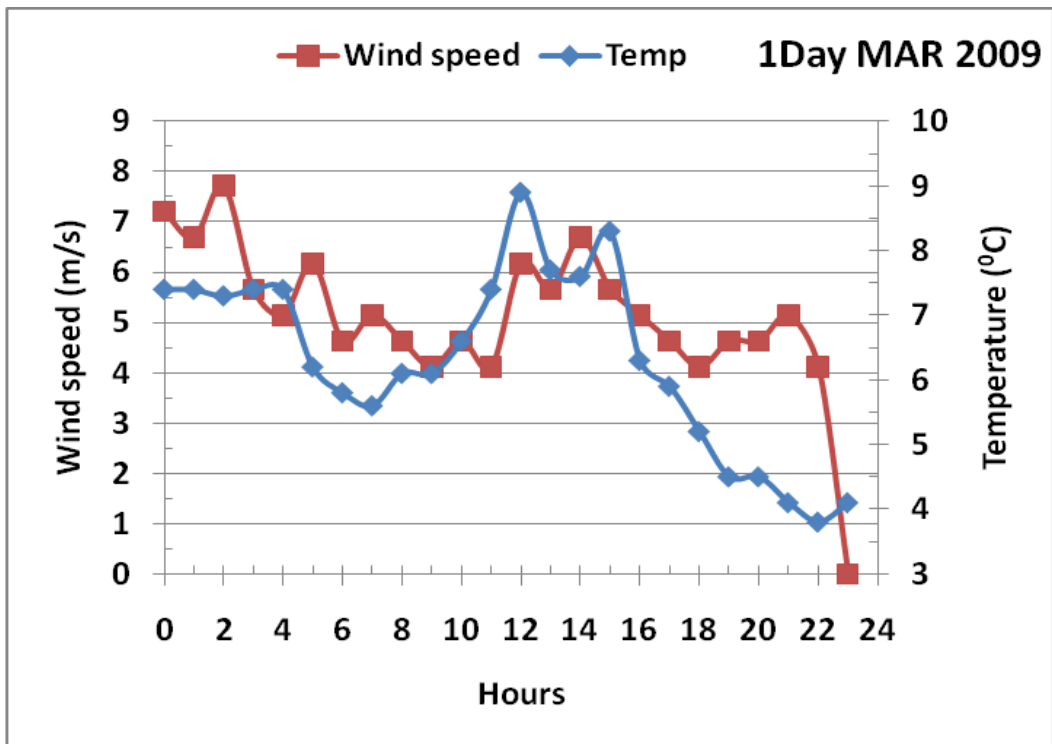


Figure 5-31: Graph of one day (i.e. 24 hours) hourly wind speed and temperature for March 2009.

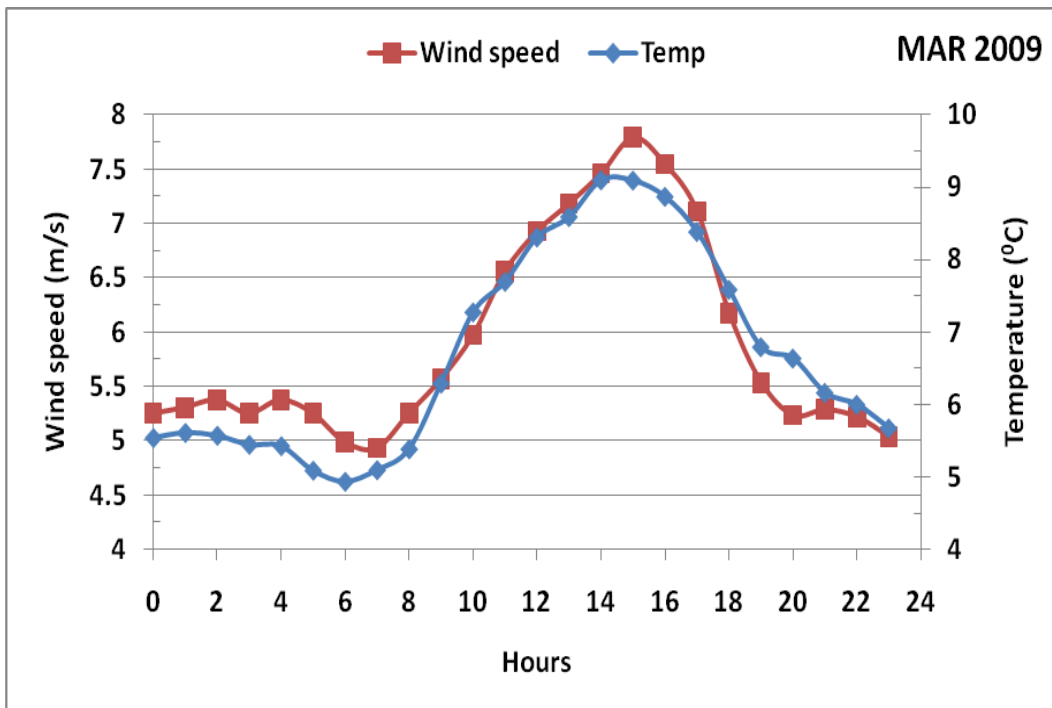


Figure 5-32: Graph of average hourly wind speed and temperature for March 2009.

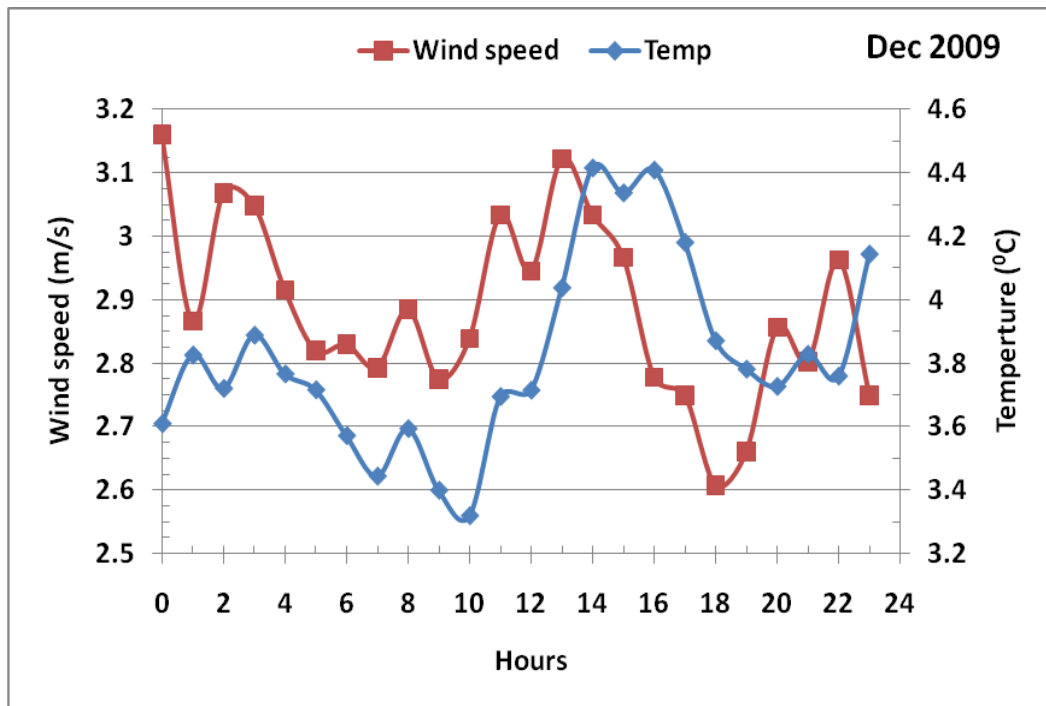


Figure 5-33: Graph of average hourly wind speed and temperature for December 2009.

To establish a relation between diurnal wind speed and diurnal temperature the coefficient of correlation was calculated between diurnal hourly average mean wind speed and diurnal hourly average mean temperature for eleven years (i.e. 1999 to 2009) as shown Table 5-6. It was found that there is a very strong positive correlation between monthly mean diurnal wind speed and temperature in all eleven years except a few months each year. To evaluate the degree of correlation, a graph of coefficient of correlation was drawn against months for eleven years as shown in Figure 5-34. Figure 5-34 shows that there is a very strong correlation (i.e. correlation coefficient more than 0.80) from March to October in all eleven years while, in the months of January, February, November and December the correlation is weaker as well as variable.

It can be concluded that in summer, when days are longer and diurnal temperature variation is higher, wind is driven in correlation with temperature variation and in winter when days are shorter and temperature variations are lower, correlation between the diurnal wind speed and temperature becomes weaker and unpredictable.

Table 5-6: Correlation coefficient between monthly mean diurnal temperature and wind speed.

Year	JAN	FEB	MAR	APR	MAY	JUN	JUL	AUG	SEP	OCT	NOV	DEC
2009	0.66	0.70	0.96	0.99	0.98	0.92	0.97	0.98	0.93	0.89	0.64	0.05
2008	0.91	0.80	0.93	0.97	0.98	0.97	0.96	0.97	0.93	0.92	0.75	-0.03
2007	0.41	0.91	0.98	0.96	0.99	0.98	0.98	0.96	0.97	0.96	0.72	0.32
2006	0.89	0.88	0.94	0.97	0.97	0.98	0.97	0.98	0.94	0.92	0.38	0.00
2005	0.79	0.95	0.90	0.99	0.97	0.97	0.98	0.95	0.96	0.94	0.74	0.60
2004	0.83	0.79	0.98	0.99	0.98	0.92	0.98	0.98	0.97	0.84	0.77	0.49
2003	-0.29	0.91	0.97	0.94	0.96	0.98	0.98	0.97	0.99	0.96	0.84	0.38
2002	0.66	0.82	0.97	0.95	0.97	0.98	0.97	0.94	0.95	0.93	0.73	0.77
2001	0.59	-0.17	0.98	0.97	0.98	0.98	0.99	0.98	0.98	0.83	0.86	0.02
2000	0.14	0.58	0.97	0.95	0.91	0.93	0.94	0.97	0.97	0.91	0.70	0.31
1999	0.76	0.94	0.99	0.98	0.99	0.97	0.96	0.98	0.97	0.82	-0.14	0.28

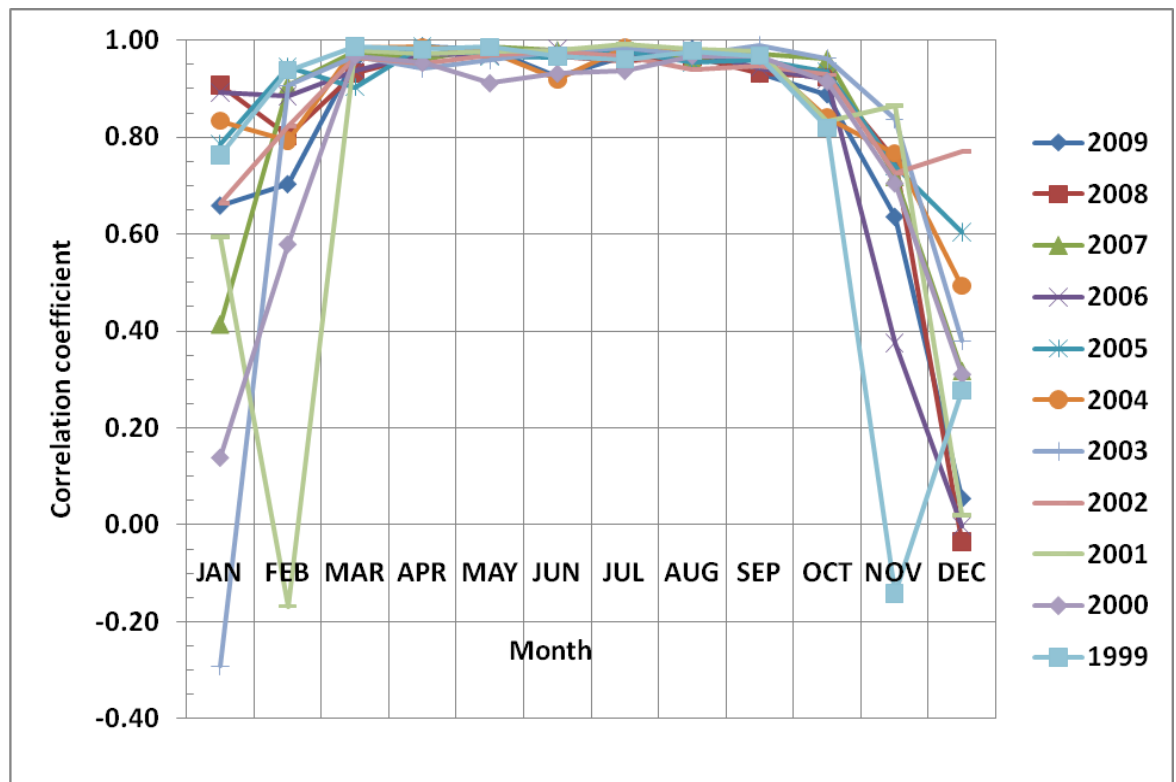


Figure 5-34: Graph of coefficient of correlation between diurnal mean wind speed and temperature against months for 1999 to 2009.

5.15.2 Atmospheric Pressure

Winds are originated by pressure differences across the earth's surface due to the asymmetrical heating of the earth by solar radiation. The spatial variations in heat transfer to the earth's atmosphere generate differences in the atmospheric pressure field that cause air to move from high to low pressure area. Usually the downward gravitational force cancels the pressure gradient force in the vertical direction. Thus, the winds blow predominantly in the horizontal plane, in response to the horizontal pressure gradients. At the same time, there are forces that strive to mix the different temperature and pressure air masses distributed across the earth's surface (Met office, 2008).

Pressure gradient is a term to express the difference in air pressure between two points in the atmosphere or on the surface of the Earth. It is very important to wind speed, because the greater the difference in pressure, the faster the wind flows (from the high to low pressure) to balance out the variation. The pressure gradient, when combined with the Coriolis Effect and friction, also influences wind direction.

To analyse the relation between atmospheric pressure and wind speed in Edinburgh, available hourly atmospheric pressure from Met office was used. Initially hourly pressure and wind speed data was drawn for one day against hours of the day as shown in Figure 5-35. It shows that wind speed decreases as atmospheric pressure decreases. Subsequently, the data for March 2009 was plotted in Figure 5-36. It shows that pressure decreases as wind speed increases for major part of the day but there is no clear correlation between both quantities. For further investigation of the relation between diurnal atmospheric pressure variation and diurnal wind speed variation, two graphs were generated based on diurnal pressure variation and diurnal wind speed variation for year 2009 as shown in Figure 5-37.

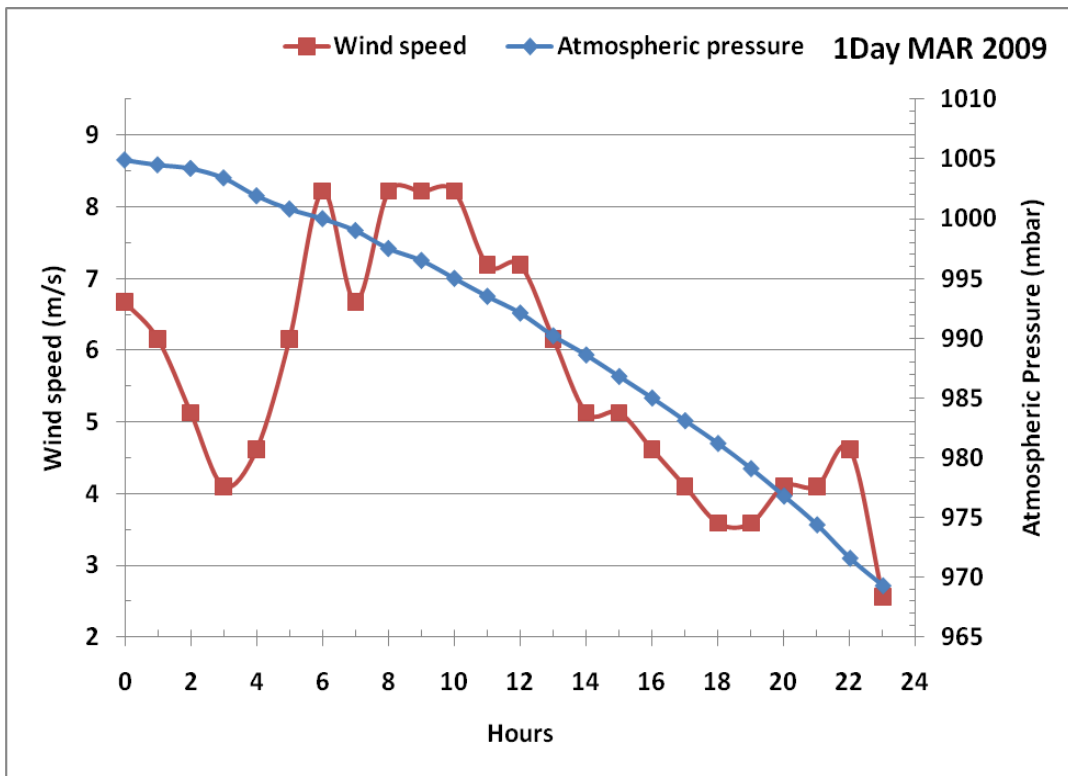


Figure 5-35: Graph of hourly wind speed and atmospheric pressure for one day.

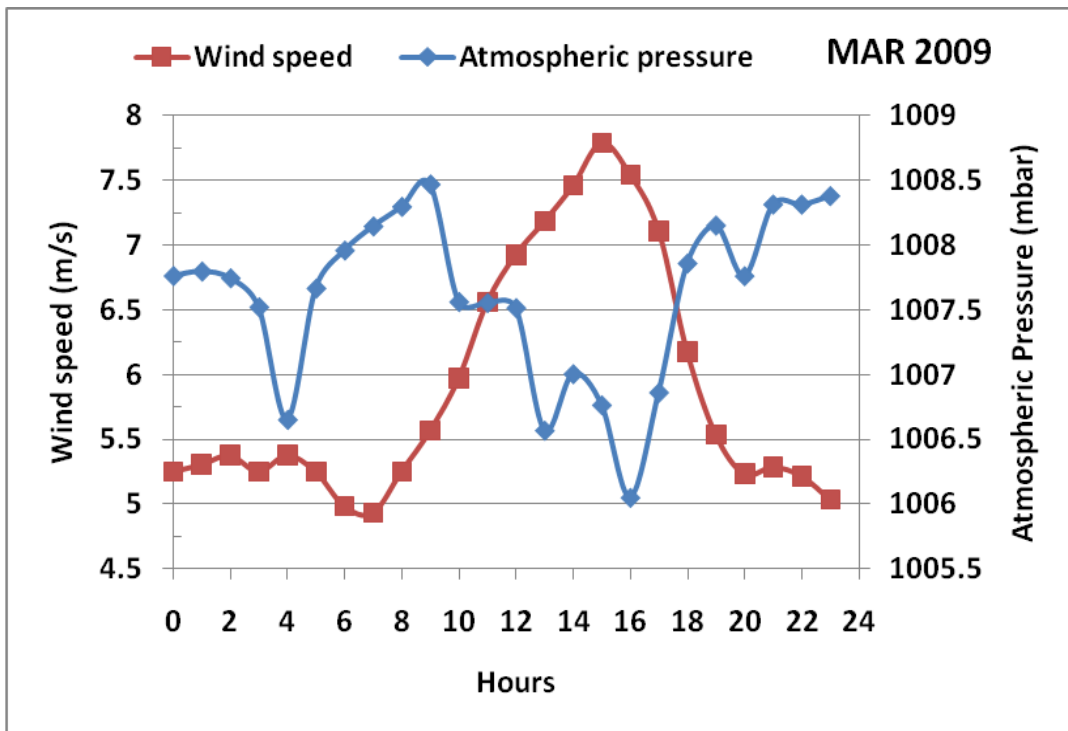


Figure 5-36: Graph of diurnal hourly average wind speed and atmospheric pressure for March 2009.

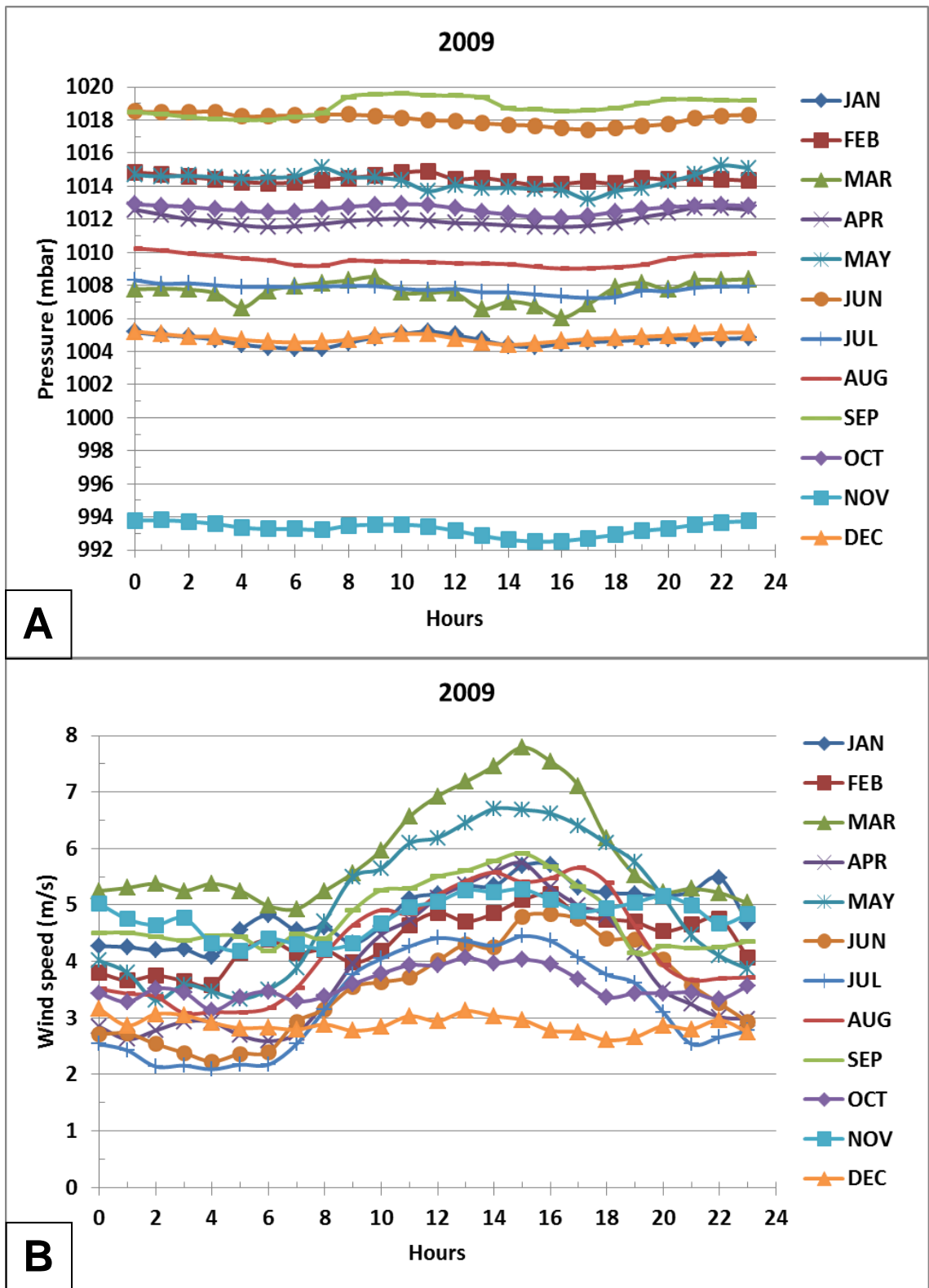


Figure 5-37: Graph **A**: diurnal atmospheric pressure variation for year 2009. **B**: diurnal wind speed variation for year 2009.

It is found that although wind speed increases when pressure decreases as in the case of November 2009, in March 2009 pressure variation is not as significant as wind speed variation, which is greater than rest of the year. In addition, atmospheric pressure was lowest in November 2009 while wind speed variation was same as in the month of Jan or Feb.

To investigate the relation of wind speed and atmospheric pressure on daily basis, thirteen days (to avoid congestion of lines) of January 2009 hourly data for wind speed and atmospheric pressure were plotted against the hours of day as shown in Figure 5-38. In Figure 5-38, wind speed increases as pressure decreases and vice versa. On further evaluation it is found that wind speed is not inversely proportional to the atmospheric pressure but instead to the gradient (rate of change) of the pressure. For instance, though day2 has the highest atmospheric pressure, it does not have the lowest wind speed. Likewise, day12 has the lowest atmospheric pressure but does not have the highest wind speed. On the other hand side, in day10 there is a rapid change in atmospheric pressure as it decreases from 1022mbar to 1006mbar in the fifteenth hour. This causes rapid increase in wind speed from 4.5 m/s to 12.6 m/s and as the rate of change in pressure decreased after the fifteenth hour so did the wind speed.

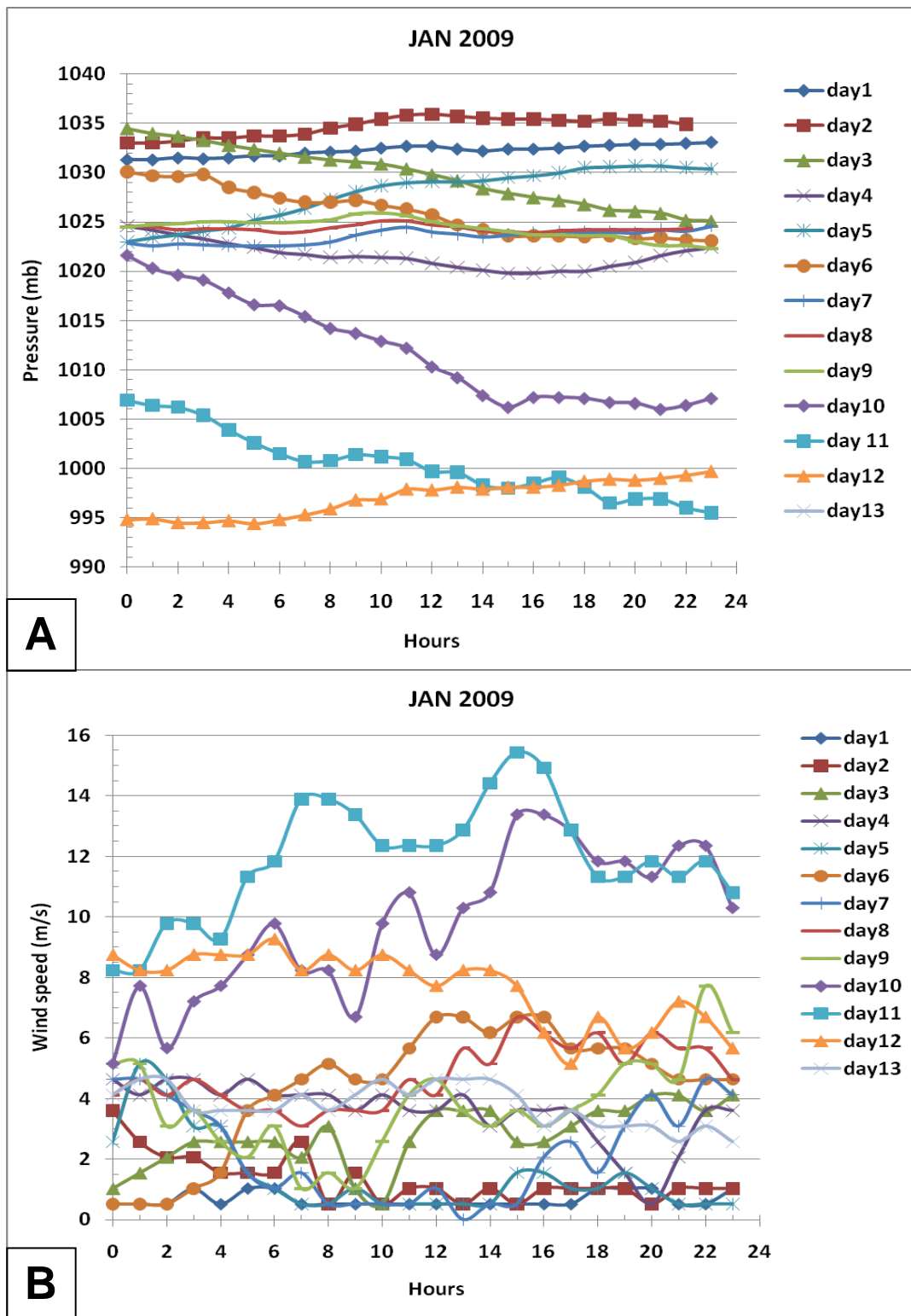


Figure 5-38: Graph **A**:Hourly atmospheric pressure variation fo Jan 2009. **B**: hourly wind speed variation for Jan 2009.

5.15.3 Relative humidity

Relative humidity is the ratio of the amount of water vapour actually in the air to the maximum amount of water vapour required for saturation at that particular temperature and pressure. Relative humidity is the prominent indicator that describes atmospheric moisture. The density of air decreases as humidity (moisture content) increases, this is because the molecular mass of water is less than the molecular mass of dry air (Ahrens, 2009).

To study the trend of relative humidity, year 2007's diurnal relative humidity was plotted as shown in Figure 5-39. In the plot relative humidity starts decreasing as the day progresses, attains a minimum at midday and then regains at the end of the day. In addition the variation in relative humidity is higher in summer than in winter. It seems that diurnal relative humidity pattern is just opposite to the diurnal wind speed pattern (as shown in Figure 5-25) and diurnal temperature pattern (as shown in Figure 5-30).

To determine if there is a relation between wind speed and relative humidity, diurnal average wind speed and relative humidity for May 2007 were plotted against hours as shown in Figure 5-40. It is found from the graph that wind speed is inversely proportional to relative humidity.

To further assess the level of relationship between relative humidity and wind speed, the coefficient of correlation was calculated as shown in Table 5-7. It shows that there is a very strong (i.e. more than 0.80) negative correlation in summer months, even for some cases in January, February and November as well. To visually elaborate the degree of correlation in different months a plot of coefficient of correlation was drawn as shown in Figure 5-41. The plot depicts very strong correlation between diurnal wind speed and relative humidity from March to October which becomes weaker and unpredictable in the months of January, February, November and December.

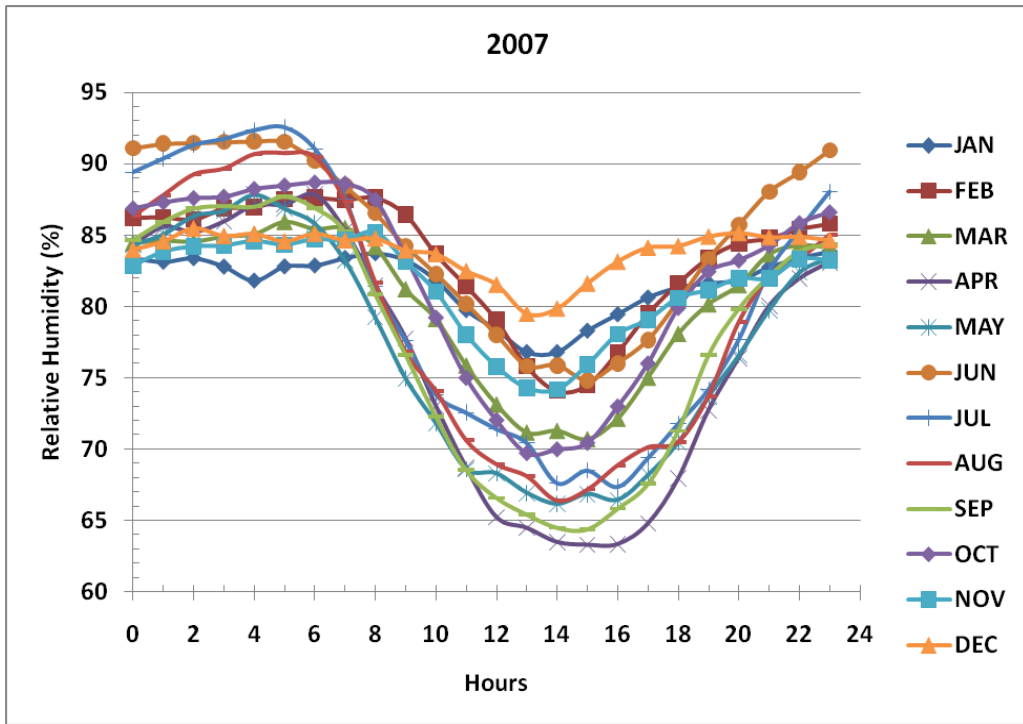


Figure 5-39: Graph of diurnal hourly average relative humidity for May 2007.

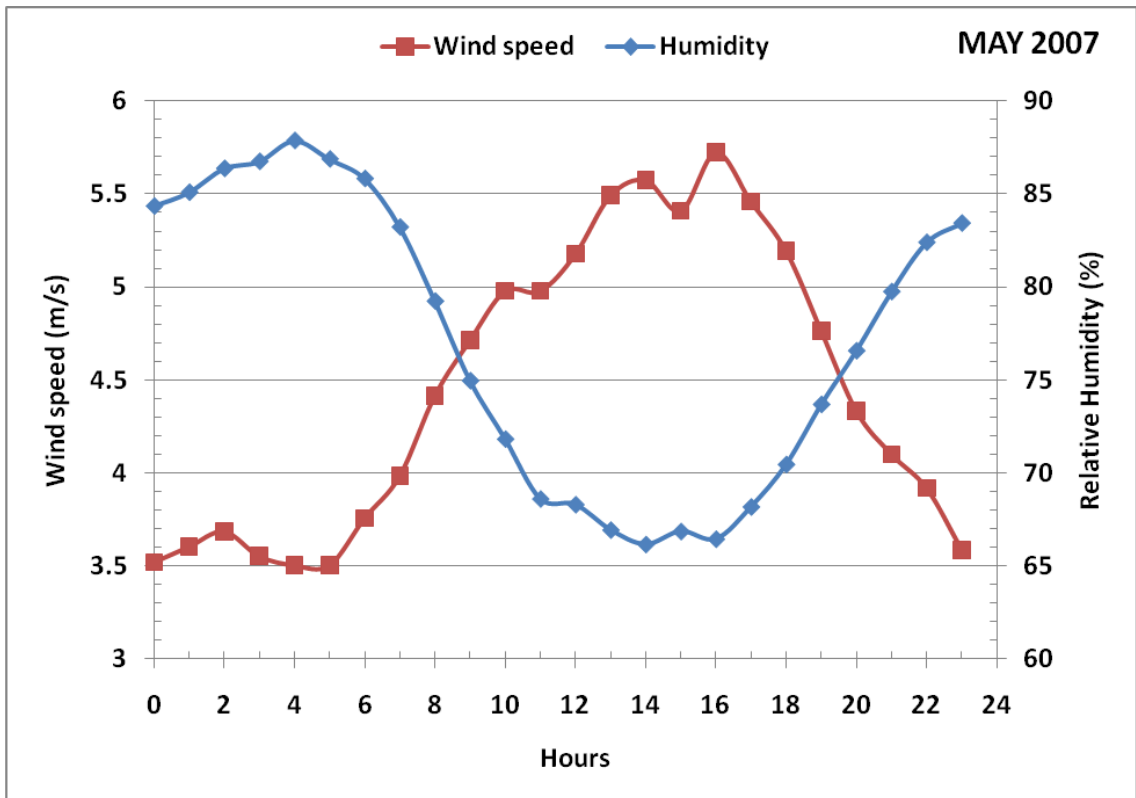


Figure 5-40: Graph of diurnal hourly average wind speed and relative humidity for May 2007.

Table 5-7: Correlation coefficient between monthly mean diurnal relative humidity and wind speed.

YEAR	JAN	FEB	MAR	APR	MAY	JUN	JUL	AUG	SEP	OCT	NOV	DEC
2009	-0.71	-0.82	-0.96	-0.99	-0.98	-0.93	-0.98	-0.98	-0.90	-0.93	-0.75	-0.24
2008	-0.64	-0.85	-0.90	-0.95	-0.98	-0.97	-0.97	-0.96	-0.97	-0.91	-0.92	0.00
2007	-0.25	-0.79	-0.99	-0.97	-0.98	-0.98	-0.98	-0.98	-0.97	-0.98	-0.66	-0.31
2006	-0.69	-0.83	-0.79	-0.97	-0.96	-0.98	-0.97	-0.97	-0.96	-0.95	-0.17	-0.51
2005	-0.66	-0.97	-0.90	-0.99	-0.95	-0.97	-0.97	-0.98	-0.95	-0.92	-0.72	-0.68
2004	-0.66	-0.93	-0.98	-0.98	-0.98	-0.93	-0.99	-0.98	-0.97	-0.89	-0.87	-0.55
2003	-0.85	-0.95	-0.96	-0.95	-0.98	-0.98	-0.99	-0.98	-0.99	-0.96	-0.78	-0.68
2002	-0.88	-0.69	-0.98	-0.96	-0.98	-0.98	-0.98	-0.92	-0.96	-0.94	-0.78	-0.80
2001	-0.70	0.17	-0.98	-0.97	-0.97	-0.97	-0.99	-0.98	-0.96	-0.85	-0.81	-0.64
2000	-0.09	-0.62	-0.98	-0.95	-0.92	-0.92	-0.93	-0.99	-0.97	-0.91	-0.68	0.24
1999	-0.46	-0.88	-0.99	-0.98	-0.98	-0.95	-0.96	-0.99	-0.98	-0.76	-0.20	-0.58

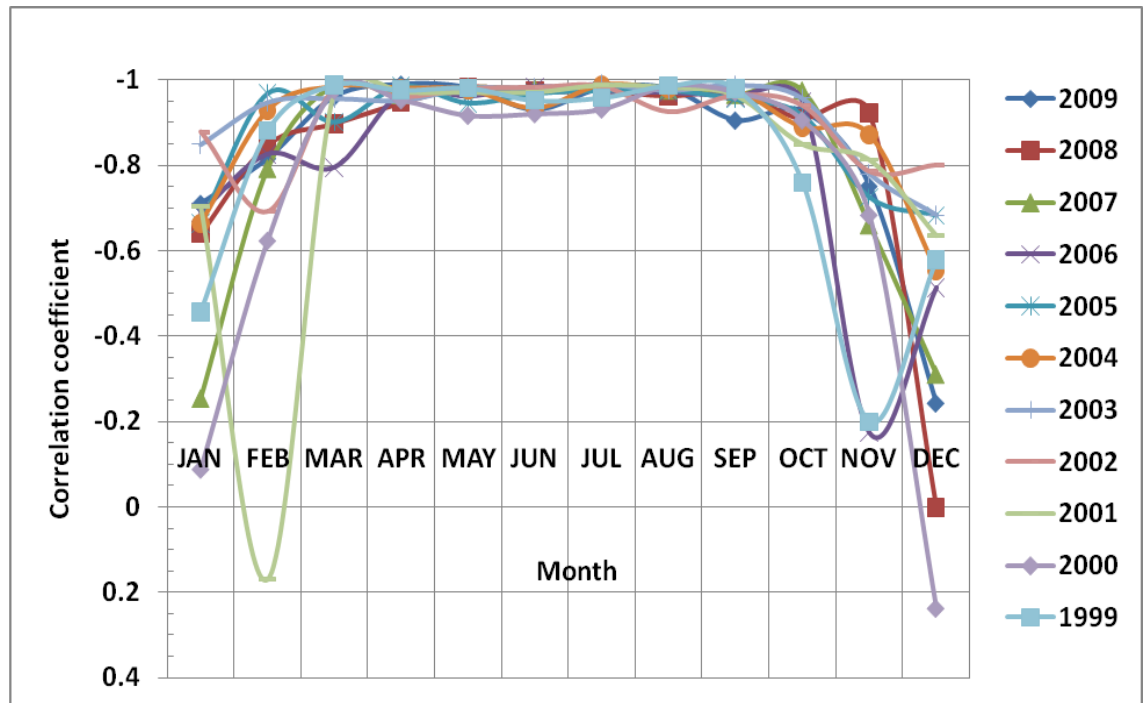


Figure 5-41: Graph of coefficient of correlation between diurnal mean wind speed and relative humidity against months for 1999 to 2009.

5.16 Air density in Edinburgh

Air density is an important factor effecting wind energy harness because the available power in wind is directly proportional to the air density. Density of air varies with the variation of moisture content and temperature of air. The amount of water vapour in air influences the density most. Water vapour is a relatively

light gas compared to diatomic oxygen and diatomic nitrogen – which are the dominant components of air. When water vapour content increases in the moist air, the amount of oxygen and nitrogen decreases per unit volume and since the mass decreases so does the air density (Engineeringtoolbox, 2005).

Air density can be calculated by given data (atmospheric pressure, temperature and humidity). It ρ_a (kg/m^3) can be expressed as:

$$\rho_a = \frac{P}{R.T} \quad \text{Equation 5-10}$$

where, P is the atmospheric pressure in (hpa)

T is temperature in Kelvin

R is Specific gas constant of dry air (287 J/Kg-K)

Moisturized air density can be expressed as (Cook 2006):

$$\rho_a = \frac{[P \times (1 + X)]}{[0.28703 \times (T + 273.16) \times (1 + 1.16078 \times X)]} \quad \text{Equation 5-11}$$

Where, P is atmospheric pressure in Kpa.

X is Humidity Ratio by Partial Vapour Pressure.

To calculate density from above formula, X needs to be known which augments the need to calculate vapour pressure (cook 2006) first. For that, saturation vapour pressure is required which can be calculated via the following formula (Bolton 1980);

$$P_{sat} = 6.112e^{\left[\frac{17.67 \times T}{T + 243.5}\right]} \quad \text{Equation 5-12}$$

where, P_{sat} is Saturation vapour pressure (hpa)

T is temperature in (C°)

Once saturation vapour pressure is known, vapor pressure can be calculated from the relation between relative humidity (ϕ), vapour pressure and saturation vapour as shown below (Barry & Chorley, 2010):

$$\phi = \frac{P_v}{P_{sat}} \times 100 \quad \text{Equation 5-13}$$

where, P_v is vapour pressure of water (hpa)

P_{sat} is saturation vapour pressure (hpa)

Humidity Ratio (X) by Vapour Partial Pressure can now be calculated from the following equation (Cook 2006):

$$X = \frac{0.622 \times P_v}{P - P_v} \quad \text{Equation 5-14}$$

Where, P is atmospheric pressure (hpa)

P_v is vapour pressure of water (hpa)

By using equation 5-11 hourly air density was then calculated and for the year 2005 maximum air density ($1.337621793 \text{ Kg/m}^3$) and minimum air density ($1.183871448 \text{ Kg/m}^3$) have also been evaluated. The mean air density and mean standard deviation (based on the density values) were found to be $1.249305187 \text{ Kg/m}^3$ and $0.028483473 \text{ Kg/m}^3$, respectively. Since standard deviation has an almost negligible value, mean air density was used for all calculations.

5.17 Wind power density and energy estimation

The wind speed is always intermittent, and thus the energy content of the wind is ever changing. The magnitude of variation depends on the weather, local surface condition and obstacles.

If previously considered equation 2-6, divide both sides by area (A_T) then theoretical wind power density ($TWPD$) i.e. the amount of wind power (watts) available per area (square meter) can be obtained as follow (Hughes, 2000):

$$TWPD = \frac{P}{A_T} = \frac{1}{2} \rho_a V^3 \quad \text{Equation 5-15}$$

Theoretical wind power density can be calculated using hourly wind data. However, hourly wind speed represents average wind speed in an hour; it does not mean that wind speed during that particular hour is same throughout. Thus, calculating wind power density from hourly data may carry some error.

One approach to evaluate wind power density is to use the monthly average wind speed to calculate wind power density over the period of a month and then take the average of wind power for the whole year. A different value of wind power density will be obtained if yearly mean wind speed is used.

Another way of expressing the wind power density P is given as (Mayhoub & Azzam 1997):

$$TWPD = \frac{1}{2} \rho_a \sum_{i=1}^N f_i V_i^3 \quad \text{Equation 5-16}$$

Where, f_i is the frequency of occurrence of wind in the i -th class, V_i is the median wind speed of the i -th class and N is the number of wind speed classes.

Available wind power density calculation included all wind speeds from very low i.e. less than 1 m/s to very high i.e. 19 m/s. But in practice, it is not feasible to make use of all wind speeds as WEC systems has cut-in and cut-out wind speed limitations. In addition, it is not physically possible to convert all wind energy into electrical energy. The maximum that can be extracted by an ideal wind turbine is 59.3% of the available wind power, known as Betz limit (Manwell, McGowan & Rogers, 2009). In wind turbine market, companies claim different efficiencies for their wind turbines (Andy Wilson, 2007). For this research, Windsave wind turbine is used which claims 33% efficiency at the 12

m/s wind speed (optimum level) according to their power curve (details in appendix 1).

Output power of any WEC can be estimated by multiplying the power coefficient C_p (efficiency/100) of the system with available power. As shown in equation below from (Burton *et al*/2001).

$$P = \frac{1}{2} C_p \rho A_T V^3 \quad \text{Equation 5-17}$$

Wind power densities were calculated using equation 5-16 is shown in Figure 5-42. It can be seen that the wind power density is low over low wind speeds even when the wind speed frequency is high and the wind power density is high over high wind speeds even when the frequency is low. It is because cubic power of wind speed is directly proportional to the available power.

To calculate wind energy density per month or per year, it is important to include all the variations in the wind speed. The results are shown in Table 5-8, but it is to be noted that these results, which also include the changes in the wind direction, can only provide an estimated figures. From the table, the overall annual average energy density in Edinburgh is about 1 MWh/m² and by including Betz limit, it can be said that 593 kWh/m² annual average energy density is available in Edinburgh to harness.

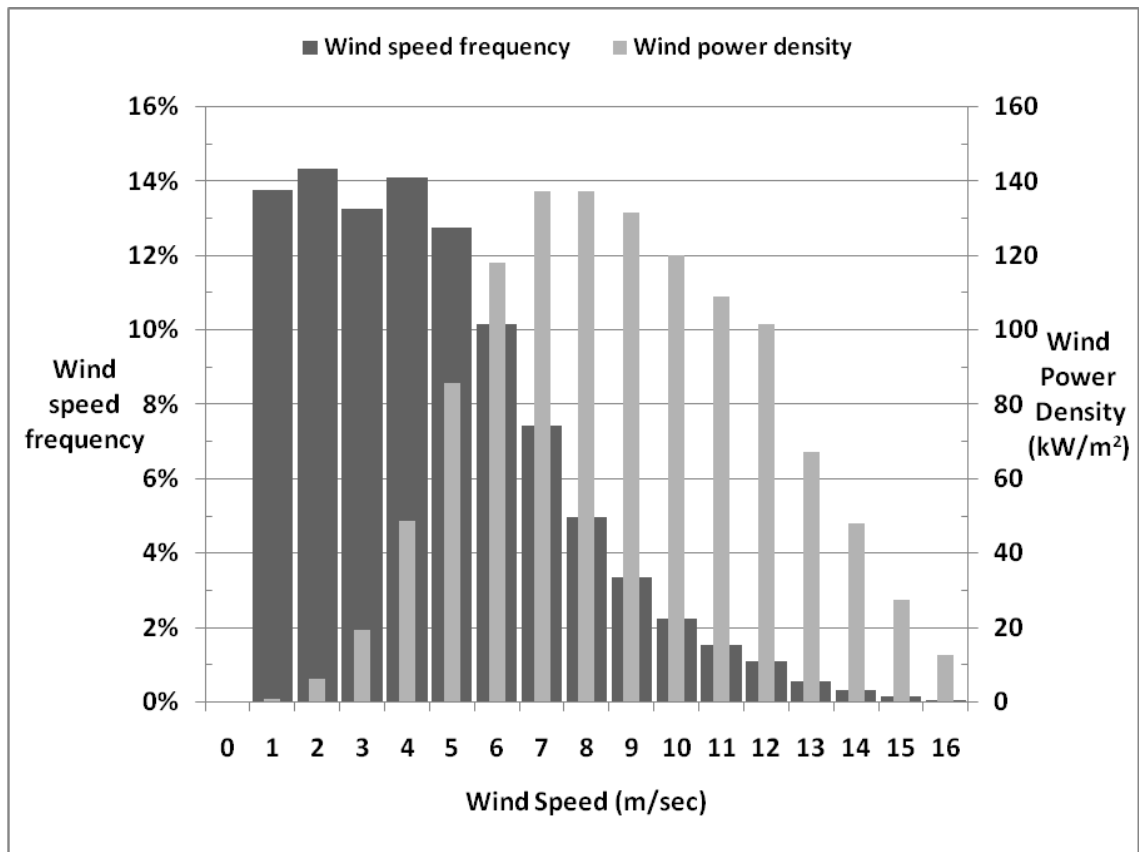


Figure 5-42: Wind power density against wind speed frequency for year 2008.

Table 5-8: Monthly available wind energy in kWh/m².

Month	1999	2000	2001	2002	2003	2004	2005	2006	2007	2008	2009
Jan	165.24	189.51	49.04	142.62	162.58	98.01	261.93	74.25	245.52	196.68	99.74
Feb	173.44	210.32	63.07	165.15	40.74	92.28	73.82	63.83	53.28	197.70	69.76
Mar	80.06	128.13	57.45	131.16	59.06	104.89	80.64	43.38	143.38	144.94	148.49
Apr	71.42	54.87	61.68	69.68	55.38	52.76	96.36	114.05	73.79	72.54	56.79
May	81.17	43.66	48.03	50.31	80.87	40.92	62.97	65.10	77.84	47.10	102.74
Jun	41.83	62.26	66.60	65.79	55.59	57.10	29.69	54.15	33.62	51.43	39.34
Jul	45.72	23.03	42.26	28.89	36.23	33.53	40.37	30.64	42.39	38.48	33.49
Aug	39.81	32.68	29.65	24.18	42.99	35.46	55.15	37.62	53.95	37.00	67.20
Sep	40.47	43.38	54.44	19.85	43.54	108.80	98.78	37.83	74.79	33.65	94.51
Oct	89.93	89.65	114.78	34.54	56.34	57.51	54.13	57.48	51.08	125.97	59.24
Nov	151.05	62.56	97.26	41.06	74.96	81.26	93.25	144.35	83.91	105.94	115.56
Dec	148.89	83.13	64.41	27.32	77.74	152.98	55.23	193.65	89.79	89.44	28.60
Total	1129.03	1023.18	748.68	800.54	786.02	915.49	1002.32	916.31	1023.35	1140.85	915.45

5.18 Savings on GHG emissions

According to the Department of Energy and Climate Change (DECC) report issued in Sep 2010 (DECC, 2010), in UK for every kWh of electricity (generated and transmitted up to end user) 542.84 grams of GHGs were released. This value represents only direct emissions; if indirect emissions are also included the figure rises to 617.07 grams of GHGs per kWh of electricity. Thus, a WEC system having an efficiency of 25% (it is noted that different companies claim different efficiencies for their respective WEC systems (Andy Wilson, 2007)) can generate approximately 250 kWh/m² of electricity from 1 MWh/m² of wind energy and it can save approximately 154.2675 kg of GHGs per m² in a year. It indicates that if a wind turbine like WindSave's WS1200PS which has swept area of 2.378 m² works with efficiency of 25% then it can generate 594.5 kWh of energy and save 366.848 kg of GHGs emission annually. Large wind turbines with greater swept area and higher efficiency can further save more GHG emissions.

5.19 Conclusion

The topography around Met office weather station was studied and it was found that there is an elevation variation around Met office weather station and no prominent obstacle in the wind flow around it. Prevailing wind direction was found to be south west. Average yearly wind speed varied from 3.90 m/s to 4.58 m/s at 10 meter above ground. Through probability distribution analysis it was established that about 40% of the time wind speed is 3 m/s or lower and that Weibull distribution fits better than Rayleigh distribution. Diurnal variation in urban area was investigated and wind speed variation was found highly correlated to temperature variation and inversely related to humidity variation. There is no diurnal variation effect on wind direction. Velocity duration curve was found to be more or less the same for ten years of data. Air density for Edinburgh was calculated to be 1.249 Kg/m³. An average of 1 MWh/m² wind energy was found to be available in Edinburgh's rural area.

6 ANALYSIS OF LOCALLY COLLECTED WIND DATA

6.1 Introduction

This chapter presents the study of location and surrounding area's topography of Merchiston campus followed by Merchiston campus wind data analysis, comparison of urban and rural wind and available wind energy in Edinburgh's urban area.

6.2 Location of Merchiston Campus

Two MetPak weather stations were installed on July 2009 at Edinburgh Napier University's Merchiston campus roof's top for the collection of wind data and logged data until February 2011. Merchiston campus is located at $55^{\circ} 55' 57.21''\text{N}$ and $3^{\circ} 12' 52.81''\text{W}$ in the urban area of Edinburgh. It is situated at 86.59 degrees from North (i.e. in east direction) on 8.08 km from Met office weather station and the elevation of the site is about 100 m as shown in Figure 6-1.

6.3 Terrain at the Merchiston Campus

As discussed in Chapter three, the city of Edinburgh offers a high value of surface roughness coefficient for wind. Elevation of Merchiston campus and its surrounding area was determined using Google Earth and was found as 100 m. To determine the elevation around Merchiston campus, Edinburgh was divided into 24 sectors with the spacing of 15 degrees and 24 lines were drawn commencing from Merchiston campus and terminating up to a length that covers 15 km distance as shown in Figure 6-2.

In Figure 6-3, the 24 graphs show elevation around Merchiston campus. They show that elevation of Merchiston campus from North to North-East is higher than the surrounding area with a very few exception from North-East to East direction. There are higher elevations of up to 165m just 3 km from Merchiston campus. From 90 degrees to 120 degrees it seems that Merchiston campus is on one edge of a valley whose other side is about 237 m high 14 km away and descent has a minimum elevation of 45 m about 10 km from Merchiston

campus. From South-East (135 degrees), there is higher and very rough elevation area even up to 513m in 210 degrees. From South-West, Merchiston campus seems to be in the decent of a valley whose other side is up to 338m. From West to North, Merchiston is higher in elevation but has vibrant elevations in front of it, except a sharp cliff having a height of 160 m and about 4 km distance at 300 degrees.

In terms of constructed obstacles for the wind flow that can cause direct shading effect, it was observed that there is no building around Merchiston campus (as shown in Figure 6-4) except one of its own campus block. This is 7.5 m higher than the wind monitoring point and just 91.6 m away at 60 degrees and it spans 56 m in front of the wind monitoring point.

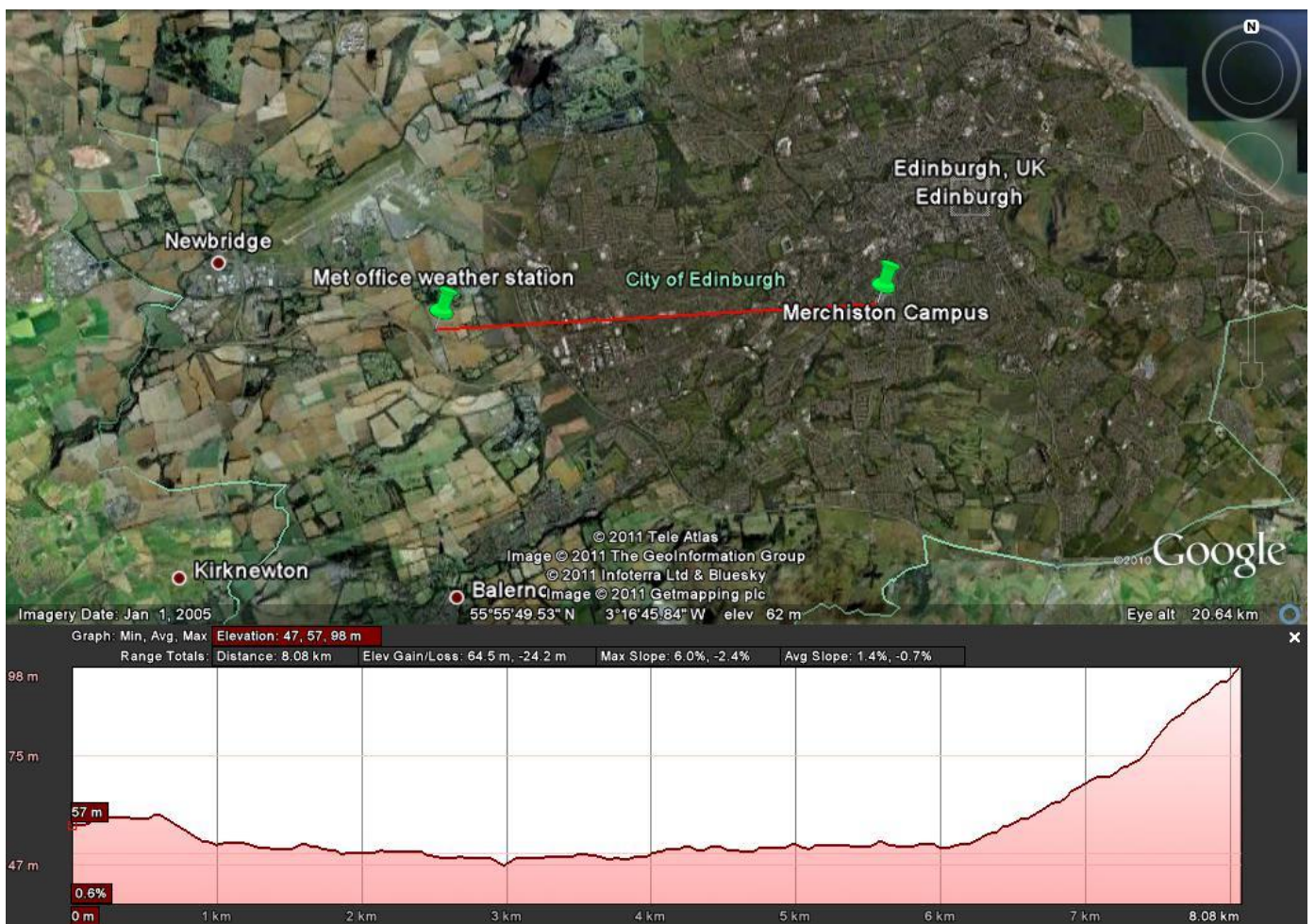


Figure 6-1: Relative location and elevation of Met office weather station and Merchiston campus (Courtesy of Google Earth).

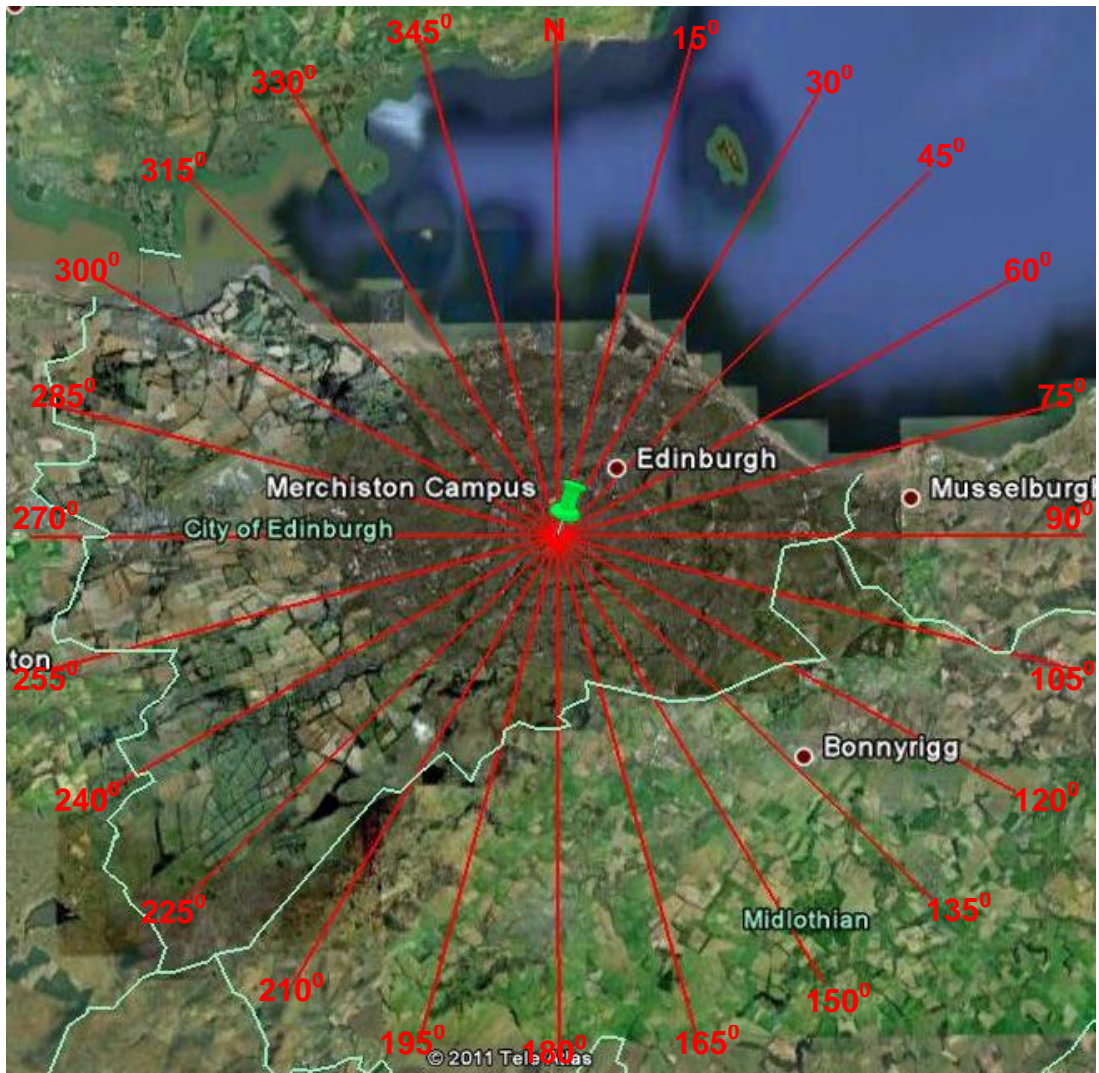


Figure 6-2: 24 Sectors around Merchiston campus drawn on Google Earth.

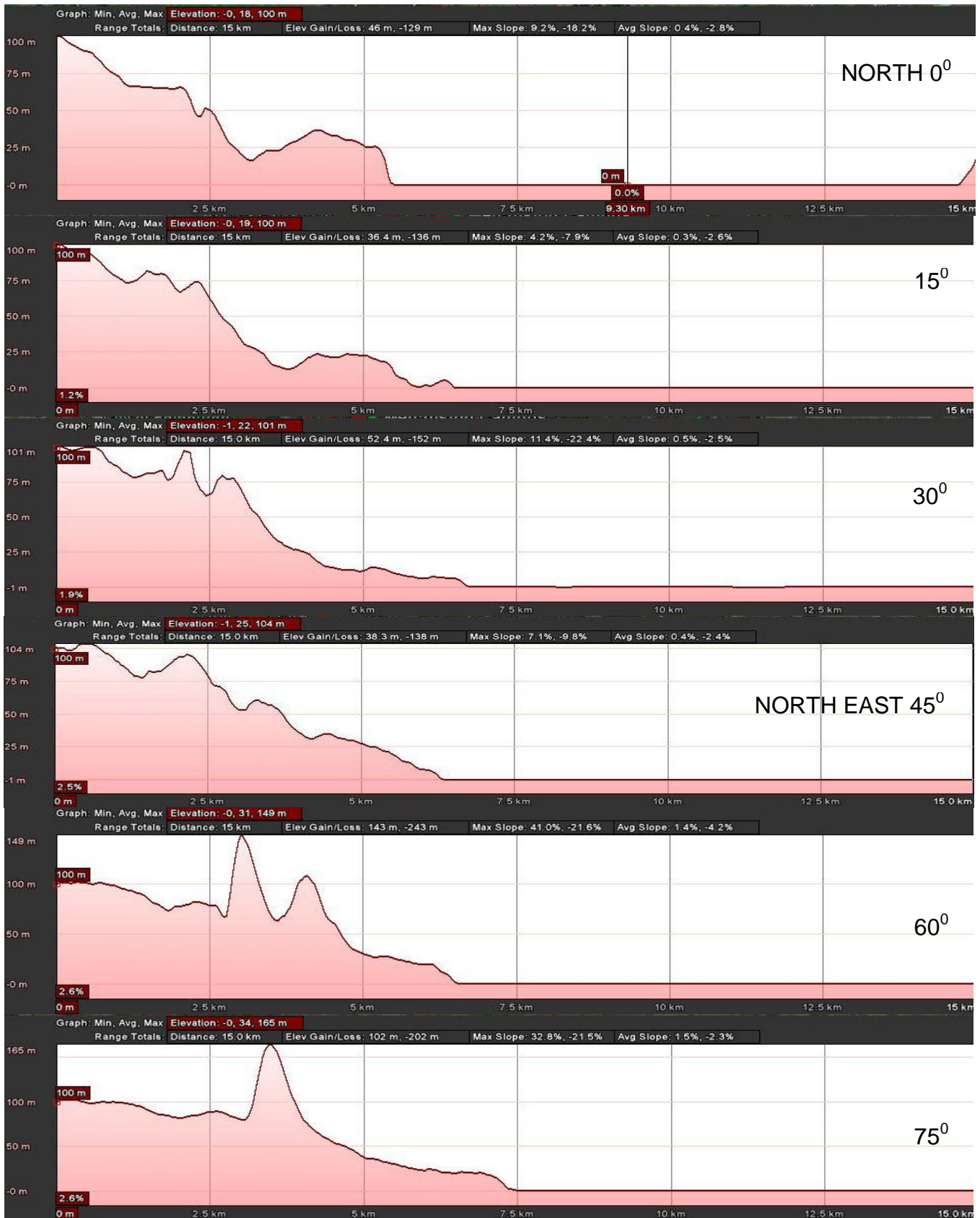


Figure 6-3: 24 Elevation graphs around Merchiston campus up to 15 km in distance (continue).

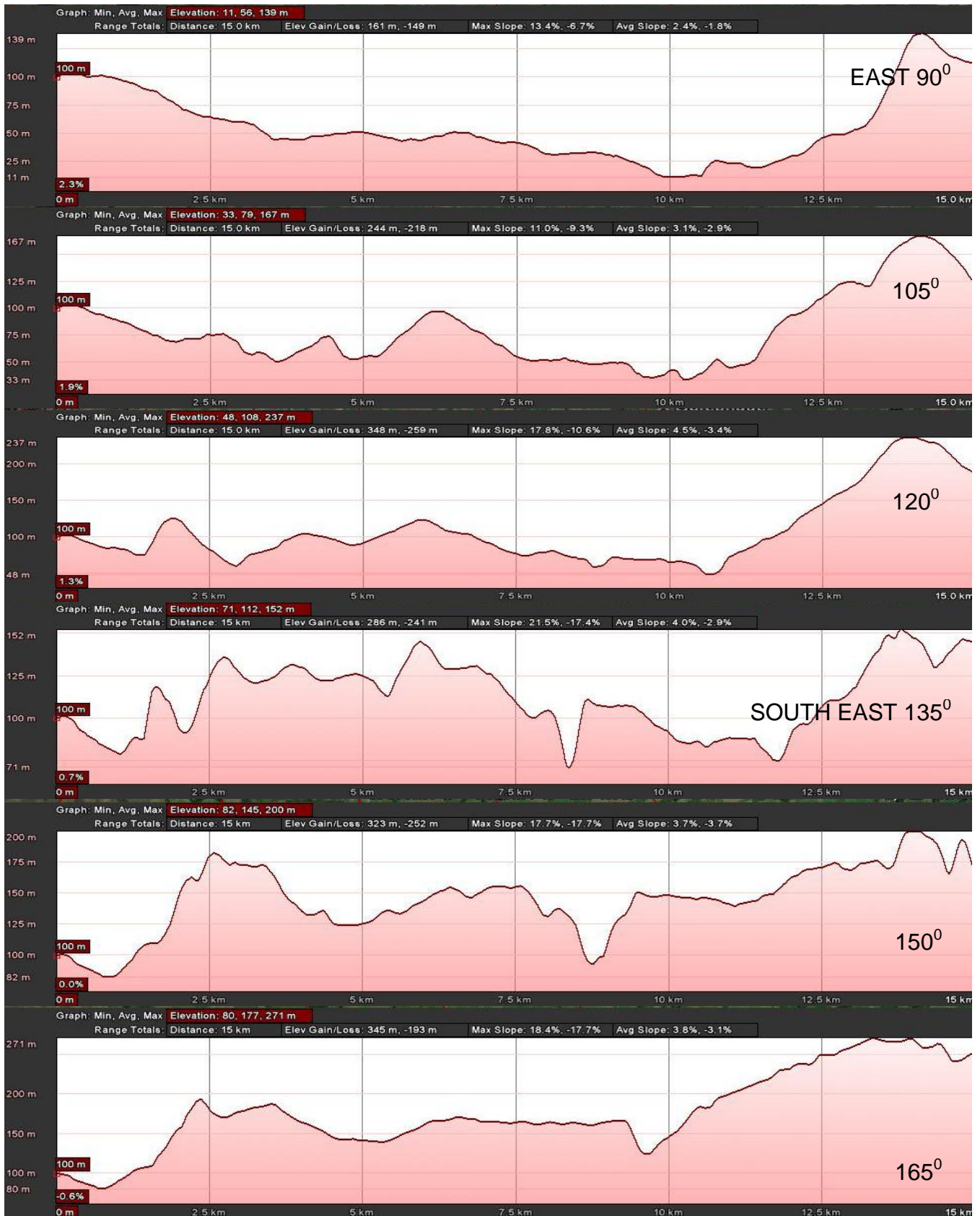


Figure 6-4: 24 Elevation graphs around Merchiston campus up to 15 km in distance (continue).

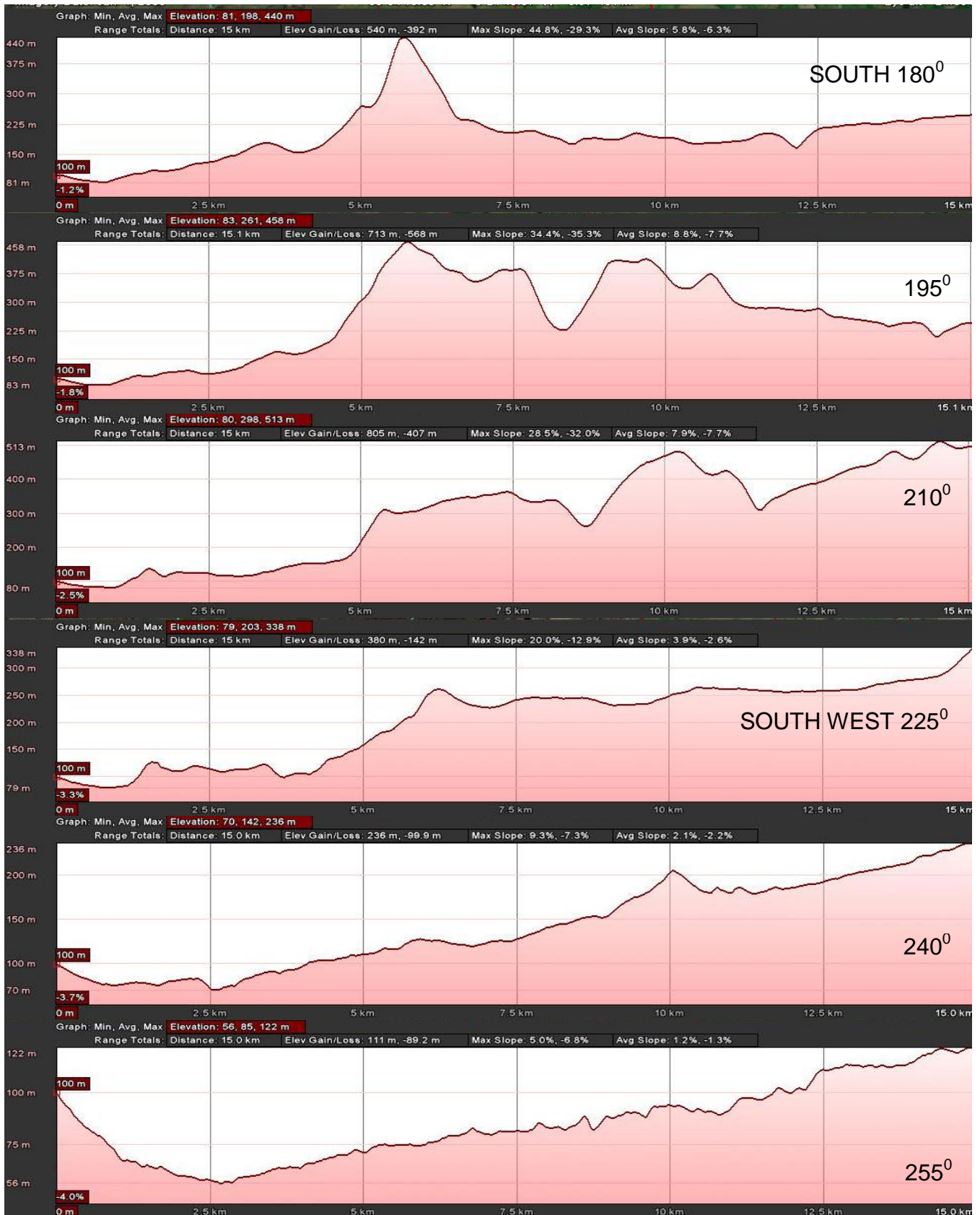


Figure 6-5: 24 Elevation graphs around Merchiston campus up to 15 km in distance (continue).

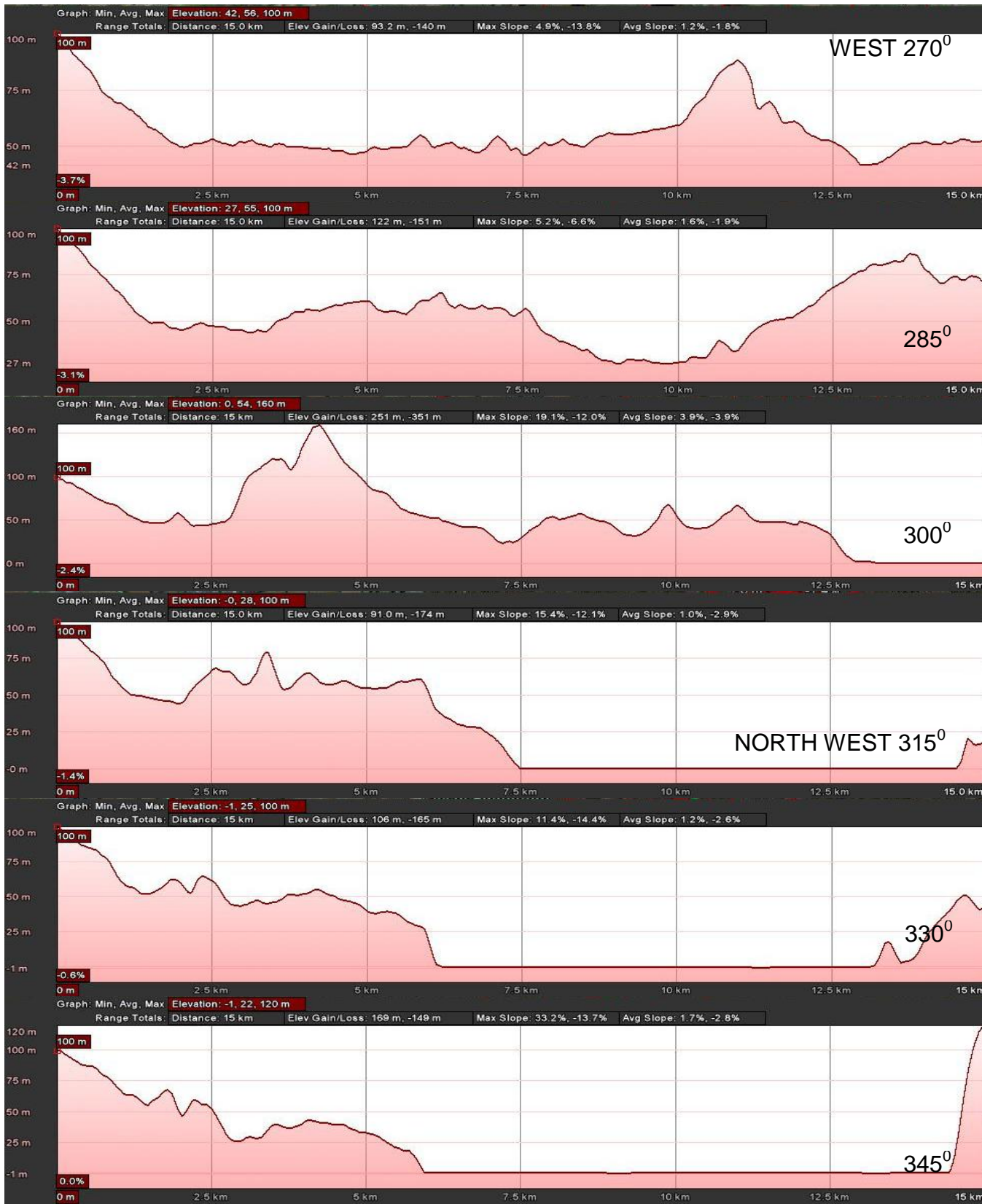


Figure 6-6: 24 Elevation graphs around Merchiston campus up to 15 km in distance.



Figure 6-7: Photographs of surrounding area from roof top of Merchiston campus (continue).



Figure 6-8: Photographs of surrounding area from roof top of Merchiston campus.

6.4 Wind data source

MetPak can provide wind speed, wind direction, temperature and relative humidity. In addition to that, atmospheric pressure data was collected separately. In MetPak stations wind speed and direction is sensed by ultrasonic sensors which can give more reliable data than a weather station with moving parts. The vertical distance between both MetPak stations is 1.5 m. Data logger attached to MetPak systems sampled the data every second and then logged the average of every two seconds.

6.5 Prevailing wind direction

At Merchiston top, wind is blowing from all directions as shown in the monthly wind rose diagrams (Figure 6-11) but overall dominant direction is South-West. Wind blow from North or South direction is very rare and easterly westerly winds are more frequent at Merchiston. There are minor differences in wind direction data, logged at higher MetPak (MetPak1) and lower MetPak (MetPak2). Wind flow in some months is very directional than in others. For instance, in August and December wind flow only occurs from West or South West direction. On the other hand in the month of June wind flows from both East and West directions.

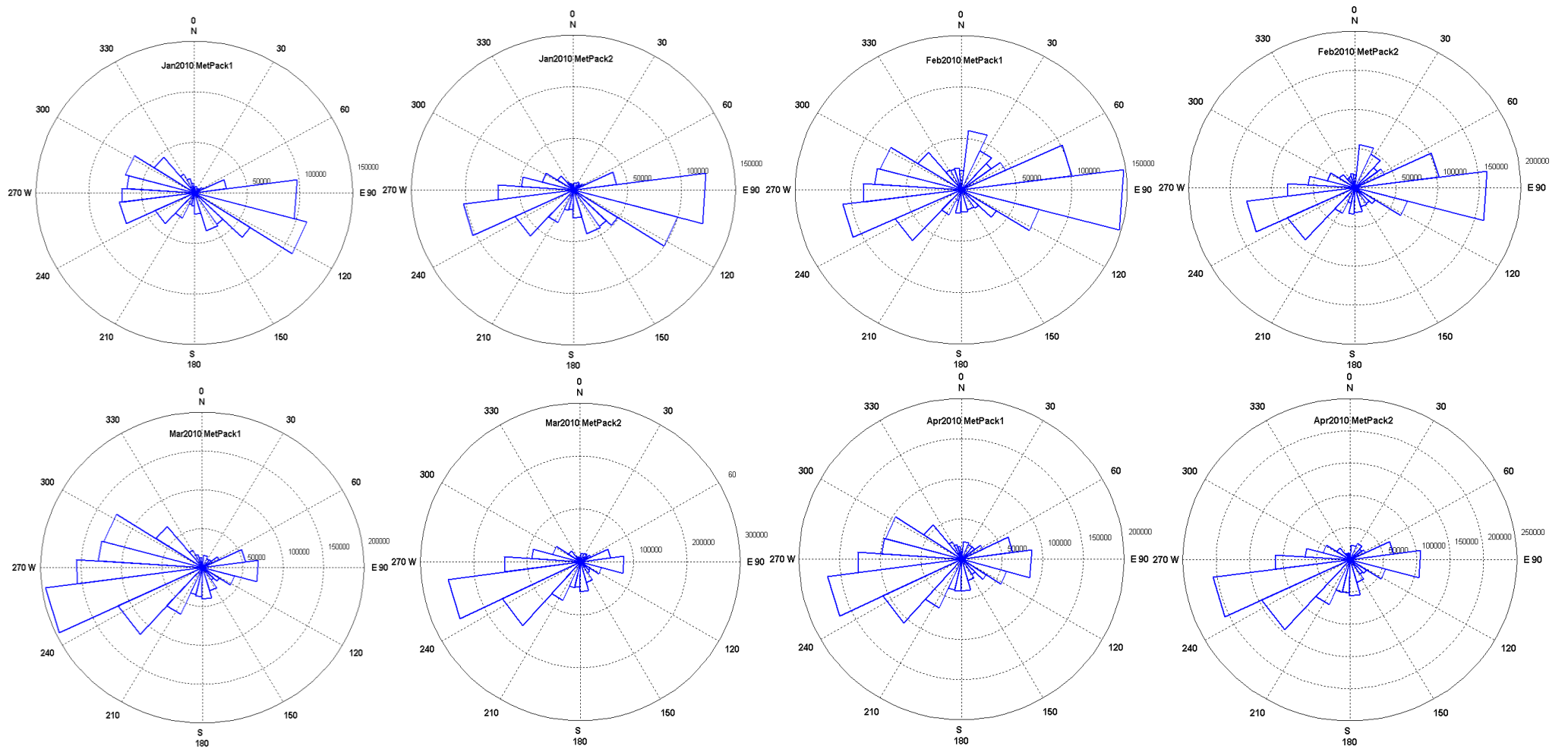


Figure 6-9: Wind rose diagrams of wind flow direction at Met Pack1 & 2 from July 2009 to June 2010 (continue).

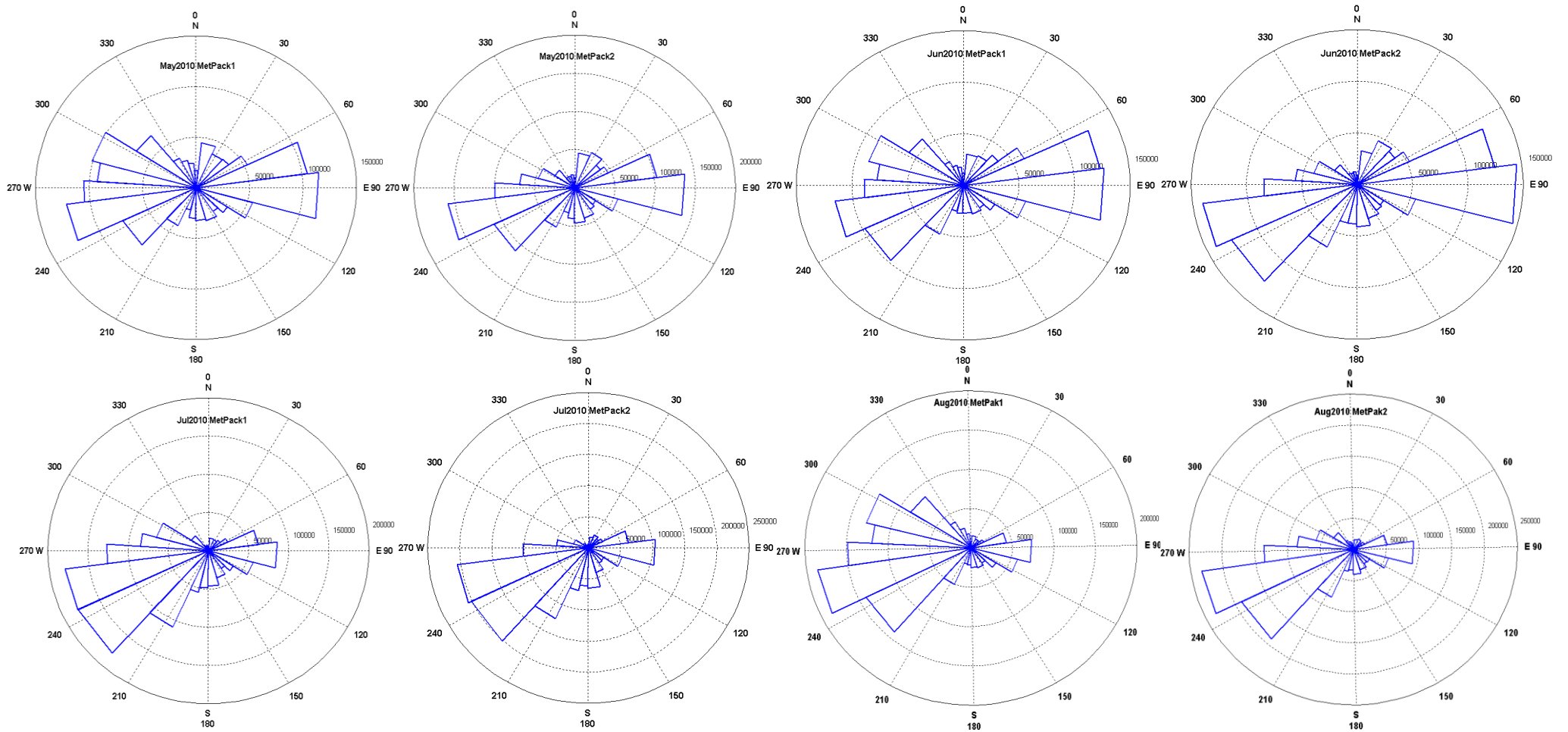


Figure 6-10: Wind rose diagrams of wind flow direction at Met Pack1 & 2 from July 2009 to June 2010 (continue).

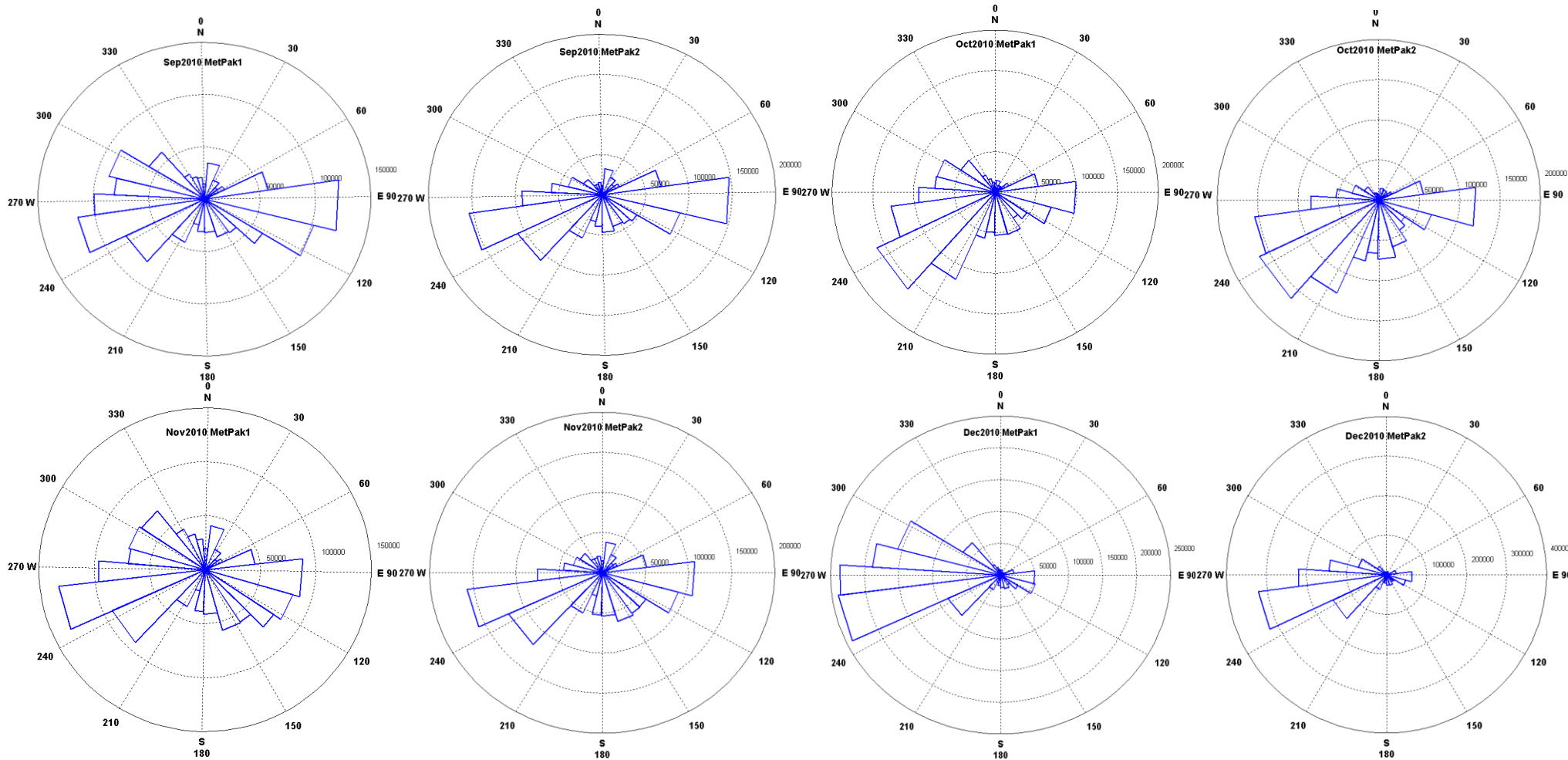


Figure 6-11: Wind rose diagrams of wind flow direction at Met Pack1 & 2 from July 2009 to June 2010.

6.6 Mean wind speed and standard deviation

As discussed in last chapter, the average or mean wind speed is most widely used and most generally understandable statistical figure which indicates the suitability of wind regime. In addition to mean wind speed, standard deviation tells about the dispersion in the data. Table 6-1 shows the monthly average wind speed, standard deviation and the available data in percentage. It shows that average annual mean wind speed at higher MetPak (i.e. MetPak1) is 3.71 m/s and at lower MetPak (i.e. MetPak2) is 3.06 m/s, which may not necessary be sufficient for wind energy generation by using micro-wind turbine. It is noticed that the maximum mean wind speed is recorded in November months, 4.9 m/s and 4.57 m/s respectively. At the same time, the standard deviation of data is also higher in Novembers, averaged value equal to 3.3 m/s, which means that there is lack of consistency in wind speed and wind is rather gusty than steady. Last column of Table 6-1 shows the percentage of available data in the month. The shortfall of data in Sep 2009 and Oct 2009 caused by the major renovation work at roof and shortfall of data in Dec and Jan caused by Christmas and New-year holidays as data logger system has memory limitations.

Figure 6-12 shows that there is about a constant ratio between lower and higher MetPak i.e. 1.21 on average. It means the mean wind speed increases 1.21 times, or 16%, when there is a 1.5 m height increase at Merchiston roof. On the other hand, standard deviation increases by 7% with the same increase in height as evident in Table 6-1.

Table 6-1: Mean wind speed and standard deviation based on MetPak H (MetPak1) and MetPak L (MetPak2) data.

Month	Mean wind speed (m/s)		Standard deviation (m/s)		Available data %
	MetPak H	MetPak L	MetPak H	MetPak L	
Jul-09	3.43	2.90	2.03	1.84	99.99
Aug-09	4.47	3.83	2.51	2.25	99.99
Sep-09	4.02	3.25	2.46	2.16	54.82
Oct-09	3.46	3.05	1.94	1.84	17.73
Nov-09	4.90	4.24	3.07	2.85	99.99
Dec-09	3.32	3.18	2.02	2.90	85.12
Jan-10	4.15	3.46	2.43	2.27	66.15
Feb-10	2.80	2.38	1.78	1.73	99.99
Mar-10	4.11	3.41	2.86	2.52	99.99
Apr-10	3.80	3.18	2.50	2.30	99.76
May-10	3.04	2.44	1.69	1.46	99.99
Jun-10	3.06	2.47	1.73	1.49	99.99
Jul-10	4.35	3.65	2.47	2.19	99.99
Aug-10	3.33	2.66	1.94	1.68	99.99
Sep-10	3.78	3.10	2.45	2.16	96.77
Oct-10	4.28	3.60	2.39	2.26	99.99
Nov-10	4.57	3.80	3.46	3.01	99.99
Dec-10	3.18	2.56	1.89	1.62	98.21
Jan-11	4.07	3.42	2.52	2.39	85.55
Feb-11	4.38	3.71	2.97	2.72	99.99
2010 Annual Average	3.71	3.06	2.30	2.06	

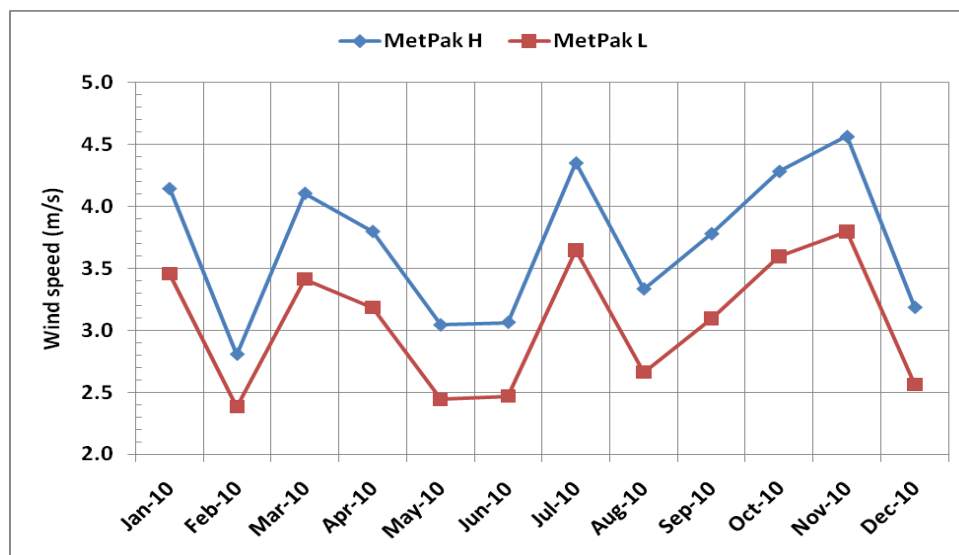


Figure 6-12: Comparison of monthly mean wind speed from MetPak 1 and MetPak 2.

6.7 Probability distribution function (PDF)

Probability distribution of MetPak-H data shows that there is very high probability for low wind speed (i.e. less than 4 m/s) as shown in Figure 6-15. The distribution is unimodal as indicated (for Met office data) in the preceding chapter. Weibull distribution results are closer to the real data distribution than Rayleigh distribution.

Table 6-2 gives the parameter values for Weibull and Rayleigh distributions with the value of shape factor k going up to a maximum of 1.89 and down to a minimum of 1.35, having a mean value of 1.71. The values for the Weibull scale factor c have a maximum value of 4.98 and a minimum of 3.13, having a mean value of 4.14. Higher value of scale factor suggests greater probability for higher wind speed and vice versa. A high value of shape factor means distribution is more concentrated around one value where as a low shape factor means distribution is more disperse.

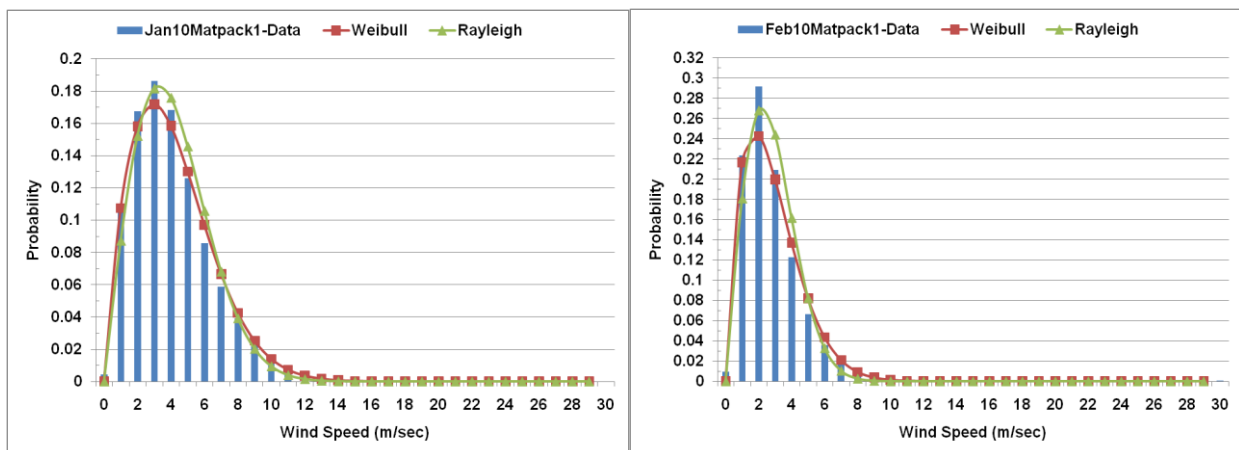


Figure 6-13: Comparison between Probability distribution of MetPak-H (MetPak1) data, Weibull distribution and Rayleigh distribution for year 2010 (continue).

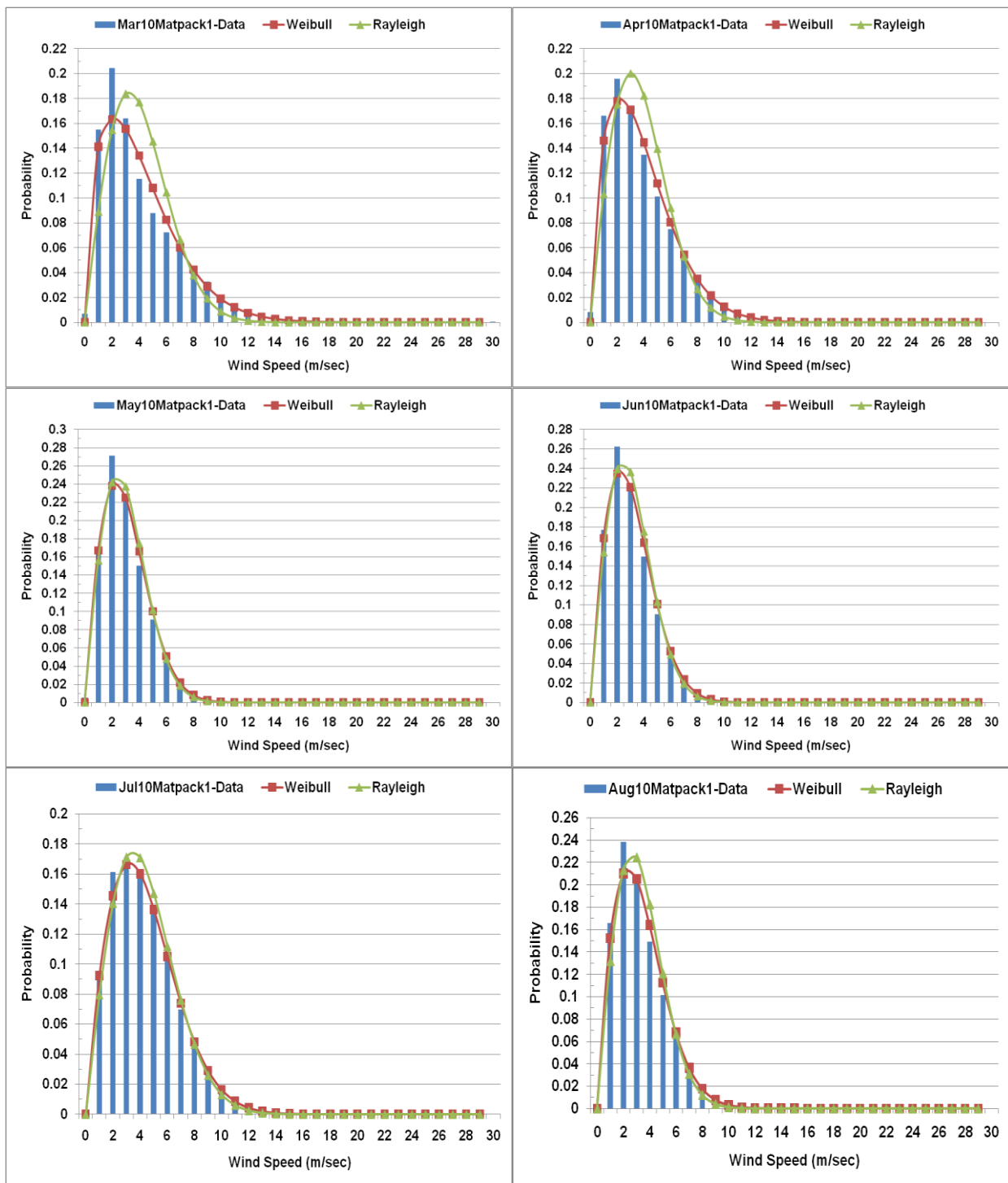


Figure 6-14: Comparison between Probability distribution of MetPak-H (MetPak1) data, Weibull distribution and Rayleigh distribution for year 2010 (continue).

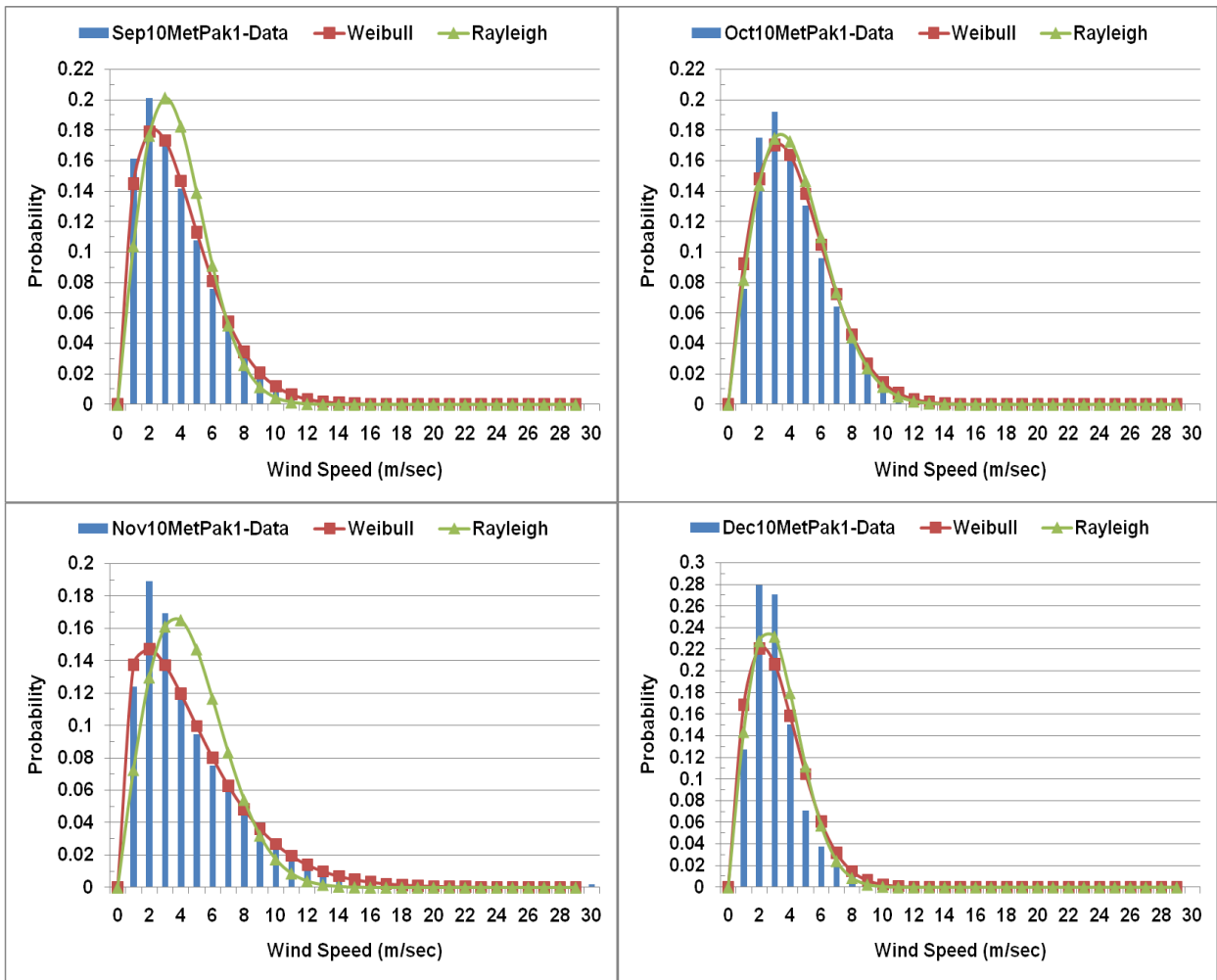


Figure 6-15: Comparison between Probability distribution of MetPak-H (MetPak1) data, Weibull distribution and Rayleigh distribution for year 2010.

Table 6-2: Weibull and Rayleigh parameters for MetPak-H wind speed data for year 2010.

Month	Weibull parameters		Rayleigh parameters
	Shape parameter (K)	Scale parameter (C)	Scale parameter (C)
Jan-10	1.78	4.66	4.68
Feb-10	1.63	3.13	3.16
Mar-10	1.48	4.54	4.63
Apr-10	1.58	4.23	4.29
May-10	1.89	3.43	3.43
Jun-10	1.86	3.45	3.46
Jul-10	1.85	4.90	4.91
Aug-10	1.80	3.75	3.76
Sep-10	1.60	4.22	4.27
Oct-10	1.88	4.83	4.83
Nov-10	1.35	4.98	5.15
Dec-10	1.76	3.58	3.59

6.8 Cumulative distribution function (CDF)

Cumulative distribution function indicates the fraction of time for which the wind is at a given velocity. The cumulative distribution graph for MetPak-H in Figure 6-17 shows that wind speed was lower than 4 m/s for more than 80% of the time in the months of Feb, May, Jun and Dec and more than 60% to 65% of the time in the rest of the year. Moreover, wind speed rarely blows above 10 m/s.

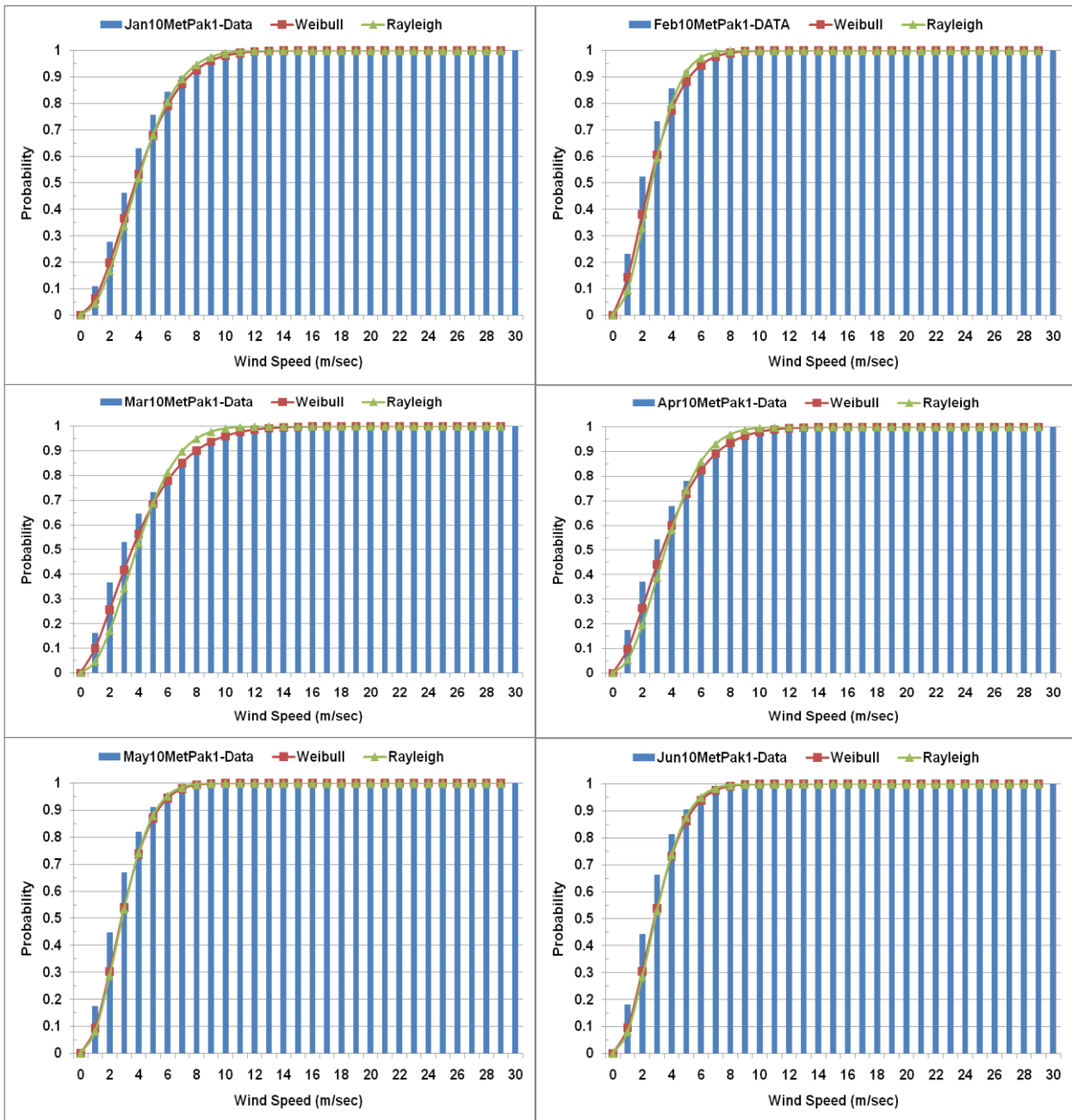


Figure 6-16: Comparison between monthly cumulative distribution of real data, Weibull distribution and Rayleigh distribution year 2010 (continue).

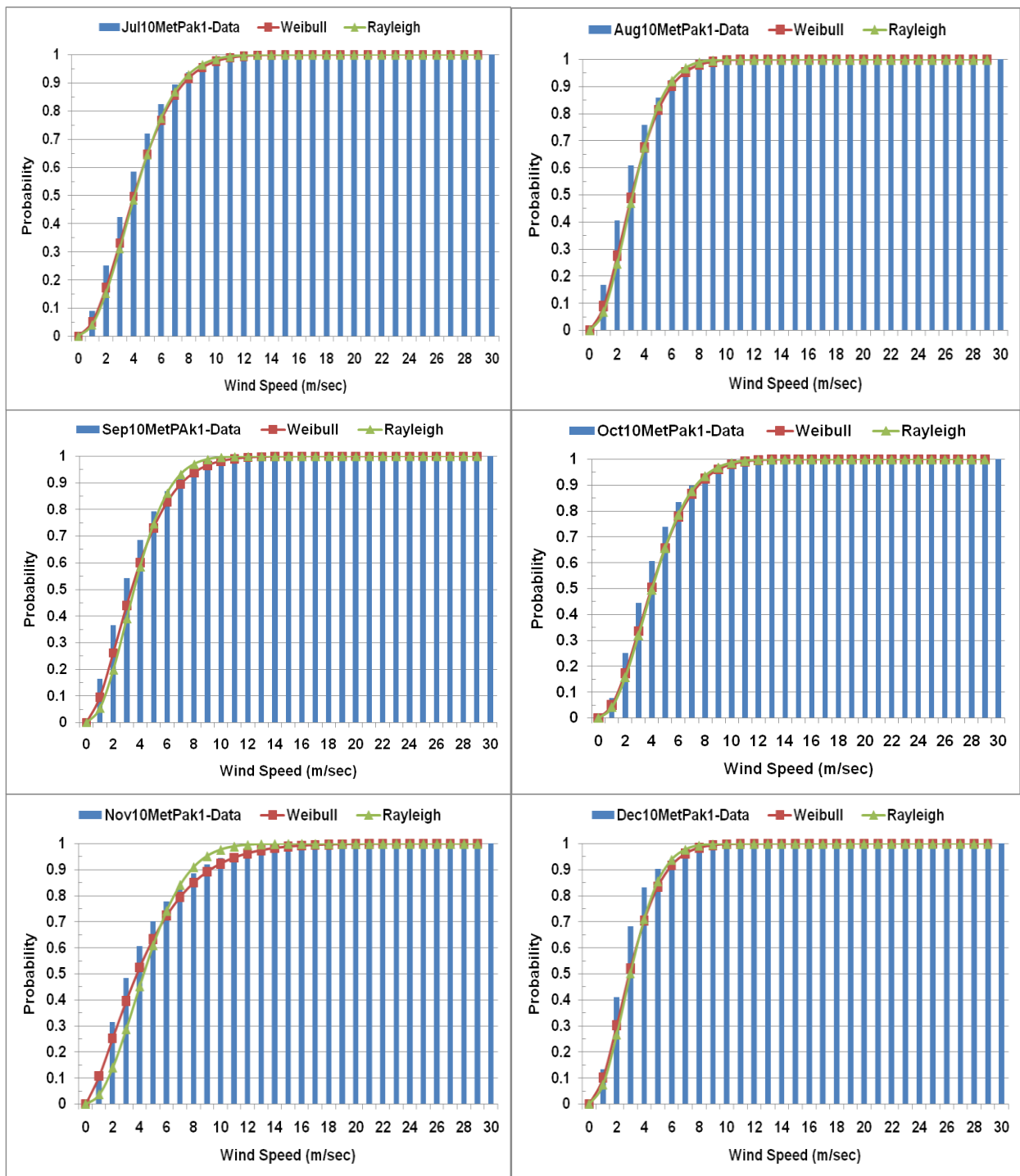


Figure 6-17: Comparison between monthly cumulative distribution of real data, Weibull distribution and Rayleigh distribution year 2010.

6.9 Effect of sampling time on frequency distribution of data

At Merchiston campus, wind data was sampled every second and then logged as an average of every two seconds. It is different from Met office data which was recorded hourly. In order to analyse the effect on the data with different sampling rate, July 2010 MetPak-H data was used, since it has maximum number of logged data (i.e. 1339124 out of 1339200). A MATLAB program was created to convert 2 second data into 1, 10, 20, 30, 40, 50 and 60 minutes averaged data. The data derived from this process is used to draw probability distribution function as shown in Figure 6-18. It seems that with increasing sampling time there is a minor shift in real data bar graphs. This trend was statistically analysed and the results are presented in Table 6-3. Standard deviation decreases as sampling time increases while mean wind speed remains unaffected. The value of shape factor (k) for Weibull distribution increases with increasing sampling time but there is no change in Weibull scale factor (c) and Rayleigh distribution parameters. The increase in Weibull shape factor with increase in sampling time indicates a decrease in the width of the curve giving an impression that wind data is more concentrated in the middle of the curve. This is a natural outcome, because with increased sampling time the data otherwise lying on the edges of the distribution now merges into the values available near to the centre as shown in Figure 6-18.

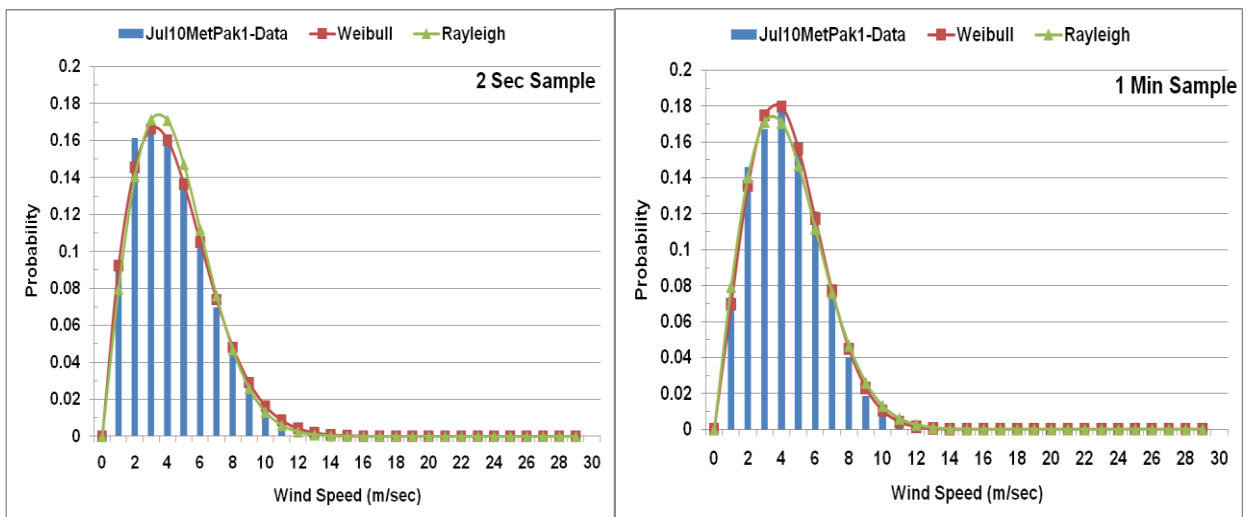


Figure 6 9: Comparison between Probability distribution of real data, Weibull distribution and Rayleigh distribution based on different sampling time (continue).

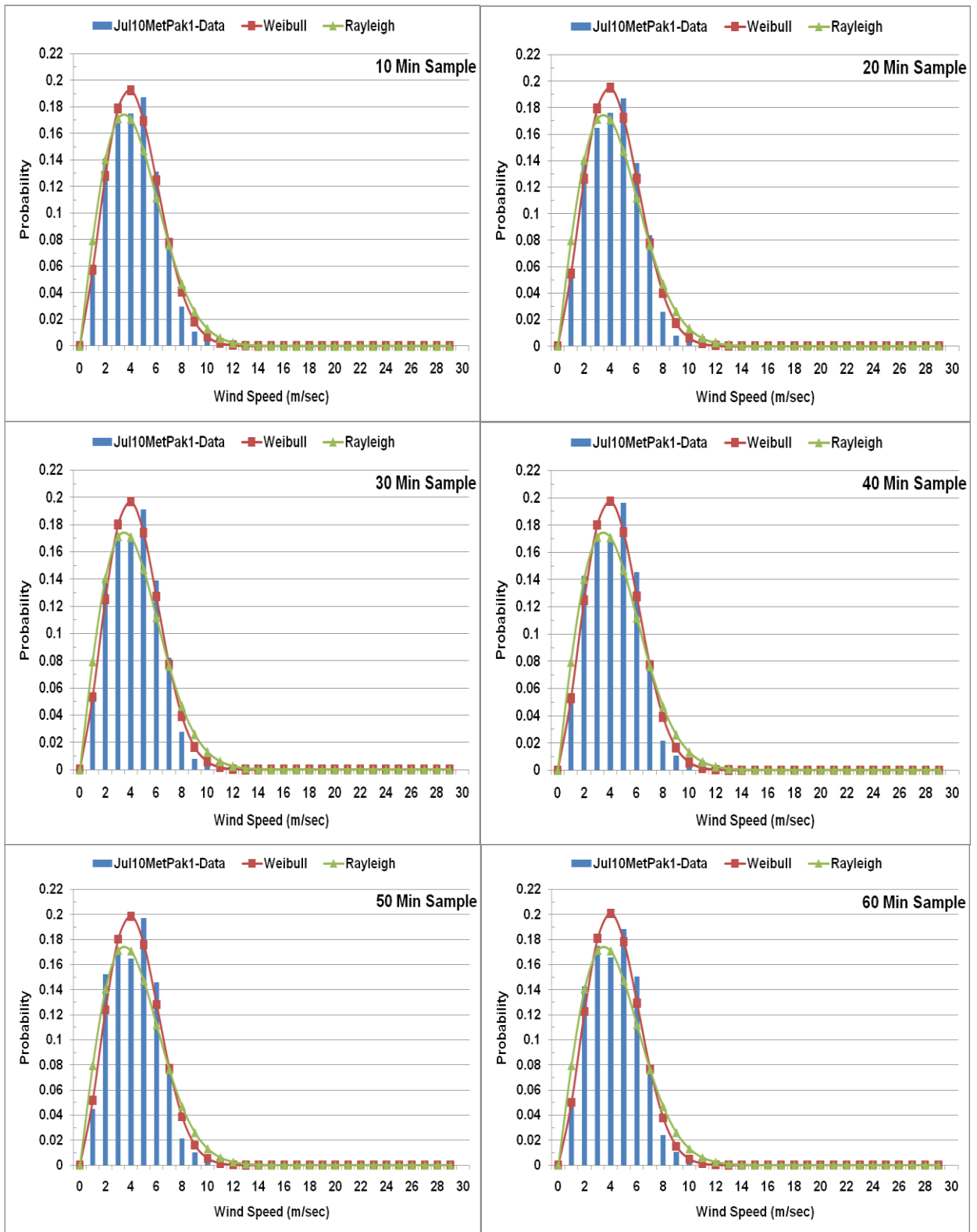


Figure 6-18: Comparison between Probability distribution of real data, Weibull distribution and Rayleigh distribution based on different sampling time.

Table 6-3: Mean, standard deviation and PDF parameters based on different sampling time.

Sampling time	Mean	Std dev	Weibull		Rayleigh
			K-Shape factor	C-Scale factor	C-Scale factor
2sec	4.35	2.47	1.85	4.90	4.91
1min	4.35	2.18	2.12	4.91	4.91
10min	4.35	2.02	2.30	4.91	4.91
20min	4.35	1.99	2.34	4.91	4.91
30min	4.35	1.97	2.37	4.91	4.91
40min	4.35	1.96	2.38	4.91	4.91
50min	4.35	1.95	2.39	4.91	4.91
60min	4.35	1.93	2.42	4.91	4.91

6.10 Velocity duration curve

To get an idea of the nature of wind regime, velocity duration curve was drawn based on MetPak-H and MetPak-L data as shown in Figure 6-19. The plots show MetPak-L curve to be flatter than MetPak-H. While flatter curve indicates more constant and low wind speeds, steeper curve signifies more irregular and high wind regime. Velocity duration curve in Figure 6-19 also suggests that at MetPak-L about 3500 hours wind speed was 4 m/s or higher (i.e. 40% in entire year) and at MetPak-H about 4700 hours wind speed was 4 m/s or higher (i.e. 54% in entire year). But only 0.16% of MetPak-L and 0.41% of MetPak-H data reached up to 12 m/s. These show that the wind speed at Merchiston campus is hardly reaching the rated wind speed, for most of the small wind turbine (i.e. 12 m/s). This is strong evidence that the wind turbine may not achieve the rated power output due to the lack of wind energy resource.

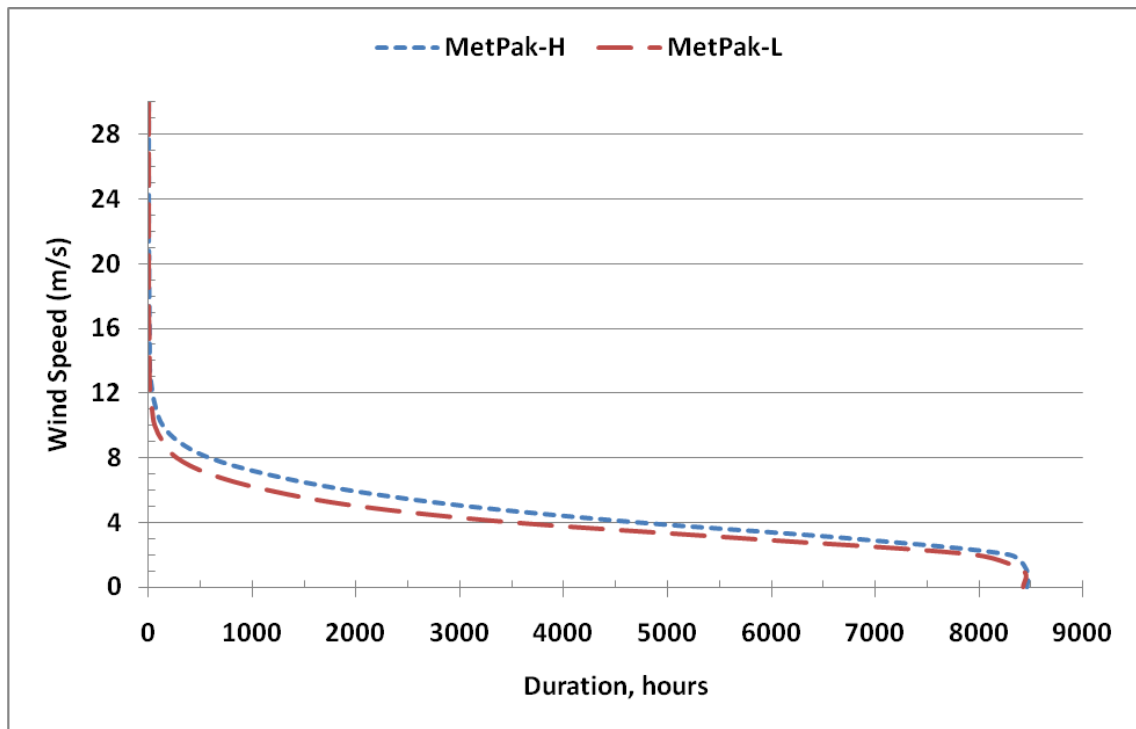


Figure 6-19: Velocity duration curve of MetPak-H and MetPak-L for year 2010.

6.11 Diurnal variation in data at Merchiston

Diurnal wind speed variation is due to differential heating of the earth's surface during the everyday radiation cycle. A typical diurnal variation comprises of an increase in wind speed during the day with it being lowest during the hours from midnight to sunrise. To study wind speed variation in the present research, hourly wind speed data was used to take average for each hour of a day up to a month, the results are shown in Figure 6-20. There is a noticeable increase in wind speed from 7th hour to 20th hour in some of the months but it is not significant as in Met office data (in a rural site). Moreover, the diurnal wind variation at MetPak-L is lower than that of MetPak-H. MetPak-H witnessed highest diurnal wind speed variation in July 2010, in which average wind speed increases from 3.3 m/s to about 5.4 m/s. This 2.1 m/s difference is lower than the typical diurnal variation at Met office weather station (which can go up to more than 3 m/s). For the same month (i.e. July 2010) diurnal wind speed variation at MetPak-L is 1.73 m/s (i.e. 4.5 m/s - 2.8 m/s) only. These results are important as they emphasise that diurnal wind speed variation in urban area is lower than in rural area.

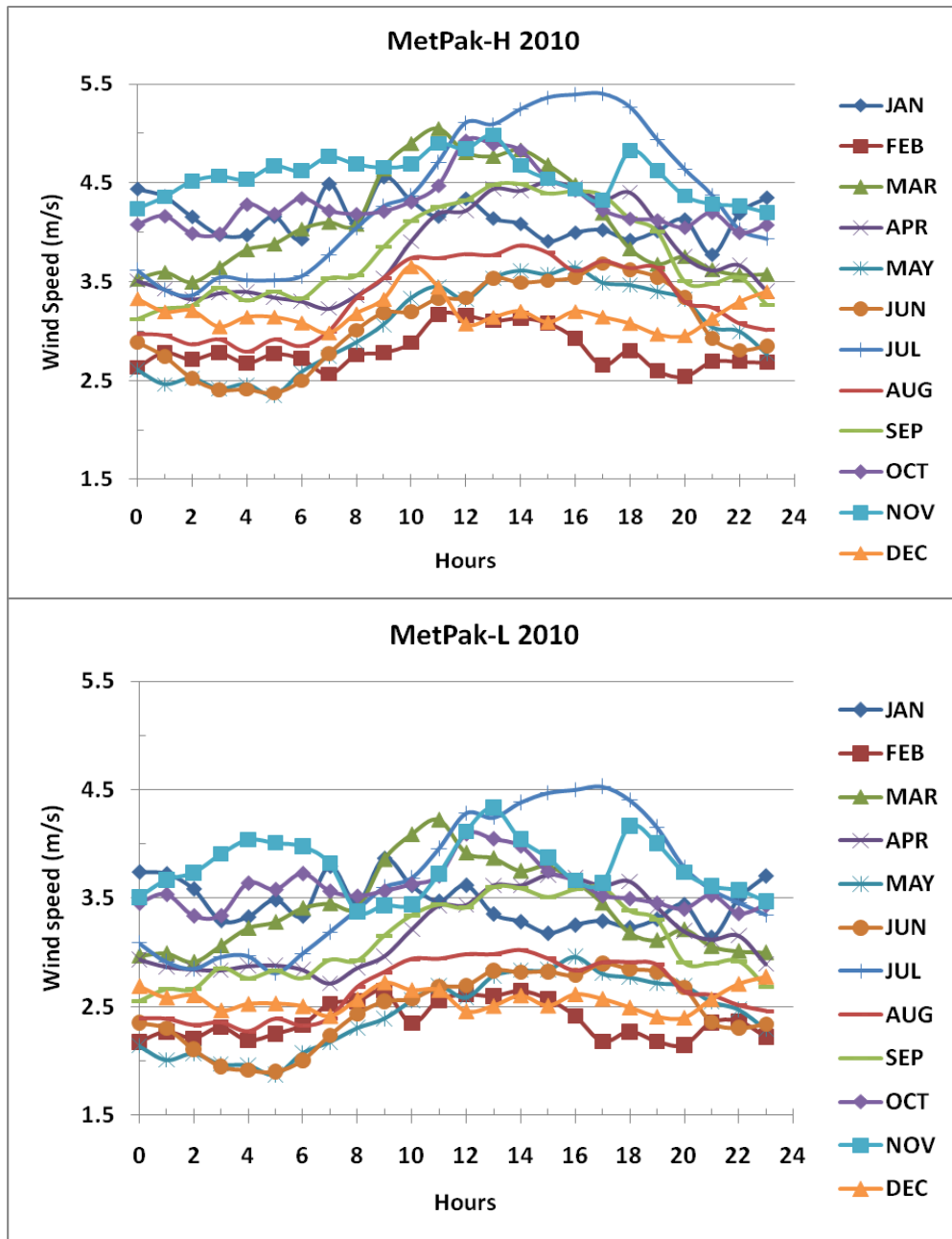


Figure 6-20: Graph of monthly diurnal wind speed at MetPak-L and MetPak-H for 2010.

Diurnal variation in temperature at Merchiston (as shown in Figure 6-21) is in the same fashion as in Met office data except that the rise of temperature in summer is more than the corresponding rise in Met office data. By testing the correlation between diurnal wind speed and diurnal temperature variation, it is found that at Merchiston campus for the year of 2010; only the correlations from

April to September are higher than 0.8 while rest of the months do not show much correlation as shown in Figure 6-22.

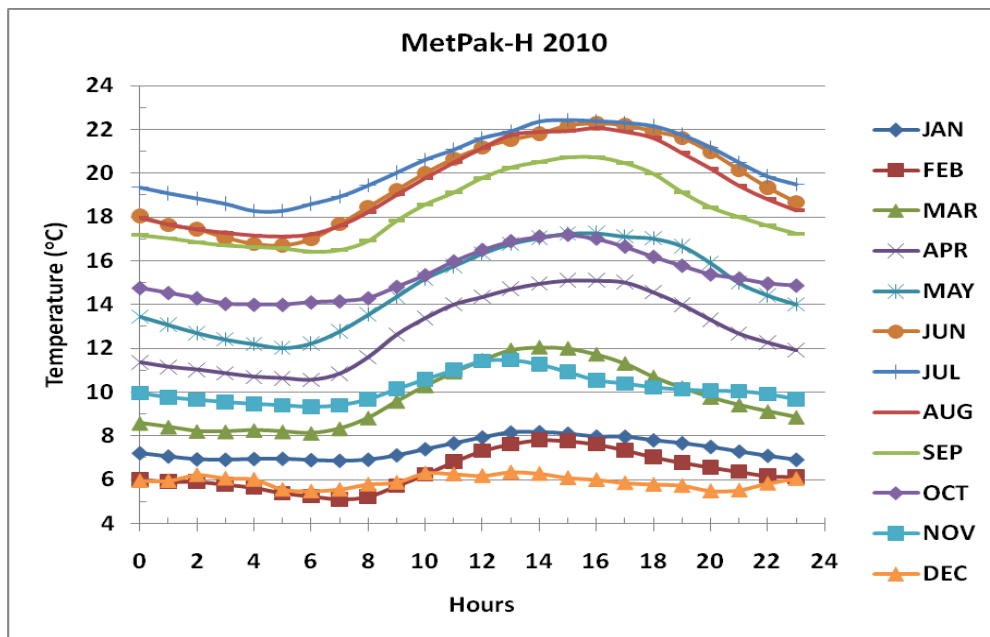


Figure 6-21: Monthly diurnal temperature variation at Merchiston campus for 2010.

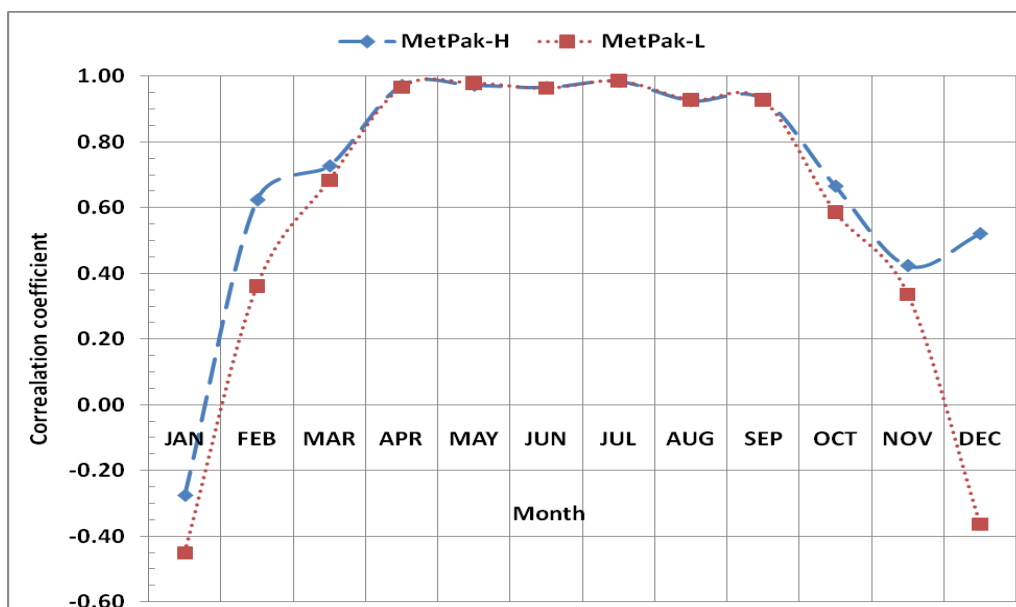


Figure 6-22: Graph of coefficient of correlation for MetPak-H and MetPak-L between diurnal mean wind speed and temperature against months for 2010.

To determine diurnal variation in wind direction at Merchiston campus, the wind flow of two days of July 2010 were drawn as presented in Figure 6-23. July was chosen to study the wind direction since the diurnal temperature and wind speed variation are the highest as well as their correlations. By observing the daily wind flow rose diagrams (as shown in Figure 6-23), it is found that there is no diurnal effect on wind flow direction at Merchiston campus same as in the case of Met office weather station data.

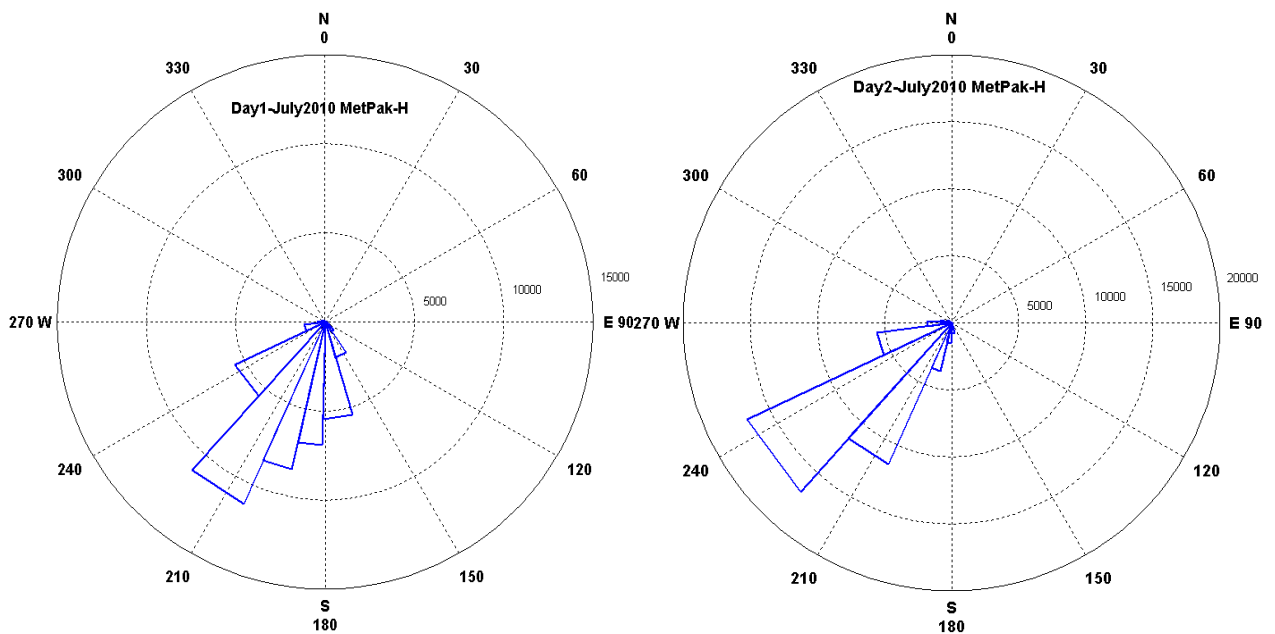


Figure 6-23: Daily wind direction in rose diagram for 2 days of July 2010.

6.12 Comparison of Met office and Merchiston wind data

Having wind data from both sites (i.e. Met office and Merchiston campus) for the same period i.e. July 2009 to December 2009, proved to be beneficial in analysing the differences in rural and urban area wind resource. Table 6-4 shows six months comparison between Merchiston campus and Met office data. Monthly average wind speed for July 2009 was 3.4 m/s, with a standard deviation of 2 m/s at Merchiston campus. For the same period of time, averaged wind speed at Met office site (at Gogarbank) was found to be 3.2 m/s with a standard deviation of 1.88 m/s. It shows that MetPak-H mean wind speed and standard deviation is more or less the same as Met office wind data. However, as discussed in previous chapter the elevation of Merchiston campus is 43 m

(100 m – 57 m) higher than the Met office weather station site. More so, the height of the MetPak-H above ground level is 23.6 m (20.5 m + 3.1 m) while the Met office weather station is only 10 m high above ground level. Considering the height factor, it can be concluded that there is a reasonable difference between urban and rural area's vertical wind profile and because of higher urban roughness wind becomes slower there even at considerable height.

Table 6-4: Monthly mean wind speed and standard deviation at Met office weather station and Merchiston campus.

Month	Mean wind speed (m/s)			Standard deviation (m/s)		
	Met office	MetPak H	MetPak L	Met office	MetPak H	MetPak L
Jul-09	3.24	3.43	2.90	1.88	2.03	1.84
Aug-09	4.28	4.47	3.83	2.23	2.51	2.25
Sep-09	4.81	4.02	3.25	2.58	2.46	2.16
Oct-09	3.58	3.46	3.05	2.41	1.94	1.84
Nov-09	4.79	4.90	4.24	3.04	3.07	2.85
Dec-09	2.89	3.32	3.18	1.97	2.02	2.90
Average	3.93	3.93	3.41	2.35	2.34	2.31

6.13 Wind power density and energy estimation

By using available wind data, theoretical wind power density can be calculated. One way to estimate wind power density is to use the monthly average wind speed to calculate wind power density over the period of a month; the other is to calculate by using hourly wind data. Equation 5-15 was used to calculate wind power density; results are shown in Table 6-5. Equation 5-15 suggests that wind power density depends only on the wind speed and air density. However, there is another very important factor, which is the consistency in wind speed during a time period as it makes a big difference. From Table 6-5, it is noticed that yearly average wind power density derived from hourly wind data is almost doubled than the wind power density derived from monthly mean wind speed. This is because when a mean value is taken, it equalizes the weight or importance of those values; but in calculating wind energy, values of wind speed ought not to be equalized because the power in wind is directly proportional to the cubic power of the wind speed. If wind speed increases twice, the power in wind increases eight times. That's why when monthly mean wind speed is taken, it simply equalizes the weighting of higher values to the

weighting of lower values and resulting in inaccurate calculation of wind power density. For the present research, wind power density was therefore calculated from hourly mean wind speed, then summed up for a month and then divided by the number of hours in the month. Although it is better than the other method, it is still not the most accurate one as the wind does not blow with constant intensity for a whole hour.

Table 6-5: Monthly mean wind speed, power density derived from mean wind speed and from hourly data.

Months	MetPak-H mean Wind speed (m/s)	Wind Power density (watt/m ²) from Mean wind speed	Wind Power density (watt/m ²) from hourly data
Jan-10	4.15	44.50	52.83
Feb-10	2.80	13.78	26.38
Mar-10	4.11	43.28	93.51
Apr-10	3.80	34.24	68.19
May-10	3.04	17.58	27.15
Jun-10	3.06	17.95	28.79
Jul-10	4.35	51.52	83.80
Aug-10	3.33	23.13	38.96
Sep-10	3.78	33.76	65.74
Oct-10	4.28	49.14	80.78
Nov-10	4.57	59.49	163.51
Dec-10	3.18	20.16	39.59
Yearly Average	3.71	34.04	64.10

According to Equation 5-16 the wind power density associated with the wind speed frequency can be calculated as shown in Figure 6-24. It shows wind power density and wind speed frequency in relation with different wind speeds.

Table 6-6 shows the comparison between results obtained from different methods of estimating total wind energy for the year 2010. It shows that energy calculated on the basis of monthly mean wind speed is very low. To calculate wind energy from monthly mean wind speed, mean wind speed was multiplied by the number of hours in the month and then all monthly estimated energy was totalled up. On the other end yearly estimated wind energy, based on frequency distribution, is much higher. This is because in this method different wind speeds in a bin are tagged as median wind speed which is sometimes higher and sometimes lower than the median value (results show that most of the time low wind speed was tagged high, thus yielding high result values). Yearly wind

energy estimated by hourly wind data is more reliable as it includes all hourly averaged wind data.

As in Table 6-6, hourly wind data yields an energy estimation of 563 kWh for the year 2010 at Merchiston campus MetPak-H, which is almost half of the energy calculated by Met office wind data (i.e. 1MWh) located in rural area of Edinburgh. In contrast, there is not much difference in yearly mean wind speeds of both data. In years 2002 and 2003, yearly mean wind speed at Met office weather station was 3.9 m/s (as shown in Table 5-1) and estimated yearly wind energy was 801 kWh and 786 kWh (as shown in Table 5-8), respectively. However, at Merchiston MetPak-H yearly mean wind was 3.71 m/s but estimated wind energy was only 563 kWh. It shows that the wind energy available in urban area is about 30% less than that in rural area although the sites are only 8 km apart.

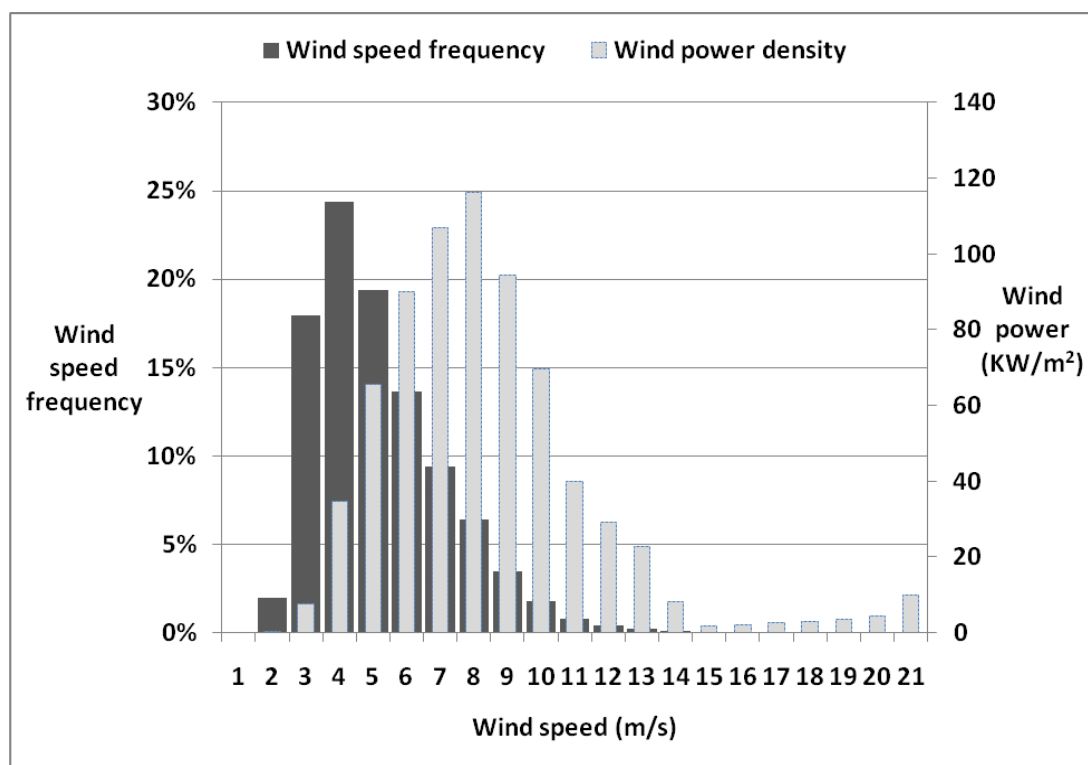


Figure 6-24: Wind power density bar graph in relation with Wind Speed Frequency distribution for year 2010 at MetPak-H.

Table 6-6: Comparison of results for wind energy estimation based on different methods for year 2010 MetPak-H.

Total wind energy estimation for year 2010 based on MetPak-H data		
By monthly mean wind speed	By hourly mean wind speed	By wind speed frequency distribution
299.46kWh/m ²	562.58kWh/m ²	722.28kWh/m ²

6.14 Turbulence analysis

6.14.1 Introduction

In addition to the pressure gradient and gravitational forces, inertia of the air, the earth's rotation and friction with the earth's surface (resulting in turbulence) also affect the atmospheric winds.

Natural wind is defined as consisting of turbulent fluctuations superimposed on a quasi-steady mean wind speed. From the sample of wind speed in Figure 6-25, it is obvious the variations are irregular and cannot be described in a deterministic manner. Wind turbulence is best characterized using its statistical properties because statistical techniques have been developed for analysis of randomly fluctuating signals (Freris, 1990).

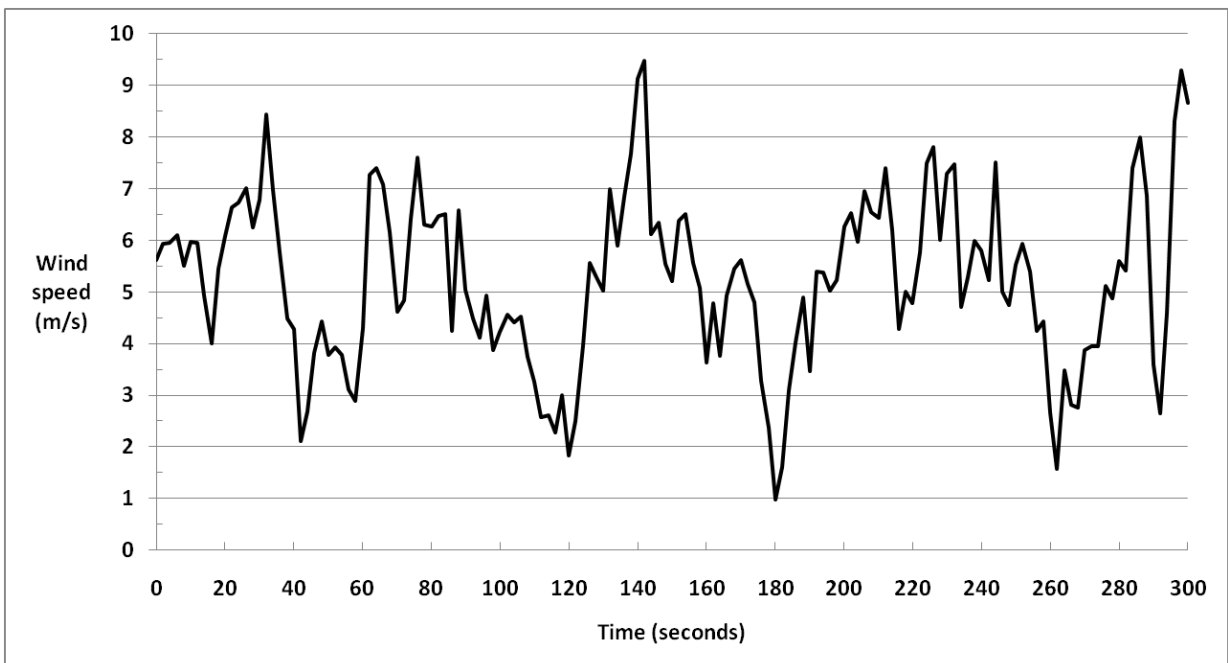


Figure 6-25: Wind speed data for a 5-minutes sampling period at 0.5 Hz.

Statistically, turbulence is the deviation of the instantaneous wind speed $U(t)$ from the quasi-steady mean wind speed \bar{U} .

$$u(t) = U(t) - \bar{U} \quad \text{Equation 6-1}$$

The variability of the wind speed is best described in terms of the variance σ_u^2 , where

$$\sigma_u^2 = \bar{u}^2 = \frac{1}{T} \int_{t_0 - T/2}^{t_0 + T/2} [U(t) - \bar{U}]^2 dt \quad \text{Equation 6-2}$$

Turbulence intensity I_u , a measure of the gustiness of the wind, is then defined as;

$$I_u = \frac{\sigma_u}{\bar{U}} \quad \text{Equation 6-3}$$

Inside the atmospheric boundary layer at a fixed height, turbulence intensity usually decreases with increase in height because mean wind speed increases more rapidly than the variance (Freris, 1990).

6.14.2 Sampling time for turbulence intensity

As shown in Equation 6-3, turbulence intensity is the ratio of standard deviation to mean wind speed both of which depend on sampling period. Figure 6-26 shows that standard deviation varies more than the mean wind speed with change in sampling period thus also affecting the turbulence intensity.

A MATLAB program was written to analyse different sampling periods for one particular time series. It was used to generate averaged values of turbulence intensity for each sampling period. This output was then plotted as shown in Figure 6-27. It is noted that the monthly average turbulence intensity (TINT) increases with a power trend or regression as sampling period increases.

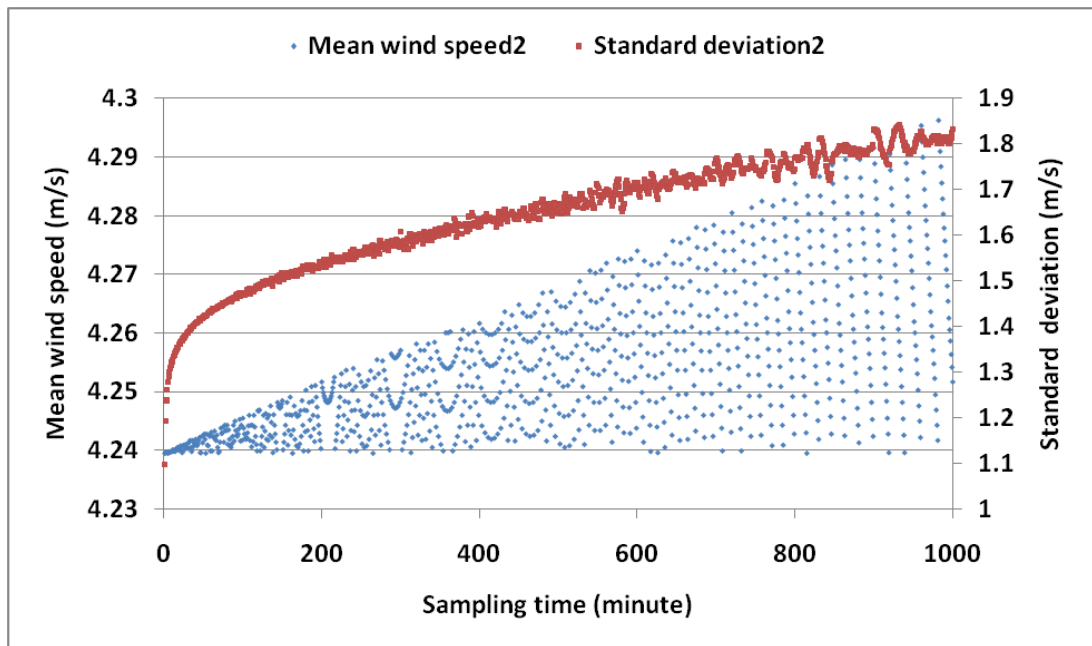


Figure 6-26: Mean wind speed and standard deviation versus sampling period.

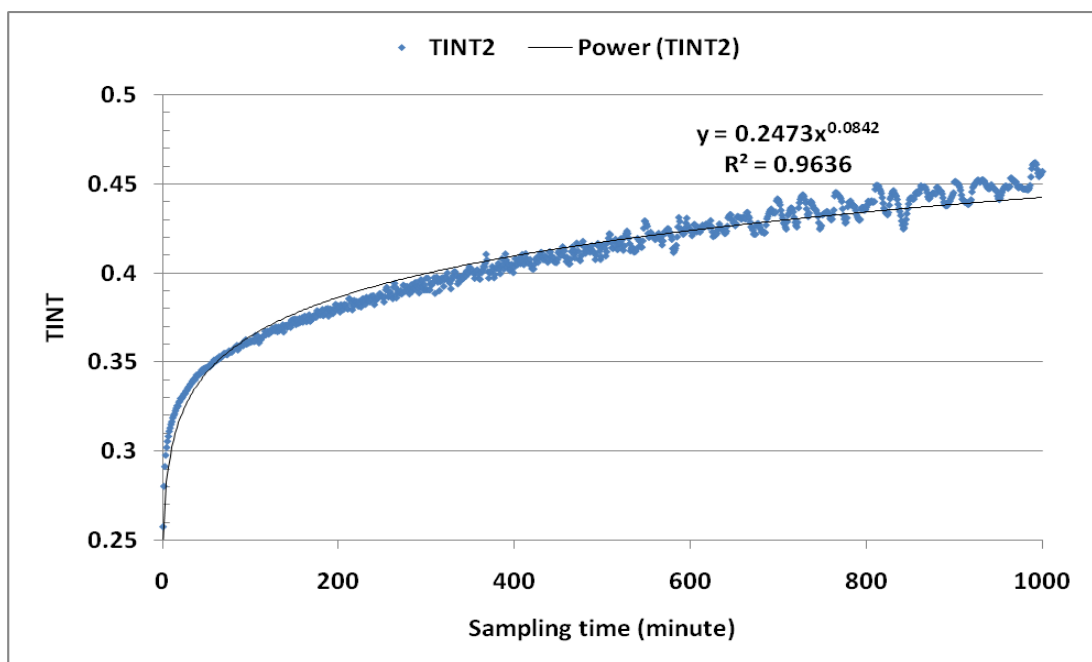


Figure 6-27: Turbulence intensity (TINT) versus sampling period with power trend.

Turbulence intensity against sampling time period of 1-60 minutes is plotted in Figure 6-28. It is found that turbulence intensity changes rapidly as sampling period increases from 1 to 10 minutes. The rate of change becomes lower

between 10 to 60 minute sampling periods. It is also evident from Figure 6-29 that the rate of change or slope of TINT is between -0.002 and 0.002 from 10 to 60 minute sampling period. Similar research conducted at the Risø National Laboratory in Denmark suggests averaging times of 10-60 minutes (Petersen *et al.*, 1998). An overview of TINT taken from 10-60 minute sampling period is shown in Figure 6-30. Average of TINT of 10-60 minutes sampling period is 0.33657 which is very close to TINT of 30 minute sampling time (i.e. 0.33605). Supported by these evidences, it is decided that in all TINT calculations, a 30 minute sampling time will be taken into account.

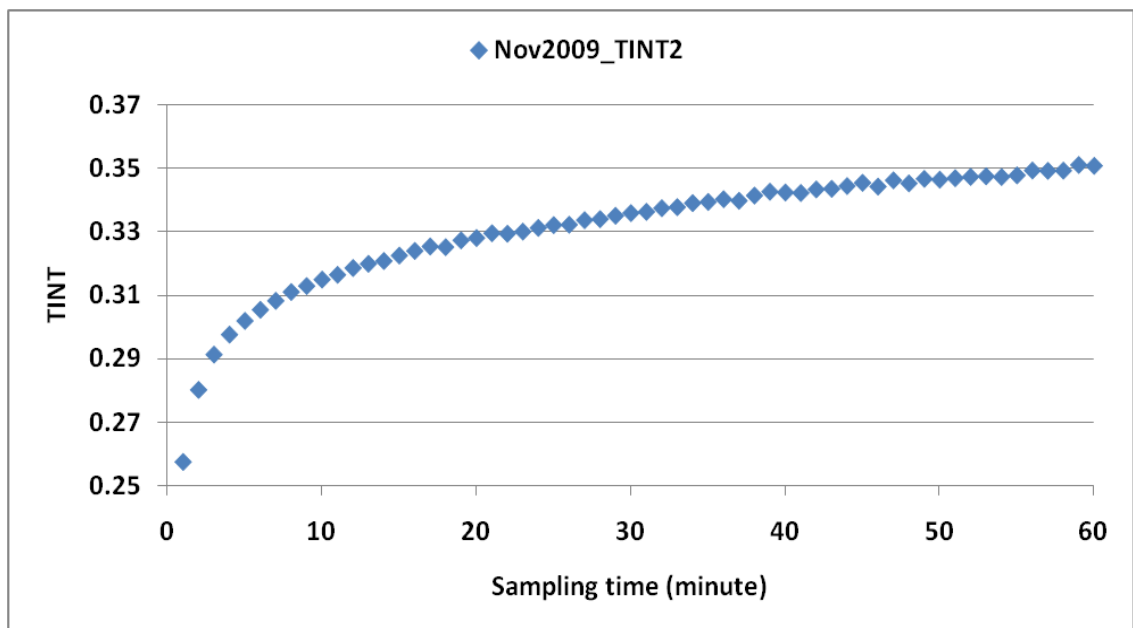


Figure 6-28: Turbulence intensity versus sampling period of 1 to 60 minutes.

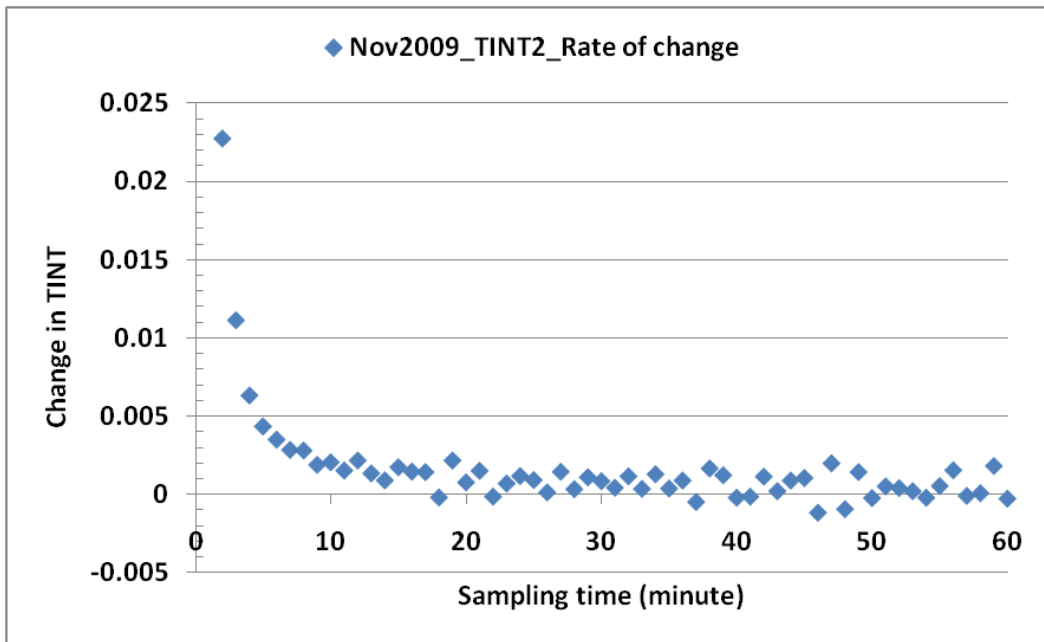


Figure 6-29: Rate of change (slope) between consecutive turbulence intensity values.

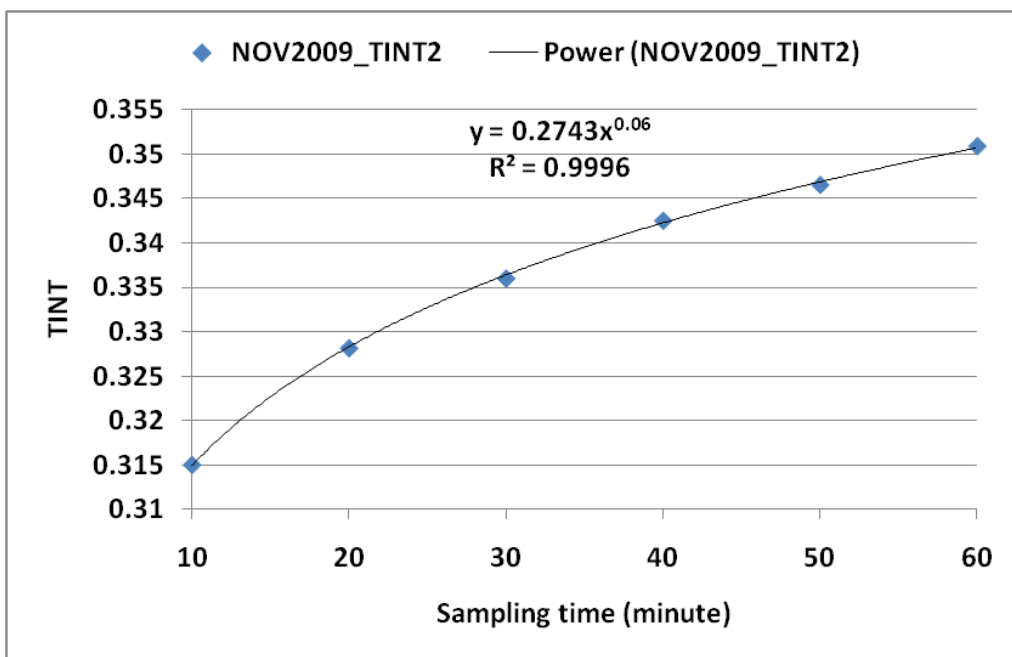


Figure 6-30: Turbulence intensity versus sampling period 10 to 60 minutes.

6.14.3 Standard deviation and mean wind speed

To study the relation of TINT with standard deviation and mean wind speed, it is important to first analyse the relation between mean and standard deviation of

wind speed. Figure 6-31 shows that there is a linear relation between mean wind speed and standard deviation in wind data, i.e., standard deviation increases as mean wind speed increases. Although there is no recognisable relation between mean wind speed and TINT, at low mean wind speed, variation in TINT is much higher than at high mean wind speed (as shown in Figure 6-32). It shows that as mean wind speed increases, the value of TINT converges to a constant value (in this case 0.3) as shown in Figure 6-32. On the other hand, variation in TINT with respect to standard deviation is random; it varies around its mean value (i.e. 0.3) no matter if standard deviation is high or low as shown in Figure 6-33.

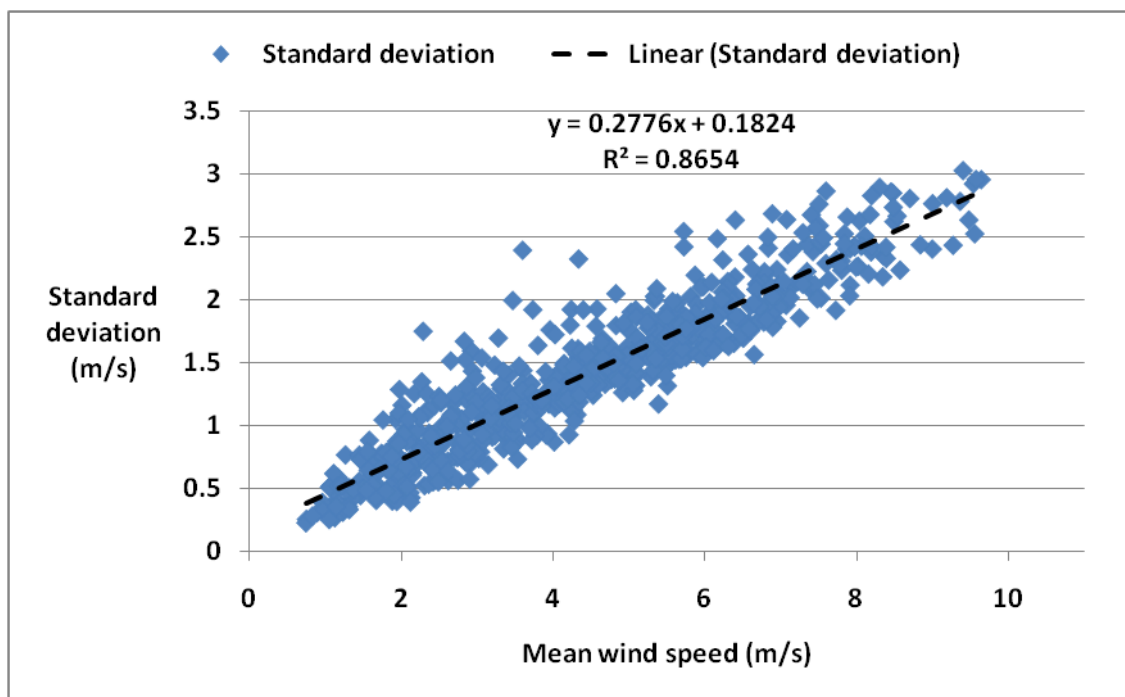


Figure 6-31: Standard deviation versus mean wind speed.

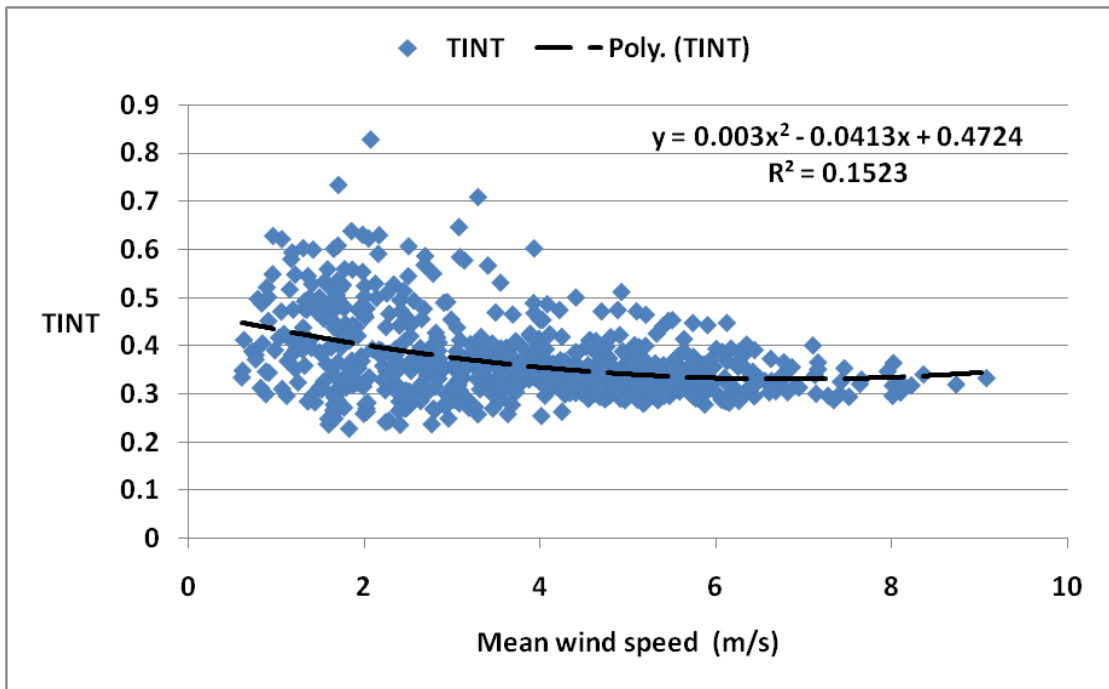


Figure 6-32: Turbulence intensity (TINT) versus mean wind speed.

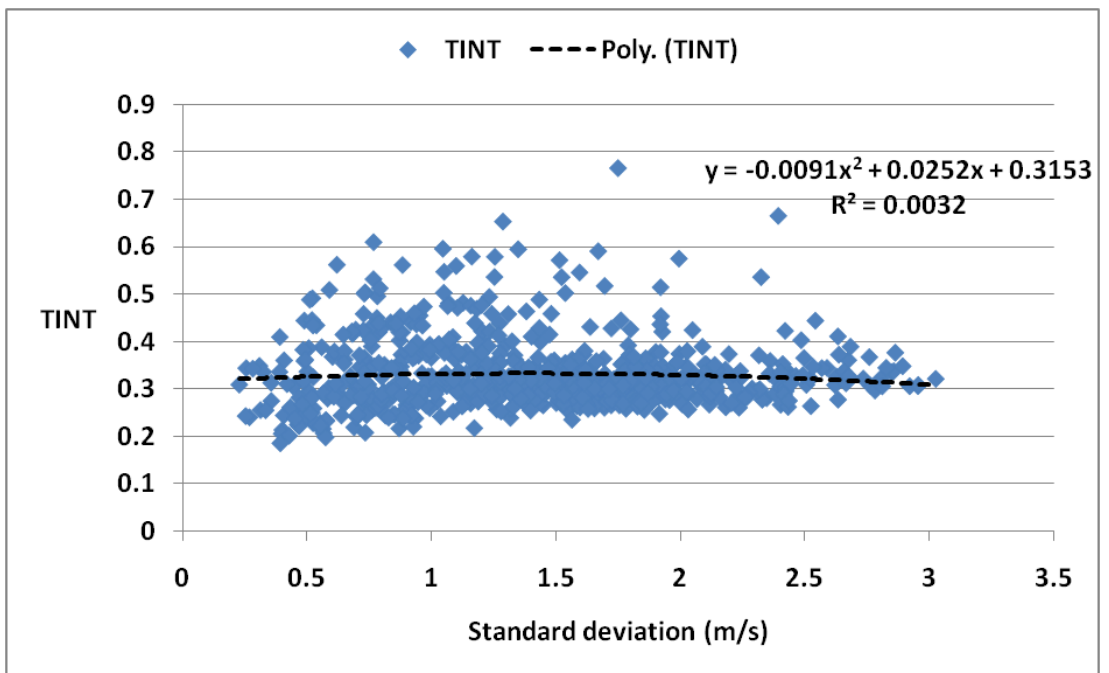


Figure 6-33: Turbulence intensity versus standard deviation in wind speed.

6.14.4 Variation in wind profile with height near to buildings

In this research vertical distance between MetPak-H and MetPak-L is 1.5 m and the height of the MetPak-L from roof is 1.6 m. This created an opportunity to be able to study change in wind profile with height in the vicinity of an urban building. Figure 6-34 shows that there is very strong linear relation in mean wind speed of lower and higher MetPak. Reiterating from Section 6.6, wind speed at MetPak-H is 16% higher than MetPak-L while standard deviation increases by only 7%.

Figure 6-35 shows that there is a linear relation between TINT at MetPak-L and TINT at MetPak-H. On further investigation, it was found that the ratio between TINT-L and TINT-H is high when turbulence is low and is low when turbulence is high. In other words, in a state of high wind turbulence the difference between lower and upper turbulence value becomes low while during low wind turbulence this difference becomes high. From Equation 6-3, it can be stated that turbulence intensity is directly proportional to standard deviation. Therefore, when standard deviation becomes high, the change in TINT with height decreases. Or, since turbulence intensity is inversely proportional to the mean wind speed, therefore, when mean wind speed decreases, the change in TINT with height also decreases and vice versa.

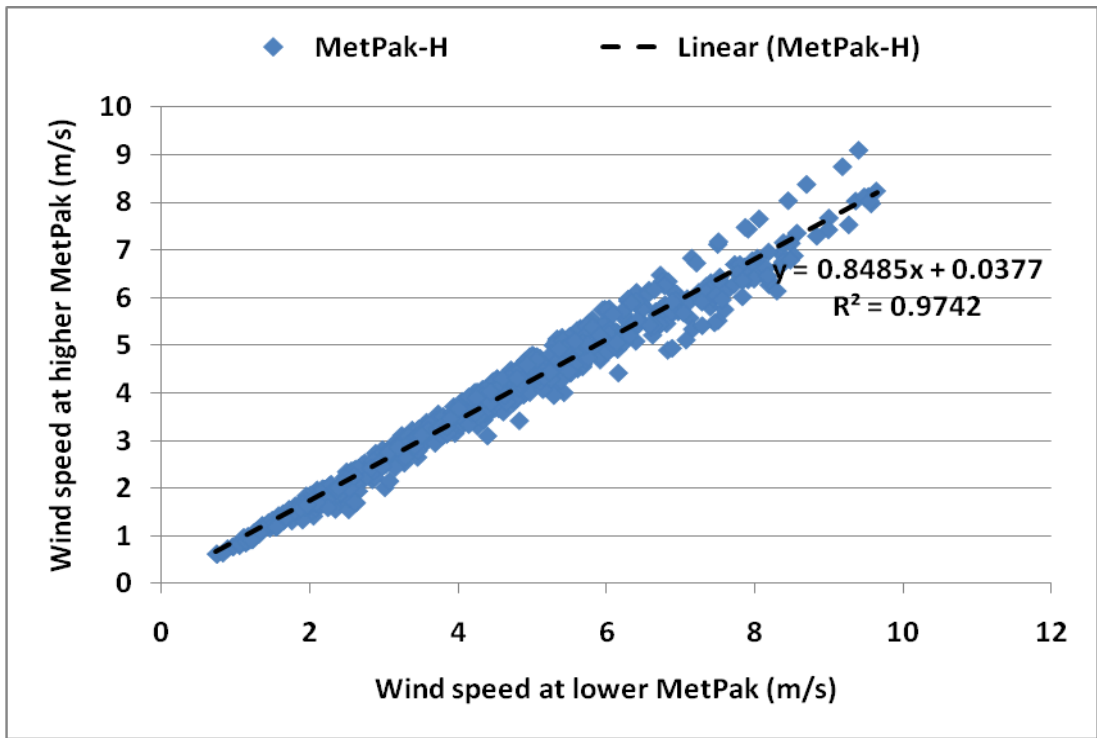


Figure 6-34: Wind speed at lower Matpak versus wind speed at higher Matpak.

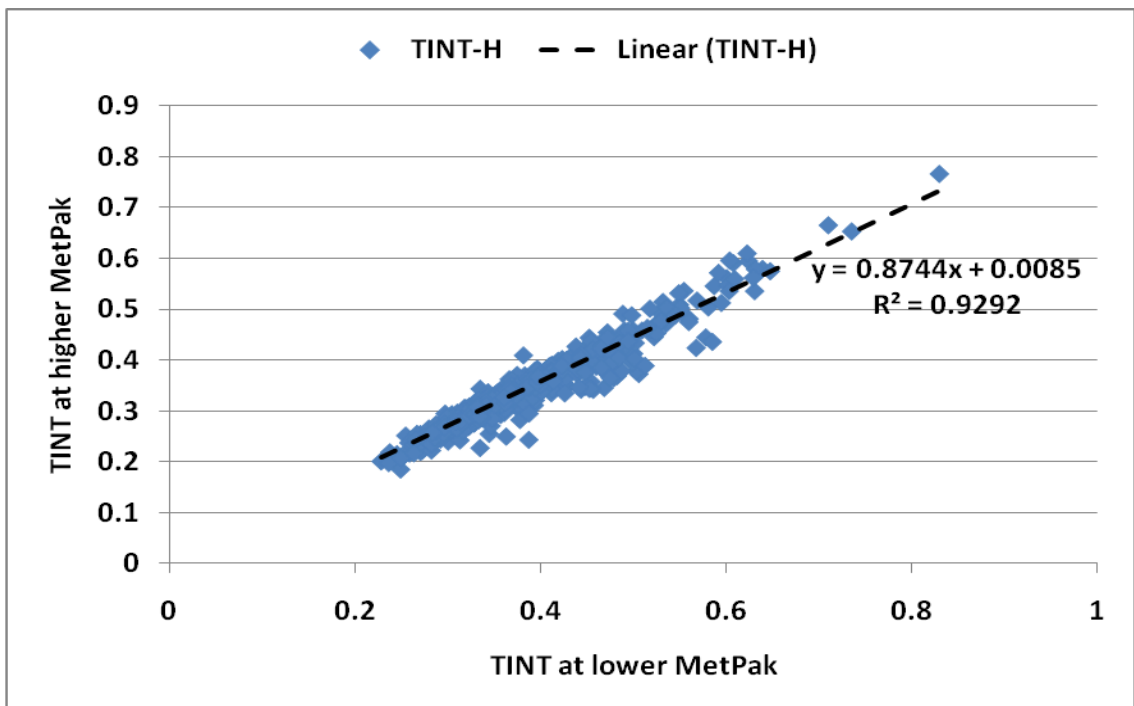


Figure 6-35: TINT at lower Metpak versus TINT at higher Metpak.

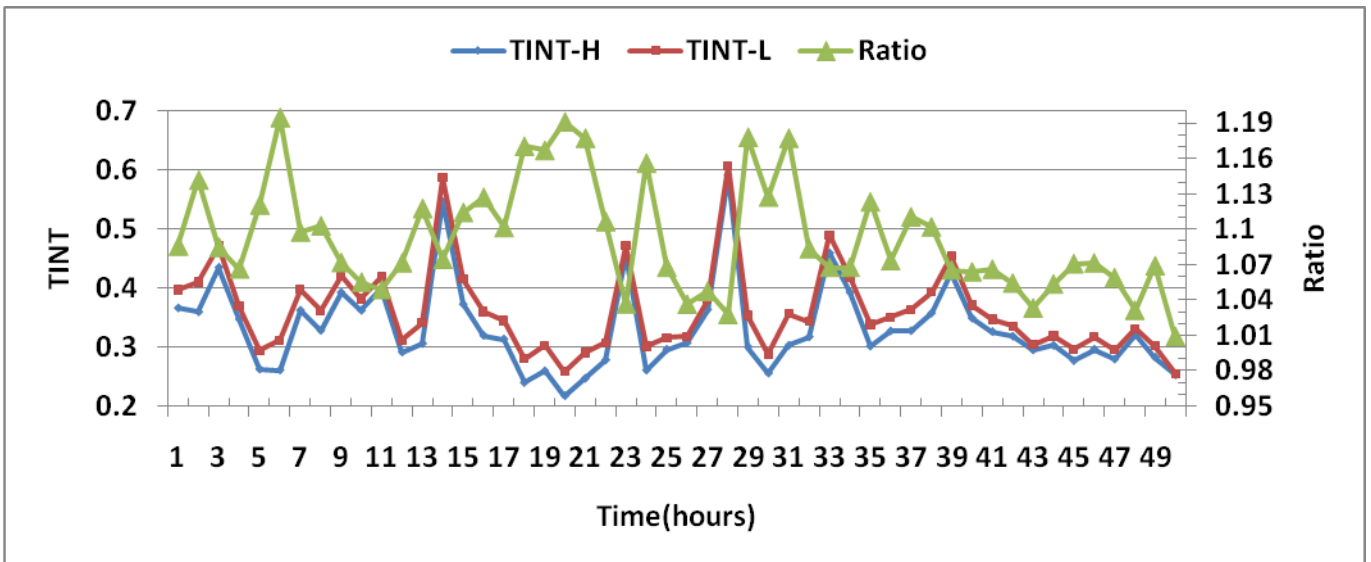


Figure 6-36: Lower MetPak turbulence (TINT-L) and higher MetPak turbulence (TINT-H) on hourly time scale and ratio between them.

By drawing probability distribution of lower and higher MetPak it is clearly identified that TINT-L has more probability for high turbulence intensity than TINT-H as shown in Figure 6-37. In other words, TINT decreases at Merchiston campus roof top by 10% as height increases by 1.5 m.

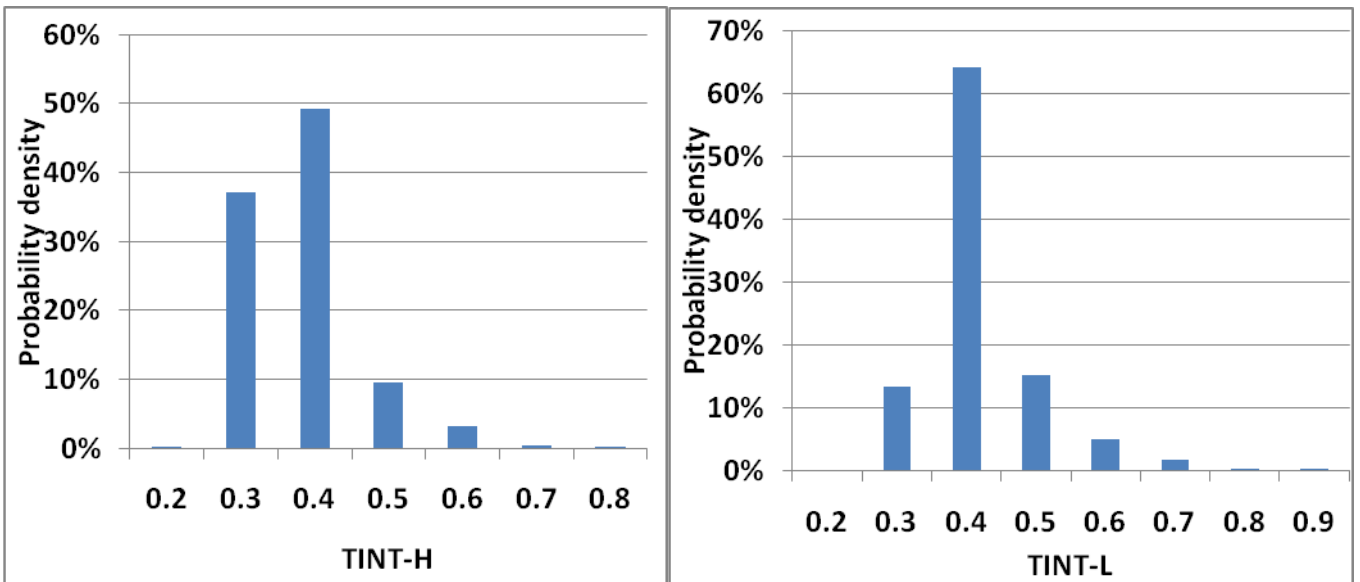


Figure 6-37: Probability density of wind turbulence intensity at higher MetPak (TINT-H) and lower MetPak (TINT-L).

6.15 Variation in wind direction

Urban area wind also has directional variations in addition to general wind speed variation. The swirling nature of wind found in many urban areas has two main consequences that reduce the amount of energy captured by a lift-based (horizontal-axis) wind turbine. Firstly, the turbine is constantly attempting to turn (yaw) into the wind direction, hence causing reduction in the amount of time it is aligned with the flow. Secondly, even when wind turbine is aligned with the main wind flow direction, the air arrives at the blades at a non-optimal direction for the blade design (Holdsworth, 2009).

Wind data from Merchiston campus shows that there is reasonably significant variation in the wind direction as shown in a snap shot of wind directional data in Figure 6-38. It is difficult to quantify and present the variation in wind direction because a line graph as shown in Figure 6-38 shows very high directional difference between 0 degrees and 350 degrees, but as a matter of fact there is only 9 degrees angular difference between them. Moreover, a rose or compass graph cannot depict the variation with the time scale.

In addition to that, an error was also identified in wind directional data, which was caused by the logging of sample averages. By looking at Figure 6-38 it can be seen that in a series of time, wind changes its direction from 0 degree to 180 degrees. Then it blows from 350 degrees within a span of six seconds and its direction continues to vary between 180 and 350 degrees, sometimes also going down to 0 degree. The angular difference between 0 and 350 degrees is only 9 degrees, that's why it is understandable that wind direction varies in between these angles. But the angular difference between 350 and 180 degrees is 170 degrees and between 0 and 180 degrees it is 180 degrees. This huge and sudden change in atmospheric air flow in normal circumstances is not possible. Careful inspection of wind directional data reveals that this error appears when one of the two per second samples of wind direction taken by data logger was on one side of the 0 degrees (i.e. 0 to 10 degrees) while the other was on the other side (i.e. 350 to 359 degrees). To put it simply, when wind direction varies across the North (0 degree) direction in each sample, it

causes the arithmetic average of both samples, deviate about 180 degrees from each other, to be logged by the data logger. At Merchiston campus, wind blows occasionally from north direction as shown in Figure 6-11, the aforesaid error only affects the data by very minor percentage. In fact there is only 1 entry out of 100 in the monthly data showing a change of more than 170 degrees in wind direction. Therefore such error can safely be neglected in wind directional calculations.

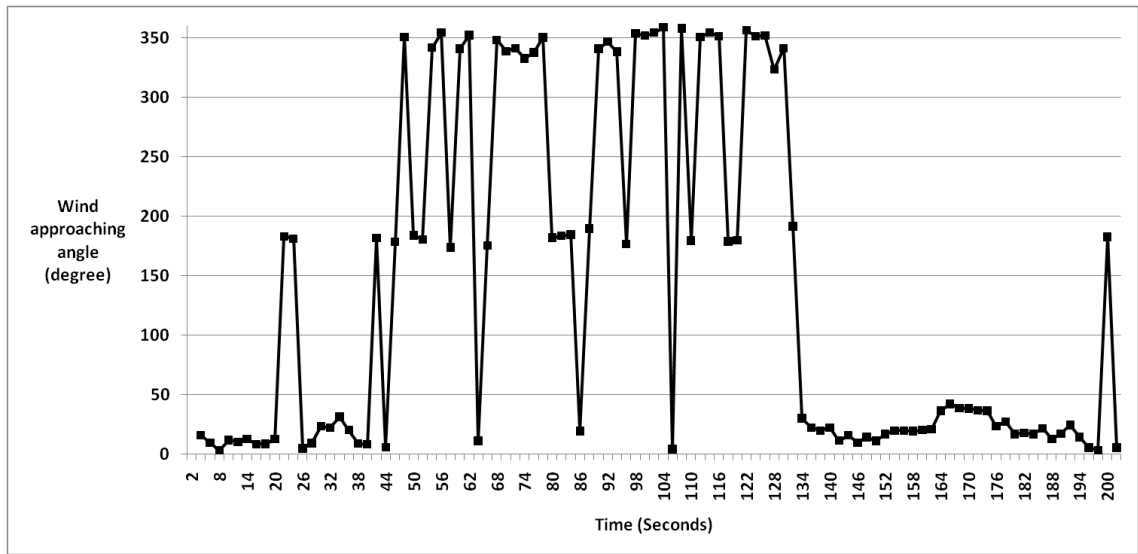


Figure 6-38: Wind approaching angle with the increment of time.

To quantify the directional variation, an angular difference in each directional data is calculated. In this approach, the difference between each successive data points has been taken and to avoid the misinterpretation of the difference between extreme angles (e.g. 1 degree and 350 degrees), 360 is subtracted from all results having a difference of more than 180 degrees.

The cumulative probability distribution graph in Figure 6-39 shows that in every two seconds wind changes its direction at least two degrees and this change increases logarithmically. It also shows that the variation in wind direction in different months is more or less the same.

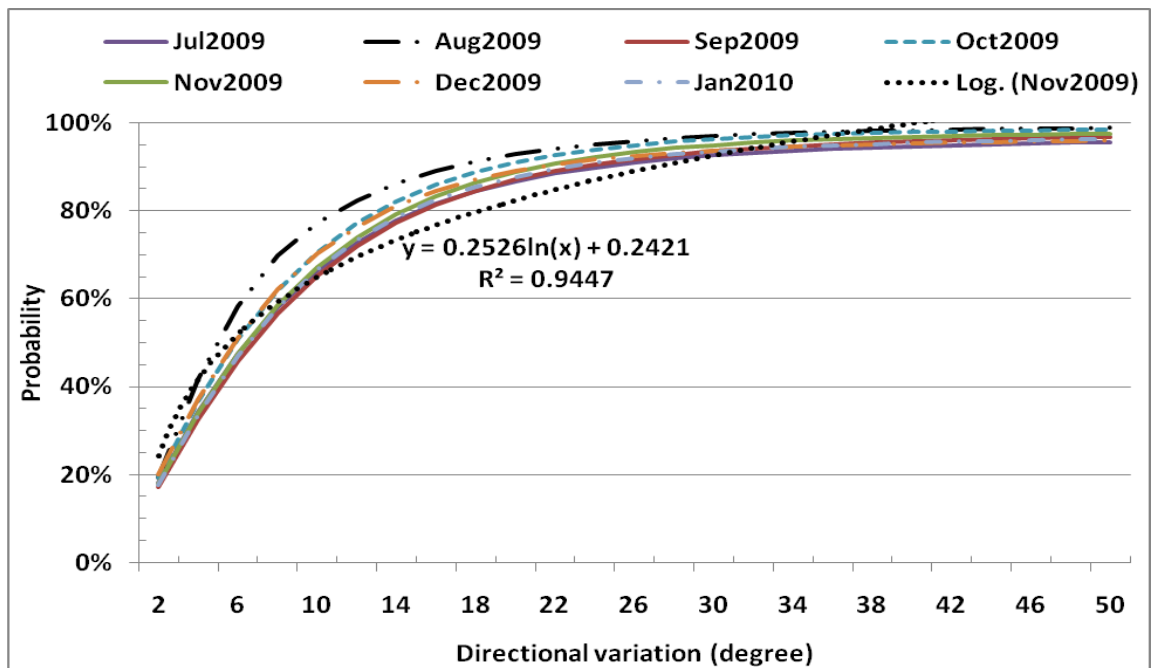


Figure 6-39: Cumulative probability distribution of wind direction variations for different months and logarithmic trend line.

To evaluate the strength of directional variation, turbulence intensity for wind directional variation was calculated by using Equation 6-3. For this calculation, standard deviation and mean of change in wind directional values for 10 minutes were used. It is found that the value of TINT in wind direction is much higher than the value of TINT in wind speed (i.e. for wind speed average TINT is about 0.3 and for wind direction variation average TINT is about 1). To study the relation between the wind directional variation and wind speed, a plot was drawn as presented in Figure 6-40. It shows that as wind speed increases, TINT in wind direction decreases. The probability of variation in wind direction is higher at low wind speed than at high wind speed.

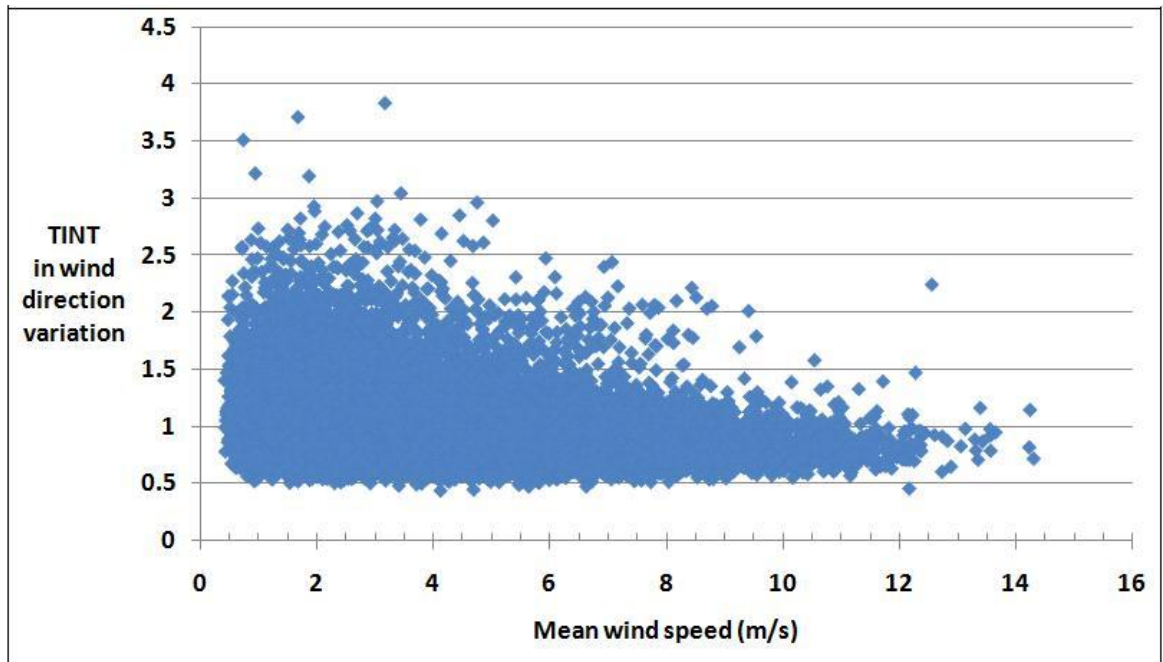


Figure 6-40: Turbulence intensity (std dev / mean) of wind directional variation versus mean wind speed.

6.16 Conclusion

Topography around Merchiston campus was analysed and a lot of elevation variations were found around the campus. Prevailing wind direction at Merchiston is primarily south-west but wind also blows from east and west, and very rarely from north and south. Average yearly wind speed 3m above the roof is found to be 3.71 m/s. Through probability distribution analysis, it was established that about 65% of the time wind speed was 4 m/s or lower and Weibull distribution fitted better than Rayleigh distribution. Diurnal variation in urban area is not as significant as in rural area. There is about 30% less wind energy available in Edinburgh's urban habitation when compared to the rural area even if the mean wind speeds were roughly the same. The choice of method used to calculate the available wind energy plays a crucial role and calculation from hourly average wind speed is found to be more accurate than others. Wind energy available for year 2010 at Merchiston campus is calculated as 563 kWh/m². Turbulence in wind speed and wind direction was also analysed and its intensity was found to be higher in the latter.

7 CFD ANALYSIS

7.1 Introduction

This chapter details the information about the CFD software and sheds light on the modelling approach adopted for investigating the wind flow around the rooftop of the building structure under study. The CFD simulation results have also been presented in this chapter. The aim of this exercise (CFD analysis) is to explore the wind flow pattern and the differences in wind speed at two predetermined target points.

7.2 PHOENICS CFD software

7.2.1 Introduction

For this research, PHOENICS CFD software has been used as it has more ready-made tools than any other CFD software. The name is an acronym for "Parabolic Hyperbolic Or Elliptic Numerical Integration Code Series". It is a commercial "CFD code", i.e. a member, of that family of software packages which embody the techniques of Computational Fluid Dynamics. It is established software used by the industry for complex flow problems and hence is well tested and benchmarked. It is also a "SFT code" (Solid-Fluid-Thermal) and has additional capability of calculating stresses-in-solids. Being a general-purpose software package it quantitatively calculates how fluids (air, water, steam, oil, blood, etc) flow in and around; engines, buildings, human beings, lakes, river, oceans etc. PHOENICS can estimate the associated changes of temperature, pressure, velocity etc of different chemical and physical composition.

7.2.2 The components of PHOENICS

PHOENICS has different modules, for the input (problem definition), data-processing and output. Each of these stages/functions is detailed below:

- a) Problem definition (i.e. pre-processing), in which the user prescribes the situation to be simulated and the questions which are to be answered.

- b) Simulation (i.e. data-processing), by means of computation, of what the laws of science imply in the prescribed circumstances.
- c) Presentation (i.e. post-processing) of the results of the computation, by way of graphical displays, tables of numbers, and other means.

PHOENICS is therefore, like many but not all CFD codes. It has a distinct software module or set of modules, for each of the above three functions. This sub-division allows functions to be performed in a better and easier way than other CFD software. The three (sets of) modules of PHOENICS are called:

- SATELLITE (which incorporates also the Virtual-Reality Editor and Viewer)
- EARTH (the solver module); and,
- PHOTON (which incorporates the graph-plotter, AUTO-PLOT).

Their interrelationships are shown in Figure 7-1. In the figure although the VR-Viewer is displayed on the post-processing side, it is part of the SATELLITE module.

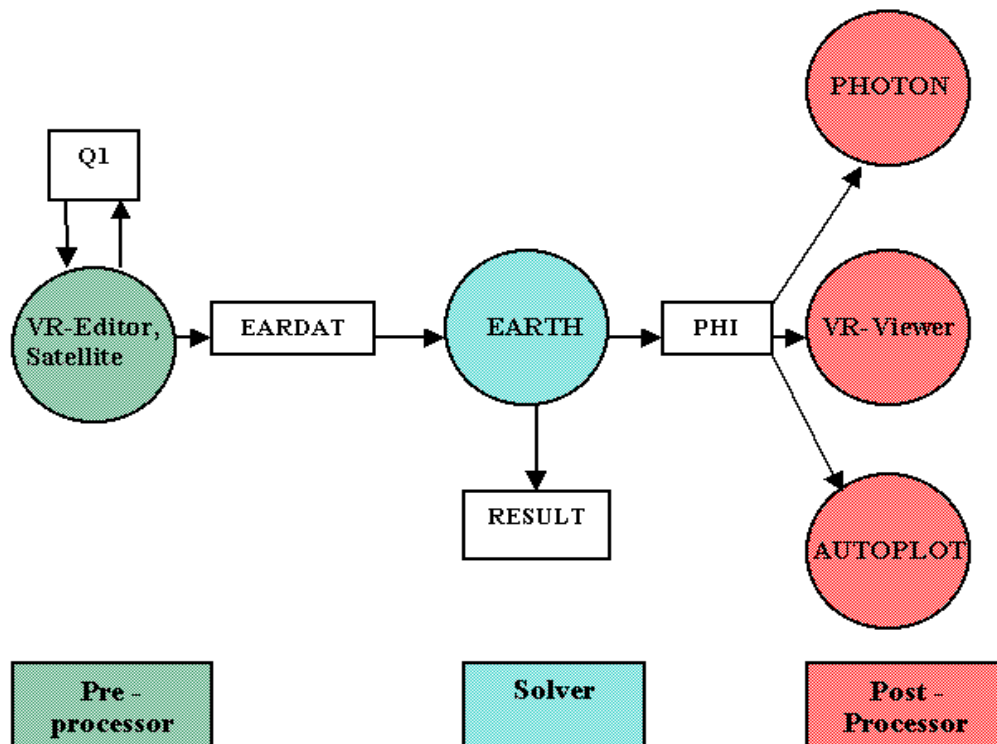


Figure 7-1: interrelationships of different modules of PHOENICS.

The four names in white rectangular boxes in above diagram refer to files which are used for communication between modules, as follows:

- Q1, the user-readable input-data file, which is written in PIL, the PHOENICS Input Language, and is the main expression of what the user wishes to achieve.
- EARDAT, an ASCII file which expresses in EARTH-understandable form what the user has prescribed by way of Q1.
- PHI, which is written by EARTH in accordance with a format which enables PHOTON, AUTO PLOT and the Viewer to display the results of the computation graphically.
- RESULT, which is an ASCII file expressing the results in tabular and line-printer-plot form.

7.2.3 Geometry Construction

Computationally accurate construction of the subject geometry is paramount and plays a crucial role in the CFD simulation. Results downstream of the computation process can be extremely erroneous if the model geometry setup is incorrect. However, if the geometric model is detailed then it increases the computational requirement. On the other hand over simplification leads to representing false conditions.

The geometry of the target building in this research was simplified with consideration so that it remained comparable with the real urban environment. Only the basic building blocks themselves were modelled; vegetation (trees, hedges, etc), fences, boundary walls and chimneys were ignored because including these features would increase the computational demand beyond available system's current ability given the relatively small scale of these elements compared to the building dimensions. Moreover the value added to the results would have been insignificant.

The COST guidelines (Franke *et al.* 2007) suggests that any similar sized obstacle which is up to a distance of six times the height of the building under observation can affect the approaching flow. This suggestion was used to

determine whether the subject model required any other geometry to be included in the flow problem. But there is no obstacle in similar size around the Merchiston campus; moreover the altitude of the campus is higher than the surrounding area.

There are many external geometry-creation programs, which can create the geometry of the model that can be imported into PHOENICS. However in many cases it is convenient to create the surface geometry of a desired object without using external programs.

One way of creating geometry in PHOENICS is to use simple FORTRAN (or other high-level-language) program. Another approach is top down modelling i.e. Import an object into working domain of PHOENICS VR (Virtual-Reality) and then change their position, size and orientation through controls which are provided. Shape-maker is another potential solution. It is a stand-alone executable program which can be used for the creation of geometry corresponding to a variety of mathematically-defined shapes. These geometry files have the extension ".dat", accepted by the PHOENICS VR Editor and Viewer. The parameters of the shapes, for example length, radii of curvature, number of facets, etc, may be set interactively, and stored in a file with .geo extension; and the resulting body can be imported as an "object".

The first step for this research is to create a geometrical cuboid with dimensional resemblance to the Merchiston campus building, for investigating the effect of change of height and length on the wind profile and turbulence. Then a full scale geometrical model of Merchiston campus is created to investigate the wind flow at the target points as shown in Figure 7-2.

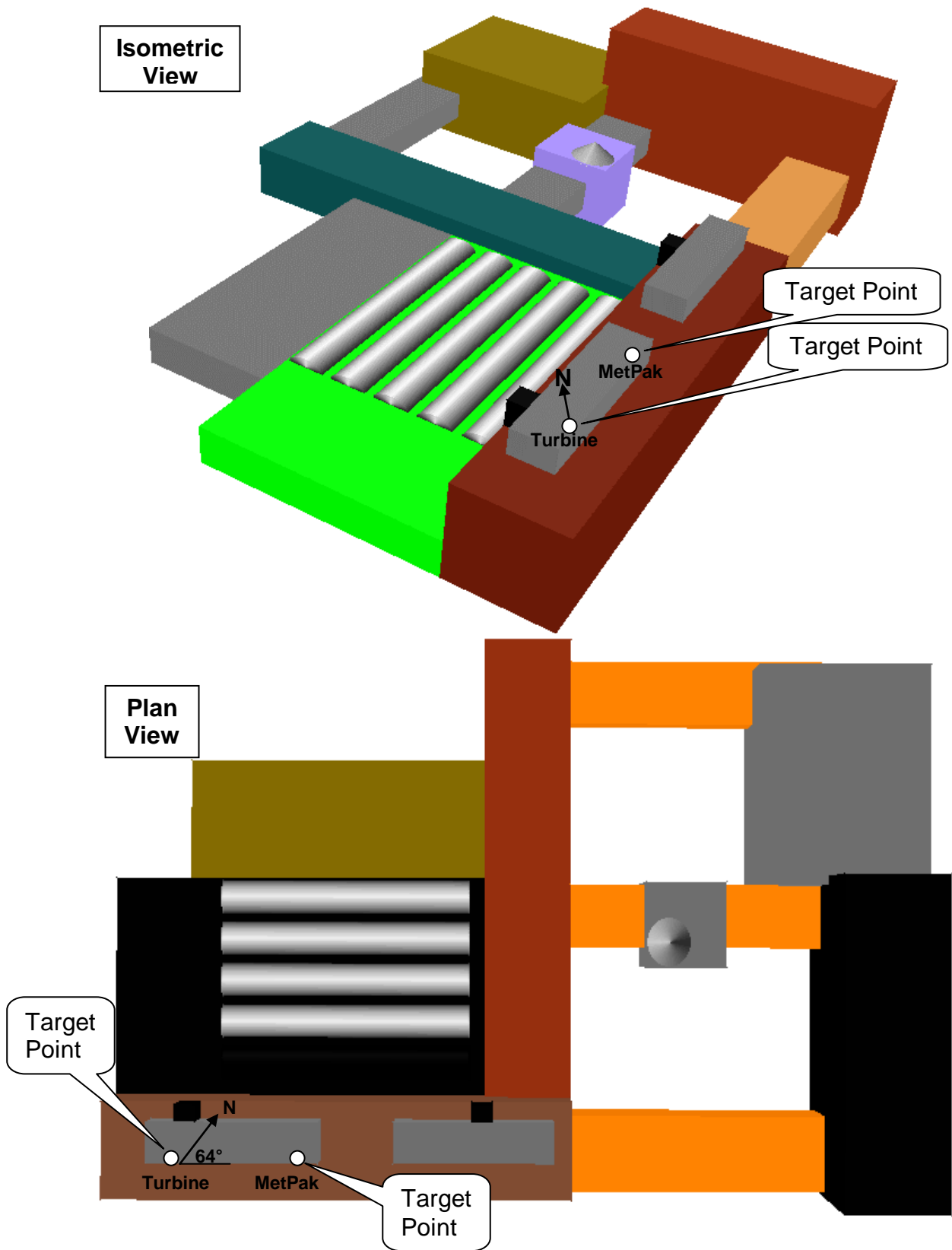


Figure 7-2: Isometric and Plan view of Merchiston campus CFD geometric model.

7.2.4 Domain creation

In CFD, domain is a three dimensional enclosed area in which target geometry has to be placed to create required environment for simulation. Creation of a domain is dependent upon the flow problem, to be solved. For a three dimensional domain with a single building and no surrounding obstacles, it is recommended by Hall, (1997) that the inlet, lateral extents and the top boundary to be a distance of at least $10H$ from the building, where H is the height of the highest building as shown in Figure 7-3. If the building has a larger lateral dimension then the blockage ratio should be less than 3%. The 'blockage ratio' is the ratio of the surface area of the face of the building perpendicular to the flow direction to the area of the domain plane perpendicular to the flow. The outflow boundary should be a distance of at least $30H$ behind the building (Prevezer *et al*, 2002).

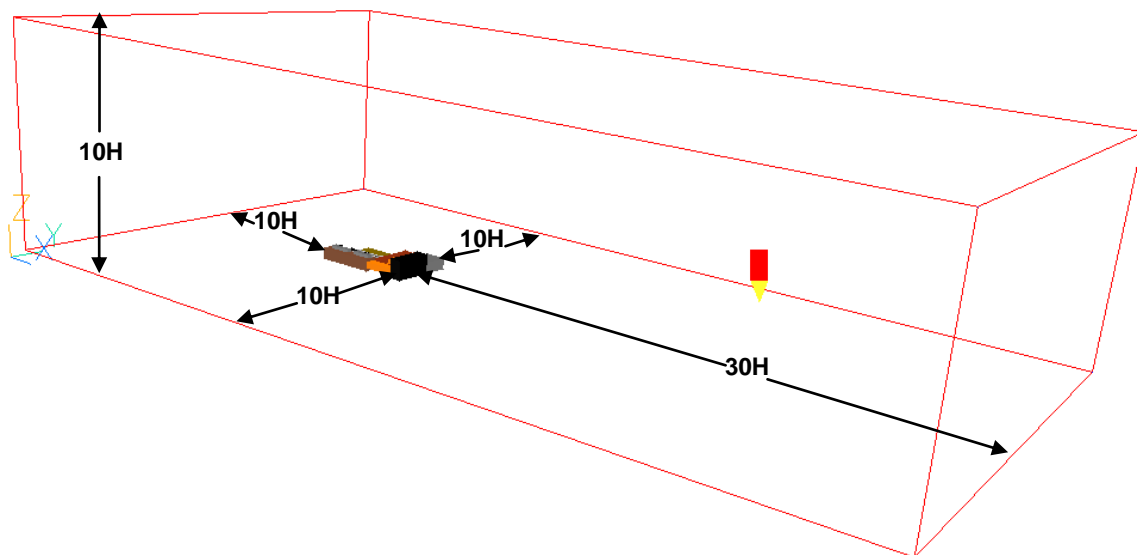


Figure 7-3: Domain dimensions of CFD model.

7.2.5 Mesh sizing

While setting up a CFD simulation, most of the time is consumed in the definition of domain geometry and the mesh generation. This area is widely recognised to be the most important and skill intensive area of CFD analysis. The quality of the mesh is paramount so much so that the use of an advanced

turbulence model can be completely cancelled out by a bad grid (Mertens, 2006). There are two types of mesh, structured and unstructured. Structured meshes are defined by the user such that cells can be assigned and identified in the domain with a row and a column number. This can be fairly time consuming for complicated geometries whereas for unstructured tetrahedral meshes, bulk of the work in dissecting geometry into small cells is done by computer and thus requires significantly less user input. In PHOENICS, individual objects can be selected to control the grid shape and the number of cells around the object. Otherwise the program automatically assigns grid size with respect to the geometry and user defined parameters in other region. Although this automated meshing can cause errors due to obtuse flow angles, these can be minimised by increasing the number of cells in regions of interest. In this research work, structured grid has been chosen in all CFD simulations to utilise the available resources as good as possible for the target area.

In grid design, regions with large flow gradients require smaller cells. Ideally the flow through all cells should be normal to the inlet as well as normal to the outlet side of the cell. Non-uniform grids should have a small growth rate (i.e. the rate of change of size of the cells). Cell sizes are changed by factors of 0.5 and 1.3 in the simulations. A growth rate of 1.3 is not ideal but for the simulation of Merchiston building, it is a reasonable compromise because of the computing resource limitations as shown in Figure 7-4. At times addition of just one cell caused problems in simulation as shown in Figure 7-5. This indicated that virtual memory of the computer has been fully consumed. Although this problem has been addressed by increasing the RAM (random access memory) up to its maximum limit (i.e. 3.25 Giga Byte). Even so problem would occasionally resurface.

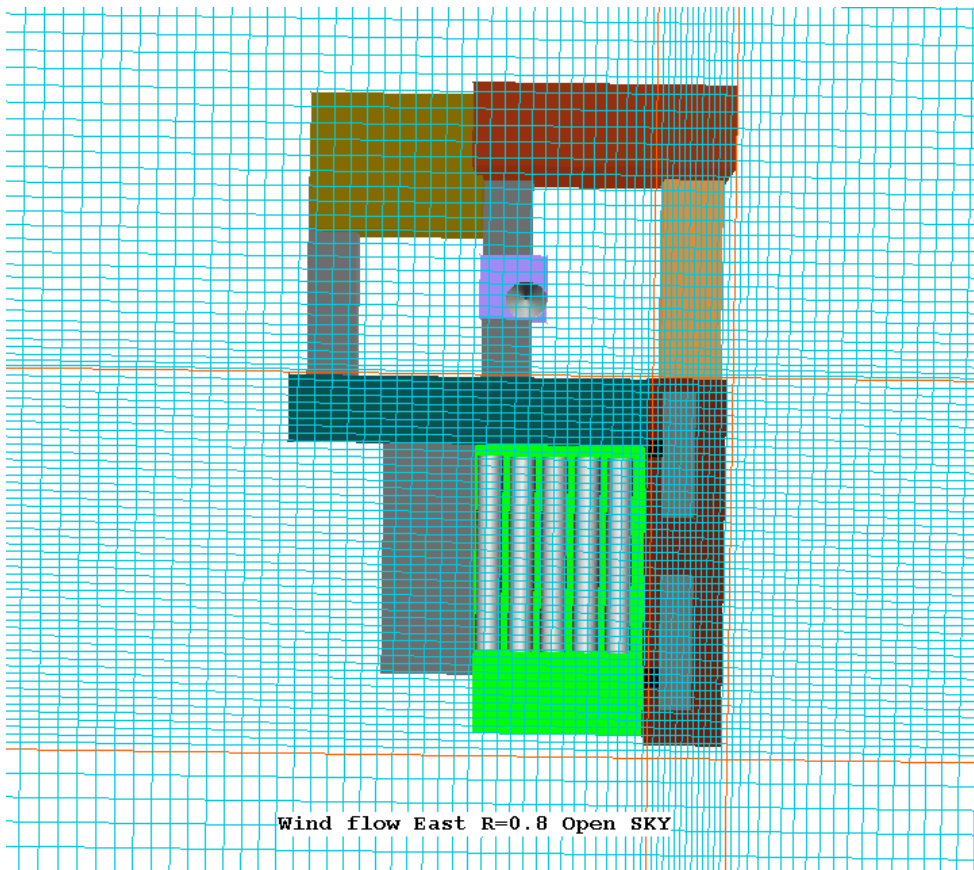


Figure 7-4: Grid on Merchiston model.

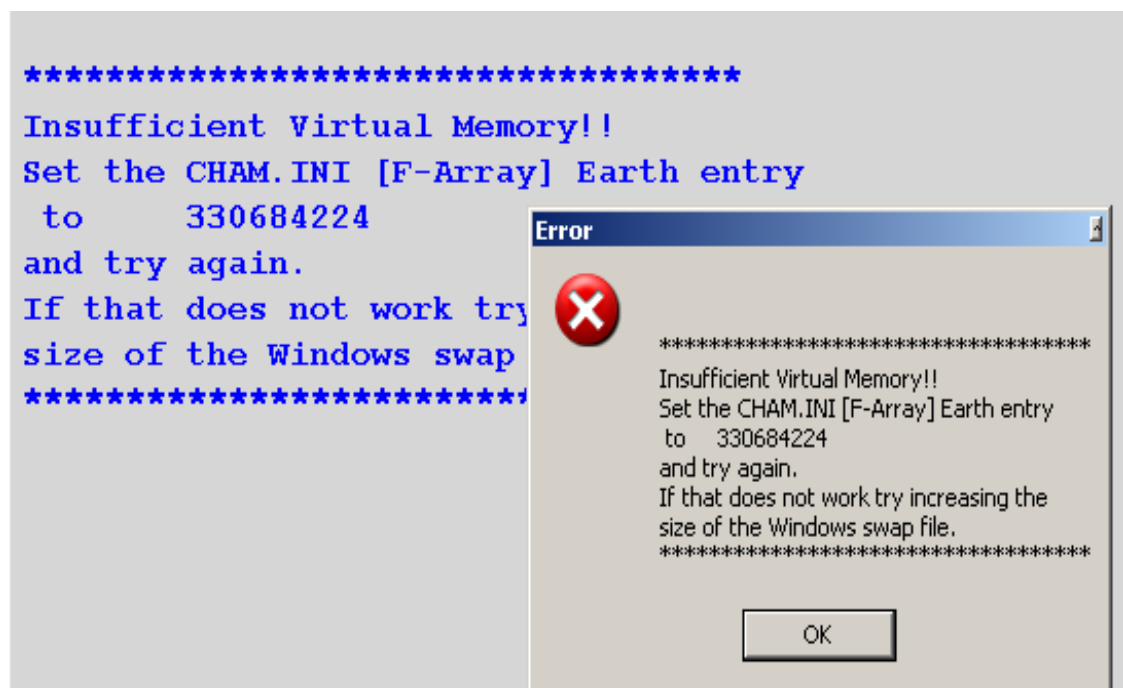


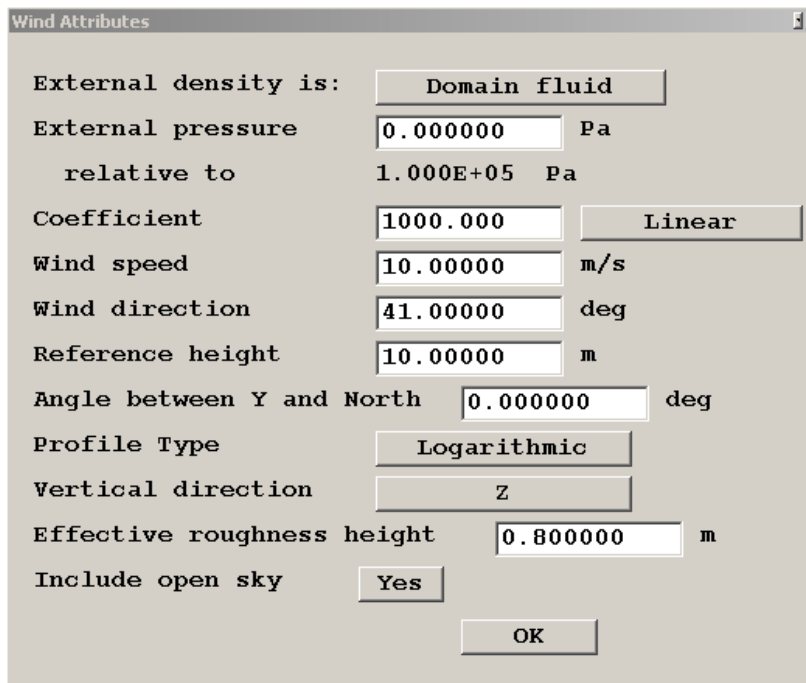
Figure 7-5: CFD software error because of resources deficiency.

7.2.6 Boundary conditions

The boundary conditions are the rules by which fluid in domain interacts with surroundings or external space. These can be divided into inflow boundaries, lateral boundaries, outflow boundaries, wall boundaries and top or sky boundaries. In PHOENICS, there is a selection of *wind object* option (an additional tool) hence; flow value at all boundaries can be assigned. The *wind object* option is for the wind analysis on any object in the domain. In any one domain, only one Wind object is allowed, and it always fills the entire domain. Based on the wind direction, it creates inflow boundaries at the domain edges using logarithmic or power law profiles on the upwind faces, and fixed pressure boundaries on the downwind faces. In addition, the upper, or sky boundary can also be made into a fixed pressure boundary.

7.2.6.1 Wind object

In PHOENICS wind object is used not only to set boundary conditions but also it provides options to set features of wind flow. The options which can be set in wind attributes are shown in Figure 7-6.



The screenshot shows the 'Wind Attributes' dialog box with the following settings:

External density is:	Domain fluid
External pressure	0.000000 Pa
relative to	1.000E+05 Pa
Coefficient	1000.000 Linear
Wind speed	10.00000 m/s
Wind direction	41.00000 deg
Reference height	10.00000 m
Angle between Y and North	0.000000 deg
Profile Type	Logarithmic
Vertical direction	Z
Effective roughness height	0.800000 m
Include open sky	Yes
OK	

Figure 7-6: Screen short of Wind attributes dialog box.

A detailed look at these wind attributes are given below;

- **External density:** The external density is used to calculate the mass inflow. It can be taken to be the same as the domain material density, or set to a user-specified value. If the domain density is a function of pressure (and/or temperature), the External pressure (and/or External temperature) will be used to evaluate it. In all simulations “domain fluid” option has been selected.
- **External pressure:** This sets the pressure outside the domain. It is taken to be the same at all open faces. It may be used to calculate the inlet density. The external pressure is set relative to a fixed reference pressure. For all simulations it has been set zero to avoid any influence with domain flow.
- **Coefficient:** This controls how closely the internal pressure at the downstream boundaries (and upper boundary if Sky is active) approaches the set external pressure. When set to Linear, the mass flow through the pressure boundaries is a linear function of pressure difference. A fairly large value of the order of 1000 will keep the internal pressure very close to the external, it restraining any internal pressure gradients at the boundaries.
- **Wind speed:** This sets the absolute value of the wind velocity in m/s at the reference height.
- **Wind direction:** This sets the direction in degrees, relative to North that the wind is blowing from. A value of zero means that the wind is blowing from due North. The angle increases clockwise to 90 for East, 180 for South and 270 for West. It can be set on any value in the range 0.0 - 360.0.
- **Reference height:** This sets the height at which the Wind Speed is specified.

- **Angle between Y axis and North:** This and the Vertical direction determine the orientation of the domain with respect to North. Although in Merchiston model North is 64 degrees from X-axis and 26 degrees from Y-axis (as shown in Figure 7-2), the value in this option set to zero to avoid confusion which author faces in initial simulations. And add 26 degrees in all angles to correct the angular difference in the model and real object.
- **Profile type:** The boundary layer velocity profile can be a logarithmic or power-law function of height above the ground. This is measured from the first open cell. It set as logarithmic for all simulations.
- **Vertical direction:** This controls which axis will be pointing up.
- **Effective roughness height:** This option sets the roughness height at the edge of the domain. Typical roughness values are given in Table 5-5. Some of the literature (Burton *et al.* 2001) mentioned the roughness height as 0.7 for city area and some (ISES, 2007) mentioned 1 for the city area. For all CFD simulation in this research author take 0.8 as roughness height.
- **Include open sky:** When the option set to “No”, the upper boundary is treated as a frictionless impermeable lid. When set to “Yes”, the upper boundary is treated as a fixed pressure boundary. The external pressure, pressure coefficient and temperature are the same as at the downwind boundaries. In all simulations open sky option set as “Yes”.

7.2.7 Selection of turbulence model

Turbulence is an essential entity of urban or built-up environment which cannot be avoided or neglected in CFD simulations of wind flow. Many turbulence models have been developed including the k- ϵ model and the k- ω models but there is not a single model that has been universally accepted to solve all turbulent flow problems. Therefore choice of a turbulence model is based on the nature of the problem. All available turbulence models in PHOENICS are described in the POLIS Encyclopaedia (POLIS Encyclopaedia, 2007) under

'Turbulence', where each has its own descriptive article and its pros and cons. Until recently the standard k - ϵ turbulence model (where k is the turbulent kinetic energy and ϵ the turbulent dissipation rate) was the model of choice for micrometeorological simulations. However it was reported that it tends to overestimate the distance downstream for flow reattachment (Heath, Walshe & Watson, 2007). On the other hand, some of the literatures (Li. *et al*, 2006, Mertens, 2006) suggest that k - ϵ turbulence model is the best suited model for the flow problems in the roughness sub-layer. In PHOENICS there are several variants of the k - ϵ model (as mentioned below) usually giving enhanced performance for recirculation flow (Ludwig, 2009).

- **KECHEN** - Chen-Kim two-equation k - ϵ model. Gives better prediction of separation and vortexes.
- **KERNG** - RNG derived two-equation k - ϵ model. Gives better prediction of separation and vortexes. However, the user is advised that the model results in substantial deterioration in the prediction of plane and round free jets in stagnant surroundings.
- **KEMMK** - Murakami, Mochida and Kondo k - ϵ model for flow around bluff bodies as encountered for example in wind-engineering applications.
- **KEKL** - Kato-Launder k - ϵ model for flow around bluff bodies as encountered for example in wind-engineering applications.
- **KEMODL-YAP** - k - ϵ model with Yap correction for separated flows.
- **TSKEMO** - Two scale k - ϵ model for flows in which there is an appreciable time lag between the turbulent production and dissipation processes.

In light of the above description, KECHEM model is found most suitable to the project under consideration and so it is used in all CFD simulations.

7.2.7.1 KECHEN Turbulence model

In PHOENICS the standard high-Reynolds-number forms of the two-equation eddy-viscosity k - ϵ KE-EP turbulence model is chosen. To characterise the various dynamic processes occurring in turbulent flows, this model employs a single time scale (KE/EP). The source, sink and transport terms contained in the closed set of model equations are held to proceed at rates proportional to EP/KE.

In turbulence, fluctuating motions vary with a spectrum of time scales. Therefore, a single-scale approach is adequate in all circumstances because different turbulence interactions are related with different parts of the spectrum. For the remedy of this deficiency in the standard model, Chen and Kim (Chen & Kim, 1987) proposed a modification which improves the dynamic response of the EP equation by introducing an additional time scale (KE/PK), where PK is the volumetric production rate of KE. In addition to this several standard-model coefficients are also adjusted so that the model maintains good agreement with experimental data on classical turbulent shear layers. Because of model's success for a number of separated-flow calculations, the CK modification is provided as an option in PHOENICS (POLIS Encyclopaedia, 2007).

7.2.8 Convergence criteria

A simulation is said to be converging when the residuals (or errors) in the equations decrease as the iterative solution proceeds. In PHOENICS, the residuals are usually displayed on the screen by EARTH and stored. It can be checked by monitor plot option in EARTH solver as shown in Figure 7-7.

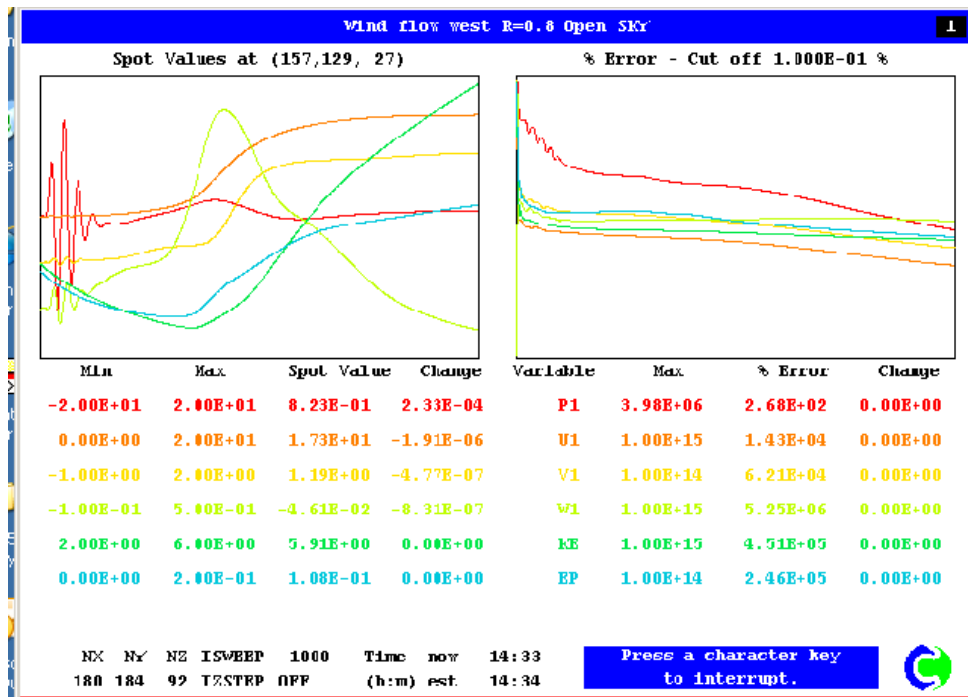


Figure 7-7: Convergence monitor plot generated by the EARTH solver.

7.2.9 Limitations and potential Errors in CFD analysis

When using CFD code to solve a fluid dynamics problem it is important to understand the errors and uncertainties that cause inaccuracies in the solution. It is then possible to realise the limitations of the model and minimize these errors. There are several classifications of errors available, recommended by several different sources (Coleman, Stern, 1997), (Franke *et al.* 2007), (Schatzmann & Britter, 2005). This study has used the ones outlined in the COSTBest Practice Guidelines (Franke *et al.* 2007) which divide the errors into two broad categories:

1. Errors and uncertainties in modelling the physics
2. Numerical errors and uncertainties

The physical errors usually derive from the input of the flow problem and can be categorised as follows:

- Simplification of physical complexity
- Usage of previous experimental data

- Geometric boundary conditions
- Physical boundary conditions
- Initialisation

As the numerical errors occur from the numerical solution of the mathematical model and mainly consist of:

- Computer programming
- Computer round-off
- Iterative convergence

All possible effort has been made during this study to minimise the number of physical and numerical errors by following best practice guidelines and building upon the experience of similar existing CFD studies. The main limiting factor to further minimising errors was the available computational processing power. This limited both the complexity of the geometry that could be created, the size of the mesh and also the processing time of the solver. Typical solving times for the domains analysed here were 20 to 24 hours for Merchiston campus simulation.

7.3 Simulation Results

7.3.1 CFD investigation of wind flow over a cubic obstacle

The preliminary, CFD investigation has been done on wind flow over a cubic obstacle (as Merchiston campus building is a combination of different cubic blocks). For this simulation three different models have been created with different dimensions to look at the effect of dimension variations on wind flow. One of the models has twice height of the basic model and another has twice length of the basic model as mentioned below.

1. X=20m, Y=20m, Z=15m
2. X=20m, Y=20m, Z=30m
3. X=30m, Y=20m, Z=15m

7.3.1.1 Wind speed results and analysis

Wind speed monitoring at the roof top of the cubic buildings found that the upstream flow (at the leading edge) always has higher wind speed than downstream or on rest of the roof. Maximum wind speed can be found just 3m above the roof top at leading edge of the building. This wind speed increases about 18% when height becomes twice. And trailing edge of the cubic building always has the lowest wind speed. Wind flow over the cubic building followed a curved path which starts 1 m from leading edge till end of the roof. This curve has different layers of wind speed; layer near to the roof surface has lower wind speed than the layer higher from the surface. The wind speed curve (affected region) increases in thickness when the surface length of the roof increases as shown in Figure 7-8. In order to assess how wind speed varies with height, a vertical wind profile has been plotted at middle of the roof. A ratio has been calculated between wind speed at the roof top of cubic block and wind speed at reference height (i.e. 10 m/s) as shown in Figure 7-9. It has been found that the change above the roof top follows the trend of power as well as log equation with very high accuracy as R^2 value for the both trends is 0.97.

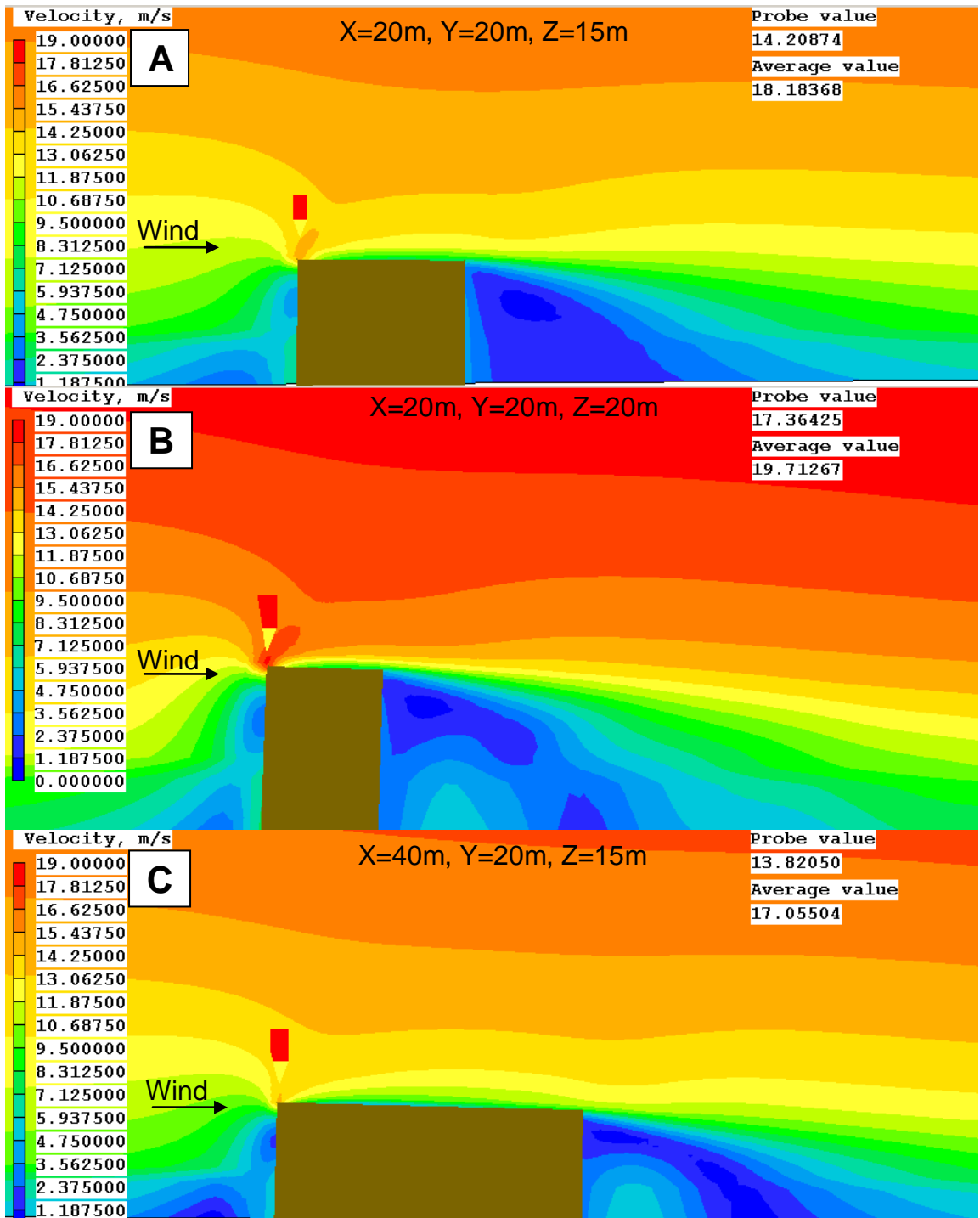


Figure 7-8: Wind flow pattern over cubic blocks, view; X-Z plan Y=0.

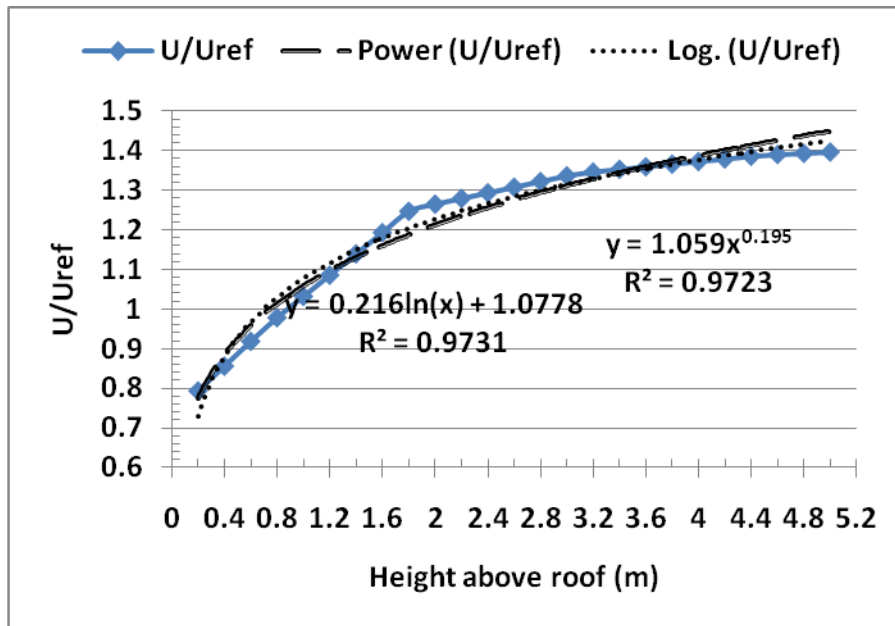


Figure 7-9: vertical wind speed profile at roof top of cubic building.

From Figure 7-10 which shows view; Y-Z plan $X=0$, it can be noted that when wind blows directly on a cubic building, the high wind speed layer over the top of the roof is higher in the middle and lower towards the corners of the building. Moreover there is high wind speed on both sides of the building as well, but it fades away about 1 m away from building.

Figure 7-11 shows (view; X-Y plan $Z=0$) the effect of cubic building on the wind flow over the rooftop of the building. It shows that as height increases over the top of the roof, the wind speed increases and it increases on the sides or edges of the building more rapidly as compared to the middle of the roof. The lowest wind speed at the cubic rooftop can be found in the middle of the roof. And the high speed region created at the front edge of the building prevails even at 6 m above the roof but reduces in its size with further height increase. It also shows that the wind shadow of the building lasts up to 5 m above the building which is 33.33% of the height of the building.

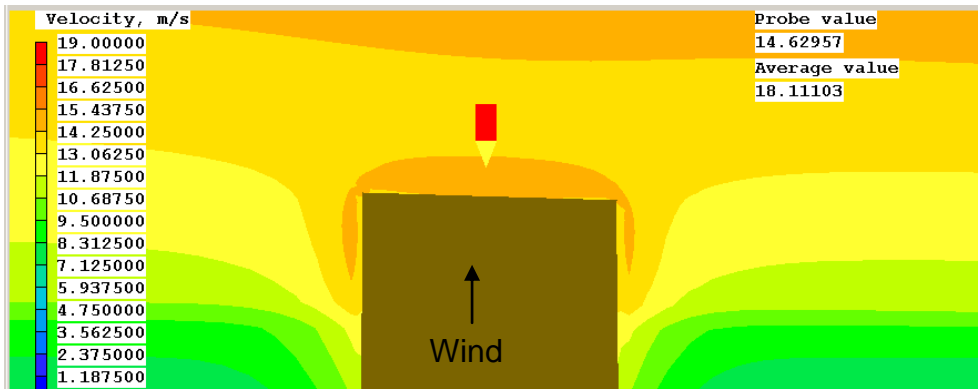
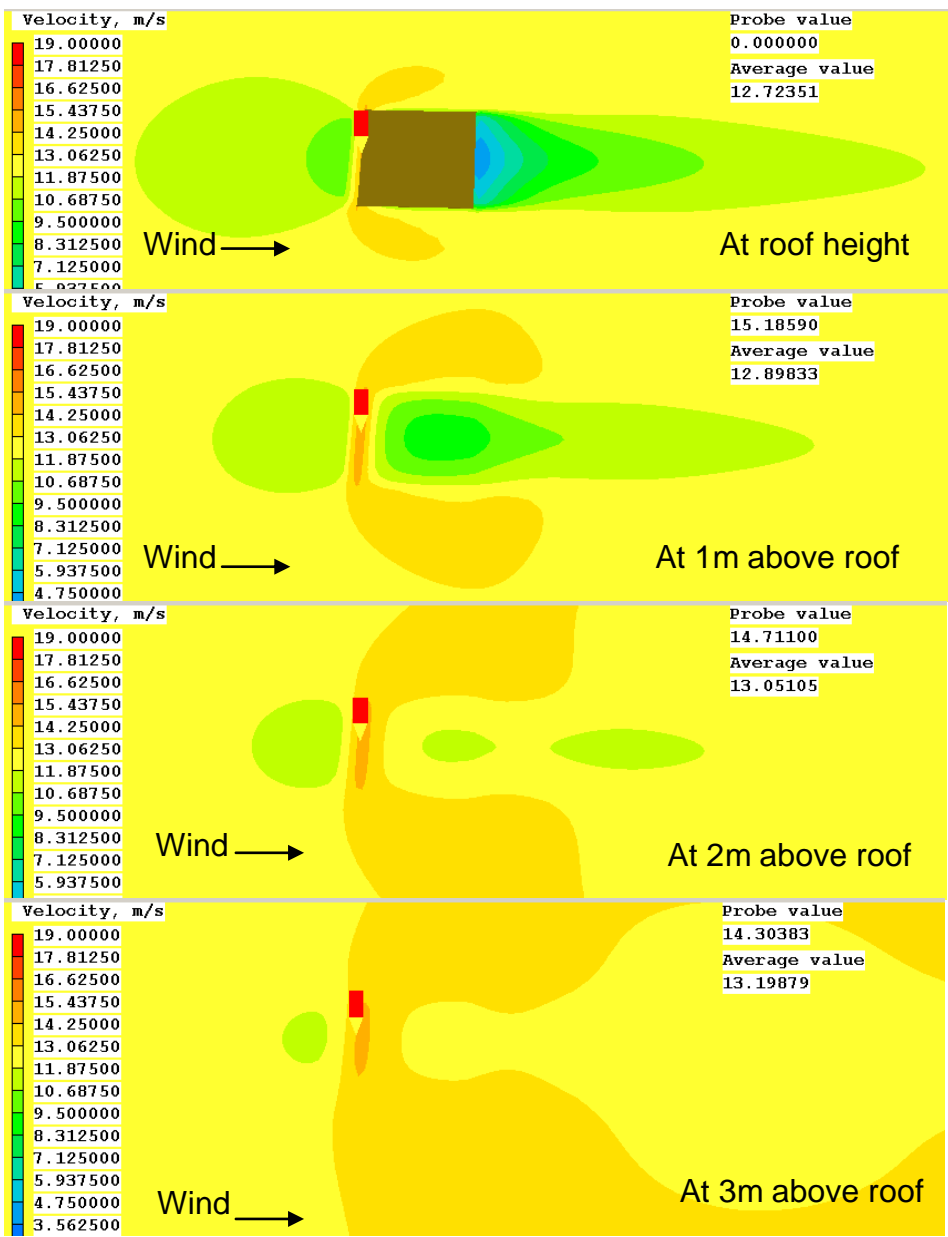


Figure 7-10: Wind speed at the leading edge of the building, wind blowing from front, view; Y-Z plan X=0.



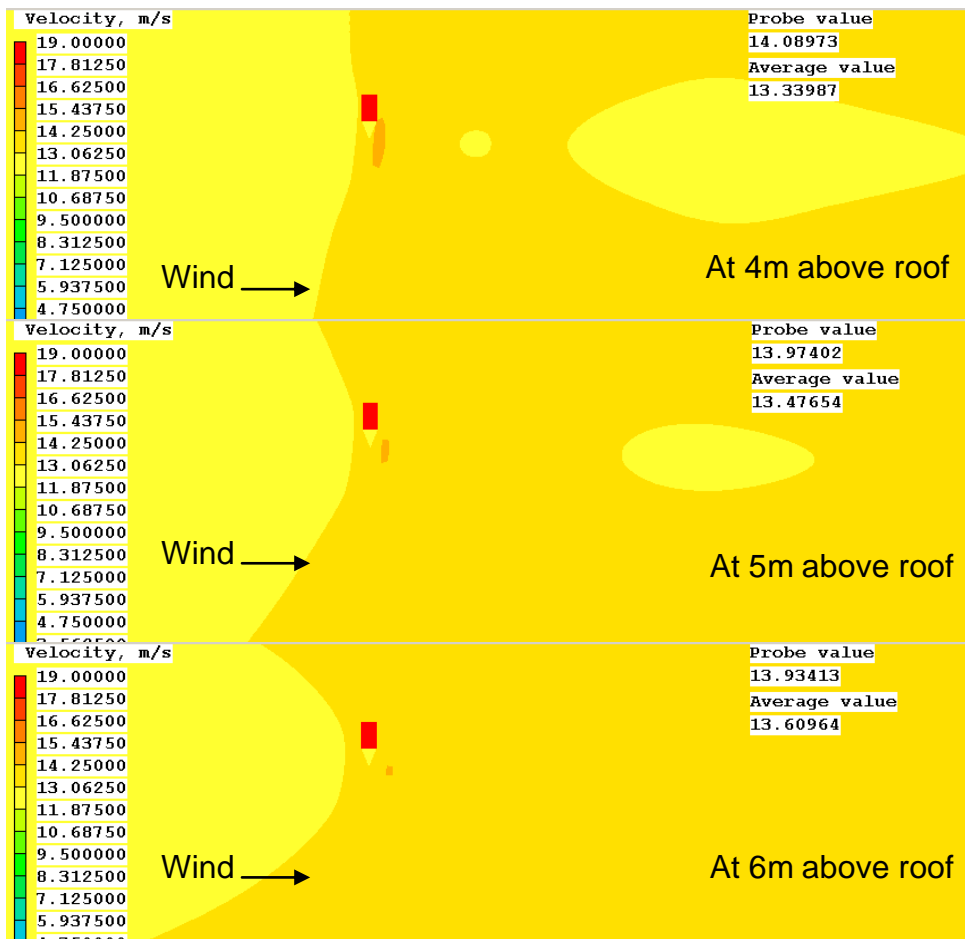


Figure 7-11: Wind speed variation over cubic building with respect to height plan view (X-Y plan Z=0).

7.3.1.2 Turbulence intensity analysis

Turbulence intensity was found low very near to the roof surface of the building and it increases after the buffer layer of the low turbulence, as shown in Figure 7-12 A and B. And after a certain height it starts decreasing again. It can be deduced that it starts decreasing when the effect of the building reduces over the roof top. Figure 7-12B shows that turbulence intensity is higher at the leading edge of the build than the trailing edge as leading edge has high wind speed with respect to trailing edge. The highest value of turbulence intensity is obtained at the same point where the highest wind speed is recorded i.e. at the leading edge of the building. In Figure 7-12B grey area in front and rear side of the building is actually indicates higher turbulence region which has value higher than the upper range of the scale on the right, and hence it is blank.

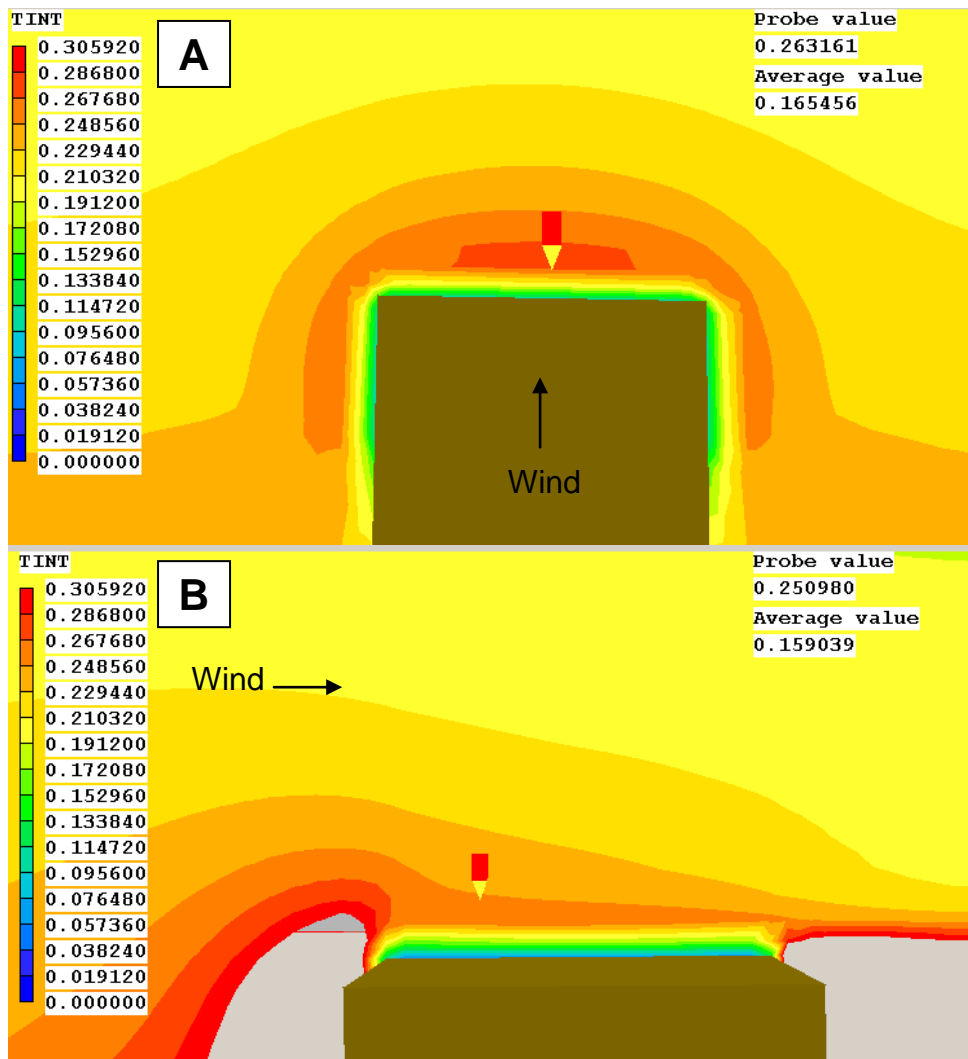


Figure 7-12: Turbulence layer over the top of the cubic building **A**: view; Y-Z plan X=0, where wind coming from front. **B**: View; X-Z plan Y=0, where wind coming from left.

7.3.2 CFD simulation over Merchiston campus

In the CFD simulation of Merchiston campus two target points have been set where wind speed has to be monitored and analysed. These points are the position of MetPak and turbine location as shown in Figure 7-13. As Merchiston campus building is not symmetric, it has different effects on wind flow when wind blows from different directions.

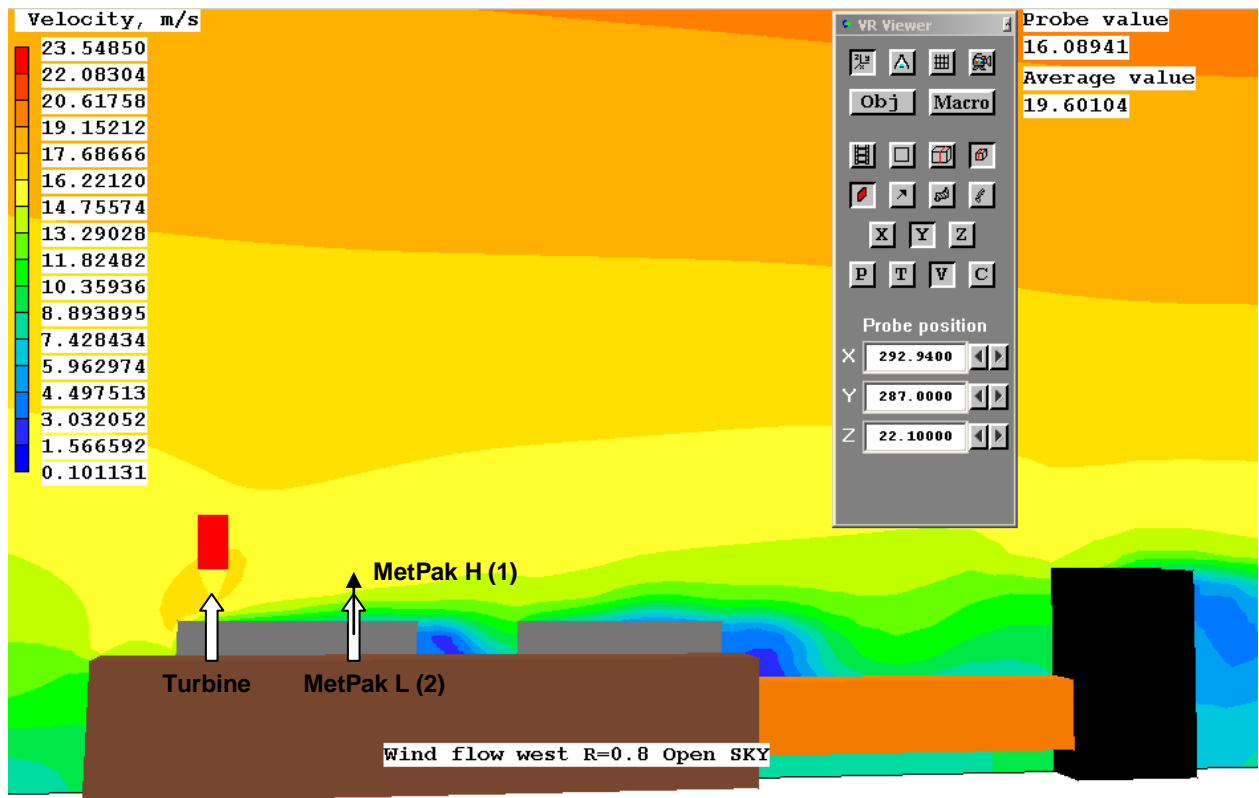


Figure 7-13: Simulation of wind flow at Merchiston, view; X-Z plan Y=0.

7.3.2.1 Effect of roughness height on wind flow

Before investigations of the wind flow variation due to different directions, it is important to test the effect of roughness on the flow pattern. As Merchiston campus is situated in an urban area, 0.8 roughness height has been selected in the *wind object* menu of the PHOENICS software. To test what effect it takes on the wind flow three simulations have been done with roughness height of 0.8, 0.7 and 0.6 as shown in Table 7-1. Table 7-1 shows that wind speed decreases on both locations (i.e. at MetPak-L and turbine) as the roughness height decreases but the ratio of the wind speed at MetPak-L and turbine remains same. It shows that the roughness height has no effect on the pattern of the wind flow.

Table 7-1: Effect of roughness height on wind flow.

Roughness height m	Wind speed at turbine (WS_T) m/s	Wind speed at MetPak L (WS_{ML}) m/s	WS_{ML}/WS_T
0.8	16.1046	13.14827	0.816
0.7	15.8176	12.89387	0.815
0.6	15.5236	12.6329	0.814

7.3.2.2 Vertical wind flow pattern at Merchiston campus

In order to assess the wind speed variation with height, vertical wind profiles have been plotted at the MetPak position with two different wind directions. One profile was made, when wind blowing from 240 degrees (as shown in Figure 7-14A) which is the most frequent wind direction at Merchiston. And other profile has been made when wind blowing from 60 degrees (as shown in Figure 7-14B), which is the most effected direction by the shading effect of the highest building of the campus.

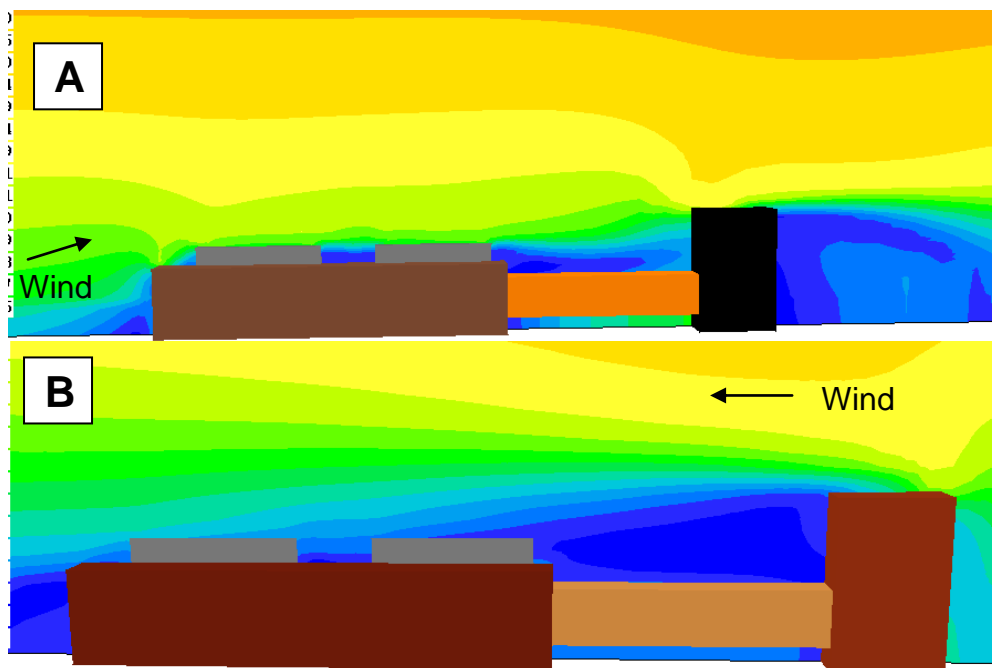


Figure 7-14: Vertical wind profile at Merchiston (view; X-Z plan $Y=0$) when **A**: wind blow from 240 degrees. **B**: when wind blow from 60 degrees.

Profile graph in Figure 7-15A shows that the vertical wind profile follows a linear trend with R^2 value of 95 when wind is blowing from 240 degrees. Figure 7-15B shows that vertical wind profile follows linear trend more strongly and closely

when wind blows from 60 degrees. There are two differences in both vertical profiles, one is the shift of magnitude on vertical axis values (i.e. from 1.16-1.4 to 0.50-0.78) and the other is the constant of the trend line equation (i.e. linear equation constant 1.1823 to 0.5337). But the slopes of the trend lines remain close to each other which show that the increments in the profile value with increase of height in both profiles are about same.

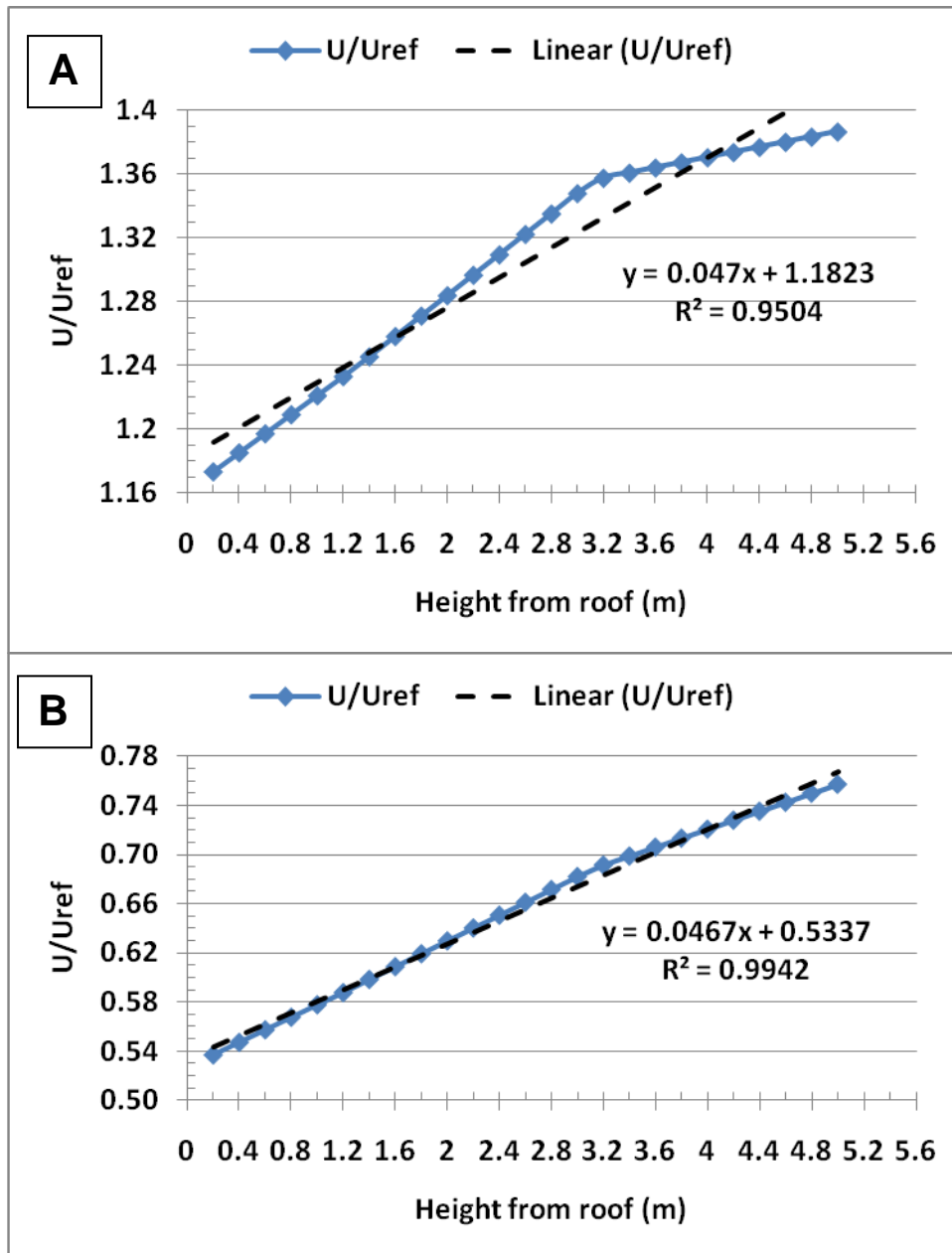


Figure 7-15: Vertical wind profile graph for Merchiston at MetPak location, when **A**: wind blow from 240 degrees. **B**: when wind blow from 60 degrees.

7.3.2.3 Effect of wind direction on wind flow

As wind turbine and MetPak-L are apart from each other by 20.45m it is obvious that both have different bearing by the wind flow. Turbine is located near the edge of the building just 4.14m from the edge and Met Pak-L is about in the middle of the roof. Thus the obvious question that arises is how much the difference will be in wind speed at both locations? To get the answer, wind simulation has been done on a full scale model of Merchiston campus. As investigated in section 7.3.2.1 that the change in roughness height can affect on the wind speed but less affect on the ratio of the wind speed at both locations.

Table 7-2: Wind speed at turbine and MetPak positions when wind blow from different angles and their ratio.

Wind direction (degree)	Wind speed (m/s)		
	at Turbine	At MetPak-L	Ratio (WS_T/WS_{ML})
North 0	8.83	11.15	0.792
15	6.13	9.06	0.677
30	8.00	11.30	0.708
45	9.60	10.07	0.954
60	7.48	6.09	1.228
75	13.48	13.36	1.009
East 90	12.51	13.25	0.944
105	9.74	10.50	0.928
120	14.53	14.82	0.980
135	15.20	15.12	1.005
150	15.84	15.43	1.027
165	15.68	15.48	1.013
South 180	15.67	15.77	0.994
195	15.60	15.56	1.002
210	15.34	15.03	1.021
225	14.63	13.00	1.125
240	13.65	12.80	1.066
255	14.24	13.96	1.019
West 270	16.24	13.34	1.217
285	16.09	11.81	1.362
300	12.92	11.28	1.145
315	11.26	9.05	1.245
330	11.57	9.11	1.270
345	10.69	9.88	1.082

Because of the differences of locations it was very much expected that the change in wind direction affects the wind speed ratio of both locations. To investigate this effect, 24 wind simulations have been done with different wind directions. The wind direction variation in 360 degrees was divided into 24 sectors i.e. 15 degrees directional intervals. From the simulation results it is found that at Merchiston campus the wind direction matters significantly. Table 7-2 shows wind speed at turbine and MetPak locations from different angles. It shows that wind turbine receives maximum wind speed when wind blow from west (270 degrees) and MetPak gets maximum wind speed when wind blow from south (180 degrees). To elucidate the wind speed differences further, a rose diagram has been plotted as shown in Figure 7-16A. Figure 7-16A shows clearly the wind speed differences at turbine and MetPak locations, it shows that turbine receives more wind, when wind blows between 225 degrees to 345 degrees. MetPak receives most wind from 0 degree to 105 degrees and there is almost no difference in wind speed on both locations' from 120 degrees to 210 degrees. Figure 7-16B indicates more clearly about the magnitude and directional bearing on both locations.

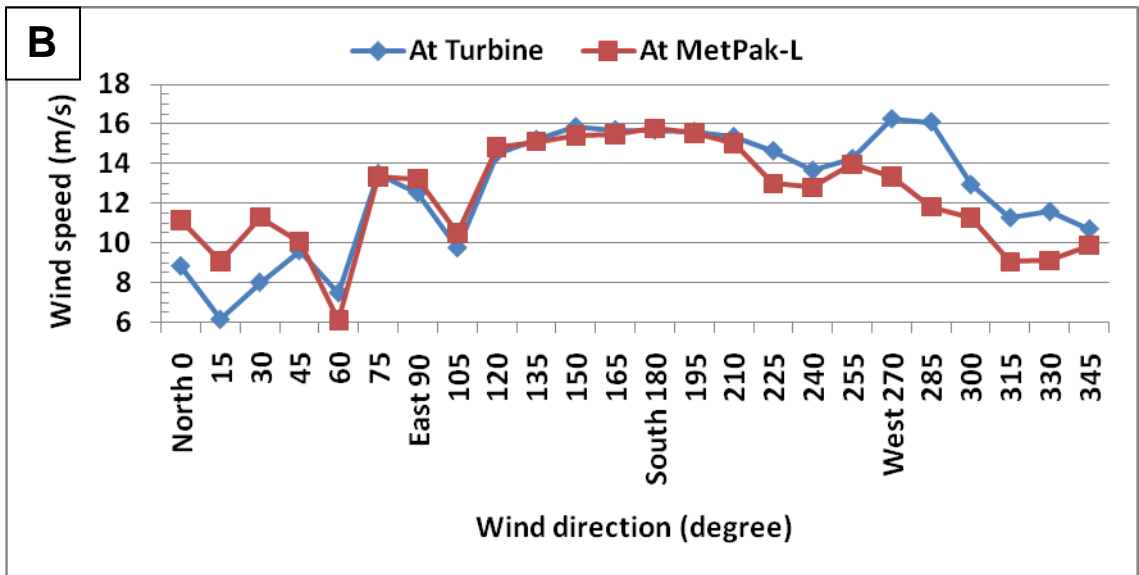
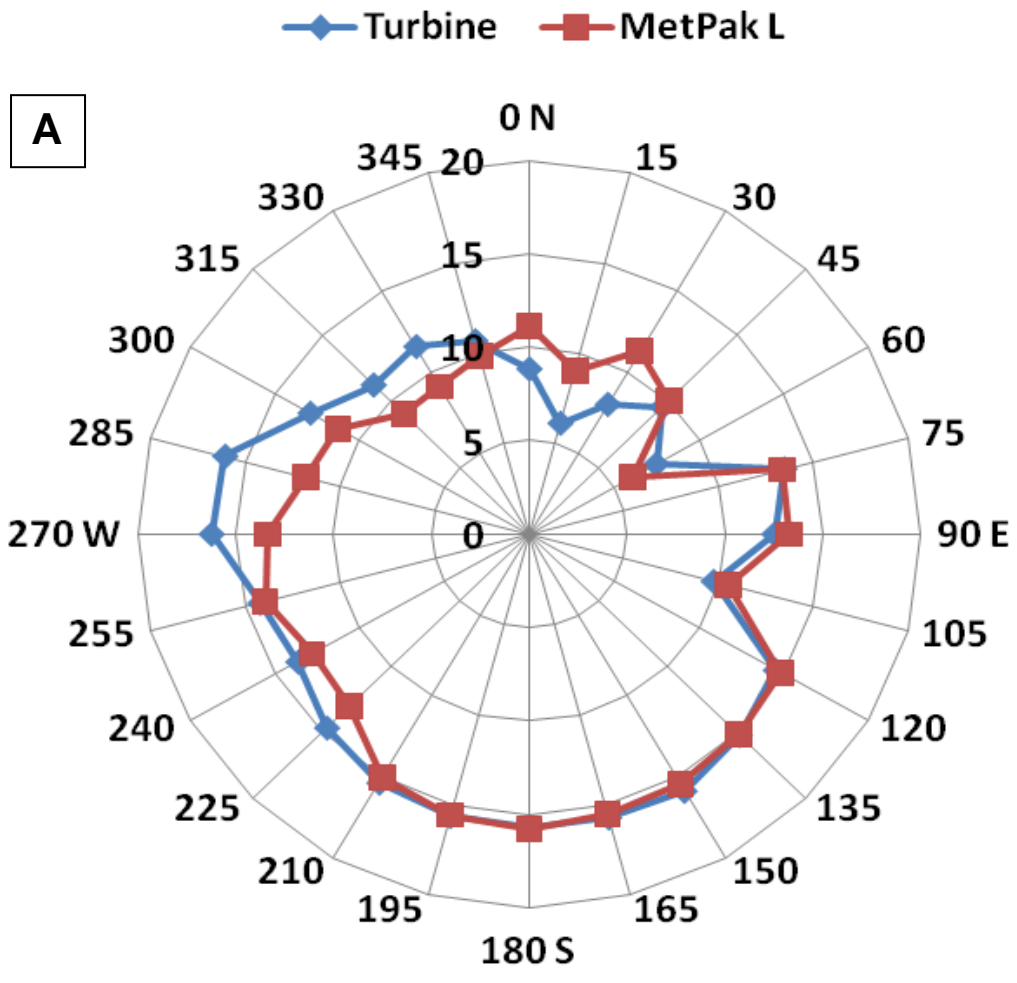


Figure 7-16: Wind speed at turbine and MetPak-L positions from different angles. **A**: Rose diagram. **B**: X-Y plot.

7.3.2.4 Turbulence intensity analysis at Merchiston

It has been found that there is great variation in wind speed because of the directional variation of wind. Therefore, investigating the difference in turbulence intensity due to the direction of wind cannot be ignored. Figure 7-17A shows the turbulence intensity in coloured layers when wind flows from 240 degrees. It shows that the low TINT (Turbulence Intensity) layers near the surface of the roof are straight (i.e. not increasing or decreasing with distance). This means TINT from left to right (i.e. turbine to MetPak) will be same when wind blows from 240 degrees. Figure 7-17B shows that when wind blows from 60 degrees the TINT increases from right to left (i.e. MetPak to turbine side). This is because of the shading effect of the big building block on the right side. White patch in Figure 7-17B, shows the high TINT which is above the upper limit of the TINT scale.

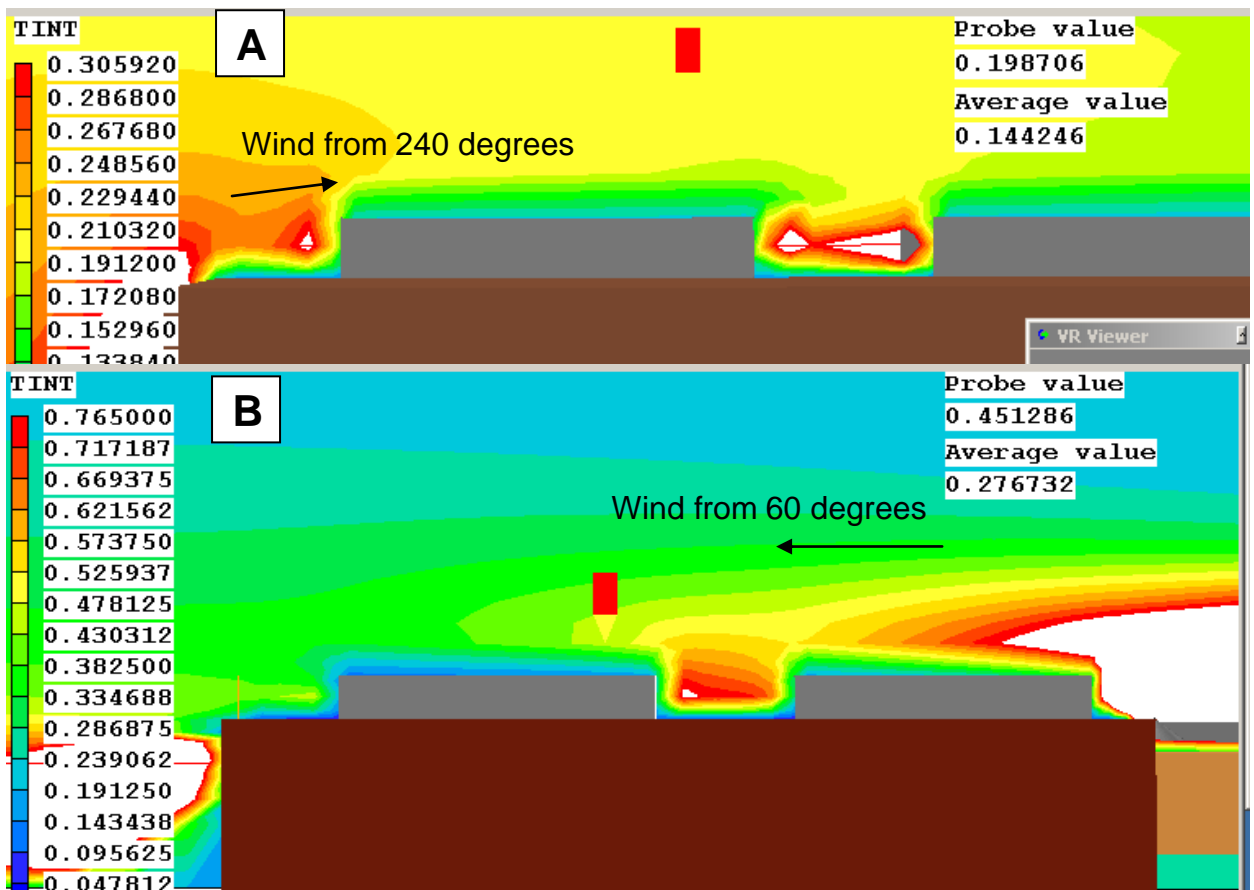


Figure 7-17: Turbulence intensity at Merchiston (view; X-Z plan Y=0). A: When wind flow from 240 degrees. B: When wind flow from 60 degrees.

To find out the effect of direction of wind flow on TINT at a particular position (i.e. in this case MetPak location) a graph has been plotted as shown in Figure 7-18. It shows that TINT increases at MetPak location with height very rapidly up to 3m above the roof and then starts decreasing slowly with the increase of height. This suggests that 3 m or above is a good height to get minimum turbulence effect at 60 degrees blow. On the other hand TINT increases fairly gradually with the increase of height when wind blow from 240 degrees until 3 m and then becomes constant upto 10 m above the roof.

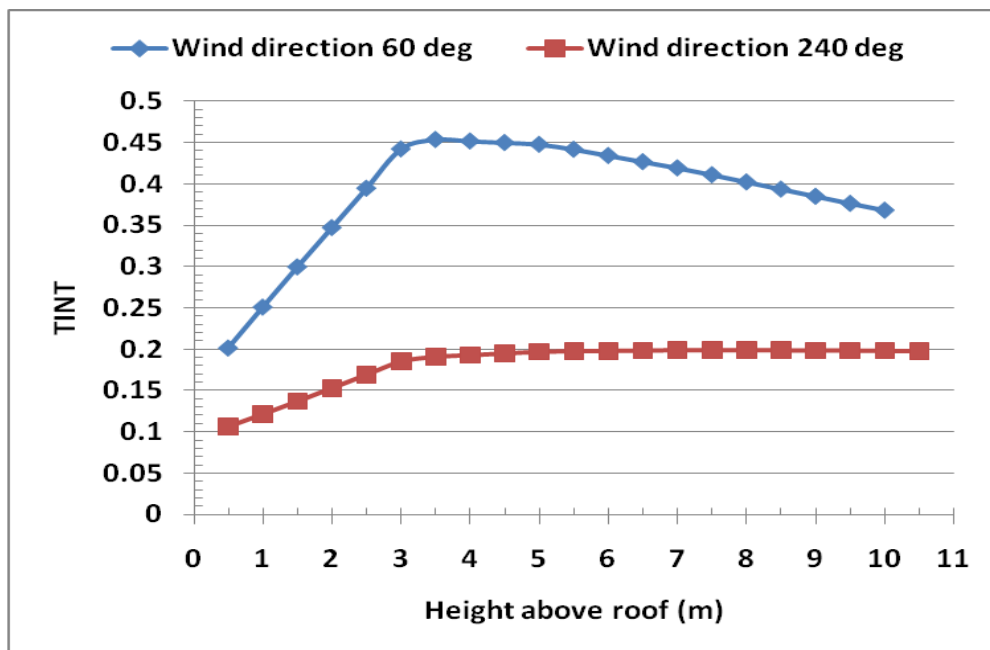


Figure 7-18: Change in TINT with height at MetPak location for different wind directions.

7.4 Limitations of this CFD study and future directions

There are large amount of configurations of buildings and layouts in Edinburgh that can be investigated using CFD. As a different grid had to be created for each wind speed direction, each simulation required large amount of time to setup and solve. Over thirty domains were created for the results presented in this chapter and many more during learning and experimental procedure. Further research into how to accurately model areas with different kind of objects like trees, houses, building blocks and variation of elevation (i.e. hills) in a single domain, is required as the lack of this detail is seen as one of the key

limitation of this study. By increasing computing power and modelling a relatively large area in a single domain can give more clear and realistic results. It is also expected that further development of CFD software and increase in computer processing ability will simplify and speedup the creation and solving of fluid dynamics flow problems in the built environment sector.

7.5 Conclusion

A number of CFD simulations have been presented in this chapter on cuboid building blocks and Merchiston campus model. It has been found that maximum wind speed over the rooftop of a cubic building can be found just 3m above the roof on leading edge and the wind speed increases by 18% when height of the building doubles. Vertical wind profile over a cubic building follows the power and logarithmic trend. Wind speed increases rapidly with the increase of height over the roof at the edges and very slow in the middle of the building. The wind shadow of the cubic building lasts up to 5m above the building which for the case under consideration is 33.33% of the height of the building. Turbulence intensity over the cubic roof first increases with height and then decreases. Above results also reported in doctoral thesis of Rogers (2009).

In the simulations of Merchiston Campus building, it has been found that there is no effect of the roughness height on the pattern of wind flow. The decrease of roughness height just decreases the magnitude of the wind velocity. Vertical wind profile has been same for two opposite wind flows but the magnitude is affected by the direction. The wind available at MetPak and turbine depends on wind direction and it has different ratios for different wind directions. Wind directions of 360 degrees were divided into 24 sectors for which ratio of wind speed at turbine and MetPak have been calculated. It was also noted that vertical profile of TINT over the Merchiston roof also depends on the wind direction.

Results of wind speed ratio of turbine and MetPak locations have been used in next chapter to calculate the wind resource at turbine location.

8 Performance analysis of WEC system

8.1 Introduction

This chapter analyses wind resource differences between MetPak and turbine location and investigates the efficiency of the WEC system in exporting energy into the grid. There is six months (Jul-Dec 2009, barring the month of Sep) turbine data available for both MetPak-L and WEC system, after which the WEC system's inverter failed. Unfortunately, the inverter could not be repaired nor replaced because the WindSave Company had gone into administration.

8.2 Wind resource at MetPak-L and WEC location

MetPak systems were installed 20.5 m away from the wind turbine because the choice of installing MetPak is limited due to the layout and availability of location on the roof (as shown in Figure 8-1). Since the logging equipment is not at the same location as the wind turbine, performance of the turbine system could not be monitored. To resolve this issue CFD simulations were done (in Chapter 7) to find out the wind resource difference between both locations.

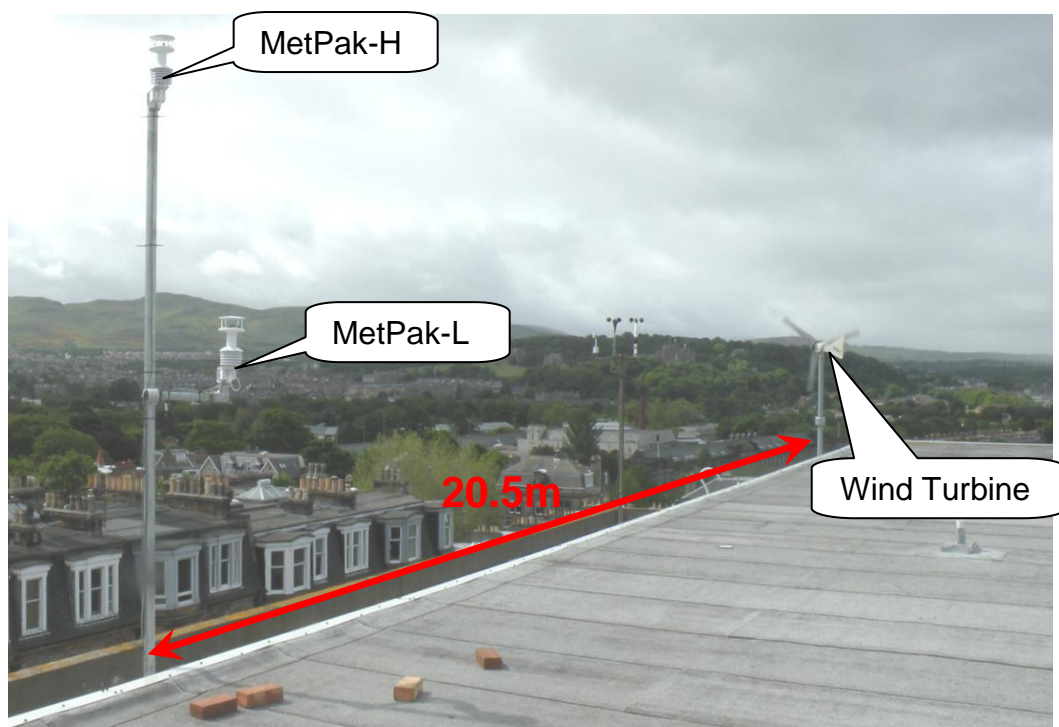


Figure 8-1: Relative location of MetPak and wind turbine at the top of Merchiston Campus roof.

In CFD analysis it was found that because of the relative location of MetPak and wind turbine, the wind flow pattern highly depends on the wind direction. Therefore, it would be beneficial to first look at the MetPak recorded monthly wind directions over Merchiston campus. Figure 8-2 shows that at Merchiston campus wind blew mostly around 240 degrees except in Oct 2009 when it blew between 90 to 240 degrees. In Figure 7-16 (Chapter 7), it was found that when wind blows between 225 to 345 degrees apart from 255 (where both locations get same wind) wind turbine receives higher wind than MetPak. To convert MetPak data in to turbine location wind data, a VBA (visual basic application) code was written which checks the wind direction of the wind data and multiplies the wind speed with the related ratio factor calculated in Table 7-2 of Chapter 7.

After calculating wind speed for turbine location, one month (Jul 2009) frequency distribution of wind speed and available power is plotted (as shown in Figure 8-3) to investigate the differences in available wind resources in both locations. It was found that the turbine location has higher wind speed than MetPak location, and therefore, more generated power.

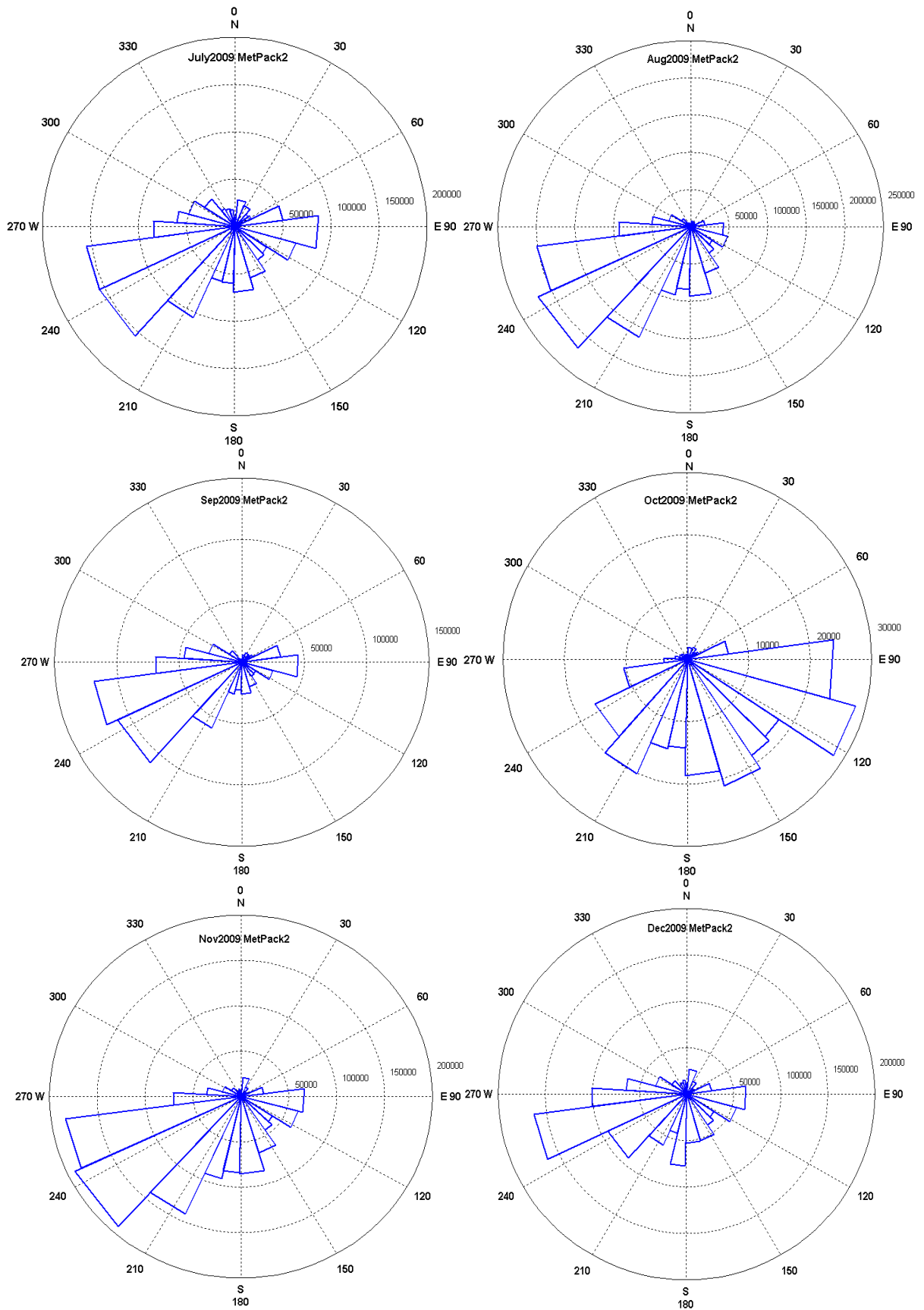


Figure 8-2: Rose diagram for MetPak-L wind directional data

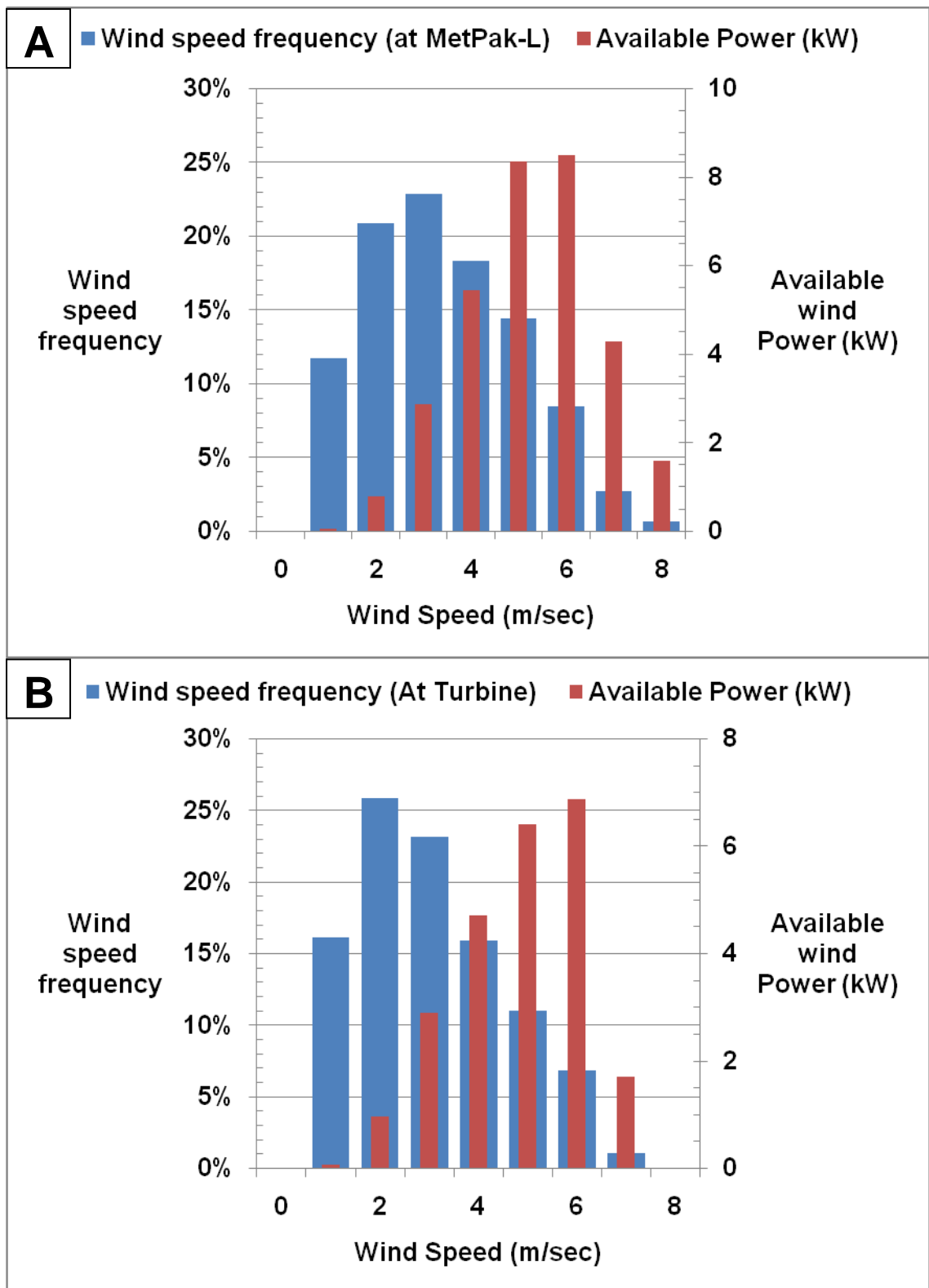


Figure 8-3: Hourly wind frequency and power available in wind per m². A: at MetPak-L location. B: at Turbine location.

Table 8-1 presents the comparison of wind speed and wind energy available at MetPak-L and turbine location. It also shows the % increase in available wind energy at turbine location; 16.92% to 18.44% from Jul to Sep 2009. In Oct 2009 there is only 3.41% increase as there is insignificant difference in the wind flow at both locations.

Table 8-1: Comparison of wind speed and wind energy available at MetPak-L and turbine location.

Month	Mean wind speed (m/s)		Available Wind energy (kWh/m ²) Calculated from hourly data		Increase in Energy at turbine Location (%)	Available Data (%)
	At MetPak-L	At Turbine	At MetPak-L	At Turbine		
Jul-09	2.90	3.04	19.89	23.26	16.92	99.87
Aug-09	3.83	4.01	41.93	49.11	17.12	99.87
Sep-09	3.25	3.46	16.23	19.22	18.44	54.72
Oct-09	3.04	3.06	3.82	3.95	3.41	17.07
Nov-09	4.24	4.37	68.46	75.43	10.18	99.86
Dec-09	3.19	3.28	54.67	55.93	2.31	81.32

8.3 Performance of WEC system

8.3.1 Available wind resource for WEC

On the basis of estimated data for the turbine location, wind data is categorised in terms of wind turbines cut-in and operating range as shown in

Figure 8-4. It shows that in six months an average of 61% wind data is below cut-in wind speed. Not a single data point reached up to cut-out wind speed or even to the optimum wind speed for rated power (i.e. 1 kW at 12.5 m/s).

Figure 8-4 shows that wind speed during Jul to Dec 2009 was below 9.51 m/s through-out.

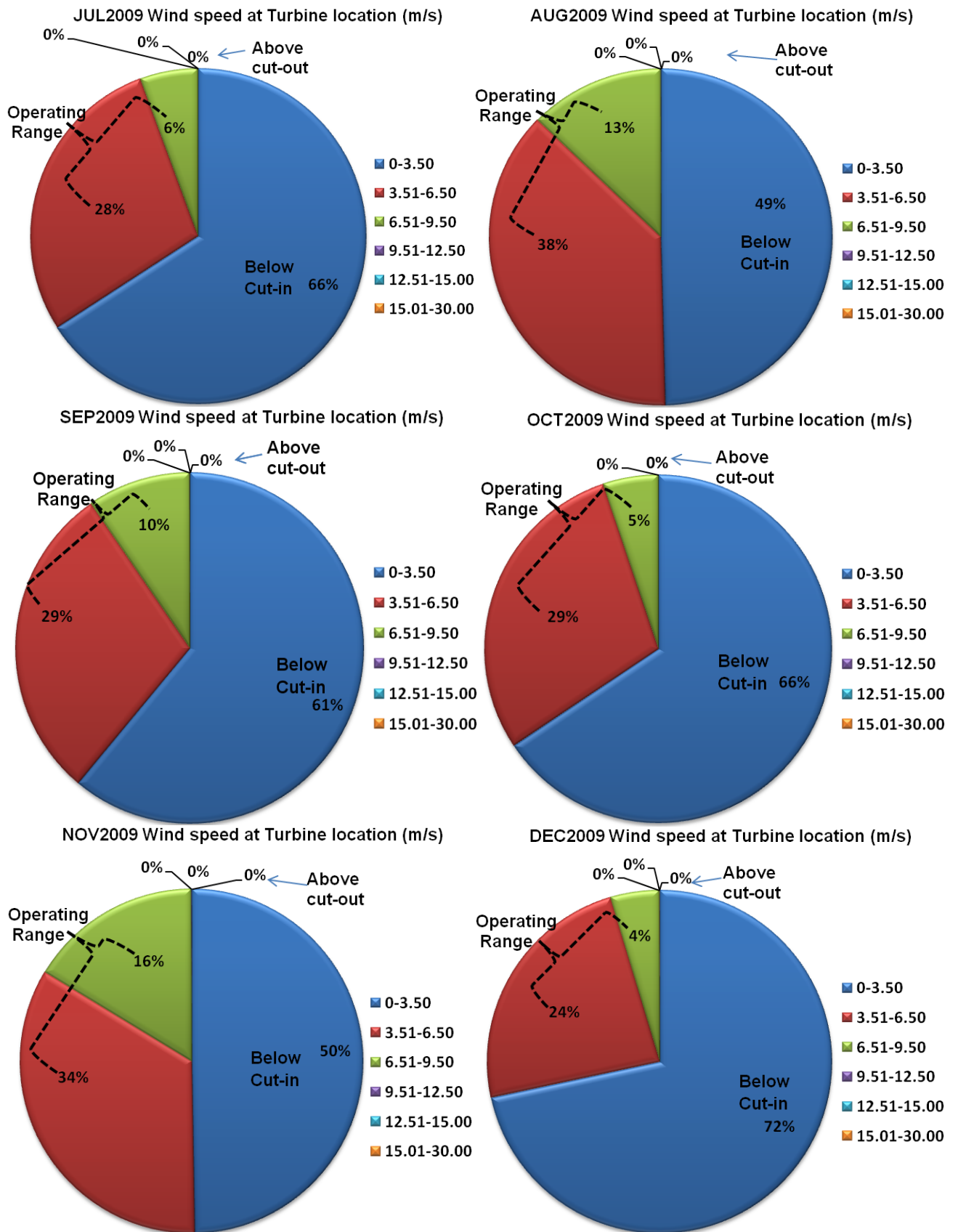


Figure 8-4: Available wind speed at turbine location in terms of turbine operation.

8.3.2 Performance of wind turbine

Several areas to be consider in assessing the performance of wind turbine, as given below:

- The aerodynamical performance of turbine's blades and yaw mechanism to catch the wind
- Mechanical performance of turbine rotor, and
- Electrical performance of the turbine generator to convert mechanical power in to electrical power.

To investigate the performance of the wind turbine the only available parameter is the DC voltage output of the wind turbine. Turbine's DC voltage data is classified into four categories;

1. Zero output (i.e. voltages equals to zero)
2. Less then 20volt
3. Wasted output (voltages between 20.10-198 volt)
4. Out put that can be utilised (voltages between 198.10-350 volt)

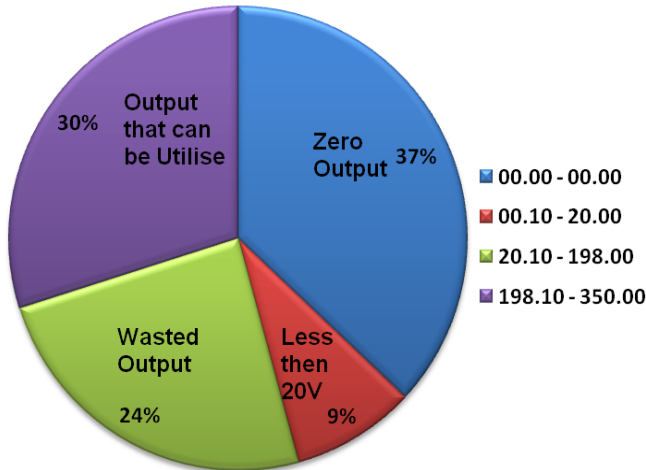
Voltages are classified as wasted and utilised output because the inverter connected to the wind turbine is only switched on to convert DC supply of wind turbine into AC when voltages level reach up to 210 volts DC and is kept exporting until DC voltage level drop down to 198 volts according to the WindSave user manual.

For the month of July 2009, Figure 8-5 shows that only 37% of the time windturbine did not generate DC voltages while Figure 8-4 shows that 66% of the wind data was less than the cut-in wind speed. It was an unexpected conflict in the data and raised the question as to how wind turbine harnessed 29% of below cut-in wind. By carefully investigating the per two second logged data it was realised that this conflict is because of the sensitivity (or response time) difference between ultra sonic MetPak and rotating wind turbine. As MetPak is

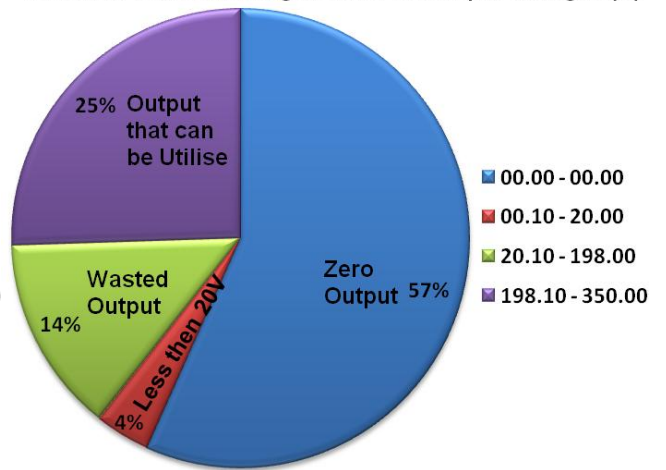
very sensitive and has an extremely quick response time, it changes very rapidly (compare to wind turbine). On the other hand, wind turbine has revolving blades and once it catches a speed in response to a wind gust it takes time to slow down or completely stop. Because of this discrepancy, it was not possible to determine how much wind was available and how much of it wind turbine harnessed to convert it into electric voltages.

It is to be noted that Sep 2009 wind turbine data is not available as during that period wind turbine was stopped for roof renovation work.

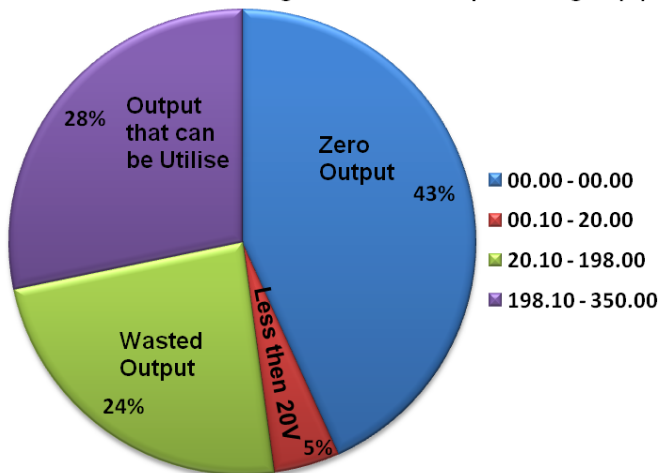
JUL2009 Wind turbine generator DC output voltages (V)



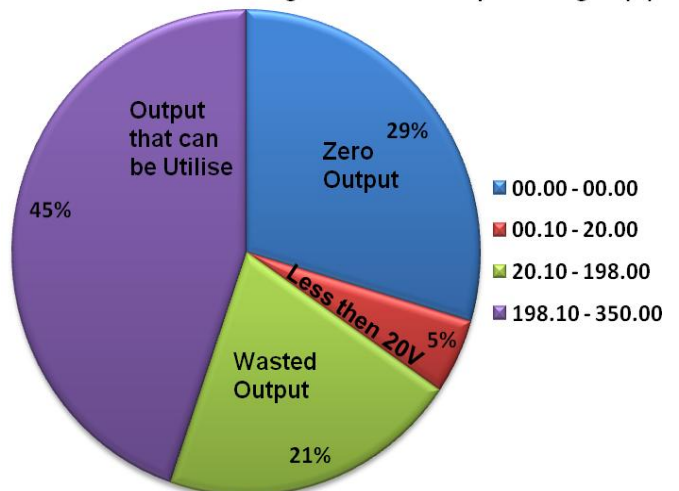
AUG2009 Wind turbine generator DC output voltages (V)



OCT2009 Wind turbine generator DC output voltages (V)



NOV2009 Wind turbine generator DC output voltages (V)



DEC2009 Wind turbine generator DC output voltages (V)

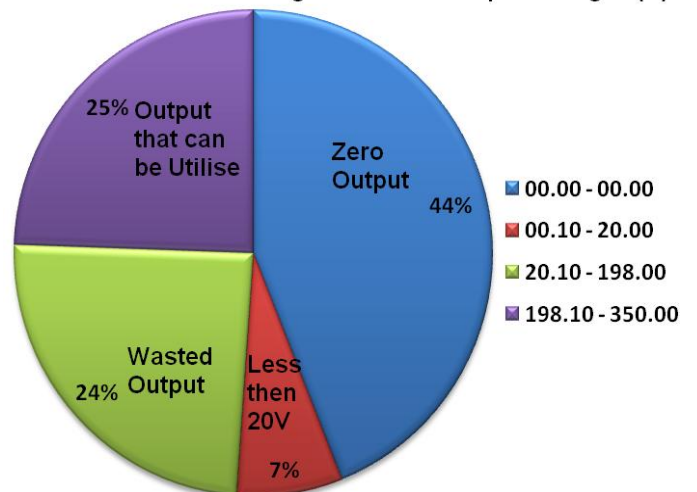


Figure 8-5: Monthly voltage output of wind turbine generator.

8.3.3 Performance of inverter system

As discussed before, the WEC used in this research has a grid connected inverter and it starts exporting DC voltages of wind turbine generator when they reach the level of 210 volts and continues until DC voltages drop down to 198 volts according to the user manual. To assess what had actually happened, a graph was plotted between DC voltages and DC current as shown in Figure 8-6. It shows that the DC current of 0.07A starts flowing when DC voltage reaches 207 volts (by adding compensation of 1.03% error by VDC it turn into 209 volts) and with current flow of 0.06A until DC voltages drop down to 196 volts (by adding compensation of 1.03% error by VDC it turn into 198 volts). Although there is some indication of current flow when voltage is 194 -195 volt but the current was low and the data points in that range were so few that they have been neglected. The maximum DC voltages logged by the system is 235.5 volts (by adding compensation of 1.03% error by VDC it turn into 237.5 volts).

As in Section 4.2.1.1, Table 4-2 shows error of 2 volts (i.e. error of 1.03%) in data logger reading at 200 volts input, which is compensated in the calculation of input and output power of the inverter system.

A VBA code was written to calculate inverter's input energy. In the calculation of input energy, all DC voltages greater than 196 volts and current more than 0.06 A were included. A compensation of 1.03% was applied to the DC voltages and multiplied with current and then time (i.e. 1/1800 hours in 2 sec) to calculate DC power and input energy, respectively.

To find out the AC side activity of inverter, a plot was drawn between DC voltages and AC side current as shown in Figure 8-7. Figure 8-7 shows that there is a continuous flow of 0.2 A current on the AC side of the inverter. This means inverter consumes 46 Wh ($230\text{ V} \times 0.2\text{ A} \times 1\text{ h} = 46\text{ Wh}$) energy per hour or 34.224 kWh ($744\text{ h} \times 46\text{ Wh} = 34224\text{ Wh}$) energy per month (31 days = 744 hours) from the grid.

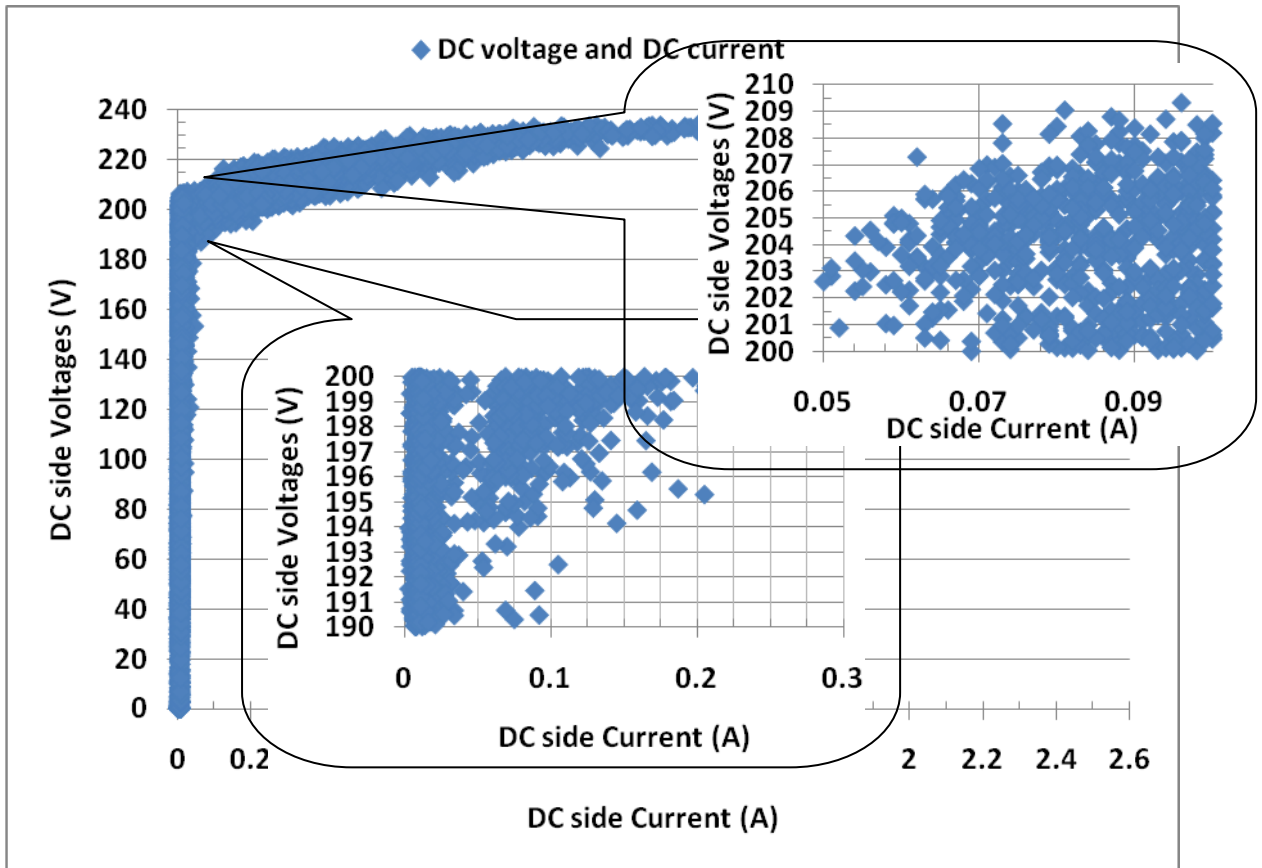


Figure 8-6: Graph of DC voltage and DC current of 30000 data points.

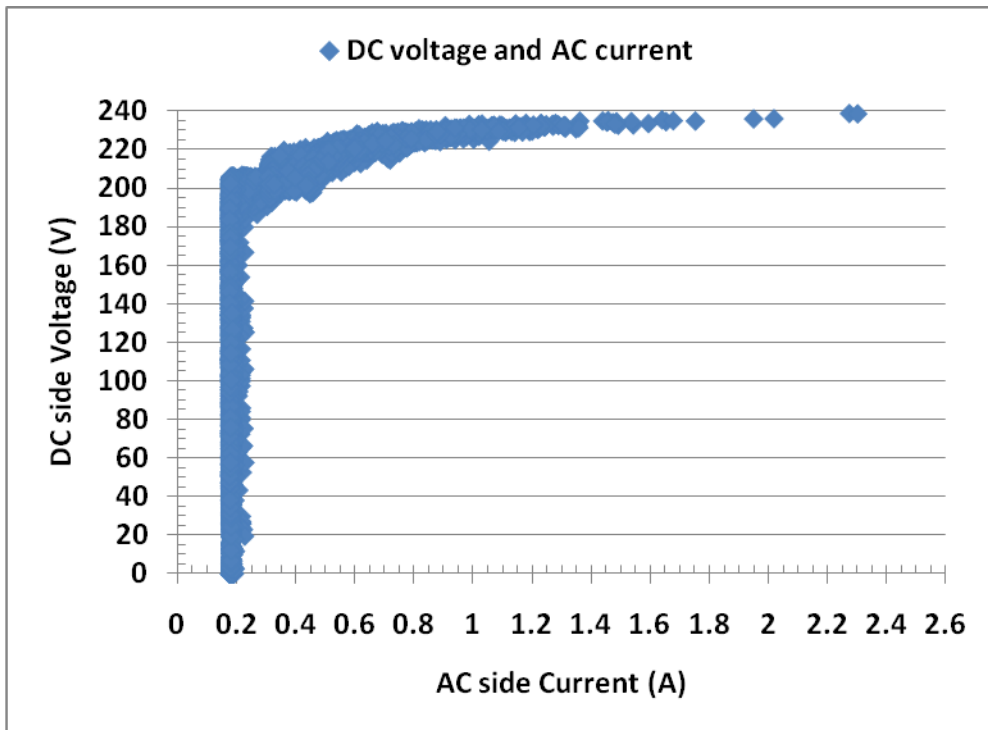


Figure 8-7: Graph of DC voltage and AC current of 30000 data points.

It has been found that the AC side current of 0.45 A starts flowing when DC voltage reaches 207 volts (by adding compensation of 1.03% error VDC becomes 209 volts) and continues to flow until dropping down to 196 volts (equal to 198 volts with compensation).

A set of VBA code has been written to calculate the total energy consumed and energy output by the inverter. To calculate energy being consumed by the inverter, all current values lower than 0.45 A were multiplied by 230 volts AC and then multiplied by time (i.e. 1/1800 hours in 2 sec) to obtain energy value. These values are then added up to determine the total energy usage. To calculate energy output from the inverter, all values greater than 0.45 A (for DC voltages greater than 196 volts) were taken into account to calculate the total output energy. Table 8-2 summarises the calculation which shows that although inverter efficiency is high to convert DC into AC but the inverter also relies on the grid energy. The net output after taking account of inverter consumption becomes very low, some even with negative output, especially in the month of October and December implying that all the generated energy was being consumed by the inverter without net output .

The pay back period of the WEC system can be calculate on the bases of its net energy export. Average of five month energy output of WEC system is 10.554 kWh/month. Average price of electricity in scotland is 16.486pence per kWh, it mean WEC system used in this research have to generate 10.554 kWh/month up to 67years to pay back its price (i.e £1400).

Table 8-2: Monthly input, output energy and energy consumed by inverter with inverter efficiency and net energy export.

Month	Energy Input of Inverter from Turbine generator (kWh)	Energy output of Inverter to the grid (kWh)	Inverter Efficiency	Energy consume by Inverter system from grid (kWh)	Net Energy export by WEC system (kWh)
JUL	28.84	28.47	98.72	28.35	0.12
AUG	34.73	32.04	92.23	17.90	14.14
OCT	3.96	3.75	94.70	5.00	-1.25
NOV	79.01	70.63	89.39	22.62	48.01
DEC	18.77	16.42	87.47	24.67	-8.25

8.4 Conclusion

It has been found that there is a reasonable difference in wind speed at turbine and MetPak locations. Performance of the wind turbine generator is difficult to obtain. The power output of wind turbine cannot be calculated as a standalone system because power is the product of voltages and current which depends on the load – inverter in this case. In the present case, the inverter cannot be switched on until generator voltages reach up to 209 volts. So there is a lot of wind turbine output lost, about 25% every month. It can be utilised for battery charging if it was connected to a suitable inverter system. The conversion efficiency of the inverter system from DC input to AC output is reasonable (after switching on) but it is at the cost of energy being consumed by inverter from the grid all the time. The efficiency of inverter in generating the output power will depend on the wind condition. So, under low wind condition, the overall performance of the micro WEC system is not viable for urban use.

9 Conclusions and future work

At the start of this research, a set of aims and objectives were laid out, as well as to answer some of the questions based on the research work in this thesis. The research work was to investigate the local wind condition in Edinburgh. With the findings which might lead to determine how the wind energy is distributed in urban and rural area, as well as studying the wind variation patterns and terrain that might affect the wind flow.

In order to arrive to the answers, several hardware installations and research studies have to be considered. First and foremost is the weather station and measurement instrumentation installation. The relevant Met Office wind data parameters have been recorded for research and wind condition analysis. The research work continues with the computational fluid dynamic (CFD) simulation to investigate the turbulence near and around the wind turbine and building. Finally, the performance of the micro WEC system in urban environment was investigated.

9.1 Analysis of wind data at Met office site and Merchiston campus

The topography around Met office weather station in Edinburgh's rural area has been analysed and found to have elevation variation around the weather station, but no prominent obstacle exist for the wind flow, around it. The prevailing wind direction has been found to be from south west with average yearly wind speed varies from 3.9 m/s to 4.58 m/s at 10 meter above the ground. Through the probability density distribution analysis, it has been found that on average, about 57% of the time, the wind speed was 4 m/s or lower and that Weibull distribution fits well compared to Rayleigh distribution. The diurnal variation in urban area has been investigated and wind speed variation has been found to be highly correlated to temperature variation and inversely related to humidity variation. It was also found that there is no diurnal effect on wind direction. The yearly velocity duration curve has been found to be more or less the same from the available eleven years data and the estimated wind energy in Edinburgh's rural area is 1 MWh/m².

The topography around Merchiston campus in urban Edinburgh has been analysed and a lot of elevation variations were found around the campus. The prevailing wind direction at Merchiston is the same as Edinburgh as a whole and the average yearly wind speed at 3m above the roof top was found to be 3.71 m/s which is lower than the MET Office data (taken from an open area). The probability distribution analysis revealed that about 65% of the time, the wind speed is 4 m/s or lower and the Weibull distribution fits better than Rayleigh distribution. Diurnal variation in urban area is more or less the same as in Edinburgh as a whole. Through the research work, it has been found that the choice of data to calculate the available wind energy plays a significant role and calculation from hourly average wind speed is found more reasonable and reliable than others. The wind energy available for year 2010 at Merchiston campus was found to be 563 kWh/m². Hence, it can be concluded that with the type of micro WEC system being used in the research, it cannot reasonably provide a cost effective solution to the renewable energy generation in Edinburgh.

9.2 Results of CFD investigation

One of the important chapters in this research work was on CFD investigation. Several simulations and analysis have been deduced in this thesis. It has been found that the maximum wind speed over the roof top of a cubic building was just 3m above the roof on the leading edge. The wind speed increases 18% when the height of the building is doubled. The vertical wind profile over a cubic building has been found to follow the power and logarithmic trend and the wind speed increases rapidly with the increase in height over the roof edge and very slow in the middle of the building. The wind shadow of the cubic building has been seen to last up to 5 m above the building which, in this case, is 33.33% of the height of the building. The simulation results also showed that the turbulence intensity over the cubic roof was in the increasing trend with height and then gradually decreased. Evidence obtained from the work also showed that there is no effect of the roughness height on the pattern of wind flow. It was found that the wind available at the MetPak and wind turbine was different, which constitutes to a specific ratio and wind direction dependent. The results

have also shown that the vertical profile of turbulence intensity over the Merchiston roof depends on wind direction.

9.3 Performance of the WEC system

The final part of this research work was to investigate the performance of the WEC system. The initial monitoring of WEC system has found that the system generated DC voltages. The inverter system in use was acting as loading so that the power output could be calculated. However, the inverter could only switch on when the WEC system generates DC voltage of 209 volts and above. As a result, there is power lost, which amounted to about 25% every month. Alternatively, battery charging facility can be adopted to harness the DC voltage wastage. The conversion efficiency of the inverter system (from DC input to AC output) was found to be reasonable (after switching on). However, it is the inverter system that requires constant power supply from the grid, has reduced the overall efficiency. When the system is under good wind condition, the efficiency of the system can reach positive value and vice-versa. With due consideration, the overall performance of the micro WEC system have been deemed to have low efficiency for use in urban area.

9.4 Future work

During the course of this research, a number of key areas have been investigated as far as the application of micro WEC system in the urban is concerned. However, there are still plenty of scopes that this work can be extended further to achieve better understanding of urban wind resource assessment in the built environment. The understanding of the wind flow within the built environment has already been studied substantially within the last few years. This was mainly as a result of large scale research projects such as those carried out by the Warwick Wind Trials, 2009 (Phillips *et al.* 2008) and the Energy Saving Trust, 2009. Additional investigation into urban wind flows would further increase the understanding of the prediction of wind power yields at potential sites. There is strong evidence that CFD is able to contribute to this understanding thanks to the likely future advancements in computer processing power, simplified flow model generation, advancements of turbulence modelling

and lastly more user orientated setup techniques. Further research in investigating how to accurately model trees and other vegetation is required in a single domain. This would increase the accuracy of the modelling in suburban areas where vegetation often form obstacles as high, or higher, than the buildings being investigated.

It was obvious from the performance investigation of the WEC grid connected system that the inverter was a component that requires further improvements, in particular the correct sizing of the inverter, for the wind resource of the site. Considering different sizes of wind turbines for example medium size, to install near or around urban area would be a useful future work.

REFERENCES

- Ahrens, C. D., (1994), *Meteorology Today, an Introduction to Weather, Climate and the Environment*. (Fifth Edition), United state of America, West Publishing Company.
- Ahrens, C. D., (2009), *Meteorology Today, an Introduction to Weather, Climate and the Environment*. (Ninth Edition), China, BROOKS/COLE CENGAGE Learning.
- Andy Wilson, (2007). Debunking the Myths about Micro Wind Turbines. Available from: <http://www.sustainability.ie/microwind.html> [Accessed on 28th April 2009].
- AWS Scientific, Inc., (1997). *Wind resource assessment handbook*. United states of America.
- Barlow, J.F., Rooney, G. G., Hunerbein, S. V., Bradley, S. G., (2008). Relating Urban Surface-layer Structure to Upwind Terrain for the Salford Experiment (Salfex). *Boundary-Layer Meteorol*, 127, pp. 173-191.
- Barry, R. G., Chorley, R. J., (2010). *Atmosphere, Weather and Climate*. Ninth Edition, London: Routledge.
- BBC Weather, (2006). Available from: http://www.bbc.co.uk/weather/weatherwise/factfiles/basics/wind_localwinds.shtml [Accessed on 20th April 2010].
- BEWA, (1999). NOABL wind speed atlas for the UK. Accessed from: http://www.bwea.com/images/misc/noabl_c.gif. [Accessed on Nov 01, 2008].
- Blanch, M. J., (2002). Wind Energy Technologies for use in the Build Environment, *Wind Engineering*. 26 (3). pp 125-143.
- Bolton, D. (1980). The computation of equivalent potential temperature. *Monthly Weather Review*. 108, pp 1046-1053.

Buccolieri, R., Sandberg, M., Sabatino, D. S., (2010). City breathability and its link to pollutant concentration distribution within urban-like geometries. *Atmospheric Environment*.

Bunge, U., Mockett, C., Thiele, F., (2007). Guidelines for implementing Detached-Eddy Simulation using different models. *Aerospace Science and Technology*. 11, pp. 376–385.

Burton, T., Sharpe D., Jenkins, N., Bossanyi, E., (2001) *Wind Energy Handbook*, England: John Wiley & Sons, Ltd.

BWEA, (2009). Wind energy and the media: Real Power. Issue 15, pp25-29.
Accessed from: http://www.bwea.com/pdf/realpower/realpower_15.pdf
[Accessed on Feb 01, 2011].

BWEA, (2010). UKWED Statistics. Available from:
<http://www.bwea.com/statistics/> [Accessed on Feb 01, 2011].

Carta J.A., Ramirez, P., Velazquez, S., (2009). A Review of wind speed probability distributions used in wind energy analysis, Case study in the Canary Islands. *Renewable and Sustainable Energy Reviews*, 13, pp. 933-955.

Chang, T. P., (2010). Estimation of wind energy potential using different probability density functions. *Applied Energy*.

Chen, Y. S., Kim, S.W., (1987). Computation of turbulent flows using an extended k-epsilon turbulence closure model. NASA CR-179204.

Chiovitti, T., Dodaro, D. L., (1994). Wind Shielding Effects of Trees on Low Buildings, Stathopoulous, *Building and Environment*, Vol 29, No. 2, pp. 141-150.

Clarke, S., (2003). Fact Sheet, Electricity generation using small wind turbine at home or farm. Available from:
<http://www.omafra.gov.on.ca/english/engineer/facts/03-047.pdf> [Accessed on Feb 01, 2011].

Clark, T., (2006). *Performance testing of the Windsave WS1000 Wind Turbine*, A Report from NEL for Windsave Ltd: Glasgow; NEL.

Clobes, M., Willecke, A., Peil, U., (2011). Shape-dependent characteristics of full-scale wind profiles. *Journal of Wind Engineering and Industrial Aerodynamics*, pp. 1-12.

Coleman, H.W., Stern, F., (1997). Uncertainties and CFD Code Validation, *Journal of Fluids Engineering*, Vol 119, pp. 795-803.

Contini, D., Cava, D., Martano, P., Donato, A., Grasso, F. M., (2008). Boundary Layer Height Estimation by Sodar and Sonic Anemometer Measurements. IOP Conference Series: *Earth and Environmental Science*, Vol 1, Iss 1, pp. 012034.

Cook, D. R., (2006). Climate Research Section, Environmental Science Division: Argonne National Laboratory: explains on the following web <http://www.newton.dep.anl.gov/askasci/wea00/wea00270.htm> [Accessed on March 10, 2009].

Department of Energy and Climate Change (DECC), (2010), GHG Conversion Factors for Company Reporting. Available from: <http://archive.defra.gov.uk/environment/business/reporting/pdf/101006-guidelines-ghg-conversion-factors.pdf> [Accessed on Jan 25, 2011]

Department of Energy and Climate Change (DECC), (2011a), Energy Price. Available at: <http://www.decc.gov.uk/publications/basket.aspx?filepath=statistics%2fsource%2fprices%2fqep221.xls&filetype=4#basket> [Accessed on Jan 20, 2011]

Department of Energy and Climate Change (DECC), (2011b), 2050 PATHWAYS ANALYSIS: CALL FOR EVIDENCE. Available from: <http://www.decc.gov.uk/en/content/cms/consultations/2050pathways/2050pathways.aspx> [Accessed on June 10, 2011]

Edina Digimap, Available from: <http://edina.ac.uk/digimap/index.shtml> [Accessed on May 26, 2009].

Edinburgh city local plan, (2007). Available from: <http://map.avinet.no/website/edinburgh/plans/eclp/chap1.htm> [Accessed on May 14, 2009].

Endalew, A. M., Hertog, M., Delele, M.A., Baetens, K., Persoons, T., Baelmans, M., Ramon, H., Nicolai, B.M., Verboven, P., (2009). CFD modelling and wind tunnel validation of airflow through plant canopies using 3D canopy architecture. *International Journal of Heat and Fluid Flow*. 30, pp. 356-368.

Energy Savings Trust. Available from: <Http://www.energysavingtrust.org.uk/> [Access on Aug 14, 2009].

Engineeringtoolbox, (2005). Density of dry air, water vapor and Moist humid air. Available from: http://www.engineeringtoolbox.com/density-air-d_680.html [Access on May 14, 2009].

European wind atlas, (1989). Available from: <http://www.windatlas.dk/Europe/landmap.html> [Access on May 18, 2009].

Franke, J., Hirsch, C., Jensen, A.G., Krüs, H.W., Schatzmann, M., Westbury, P.S., Miles, S.D., Wisse, J.A., Wright N.G., (2004). Recommendations on the Use of CFD in Wind Engineering. *In: Proceedings of the International Conference on Urban Wind Engineering and Building Aerodynamics: COST Action C14 - Impact of Wind and Storm on City Life and Built Environment*. Belgium: von Karman Institute for Fluid Dynamics. pp C.1.1 - C.1.11. ISBN 2-930389-11-7.

Franke, J., Hellsten, A., Schlünzen, H., Carissimo, B., (2007). Best practice guidelines for the CFD simulation of flows in the urban environment. *Quality assurance and improvement of micro-scale meteorological models*. Cost Action 732. Belgium.

Freris, L. L., ed. (1990). *Wind energy conversion system*. Cambridge. Prentice Hall.

Georgakis, C., Santamouris, M., (2008). On the estimation of wind speed in urban canyons for ventilation purposes-Part 1: Coupling between the undisturbed wind speed and the canyon wind. *Building and Environment*. 43. pp 1404-1410.

Gill Instruments Ltd, (2006a). MetPak User Manual Doc No. 1575-PS-0001.

Issue 2. Available from:

<http://www.gill.co.uk/data/manuals/MetpakWebManual.pdf> [Accessed on Nov 10, 2008].

Gill Instruments Ltd, (2006b). Principal of operation. Available from:

<http://www.gill.co.uk/products/anemometer/principleofoperation.htm> [Accessed on Apr 15, 2009]

Gnatowska, R., (2010). Development of local wind climate as an element of rural planning. Available from: <http://www.pan-ol.lublin.pl/wydawnictwa/TOchr7/Gnatowska.pdf> [Accessed on Dec 15, 2010]

Grant Data Acquisition, (2008). SQ2020_40 user manual, Available with equipment.

Hall, R.C. Ed (1997), Evaluation of modelling uncertainty. CFD modelling of near field atmospheric dispersion. Project EMU final report, European commission Directorate- General XII Science, Research and Development Contract EV5VCT94-0531, WS Atkins Consultants Ltd. UK.

Hamburg, M., (1985). *Basic Statistics a Modern Approach*, Third Edition. United States of America: Harcourt Brace Jovanovich, Inc.

Heath, M. A., Walshe, J. D., Watson, S. J., (2007). Estimating the potential yield of small building-mounted wind turbines, *Wind energy*, 10, pp. 271-287.

Hiester, T. R., Pennell, W. T., (1981). *The Meteorological Aspects of Siting Large Wind Turbines*. United States of America: Battelle Memorial Institute. Available from: <http://www.osti.gov/bridge/purl.cover.jsp?purl=/6657537-hWaCVO/> [Accessed on February 09, 2010].

Heisler, G. M., (1989). Mean Wind Speed Below Building Height in Residential Neighbourhoods with Different Tree Densities, ASHRAE Trans. 95, Part 2.

Hughes, T., (2000). Lesson Number 1. in an Oklahoma Wind Power Tutorial Series, Available from: http://www.seic.okstate.edu/owpi_old/about/library/lesson1_windenergycalc.pdf [Accessed on Mar 10, 2009].

Holdsworth, B., (2009). *Options for micro-wind generation: Part one*. Renewable energy focus. Available from: <http://www.renewableenergyfocus.com/view/1480/options-for-microwind-generation-part-1/> [Accessed on Nov 20, 2009].

ISES, (2007). *Wind Energy pocket Reference*. China. Earthscan.

Jowder, F. A. L., (2009). Wind power analysis and site matching of wind turbine generators in Kingdom of Bahrain. *Applied Energy*. 86, pp. 538-545.

Kiehl, J. T., Trenberth, K. E., (1997). Earth's Annual Global Mean Energy Budget. *American Meteorological Society*, v78, pp. 197-208.

Kurbatskii, A. F., Kurbatskaya, L. I., (2011). The Wind-Field Structure in a Stably Stratified Atmospheric Boundary Layer over a Rough Surface. *Atmospheric and Oceanic Physics*. Vol. 47, No. 3, pp. 281–289.

Li, Q. S., Zhi, L., Hu, F., (2010). Boundary layer wind structure from observations on a 325m tower. *Journal of Wind Engineering and Industrial Aerodynamics*, v98, pp. 818-832.

- Li, X. Liu, C. Leung, D.Y.C. Lam, K.M., (2006). Recent progress in CFD modelling of wind field and pollutant transport in street canyons. *Atmospheric Environment*, v40, n29, pp 5640-5658. China.
- Ludwig, J. C., Mortimore, S., (2009). *PHOENICS-VR Reference Guide (TR326)*. London: CHAM.
- Manwell, J.F., McGowan, J.G., Rogers, A.L., (2009). *Wind Energy Explained Theory, Design and Application*. Second Edition. England: Wiley.
- Martilli, A., Santiago, J. L., Martín, F., (2007). Micrometeorological modelling in urban areas, *Física de la Tierra*. Vol. pps 133-145. Madrid.
- Mathew. S., (2006). *Wind Energy Fundamentals, Resource Analysis and Economics*. Netherlands: Springer.
- Mayhoub, A. B., Azzam, A., (1997). A survey on the assessment of wind energy potential in Egypt, *Renewable Energy*, 11(2), pp.235-247.
- Mertens, S., (2006). *Wind energy in the built environment*. UK: Multi-Science.
- Met Office, (2008). *Small-scale Wind Energy- Technical Report*. Exeter: Published on www.metoffice.gov.uk.
- Moraes, O. L. L., Acevedo, O. C., Degrazia, G. A., Anfossi, D., Silva, R. D., Anabor, V., (2005). Surface layer turbulence parameters over a complex terrain, *Atmospheric Environment*. 39, pp. 3103-3112.
- Murakami, S. (1998). Overview of turbulence models applied in CWE-1997. *Journal of Wind Engineering and Industrial Aerodynamics*. 74-6, pp.1-24.
- Murakami, S., Ooka, R., Mochida, A., Yoshida, S., Kim, S., (1999). CFD analysis of wind climate from human scale to urban scale. *Journal of wind Engineering and Industrial Aerodynamics*. 81, pp. 57-81.
- Nelson, V., (2009). *WIND ENERGY Renewable Energy and the Environment*. USA. CRC press.

Office of the Deputy Prime Minister, (2006). Planning Policy Statement 22 – Renewable energy. Available from:

<http://www.communities.gov.uk/documents/planningandbuilding/pdf/147444.pdf>

[Access on June 7th 2010]

Onat, N., Ersoz S., (2010). Analysis of wind climate and wind energy potential of regions in Turkey. *Energy*. pp. 1-9.

Palma, J. M. L. M., Castro, F.A., Ribeiro, L. F., Rodrigues, A. H., Pinto, A. P., (2008). Linear and nonlinear models in wind resource assessment and wind turbine micro-siting in complex terrain, *Journal of Wind Engineering and Industrial Aerodynamics*. 96, pp 2308-2326.

Panofsky, H. A., Press, H., (1962). Meteorological and aeronautical aspects of atmospheric turbulence, *Progress in Aerospace Sciences*. 3, pp. 179-232. [Available on line in 2003].

Petersen, E. L., Mortensen, N. G., Landberg, L., Hojstrup, J., Frank, H. P., (1998). Wind power meteorology. Part I: Climate and turbulence. *Wind Energy*, 1, pp.25–45.

Phillips, R. B., Anderson, p., Clift, J., Aguiló-Rullán, A., Pester, A. S., (2008). Micro-wind turbines in urban environments - An assessment. Blackmore, Siting micro-wind turbines on house roofs. BRE Press.

Pidwirny, M., (2010). *Atmosphere layers*. Available from:

http://www.eoearth.org/article/Atmosphere_layers [Accessed on Mar 20, 2010].

Pielke, R. A., (2002). *Mesoscale meteorological modeling*. USA: Academic Press.

POLIS Encyclopaedia, 2007. Published by CHAM.

Ponta, F. L., Seminara, J. J., Otero, A.D., (2007). On the aerodynamics of variable-geometry oval-trajectory Darrieus wind turbines. *Renewable Energy*. 32, pp.35-56.

Prevezer, T., Holding, J., Gaylard, A., Palin, R., (2002). Bluff body asymmetric flow phenomena – real effect or solver artefact? *Wind & Structures*, Vol 5, No. 2-4, pp. 359-368.

Raithby, G.D., Stubbley, G.D., Taylor, P.A., (1987). The Askervein hill project: a finite control volume prediction on three dimensional flows over the hill. *Boundary-Layer Meteorol.* 39, pp.107–132.

Rogers, T., E., (2009), Siting and performance Assessment of Micro Wind Turbines in the Built Environment. Thesis submitted to The University of Nottingham for the degree of Doctor of Philosophy. Nottingham, UK.

Schatzmann, M., Britter, R., (2005). Cost Action 732 in combination with the European Science Foundation. Quality assurance and improvement of micro-scale meteorological models. Hamburg, Germany.

Schlez, W., (2000). Voltage fluctuations caused by groups of wind turbines. *PhD Thesis*, UK. Loughborough University.

Schneider, T., (2006). *The General Circulation of the Atmosphere*. The Annual Review of Earth and Planetary Science. pp.655–688. Available from: <http://www.gps.caltech.edu/~tapio/papers/annrev06.pdf> [Access on Jun 11, 2009].

Scottish Government Publications, (2006). Appendix D Baseline Information, Available from: <http://www.scotland.gov.uk/Publications/2006/12/11102741/17> [Access on May 14, 2009].

Scottish Government Publications, (2004). Review of green belt policy in Scotland. Available from: <http://www.scotland.gov.uk/Publications/2004/08/19785/41550> [Access on May 14, 2009].

Scottish Government, (2008). Permitted Development Rights for Domestic Microgeneration Equipment. Available from:

<http://www.scotland.gov.uk/Resource/Doc/213981/0056876.pdf> [Access on June 7, 2010].

Shaw, W. J., Doran, J. C., Coulter, R. L., (2005). Boundary-layer evolution over Phoenix, Arizona and the premature mixing of pollutants in the early morning, *Atmospheric Environment*. 39, pp. 773-786.

Standards & Technical Regulations Directorate, (2005). Electrical Supply Tolerances and Electrical Appliance Safety. Available from: <http://www.bis.gov.uk/files/file11548.pdf> [Access on Feb 8, 2010]

The City of Edinburgh Council, (2006). Rural West Edinburgh Local Plan. Available from: <http://88.208.222.252/website/plans/rwelp/contents.htm> [Access on June 10, 2010]

The City of Edinburgh Council, (2007). DQ Handbook: Draft Microgeneration Guideline. Available from: http://www.edinburgh.gov.uk/download/meetings/id/8688/development_quality_handbook_draft_microgeneration_guideline [Access on June 7, 2010]

The City of Edinburgh Council, (2008). Edinburgh's Climate. Available from: http://www.edinburgh.gov.uk/internet/City_Living/Welcome_to_Edinburgh/Edinburgh%20facts/CEC_edinburgh_s_climate [Access on May 14, 2009]

The City of Edinburgh Council's Economic Development service, (2008). Edinburgh by number, Second Edition, Edinburgh: Published on: http://www.capitalreview.co.uk/pdf/research/EBN_Final.pdf [Access on May 14, 2009].

Tieleman, H. W., (1992). Wind characteristics in the surface layer over heterogeneous terrain. *Journal of Wind Engineering and Industrial Aerodynamics*. 41–44. pp. 329–340.

Tieleman, H. W., (2003). Roughness estimation for wind-load simulation experiments, *Journal of Wind Engineering and Industrial Aerodynamics*. 91, pp.1163-1173.

Ucar, A., Balo, F., (2009). Investigation of wind characteristics and assessment of wind-generation potentiality in Uludag-Busra, Turkey, *Applied Energy*, 86, pp. 333-339.

U.S. Department of Energy Information Administration (EIA), (1999). Press release. Published on: <http://www.eia.gov/neic/press/press128.html> [Access on Nov 10, 2010].

Versteeg, H. K., Malalasekera, W., (1995). *An Introduction to computational fluid dynamics; The finite volume method*. Harlow: Longman.

Warwick Wind Trials, (2009). Warwick wind trial final report, Published on: <http://www.warwickwindtrials.org.uk/resources/Warwick+Wind+Trials+Final+Report+.pdf> [Access on May 14, 2009].

Wind Atlas Analysis and Application Program, (2009). Getting Started with WAsP 9. Available from: <http://www.wasp.dk/Download/DownloadFiles/General/Getting%20Started%20with%20WAsP%209.pdf> [Access on May 12, 2009].

World Meteorological Organization, (1981). *Meteorological aspects of the utilization of wind as an energy source*. Geneva: WMO Publication [WMO-No.575].

World Wind Energy Association, (2011). Available from: http://www.wwindea.org/home/index.php?option=com_content&task=view&id=317&Itemid=43 [Access on Sep 30, 2011].

Wikimedia, (2007). Edinburgh Climate graph. Available from: http://commons.wikimedia.org/wiki/File:Edinburgh_climate_graph.png [Access on May 14, 2009].

Wordtravel, (2009). Edinburgh climate and weather. Available from: <http://www.wordtravels.com/Cities/Scotland/Edinburgh/Climate> [Access on May 14th 2009].

Xie, Z., Castro, I. P., (2006). LES and RANS for Turbulent Flow over Arrays of Wall-Mounted Obstacles. *Flow Turbulence Combustion*, 76. pp. 291-312.

Yassin, M. F., (2011). Impact of roof shape and its height of building on air quality in urban street canyons. *Atmospheric Environment*, pp. 1-10.

Zhou, Y., Stathopoulos, T., (1997). A new technique for the numerical simulation of wind flow around buildings, *Journal of Wind Engineering and Industrial Aerodynamics*. 72, pp. 137-147.

APPENDICES

Appendix A: Wind turbine efficiency

Wind turbine efficiency:

Wind turbine efficiency means how efficient turbine is to convert the wind energy into electric energy. Companies claiming different efficiencies (as shown in Table A-1) which mostly not matched with actual results, the reason for this misleading efficiency values is that manufacturers rely on the wind tunnel test results for efficiency calculation.

Table A-1: Wind turbine efficiency claimed by different companies (Andy Wilson, 2007).

Turbine	Blade Diameter in Meters (2 x Radius)	Swept Area (m²) πr^2	Manufacturers Claimed Output in kilowatts (kW) at wind speed of 12 meters per second (m/s)	Output in kilowatts (at wind speed of 12 m/s) per square meter of swept area (based on manufacturers data)	Implied level of efficiency at 12 m/s based on manufacturers data (%)
Rutland FM910	0.91	0.65	0.1	0.15	14.5
Air X	1.1	0.95	0.3	0.32	29.8
Surface Power 460*	1.4	1.54	0.43	0.28	26.4
WindSave	1.75	2.41	1	0.41	39.2
WhisperH40	2.1	3.46	0.8	0.23	21.8
Navitron 300watt	2.2	3.8	0.37	0.1	9.2
Proven WT600	2.3	4.16	0.6	0.14	13.6
Fortis Passaat	3.12	7.65	1	0.13	12.4
Proven WT2500	3.5	9.62	2.5	0.26	24.6
Fortis Montana	5	19.63	4	0.2	19.3
Proven WT6000	5.5	23.76	6	0.25	23.9
Eoltec Sirocco	5.6	24.64	6	0.24	23

Power curve for windsave WS1000 turbine:

Power curve is a graph between wind speed and the turbine power output. It can help to calculate the efficiency of the wind turbine. In one performance test report (Clark, 2006) of Windsave's WS1000 wind turbine, NEL provide power curve in results of their tests as shown in Figure A-1.

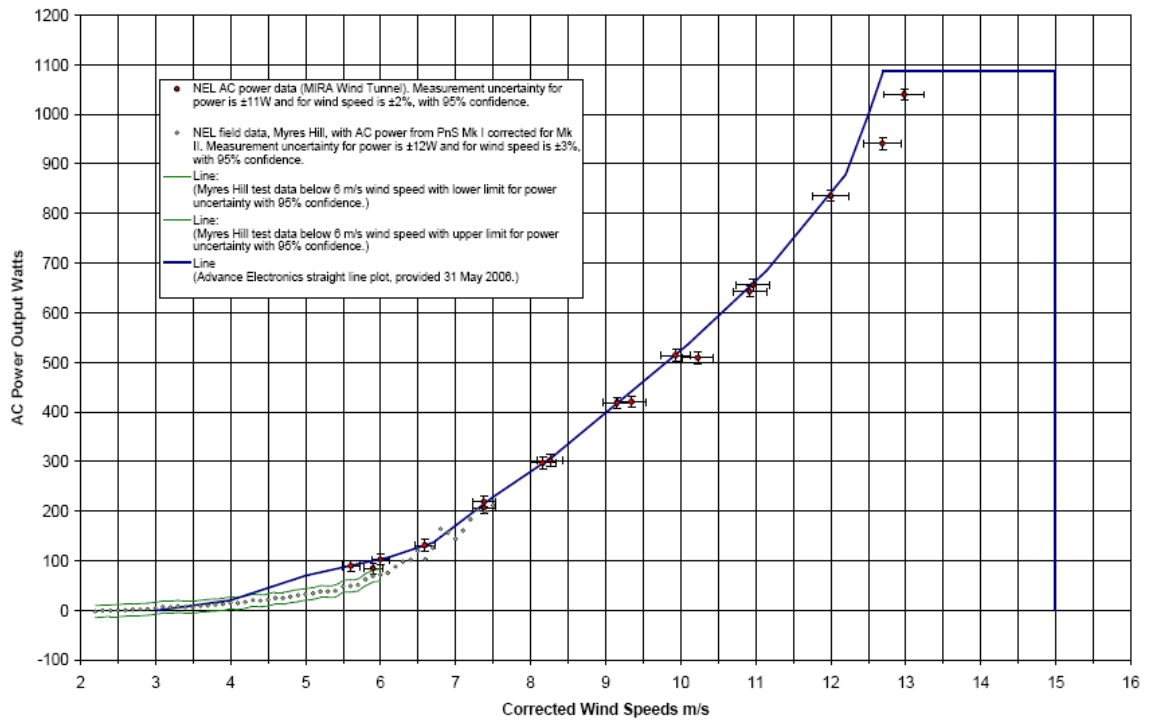


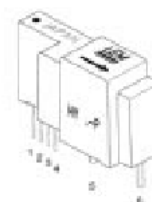
Figure A-1: WindSave WS1000 turbine power curve with 1.74m diameter blades
Published by NEL after performance testing (Clark, 2006).

Appendix B: Data sheets

Current Transducers HY 5 to 25-P

For the electronic measurement of currents : DC, AC, pulsed, mixed, with a galvanic isolation between the primary circuit (high power) and the secondary circuit (electronic circuit).

$$I_{PN} = 5 \dots 25 \text{ A}$$



Electrical data			
Primary nominal r.m.s. current I_{PN} (A)	Primary current measuring range I_p (A)	Primary conductor (mm)	Type
5	± 15	∅ 0.7	HY 5-P
10	± 30	∅ 1.1	HY 10-P
12.5	± 37.5	∅ 1.4	HY 12-P
15	± 45	∅ 1.4	HY 15-P
20	± 60	2 x ∅ 1.2 ¹⁾	HY 20-P
25	± 75	2 x ∅ 1.4 ¹⁾	HY 25-P

V_C	Supply voltage (± 5 %)	± 15	V
I_C	Current consumption	± 10	mA
I_p	Overload capability (1 ms)	50 x I_{PN}	
V_d	R.m.s. voltage for AC isolation test, 50/60Hz, 1 mn	2.5	kV
V_b	R.m.s. rated voltage, safe separation	500 ²⁾	V
R_{is}	Isolation resistance @ 500 VDC	> 1000	MΩ
V_{OUT}	Output voltage @ ± I_{PN} , $R_L = 10 \text{ k}\Omega$, $T_A = 25^\circ\text{C}$	± 4	V
R_{OUT}	Output internal resistance	100	Ω
R_L	Load resistance	> 1	kΩ

Accuracy - Dynamic performance data			
X	Accuracy @ I_{PN} , $T_A = 25^\circ\text{C}$ (without offset)	< ± 1	%
ϵ_L	Linearity ³⁾ (0 .. ± I_{PN})	< ± 1	% of I_{PN}
V_{OE}	Electrical offset voltage, $T_A = 25^\circ\text{C}$	< ± 40	mV
V_{OH}	Hysteresis offset voltage @ $I_p = 0$; after an excursion of 1 x I_{PN}	< ± 15	mV
V_{OT}	Thermal drift of V_{OE}	typ. ± 1.5 max. ± 3	mV/K mV/K
TCE_G	Thermal drift of the gain (% of reading)	< ± 0.1	%/K
t_r	Response time @ 90% of I_p	< 3	μs
di/dt	di/dt accurately followed	> 50	A/μs
f	Frequency bandwidth ⁴⁾ (-3 dB)	DC .. 50	kHz

General data		
T_A	Ambient operating temperature	- 10 .. + 80 °C
T_S	Ambient storage temperature	- 25 .. + 85 °C
m	Mass	< 14 g
	Standards ⁵⁾	EN 50178

- Notes :
- 1) Conductor terminals are soldered together.
 - 2) Pollution class 2, overvoltage category III.
 - 3) Linearity data exclude the electrical offset.
 - 4) Please refer to derating curves in the technical file to avoid excessive core heating at high frequency.
 - 5) Please consult characterisation report for more technical details and application advice.

Features

- Hall effect measuring principle
- Galvanic isolation between primary and secondary circuit
- Isolation voltage 2500 V~
- Compact design for PCB mounting
- Low power consumption
- Extended measuring range (3 x I_{PN})
- Insulated plastic case recognized according to UL 94-V0.

Advantages

- Easy mounting
- Small size and space saving
- Only one design for wide current ratings range
- High immunity to external interference.

Applications

- General purpose inverters
- AC variable speed drives
- Static converters for DC motor drives
- Battery supplied applications
- Uninterruptible Power Supplies (UPS)
- Switched Mode Power Supplies (SMPS).

981007/3

AC Current transducer AK-C-

A split Core transducer for the electronic measurement AC sinusoidal waveforms current, with galvanic isolation between the primary (High power) and the secondary circuits (Electronic circuit). Jumperselectable ranges and self powered transducers.



$I_{PN} = 10..200A$



Electrical data

Primary Nominal Current I_{PN} (A.t.RMS)	Analogue Output Signal V_{OUT} (V DC)	Type
10,20,50	5	AK 50 C5
10,20,50	10	AK 50 C10
100,150,200	5	AK 200 C5
100,150,200	10	AK 200 C10
V_c Supply voltage		Self Powered
R_L Load resistance		1 M Ω
V_d RMS Isolation voltage test, 50 Hz, 1mn		5000 V AC
f Frequency bandwidth		50-80 Hz

Accuracy - Dynamic performance data

X	Accuracy of reading @ $T_A=25^{\circ}C$	± 1	%
t_r	Response time @ 90% of I_{PN}	< 100	mS

General data

T_A	Ambient operating temperature (0-95% RH)	-20..+50	$^{\circ}C$
T_S	Ambient storage temperature	-20..+85	$^{\circ}C$
m	Mass	120	g

Note: ¹⁾ For 0-5 V output model, no saturation output up to 8 V
and for 0-10 V output model, no saturation output up to 15 V

Features

- AC measurement
- Average responding
- Self powered transducers
- Panel mounting
- Voltage output
- Isolation
- Eliminates insertion loss
- Jumper selectable ranges

Advantages

- Large aperture
- High isolation between primary and secondary circuits
- Easy to mount

Applications

- Automation systems
Analog current reading for remote monitoring (e.g. motor) and software alarms.
- Data loggers
Self-powered transducer does not drain data logger batteries.
- Panel meters
Simple connection displays power consumption.

Options on request

- DIN mounting



HCA-BARO Series

Miniature amplified barometric pressure sensors

FEATURES

- 600...1100 mbar, 800...1100 mbar barometric ranges
- Output: 0.25...4.25 V and I²C-bus (SPI and switching outputs optional)
- Precision ASIC conditioning
- Calibrated and temperature compensated
- Miniature SMT or SIL housing
- Sensortech PRO services

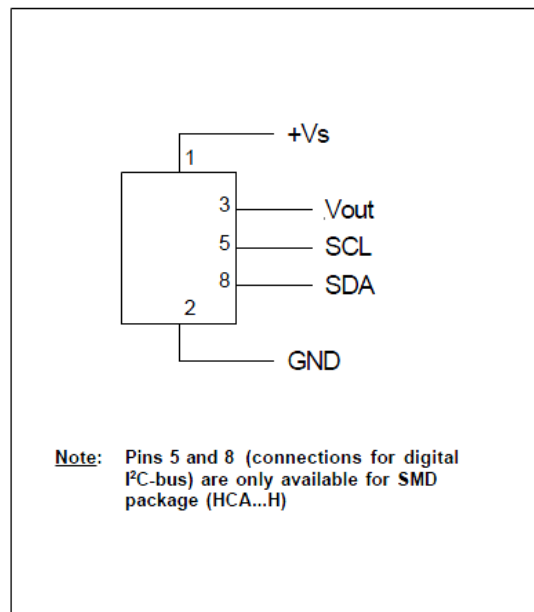


SPECIFICATIONS

Maximum ratings

Supply voltage V_s (optional 2.7 ... 3.3 V_{DC})	4.5 V ... 5.5 V_{DC}
Output current Sink	1 mA
Source	1 mA
Proof pressure ³	3000 mbara
Burst pressure ⁴	5000 mbara
Lead specifications	
Average preheating temperature gradient	2.5 K/s
Soak time	ca. 3 min
Time above 217°C	50 s
Time above 230°C	40 s
Time above 250°C	15 s
Peak temperature	260°C
Cooling temperature gradient	-3.5 K/s
Temperature ranges	
Compensated	0 ... +85°C
Operating	-25 ... +85°C
Storage	-40 ... +125°C
Humidity limits (non-condensing)	0 ... 95 %RH

ELECTRICAL CONNECTION





HCA-BARO Series

Miniature amplified barometric pressure sensors

PERFORMANCE CHARACTERISTICS

($V_s = 5.0\text{ V}$, $T_A = 25\text{ }^\circ\text{C}$, analog output signal is **ratiometric** to V_s , digital output signal is **not ratiometric** to V_s , pressure applied to high pressure port)

Characteristics	Min.	Typ.	Max.	Unit
Operating pressure range	HCA0611AR... 600		1100	mbara
	HCA0811AR... 800		1100	
Total accuracy (0 ... 85 °C) ¹			±1.0	%FSS
Response delay ^{6, 6}		2		ms
A/D resolution ⁶		15		bit
D/A resolution			11	
Current consumption (no load) ⁷		5		mA
DIGITAL PERFORMANCE CHARACTERISTICS				
Output at min. pressure		0666		Count Hex
Full scale span (FSS) ²		6666		
ANALOGUE PERFORMANCE CHARACTERISTICS				
Output at min. pressure		0.25		V
Full scale span (FSS) ²		4.00		

Specification notes:

1. Total accuracy is the combined error from offset and span calibration, linearity, pressure hysteresis, and temperature effects. Linearity is the measured deviation based on a straight line. Hysteresis is the maximum output difference at any point within the operating pressure range for increasing and decreasing pressure. Calibration errors include the deviation of offset and full scale from nominal values.
2. Full Scale Span (FSS) is the algebraic difference between the output signal for the highest and lowest specified pressure.
3. Proof pressure is the maximum pressure which may be applied without causing durable shifts of the electrical parameters of the sensing element.
4. Burst pressure is the maximum pressure which may be applied without causing damage to the sensing element or leaks to the housing.
5. Max. delay time between pressure change at the pressure die and signal change at the output.
6. The response time depends on the adjusted internal A/D resolution of the sensor. For 15 bit it is typ. 2 ms. Other A/D resolutions and reponse times are available on request. Please contact Sensortechncs for further information.
7. Sensors with lower current consumption are available on request. Please contact Sensortechncs for further information.

Appendix C: List of Publications

1. Irshad, W. Goh, K. Kubie, J., (2009). *Wind Resource Assessment in the Edinburgh Region*. IEEE conference, WNWEC 2009, Nanjing, China.

Papers under preparation:

1. Wind resources in Edinburgh's rural and urban areas.
2. Performance of micro-WEC system at roof top of urban structure.